STATIC AND DYNAMIC CHARACTERISTICS FOR A TWO-AXIAL-GROOVE BEARING AND A PRESSURE-DAM BEARING

A Thesis

by

BADER K. AL JUGHAIMAN

Submitted to the Office of Graduate Studies of
Texas A&M University
in partial fulfillment of the requirements for the degree of

MASTER OF SCIENCE

August 2006

Major Subject: Mechanical Engineering

STATIC AND DYNAMIC CHARACTERISTICS FOR A TWO-AXIAL-GROOVE BEARING AND A PRESSURE-DAM BEARING

A Thesis

by

BADER K. AL JUGHAIMAN

Submitted to the Office of Graduate Studies of
Texas A&M University
in partial fulfillment of the requirements for the degree of

MASTER OF SCIENCE

Approved by:

Chair of Committee,	Dara Childs
Committee Members,	Luis San Andres
	Stuart Scott
Head of Department,	Dennis O'Neal

August 2006

Major Subject: Mechanical Engineering

ABSTRACT

Static and Dynamic Characteristics for a Two-Axial-Groove Bearing and a Pressure-Dam Bearing. (August 2006)

Bader K. Al Jughaiman, B.S., King Fahd University of Petroleum and Minerals

Chair of Advisory Committee: Dr. Dara Childs

This thesis compares experimental static and dynamic force characteristics for a two-axial-groove bearing and a pressure-dam bearing without a relief track. The thesis also compares experimental results to predictions from a numerical analysis. The tested pressure-dam bearing has θ_s = 130°, k'=3.4~4.2, and $\bar{L}_d$ =0.75. The test results show that eccentricity for both bearings decreases as Sommerfeld number increases. However, the pressure-dam bearing maintains a minimum eccentricity of about 0.5 at high speeds. The results also show that the attitude angle for both bearings increases as Sommerfeld number increases. The maximum attitude angle for the axial-groove bearing is 90° at no-load. However, the attitude angle for the pressure-dam bearing increases above 90° at no-load as speed increases. A dynamic test shows that the pressure-dam bearing has higher direct stiffness and damping at high Sommerfeld number because of the increase in eccentricity. However, as Sommerfeld number decreases, the difference between stiffness and damping coefficients of both bearings diminishes. The dynamic test also shows that both bearings have significant added mass coefficients in the laminar flow region that decrease as eccentricity increases. The estimated axial-groove bearing whirl-frequency ratio (*WFR*) from experimental results is 0.45. The *WFR* of the pressure-dam bearing reduces to 0.41 at high Sommerfeld numbers. Numerical analysis shows that the pressure-dam bearing can have lower *WFR* if the dam arc length is increased to 150°. Numerical analysis also shows that stability can be improved further by adding a relief track. Generally, the numerical analysis under predicts the bearings' eccentricity and dynamic force coefficients with better agreement at low Sommerfeld numbers.

DEDICATION

To my parents for their care, support, and prayers
To my wife for her love, understanding, and patience,
To my son Khaled, and daughter Wasan

ACKNOWLEDGEMENTS

"Thanks to ALLAH for his guidance and help"

I would like to thank Dr. Dara Childs for his great help and support through my studies at Texas A&M University. His great knowledge was of great help to me to complete this project. My thanks are also extended to Dr. Luis San Andres and Dr. Stuart Scott for serving on my advisory committee. Also, special thanks to the Turbomachinery Research Consortium for funding the project and to Bearings Plus for providing the bearing.

I am also sure that this work could not have been achieved without the help of my friends and coworkers at the Turbomachinery Laboratory. Finally, I would like to express my deepest thanks to SAUDI ARAMCO for giving me the chance and providing all required funds to pursue my graduate studies.

TABLE OF CONTENTS

LIST OF FIGURES

Page

Page

Page

LIST OF TABLES

Page

Page

Page

NOMENCLATURE

A_x, A_y	Fourier transformation of stator acceleration
C_{ij}	Bearing damping coefficient (N.s/m)
c_{ij}	Dimensionless damping coefficient
C_r	Bearing radial clearance (m)
D	Bearing inner diameter (m)
D_x, D_y	Fourier transformation of Δx and Δy
e_x, e_y	Average bearing displacement in the x and y directions respectively (m)
f_{bx}, f_{by}	Bearing reaction forces in the x and y directions respectively (N)
f_x, f_y	Excitation forces in the x and y directions respectively (N)
F_x, F_y	Fourier transformation of f_x and f_y respectively
h	Local film thickness (m)
h_1	Film thickness before the step (m)
h_2	Film thickness after the step (m)
H_{ij}	Average dynamic stiffness (N/m)
i,j	Subscript representing x and y
K_{ij}	Bearing stiffness coefficient (N/m)
k_{ij}	Dimensionless stiffness coefficient
k'	Step film thickness ratio
L	Bearing axial length (m)
L_d	Dam axial length (m)
$\bar{L}_d$	Dam axial length ratio
L_t	Relief track axial length (m)
$\bar{L}_t$	Relief track axial length ratio
M	Rotor equivalent mass (kg)
M_{ij}	Fluid inertia coefficient (kg)
M_s	Stator mass (kg)
N	Rotor speed (Hz)
P	Bearing film pressure (N/m²)

R	Bearing inner radius (m)
Re	Reynolds number
S	Sommerfeld number
U	Rotor speed (m/s)
W	Bearing load (N)
x,y	Displacement directions
z	Bearing axial length
ρ	Lubricant dynamic viscosity (N.s/m²)
ε_0	Eccentricity ratio
ψ	Attitude angle
θ_s	Step angle
χ	Pad arc angle
ω	Rotor speed (rad/s)
Ω	Excitation frequency (rad/s)
ω_n	Rotor-bearing system natural frequency (rad/s)
ω_f	Rotor whirling frequency (rad/s)
δ_h	Horizontal preset of orthogonally displaced pressure-dam bearing
δ_v	Vertical preset of elliptical pressure-dam bearing
WFR	Whirl-frequency ratio

INTRODUCTION

Hydrodynamic fluid film bearings are commonly used in industry to support rotors. The load capacity of these bearings is generated by the rotation of the journal in the bearing clearance. This load capacity depends on many factors such as the bearing design, clearance, and lubricant viscosity.

Beauchamp Tower in the seventeenth century first discovered the high pressure generated by the hydrodynamic action of the oil film in railroad bearings. In 1886, O. Reynolds published his famous equation that provides the basis for journal bearings design [1].

$$\frac{\partial}{\partial x}\left(\frac{\rho h^3}{12\mu}\frac{\partial P}{\partial x}\right)+\frac{\partial}{\partial z}\left(\frac{\rho h^3}{12\mu}\frac{\partial P}{\partial z}\right)=\frac{1}{2}\frac{\partial}{\partial x}(\rho h U) \tag{1}$$

The equation shows that a converging film thickness is necessary to generate a positive hydrodynamic pressure. Fig. 1 illustrates how the hydrodynamic film pressure is generated in journal bearings. The figure shows that the bearing reaction force due to the rotor load has both horizontal and vertical components. While, the vertical component is in the opposite direction of the load, the horizontal direction is 90° from the load direction. This phenomenon arises from the fluid rotation and is called cross coupling.

As a result, rotors supported on hydrodynamic bearings tend to have an eccentric position e within the bearing clearance with an offset angle from the load direction called the attitude angle ψ.

This thesis follows the format of the ASME Journal of Tribology.

The equilibrium position is commonly defined in terms of a dimensionless number called Sommerfeld number *S*:

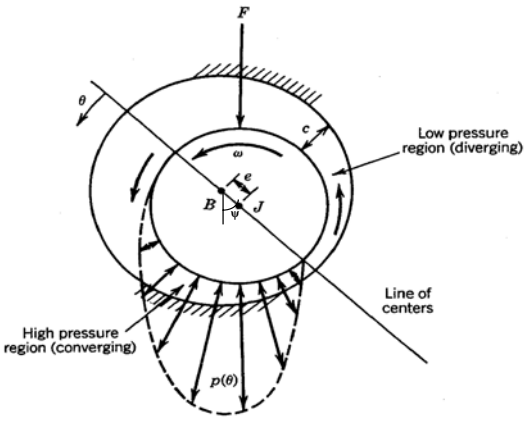

Fig. 1 Hydrodynamic pressure generation in journal bearings [2]

Lord Rayleigh [3] in 1918 analyzed the effect of varying the film thickness between two parallel surfaces on the bearing load capacity. Rayleigh found that the stepped design is the best configuration compared to a linear taper, crowned or exponential film shapes on the basis of load capacity. He also determined that the optimum ratio of the film thickness before and after the step k' is 1.7 assuming laminar flow all around the bearing including the pocket. Today, step cylindrical journal bearings are used in many different types of rotating machinery because of their higher threshold speed of instability compared to plain journal bearings. They are also easier to manufacture and have higher manufacturing tolerances than multiple-lobe bearings [4]. The improvement in stability comes from the step or dam cut in the upper surface of the bearing which produces a pressure rise near the step and a downward force on the journal. Thus, the rotor operates at higher eccentricity ratio because of this induced load. The bottom pad is sometimes deeply grooved to create a circumferential relief track. The

objective of the relief track is to reduce the effective bearing length thus reducing its load capacity and increasing journal eccentricity. Fig. 2 shows a step bearing often called pressure-dam bearing with a step at the top (unloaded pad) and a relief track at the bottom pad. The figure shows the most important design parameters for pressure-dam bearing, namely: film thickness ratio k', dam axial length ratio $\bar{L}_d$, and relief track axial length ratio $\bar{L}_t$.

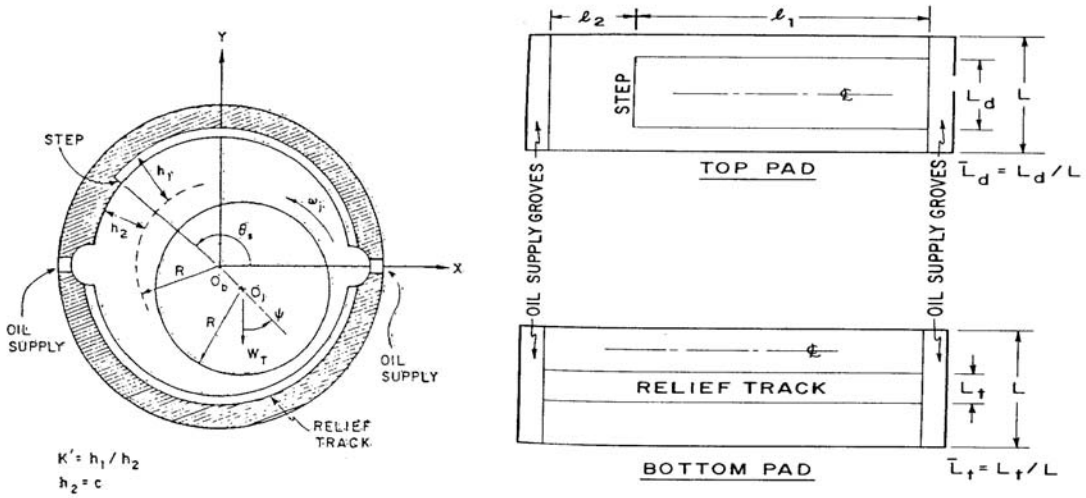

Fig. 2 Schematic view of pressure-dam bearing [4]

The evolution of bearing design continued in the late nineteenth century and early twentieth century with the extension of Reynolds equation to gas bearings and the invention of tilting pad bearings shown in fig. 3. As the name implies, the pads in this bearing are allowed to tilt as load is applied [1].

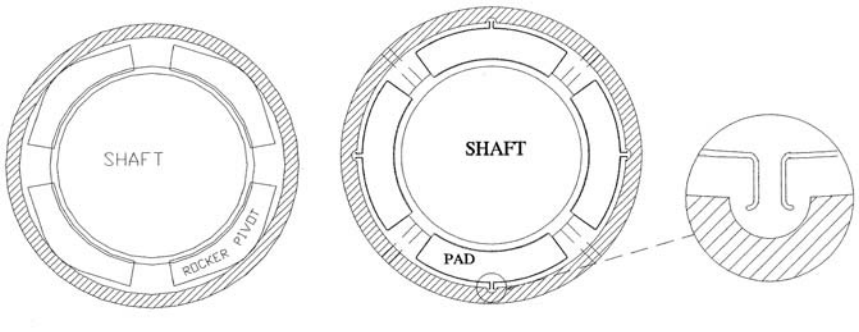

(a) (b)

Fig. 3 Tilting pad bearing a) rocket pivot b) flexure pivot [5]

In 1925, the effect of journal bearings on rotor dynamics was discovered. A. Stodola first realized that journal bearings are not firmly rigid supports. He instead represented journal bearings as springs with direct and cross-coupled stiffness [6].

Also in 1925, B. Newkirk and H. Taylor [7] observed large vibration of a rotor on plain journal bearings when reached twice its first critical speed. They also noted that the rotor was whirling at almost half of its running speed. They found that the vibration stopped when the oil supply was stopped accidentally. Newkirk and Taylor called this phenomena “oil whip” because they attributed it to the oil film action in the journal bearing clearance.

In the middle of the twentieth century, the idea of journal bearings stiffness and damping coefficients start to become popular, and a lot of work was done to study the oil whip phenomena based on these coefficients. Lund [8] in 1965 developed the concepts of the interaction between the bearing dynamic coefficients and the rotor dynamics. He showed that oil whip can be presented as an undamped resonance in which the bearing fluid film is represented by a single spring with equivalent stiffness. Lund showed that oil whip occurs when the rotor whirl-frequency is equal to the lowest rotor-bearing system natural frequency, which is determined by the bearing equivalent stiffness for rigid rotors. He also showed that rotor flexibility and bearing support flexibility lower the onset speed of instability without affecting the instability whirl-frequency ratio.

Dynamic force coefficients of fluid film bearings are calculated theoretically by assuming small amplitude journal motions about an equilibrium position and expressing the bearing reaction forces as a Taylor series expansion [9]. Therefore, for the bearing shown in Fig. 1, the reaction forces can be written as:

$$F_y = W + \frac{\partial F_y}{\partial x}\Delta x + \frac{\partial F_y}{\partial y}\Delta y + \frac{\partial F_y}{\partial \dot{x}}\Delta \dot{x} + \frac{\partial F_y}{\partial \dot{y}}\Delta y + \frac{\partial F_y}{\partial \ddot{x}}\Delta \ddot{x} + \frac{\partial F_y}{\partial \ddot{y}}\Delta \ddot{y} \tag{5}$$

$$F_x = \frac{\partial F_x}{\partial x}\Delta x + \frac{\partial F_x}{\partial y}\Delta y + \frac{\partial F_x}{\partial \dot{x}}\Delta \dot{x} + \frac{\partial F_x}{\partial \dot{y}}\Delta \dot{y} + \frac{\partial F_x}{\partial \ddot{x}}\Delta \ddot{x} + \frac{\partial F_x}{\partial \ddot{y}}\Delta \ddot{y} \tag{6}$$

The bearing stiffness, damping, and inertia coefficients are defined as follow:

$$K_{yy} = -\frac{\partial F_y}{\partial y}; K_{xx} = -\frac{\partial F_x}{\partial x}; K_{xy} = -\frac{\partial F_x}{\partial y}; K_{yx} = -\frac{\partial F_y}{\partial x} \tag{7}$$

$$C_{yy} = -\frac{\partial F_y}{\partial \dot{y}}; C_{xx} = -\frac{\partial F_x}{\partial \dot{x}}; C_{xy} = -\frac{\partial F_x}{\partial \dot{y}}; C_{yx} = -\frac{\partial F_y}{\partial \dot{x}} \tag{8}$$

$$M_{yy} = -\frac{\partial F_y}{\partial \ddot{y}}, M_{xx} = -\frac{\partial F_x}{\partial \ddot{x}}, M_{xy} = -\frac{\partial F_x}{\partial \ddot{y}}, M_{yx} = -\frac{\partial F_y}{\partial \ddot{x}} \tag{9}$$

Then, ignoring mass terms, the bearing-rotor system equivalent dimensionless stiffness for a rigid rotor as determined by Lund [8] is given by:

$$k_{eq} = \frac{k_{xx}c_{yy} + k_{yy}c_{xx} - c_{yx}k_{xy} - c_{xy}k_{yx}}{c_{xx} + c_{yy}} \tag{10}$$

The relationship between the dimensional and the dimensionless stiffness and damping coefficients are:

$$k_{ij} = K_{ij}\left(\frac{C_r}{W}\right) \tag{11}$$

$$c_{ij} = C_{ij}\left(\frac{C_r\omega}{W}\right) \tag{12}$$

The bearing whirl-frequency ratio (whirling frequency divided by rotor speed), the bearing-rotor system natural frequency and the threshold speed of instability at which oil whip occurs are given by the following equations:

$$WFR^2 = \frac{(k_{eq} - k_{xx})(k_{eq} - k_{yy}) - k_{xy}k_{yx}}{c_{xx}c_{yy} - c_{xy}c_{yx}} = (\frac{\omega_f}{\omega})^2 \tag{13}$$

$$\omega_n = \sqrt{\frac{K_{eq}}{M}} \tag{14}$$

$$\omega_s = \frac{\omega_n}{WFR} \tag{15}$$

This means that oil whip occurs when the rotor whirls at the system lowest natural frequency.

This thesis compares pressure-dam bearing force coefficients to those for a two-axial-groove bearing. The thesis also examines the effect of fluid inertia on the bearings force coefficients for laminar flow with Reynolds number on the order of 100 and compares the results to predictions from Reinhardt and Lund [10].

LITERATURE REVIEW

The classical lubrication theory established by Reynolds ignores the effect of fluid film inertia of journal bearings because of the small C_r/R ratio (<0.001) resulting in small Reynolds number (of the order of 1). Therefore, all analytical solutions for hydrodynamic journal bearings based on Reynolds theory have represented the bearings force coefficient by stiffness and damping coefficients only. The effects of flow turbulence and fluid inertia have been considered for large Reynolds number applications (of the order of 1,000). However, Reinhardt and Lund [10] suggested that fluid inertia effect could also be significant without affecting the assumption of laminar flow for Reynolds number of the order of 100. After performing a first order perturbation analysis on the fluid momentum equation keeping convective and temporal terms, Lund and Reinhardt show that a journal bearing with $L/D = 0.5; R/C_r = 10^3$, and assuming the lubricant to be oil while the journal material is steel, would have a direct added mass equal to 6 times the journal mass. This artificial mass could lower the critical speeds for short and small rotors.

Many studies have been conducted on both axial-groove journal bearings as well as pressure-dam bearings. The studies focused mainly on determining the whirl-frequency ratio, finding each bearing's stability map, and determining the optimum step depth and angle for the pressure-dam bearing.

Allaire et al. [11] used the finite element method to calculate the pressure profile for an infinite length pressure-dam bearing using laminar flow theory, linearized turbulent flow theory (turbulence shear stress parameter is determined based on Reynolds number) in the pocket without fluid inertia effect, and turbulent flow theory with fluid inertia effect that includes both turbulence and pressure drop at the step. They compared the theoretical solution to experimental results and found that the inertia theory agrees well with the experimental results. They also found that for maximum load capacity, the bearing should be designed for $k' = 2.3, \theta_s = 125^\circ$ where k' and θ_s are as

defined in Fig. 2. However, for Reynolds number up to 1500, the turbulence flow theory results deviates by only 10% from the results of inertia flow theory while laminar theory fails for Reynolds number larger than 50. Therefore, the turbulence theory can be used safely for most industrial applications.

Nicholas and Allaire [12] analyzed the stability of finite length pressure-dam bearings compared to axial-groove bearing. All bearings have *L/D* =1 and *Re*=210. They found that the two-axial-groove bearing has a 0.5 whirl-frequency ratio. Incorporating a relief track at the bottom pad of the two-axial-groove bearing with $\bar{L}_t = 0.25$, ($\bar{L}_t$ is defined in Fig. 2), reduces the whirl-frequency ratio to 0.40. Adding a step at the upper pad with $\theta_s = 125^\circ$, $k' = 3$ and $\bar{L}_d$=0.75, ($\bar{L}_d$ is defined in Fig. 2), reduces the whirl-frequency ratio further to 0.33. The whirl-frequency ratio for the pressure-dam bearing without the relief track increases to 0.45. They also predicted that the *WFR* for the pressure-dam bearing decreases as the Sommerfeld number increases. Nicholas and Allaire also found that pressure-dam bearings with $k' = 3 \sim 6$ and $\theta_s = 125^\circ \sim 160^\circ$ have the optimum stability depending on Sommerfeld and Reynolds numbers. They also found that the step is more effective at Sommerfeld number *S*>2.

Nicholas et al. [13] compared the theoretical threshold speed of instability for a two-axial-groove bearing, off-optimum pressure-dam bearing and near-optimum pressure-dam bearing supporting a flexible rotor to experimental results. The design parameters of the bearings are given in table 1. The theoretical solution predicted threshold speeds of instability at 4,900 rpm, 5,500 rpm and 8,600 rpm for the axial-groove bearing, the off- optimum pressure-dam bearing, and the near-optimum pressure-dam bearing, respectively. The experimental results show threshold speeds at 5,750 rpm, 5,600 rpm and 8,400 rpm, indicating good agreement with the theoretical solution. The experimental whirl-frequency ratio decreases from about 0.5 for the two-axial-groove bearing to about 0.35 for the near-optimum pressure-dam bearing for Sommerfeld number *S*>1.5.

Table 1. Bearing design parameters from [13]

Two-axial-groove bearing	Off-optimum pressure-dam	Near-optimum pressure-dam
$L / D = 1$ $C_r = 0.0559$ mm $C_r = 0.0660$ mm	$L / D = 1, \bar{L}_d = 0.5$ $C_r = 0.0610$ mm $C_r = 0.0737$ mm $\theta_s = 135^\circ, k' = 10.3, k' = 7$	$L / D = 1, \bar{L}_d = 0.75$ $C_r = 0.0635$ mm $C_r = 0.0737$ mm $\theta_s = 135^\circ, k' = 2.4, k' = 1.86$

Leader et al. [14] tested a rotor supported on two-axially-grooved bearings, two sets of pressure-dam bearings, and five-pad tilting-pad bearings for imbalance response and stability. The bearings specifications are given in table 2. The results show that the near- optimum pressure-dam bearing whirl-frequency ratio is 0.36, both the axial-groove bearing and the off-optimum pressure-dam bearing have 0.5 whirl-frequency ratio, and the tilting pad bearing has zero whirl-frequency ratio indicating permanent stability. However, the results show that the tilting pad bearing has the highest vibration response at the rotor critical speed, while the pressure-dam bearing and the axial-groove bearing have almost equal response.

Table 2. Bearings specifications from [14]

Axial-groove bearing	Off-optimum pressure-dam bearing	Near-optimum pressure-dam bearing	Tilting pad bearing (load on pad)
$L / D = 1$ $C_r = 0.0559$ mm $C_r = 0.0660$ mm	$L / D = 1, \bar{L}_d = 0.5$ $k' = 9$ $\theta_s = 135^\circ$	$L / D = 1, \bar{L}_d = 0.75$ $k' = 2.1$ $\theta_s = 135^\circ$	$L / D = 1$ $C_r = 0.0508$ mm $preload = 0$ $\chi = 64^\circ$ $offset = 50\%$

Lanes et al. [15] compared the threshold speed of instability for a flexible rotor supported by axial-groove bearings, near-optimum pressure-dam bearings, and preloaded three- lobe bearings. The rotor first critical speed is 2,550 rpm. The results showed that the three lobe bearing has the highest threshold speed of instability (10,400 rpm compared to 7,400 for the pressure-dam bearing and 6,550 rpm for the axial-groove bearing). Therefore, the whirl-frequency ratios are 0.24, 0.34 and 0.39 for the three-lobe bearing, the pressure-dam bearing and the axial-groove bearing respectively.

Mehta and Singh [16] studied theoretically the effect of incorporating a near-optimum pressure-dam (k' =2, θ_s = 125°, $\bar{L}_d$ = 0.75, $\bar{L}_t$=0.25) on cylindrical bearings, elliptical bearings, as well as offset halves cylindrical bearings $(L/D=1)$. The results show that cylindrical pressure-dam bearings whirl-frequency ratio is 0.29. The elliptical pressure-dam bearing $(\delta_v = 0.4)$ whirl-frequency ratio is 0.15 and the offset halves pressure-dam bearing $(\delta_h = 0.4)$ whirl-frequency ratio is 0.11.

Flack et al. [17] measured pressure drop across the dam. They reported that the highest pressure was measured at the step for bearings optimized with $k' = 2 \sim 3$ and $\theta_s = 140^\circ \sim 145^\circ$. However, the measured pressure drop was 25% compared to only 2% as predicted theoretically. He et al. [18] incorporated the effect of the temperature rise on pressure-dam bearing dynamic coefficients and threshold speed of instability. The maximum pressure of the top pad is located at the step. The temperature distribution in the bottom pad shows that the temperature increases smoothly from the leading edge to the trailing edge and is almost constant in the axial direction. For the top pad, the temperature increases smoothly in the small clearance region as oil travels from the leading edge to the trailing edge. However, the temperature is almost constant in the pocket due to the low shear stress. The analysis also showed that the journal eccentricity increases slightly compared to the isoviscous analysis. The analysis also predicts lower stiffness and damping coefficients that may alter the threshold speed of instability compared to the isothermal analysis.

The whirl-frequency ratio of axial-groove bearings and pressure-dam bearings described above from references [13, 14, and 15] was determined by measuring the rotor maximum speed before high sub-synchronous vibration is noticed. However, this method does not provide any information about the bearing stiffness, damping and inertia force coefficients that are vital for complete rotor dynamic analysis. Miller [19] developed a test rig to identify the rotor dynamic force coefficients of a plain journal bearing. The bearing force coefficients were determined by exciting the bearing housing twice using two impact guns at frequencies from 5-60 Hz and then transforming the bearing measured response data to frequency domain. Although the identified force coefficients follow the same trends as theoretical prediction, they compare poorly. De Santiago [20] discussed different available procedures to experimentally determine the force coefficients of fluid film bearings such as using impact load and imbalance response. Kostrzewsky et al. [21] used a test rig to identify the force coefficients of a two-axial-groove bearing. The test rig utilizes two electrodynamic shakers to generate synchronous sinusoidal excitations. The force coefficients were determined using the average magnitude and phase method. The measured force coefficients compared well with theoretical values.

TEST RIG DESCRIPTION

Overview

Fig. 4 shows the test rig for measurement of the static and dynamic performance of the bearing. Kaul [22] presents a de tailed account of the design and features of the test rig and facility at the Texas A&M Turbomachinery Laboratory. A summary of its main features follows.

The rig consists of a steel base that supports the main test section and the air turbine that drives the shaft. The shaft is connected to a 65 kW air turbine with a high-speed flexible disc coupling and can run up to a maximum speed of 16,000 rpm. The test shaft is made from stainless steel and machined to a precise diameter of 116.8 mm (4.6000 in) at the test section. It is supported on the pedestals through angular contact ball bearings, spaced approximately 457 mm (18 in) apart. An oil-mist lubrication system lubricates the ball bearings.

A stator section holds the test bearing and all the associated instrumentation, namely, non-contacting eddy-current proximity sensors, accelerometers, pressure transducers and thermocouples. A pneumatic loader and two hydraulic shakers apply static and dynamic loads to the bearing stator. Angular alignment between the bearing and the shaft is provided by an arrangement of six pitch stabilizers.

ISO VG32 turbine oil is delivered to the test section from an oil supply system. The oil supply system can deliver oil up to a maximum pressure of 82.7 bars and a volumetric flow of 75 liters per minute. A heat exchanger and a set of pneumatically driven valves allow for control of the oil temperature being delivered to the test section.

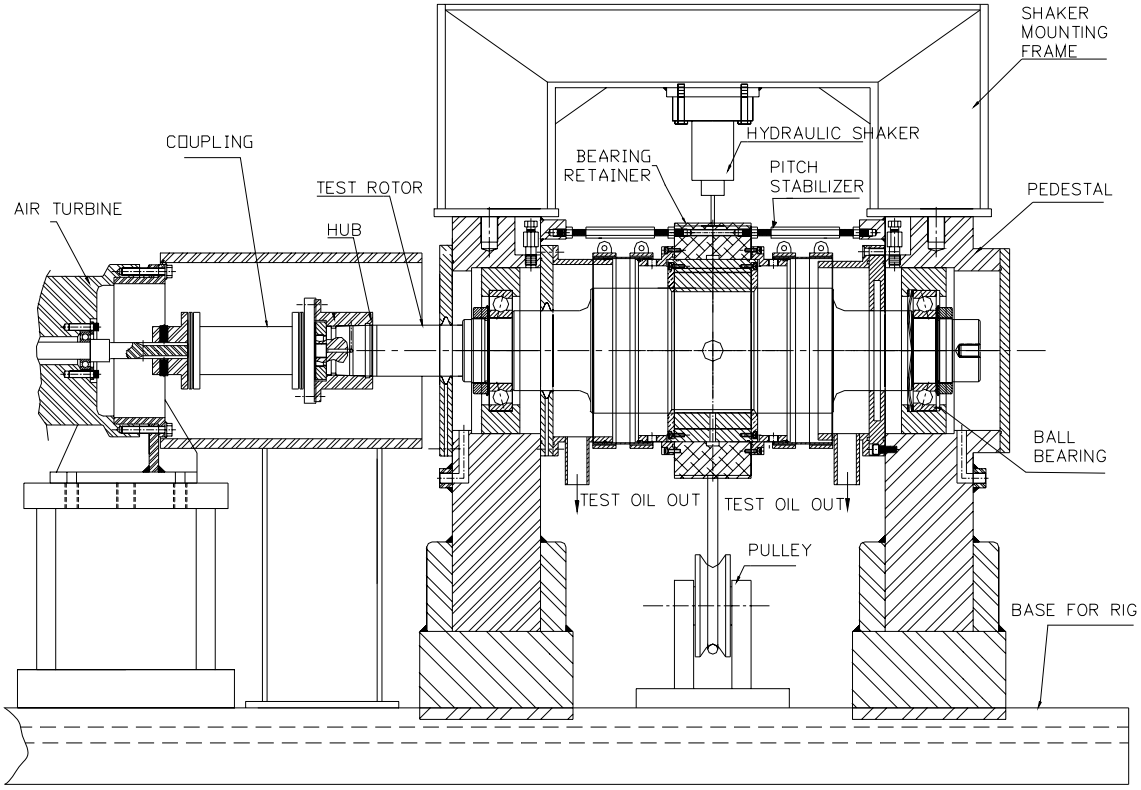

Fig. 4 Test rig main section

Loading Configuration

Two orthogonally mounted hydraulic shaker heads are attached to the stator middle section. The stator-shaker-stinger arrangement is shown in Fig. 5, as observed from the non-drive end. The shaker in the *x*-direction can excite the stator with dynamic loads up to 4,450 N in tension and compression. The shaker in the *y*-direction can excite the stator with dynamic loads up to 4,450 N in tension and 11,125 N in compression. Both shakers can provide excitation frequencies up to 1,000 Hz.

The shaker heads are attached to the stators through bar elements called stingers. Stingers isolate the test structure from the dynamics of the shakers structure. The load applied to the stator is measured with load cells bolted to the stingers on one end and the shaker head on the other end.

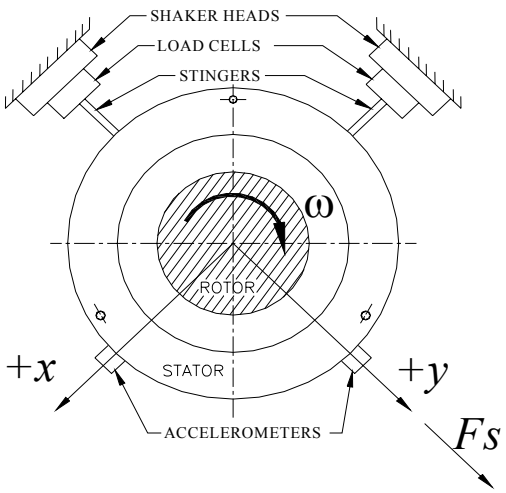

Fig. 5 Shaker-stinger arrangement

While the shakers provide dynamic loads exclusively, the pneumatic loader applies a static tensile load to the stator in one direction (see Fig. 5). The stator is displaced in the $+y$ direction due to the static load. A cable is connected to the stator assembly through a pulley and a yoke, and a spring system assures that the load is applied exclusively in one direction. The applied load is measured with a load cell attached to the cable. The rated maximum available load is 22,000 N. Fig. 6 shows a side view of the test rig with the static loader.

Instrumentation

Four proximity probes, located in the stator end caps, record the relative motion of the rotor with respect to the stator for each direction of excitation. Two proximity probes are placed in a plane at the non-drive end and two at a parallel plane at the drive end. Measurement of the stator position in two parallel planes allows monitoring of the stator's pitch and yaw.

Piezoelectric accelerometers measure the stator absolute acceleration in both the x and y directions. Temperature probes are located in the oil-inlet chamber as well as the

downstream end caps. Two thermocouples are also installed in each pad to measure the pads temperature in the circumferential direction. For the unloaded pad, the thermocouples are installed at the leading edge and at the step location. For the loaded pad, the thermocouples are installed at the middle of the pad and close to the trailing edge. A static pressure probe measures the oil pressure at the inlet and outlet locations.

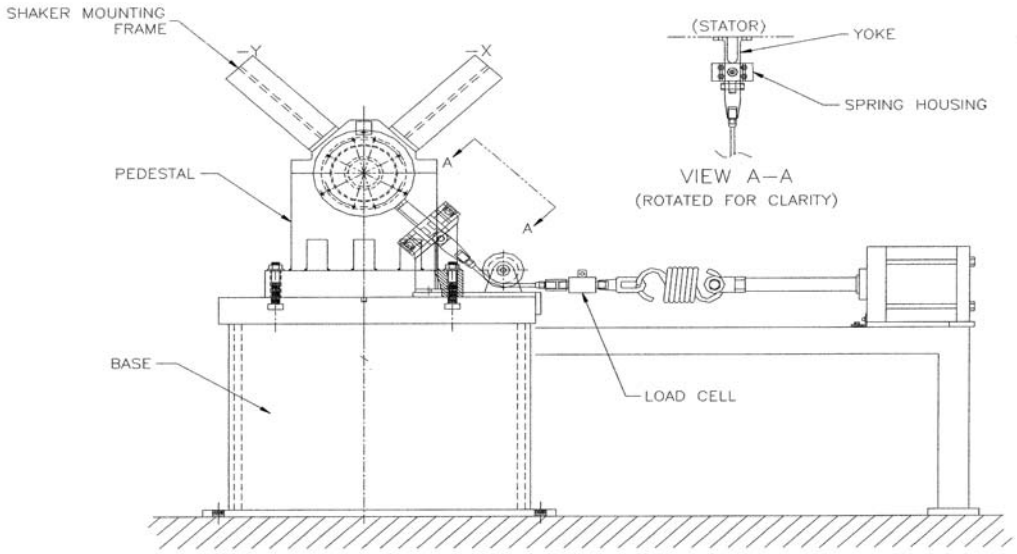

Fig. 6 Test rig side view [5]

Test Bearings

The two-axial-groove bearing was tested first. The bearing was then modified to a pressure-dam bearing and tested. Fig. 7 shows the two-axial-groove bearing as assembled in the stator. Fig. 8 shows the axial-groove bearing with a step at the top unloaded pad (All dimensions are in mm). Table 3 summarizes the bearings' important design parameters.

Table 3. Bearings design parameters

	Axial-groove bearing	Pressure-dam bearing
L	76.2 mm (3")	76.2 mm (3")
C_r	0.133±0.0063 mm(5.25±0.250 mils)	0.133±0.0063 mm (5.25±0.250 mils)
θ_s	0°	130°
k'	0	3.4~4.2
D	0.1171±0.01270 m (4.6105±0.00050")	0.1171±0.01270 m (4.6105±0.00050")
$\bar{L}_d$	0	0.75
$\bar{L}_t$	0	0

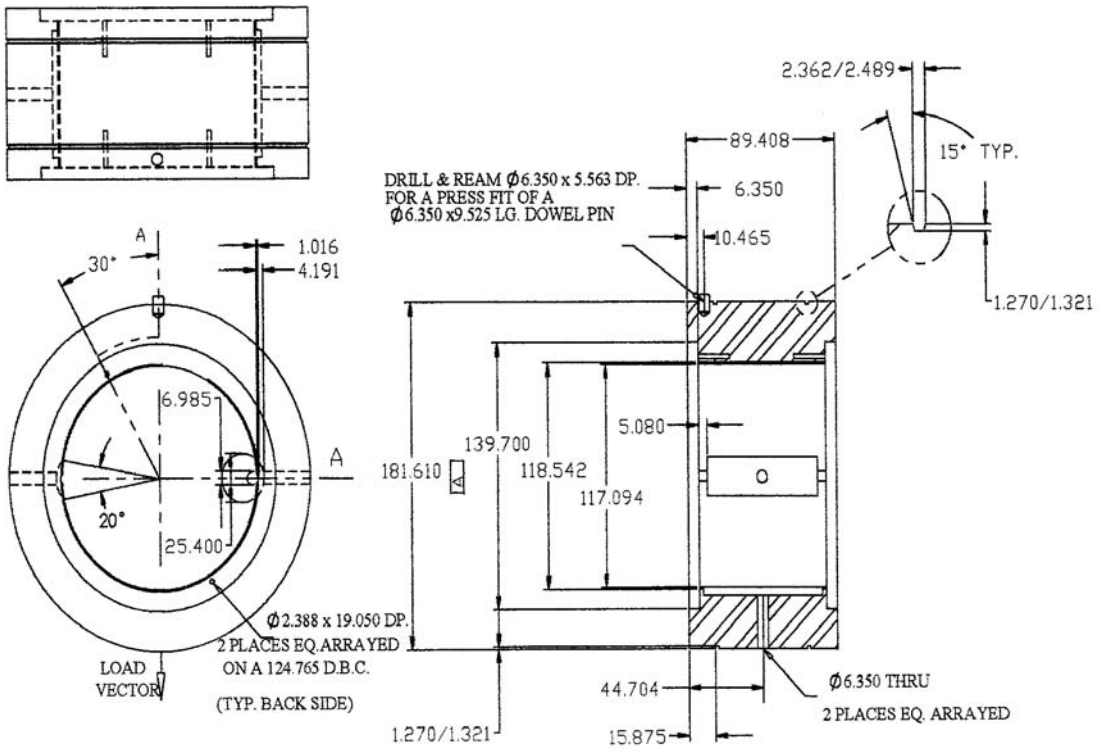

Fig. 7 The two-axial-groove test bearing

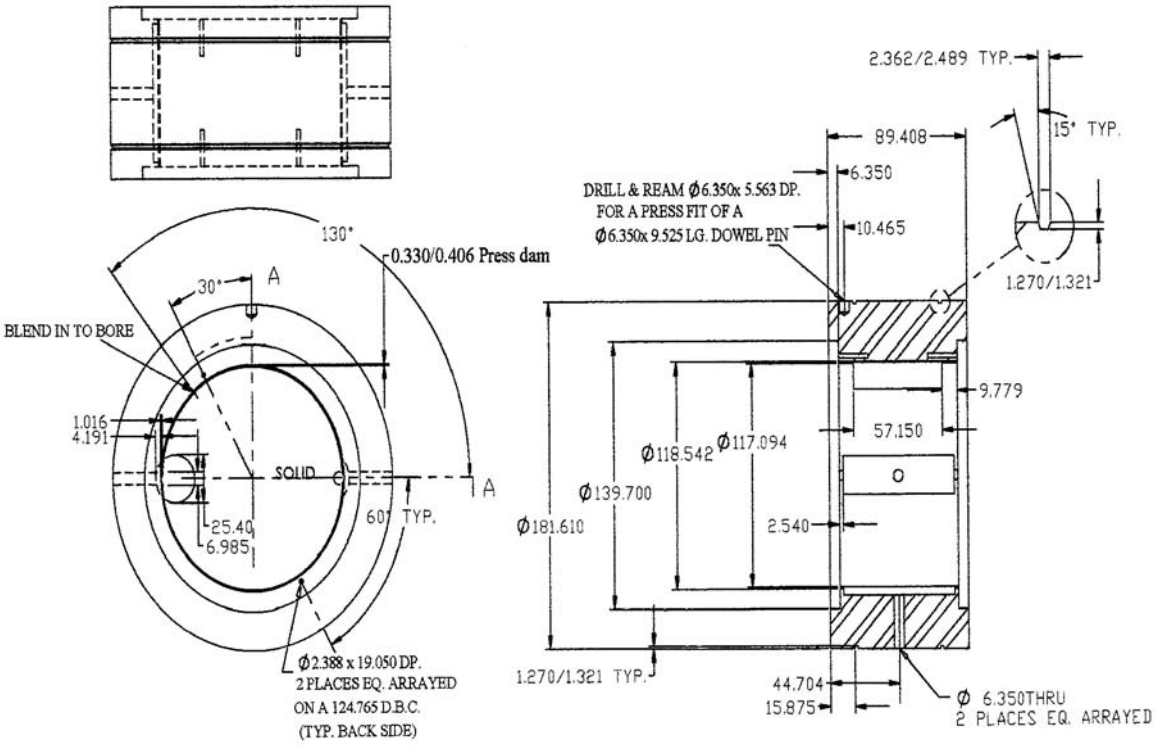

Fig. 8 Test bearing with pressure-dam at the unloaded pad

EXPERIMENTAL PROCEDURE

This section describes how the bearing static test and dynamic test are executed:

Static Test Procedure

During a typical test, the bearing stator is centered on the shaft by performing a bump test using the shakers. Once the bearing is centered ($e_x = e_y = 0$), the rotor is run at a low speed, usually 4000 rpm. Then, the bearing is loaded using the static loader to the required load. Once the rotor reaches the required steady state, the following data are taken:

1) Stator *x* and *y* position in both driven end and non-driven end planes (e_x, e_y).
2) Rotor speed, ω.
3) Oil volumetric flow rate, Q.
4) Static load applied by the static loader, W.
5) Oil inlet temperature, T_i.
6) Oil exit temperature, T_e.
7) Bearing pad temperatures.

The above procedure is repeated by increasing the bearing load, keeping the rotor speed constant until the bearing eccentricity ratio $\varepsilon_0 = 0.90$. Then, the test is repeated again at a higher speed. The test stops once the maximum allowable speed for the test rig is reached (16,000 rpm), or excessive vibration or temperature are encountered. Then, at each test condition, the bearing static characteristics which include Sommerfeld number S, eccentricity ratio ε_0, attitude angle ψ, and power loss E are calculated using the following set of equations:

$$S = \frac{\mu NLD}{W}\left(\frac{R^2}{C_r^2}\right) \tag{16}$$

$$\varepsilon_0 = \frac{e}{C_r} = \frac{\sqrt{(e_x^2 + e_y^2}}{C_r} \tag{17}$$

$$\psi = tan^{-1}(\frac{e_x}{e_y}) \tag{18}$$

$$E = Q(\rho_e C_{pe} T_e - \rho_i C_{pi} T_i) \tag{19}$$

The oil viscosity, density, and specific heat are related to temperature using the following equations:

$$\mu = 0.0453 e^{-0.03007(T-294)} \quad (N.s/m^2) \tag{20}$$

$$C_p = 3.627T + 811.75 \quad (J/kg.K) \tag{21}$$

$$\rho = -0.6616T + 1064 \quad (kg/m^3) \tag{22}$$

An effective viscosity is calculated at the average of the oil inlet and exit temperatures to calculate Sommerfeld number using equation (16).

Dynamic Test Procedure

First, the rotor is brought up to the steady state conditions of rotational speed and oil inlet temperature, for a given static load. Then, the bearing stator is alternately excited using the hydraulic shakers with a pre-specified pseudo-random dynamic excitation waveform with frequencies from 20 Hz to 300 Hz in 10 Hz increment in two orthogonal directions, i.e. *x*-direction and the *y*-direction (static load direction). Each single test consists of 32 shakes that are averaged in the frequency domain. The following data are collected for each test condition:

1) Excitation forces in both *x* and y directions (f_x, f_y).
2) Stator acceleration in both *x* and *y* directions $(\ddot{x}, \ddot{y})$.
3) Stator displacement in both *x* and *y* directions (*x*,*y*) .

The test is repeated at different load conditions keeping the rotor speed constant until the bearing eccentricity ratio $\varepsilon_0 = 0.80$. The dynamic test is stopped at lower eccentricities than the static test to make sure that the bearing will not rub against the

rotor when shacked. Then, the rotor speed is increased to a higher speed, and the same procedure is executed again. The test stops once the maximum allowable speed for the test rig is reached (16,000 rpm), or excessive vibration or temperature are encountered.

The bearing force coefficients are then calculated for each test condition using the parameter identification procedure described by Childs and Hale [23]. The equations of motion for the stator mass M_s can be written as:

$$M_s \begin{bmatrix} \ddot{x}_s \\ \ddot{y}_s \end{bmatrix} = \begin{bmatrix} f_x \\ f_y \end{bmatrix} - \begin{bmatrix} f_{bx} \\ f_{by} \end{bmatrix} \tag{23}$$

Here, $\ddot{x}_s$, $\ddot{y}_s$ are the measured components of the stator's acceleration, f_x , f_y are the measured excitation force, f_{bx} , f_{by} are the bearing reaction force components. The reaction force of a hydrodynamic journal bearing is written in terms of the bearing force coefficients:

$$-\begin{bmatrix} f_{bx} \\ f_{by} \end{bmatrix} = \begin{bmatrix} K_{xx} & K_{xy} \\ K_{yx} & K_{yy} \end{bmatrix} \begin{bmatrix} \Delta x \\ \Delta y \end{bmatrix} + \begin{bmatrix} C_{xx} & C_{xy} \\ C_{yx} & C_{yy} \end{bmatrix} \begin{bmatrix} \Delta \dot{x} \\ \Delta \dot{y} \end{bmatrix} + \begin{bmatrix} M_{xx} & M_{xy} \\ M_{yx} & M_{yy} \end{bmatrix} \begin{bmatrix} \Delta \ddot{x} \\ \Delta \ddot{y} \end{bmatrix} \tag{24}$$

Here, $\Delta x, \Delta y$ are defined as the relative motion between the rotor and the stator and K_{ij}, C_{ij}, M_{ij} are matrix elements referring to stiffness, damping and added-mass coefficients, respectively. Substituting equation (24) in equation (23) and rearranging, we obtain:

$$\begin{bmatrix} f_x - M_s \ddot{x}_s \\ f_y - M_s \ddot{y}_s \end{bmatrix} = -\begin{bmatrix} K_{xx} & K_{xy} \\ K_{yx} & K_{yy} \end{bmatrix} \begin{bmatrix} \Delta x \\ \Delta y \end{bmatrix} - \begin{bmatrix} C_{xx} & C_{xy} \\ C_{yx} & C_{yy} \end{bmatrix} \begin{bmatrix} \Delta \dot{x} \\ \Delta \dot{y} \end{bmatrix} - \begin{bmatrix} M_{xx} & M_{xy} \\ M_{yx} & M_{yy} \end{bmatrix} \begin{bmatrix} \Delta \ddot{x} \\ \Delta \ddot{y} \end{bmatrix} \tag{25}$$

The left hand vector of equation (25) is a known function of time. On the right hand side, $\Delta x(t)$ and $\Delta y(t)$ are measured functions of time. The rotordynamic coefficients are determined in the frequency domain via the Fast Fourier Transform version of equation (25) as shown below:

$$\begin{bmatrix} \boldsymbol{F}_x - M_s \boldsymbol{A}_x \\ \boldsymbol{F}_y - M_s \boldsymbol{A}_y \end{bmatrix} = - \begin{bmatrix} \boldsymbol{H}_{xx} & \boldsymbol{H}_{xy} \\ \boldsymbol{H}_{yx} & \boldsymbol{H}_{yy} \end{bmatrix} \begin{bmatrix} \boldsymbol{D}_x \\ \boldsymbol{D}_y \end{bmatrix} \tag{26}$$

The elements of the bearing dynamic stiffness function $\boldsymbol{H}$ are related to the coefficients defined in equation (24) by:

$$\boldsymbol{H}_{ij} = K_{ij} - \Omega^2 M_{ij} + \boldsymbol{j}(\Omega C_{ij}) \tag{27}$$

Equation (26) provides only two equations for four unknowns $\boldsymbol{H}_{xx}$, $\boldsymbol{H}_{xy}$, $\boldsymbol{H}_{yx}$, $\boldsymbol{H}_{yy}$. To provide four independent equations, alternate shakes about a given steady-state rotor position are conducted on the stator in orthogonal directions (x and y) yielding four equations and four unknowns, given by:

$$\begin{bmatrix} \boldsymbol{F}_{xx} - M_s \boldsymbol{A}_{xx} & \boldsymbol{F}_{xy} - M_s \boldsymbol{A}_{xy} \\ \boldsymbol{F}_{yx} - M_s \boldsymbol{A}_{yx} & \boldsymbol{F}_{yy} - M_s \boldsymbol{A}_{yy} \end{bmatrix} = - \begin{bmatrix} \boldsymbol{H}_{xx} & \boldsymbol{H}_{xy} \\ \boldsymbol{H}_{yx} & \boldsymbol{H}_{yy} \end{bmatrix} \begin{bmatrix} \boldsymbol{D}_{xx} & \boldsymbol{D}_{xy} \\ \boldsymbol{D}_{yx} & \boldsymbol{D}_{yy} \end{bmatrix} \tag{28}$$

One set of frequency-dependent dynamic stiffness coefficients ($\boldsymbol{H}_{xx}$, $\boldsymbol{H}_{xy}$, $\boldsymbol{H}_{yx}$, $\boldsymbol{H}_{yy}$) is obtained as the average of 32 separate shake tests, which are averaged in the frequency domain. For each experimental condition, ten consecutive tests are conducted to estimate the variability of the dynamic stiffness in the frequency range of 20-300 Hz. Note that data at frequencies multiple of 60 Hz, rotor running speed, and above 240 Hz have high uncertainty. Therefore, they are not included in the linear regression analysis.

Equation (27) shows that the real part of the dynamic stiffness is a quadratic function of the excitation frequency, whereas the imaginary part is a linear function. However, setting $\Lambda = \Omega^2$ transforms the quadratic into a linear relationship, thus a linear regression can be performed for both the real and the imaginary parts.

The intercept and the slope of the regression line of the real part provide estimates for the bearing stiffness K_{ij} and opposite sign of the added-mass M_{ij} coefficients, respectively. Similarly, the estimates for the damping coefficients C_{ij} are obtained from the slope of the linear regression of the imaginary part of the dynamic stiffness.

Confidence intervals are used to provide the uncertainty of the estimated rotordynamic coefficients. A confidence interval is a statistical measure of the error

bound for the estimate of the slope or the intercept, to assess the overall quality of the regression line and the accuracy of the estimates.

The formulas to compute the slope, the intercept and their associated uncertainties are obtained from Rodriguez [24]. Here, the letters x and y refer to a pair of data (x_i,y_j) for the linear regression and N refers to the number of data pairs.

Number of data pairs, (x_i,y_i): N

Regression line equation: $\hat{y} = \beta_0 + \beta_1 x$; $\hat{y}$ denotes the predicted value. (29)

Mean of the x's: $$\bar{x} = \frac{1}{N}\sum_{i=1}^{N} x_i \quad (30)$$

Mean of the y's: $$\bar{y} = \frac{1}{N}\sum_{i=1}^{N} y_i \quad (31)$$

Slope: $$\beta_1 = \frac{\sum_{i=1}^{N} y_i x_i - N\left(\bar{y}\right)\left(\bar{x}\right)}{\sum_{i=1}^{N} x_i^2 - N\left(\bar{x}\right)^2} \quad (32)$$

Intercept: $$\beta_0 = \bar{y} - \beta_1 \bar{x} \quad (33)$$

Mean Square Error, s^2: $$\frac{\sum_{i=1}^{N}\left(y_i - \hat{y}_i\right)^2}{N-2} \quad (34)$$

S_{xx}: $$\sum_{i=1}^{N} x_i^2 - N\,\bar{x}^2 \quad (35)$$

Uncertainty of the slope, $\Delta\beta_1$: $$t \times \sqrt{\frac{s^2}{S_{xx}}} \quad (36)$$

Uncertainty of the intercept, $\Delta\beta_0$: $$t \times \sqrt{s^2\left(\frac{1}{N} + \frac{\bar{x}^2}{S_{xx}}\right)} \quad (37)$$

The uncertainty in equation (37) includes a parameter denoted as t. In general, this is a multiplicative factor that depends on the desired probability that the unknown "true" parameter is contained in the interval $\beta_0 \pm \Delta\beta_0$ (or, $\beta_1 \pm \Delta\beta_1$). Since a high

confidence is desirable, the confidence parameter (t) is set to 1.960 which yields a 95% confidence level [5].

AXIAL-GROOVE BEARING TEST RESULTS

Static Test Results

Static (or steady-state) performance data presented in this section includes bearing eccentricity ratio ε_0, attitude angle ψ and estimated power losses E. Both experimental eccentricity ratio and attitude angle values will be compared to theoretical values as obtained from Someya et al. [25]. The bearing measured cold radial clearance was 0.136 mm (5.37 mils). The oil flow rate was maintained at 32 liters/min (8.5 GPM) for all test conditions which is equal to the design flow rate at 16,000 rpm. Oil was supplied at higher flow rate than design to minimize the increase in the oil temperature thus, obtaining a semi-isothermal process. The oil inlet temperate varied within 37.8 °C-48.8 °C (100 °F-120 °F) while the supply pressure was fixed at around 172 kPa (25 psi). Oil outlet temperature are listed in table 10 in Appendix A. Table 4 summarizes the test conditions for the two-axial-groove journal bearing in terms of rotor speed and static load. The letter "S" refers to static test while the letter "D" refers to dynamic test. The bearing unit load is determined using the following equation:

$$p = \frac{W}{LD} \tag{38}$$

Table 4. Text matrix for axial-groove bearing

P kPa (psi) RPM	0 (0)	172 (25)	345 (50)	517 (75)	690 (100)	862 (125)	1034 (150)	1207 (175)	1379 (200)	1655 (240)
4000	S,D	S	S,D	S	S,D	S	S,D	S		
6000	S,D	S	S,D	S	S,D	S	S,D	S	S,D	S
8000	S,D	S	S,D	S	S,D	S	S,D	S	S,D	S
10000	S,D	S	S,D	S	S,D	S	S,D	S	S,D	S

For 4000 rpm rotor speed, the maximum unit load is 1034 kPa (150 psi) because the bearing eccentricity reached the maximum allowable ratio $\varepsilon_0 = 0.80$. Also, table 4 shows that the test stopped at 10,000 rpm rotor speed because of the appearance of high subsynchronous vibration at 12,000 rpm (200 Hz) rotor speed as shown in Fig. 9.

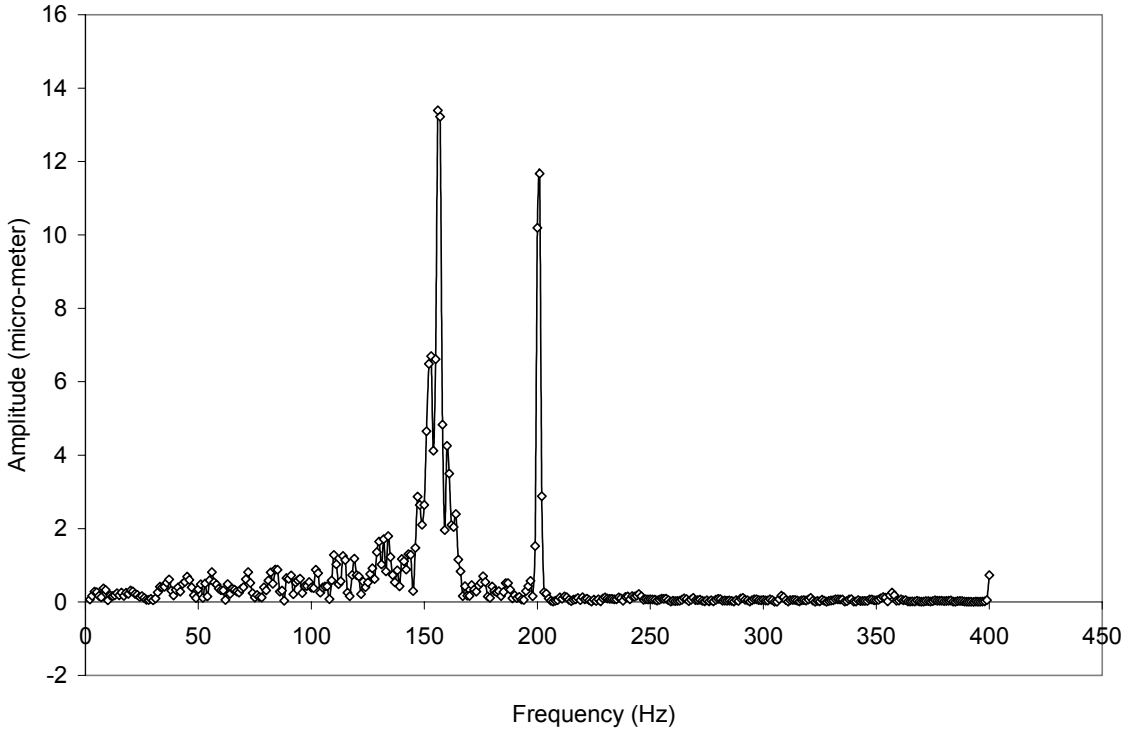

Fig. 9 Rotor frequency spectrum at 12,000 rpm rotor speed with axial groove bearing

Eccentricity

Fig. 10 shows the bearing eccentricity ratio ε_0 for 4000 rpm, 6000 rpm, 8000 rpm, and 10,000 rpm rotor speed versus unit load applied. The figure shows that as the load is increased at a fixed speed, the bearing eccentricity increases. However, for a fixed load, the bearing eccentricity decreases as the rotor speed increases. The bearing

maximum load is 1034 kPa (150 psi) at 4000 rpm and 1379 kPa (200 psi) at 6000 rpm, 8000 rpm and 10,000 rpm. The figure also shows that eccentricity is not linearly proportional to either applied load or rotor speed.

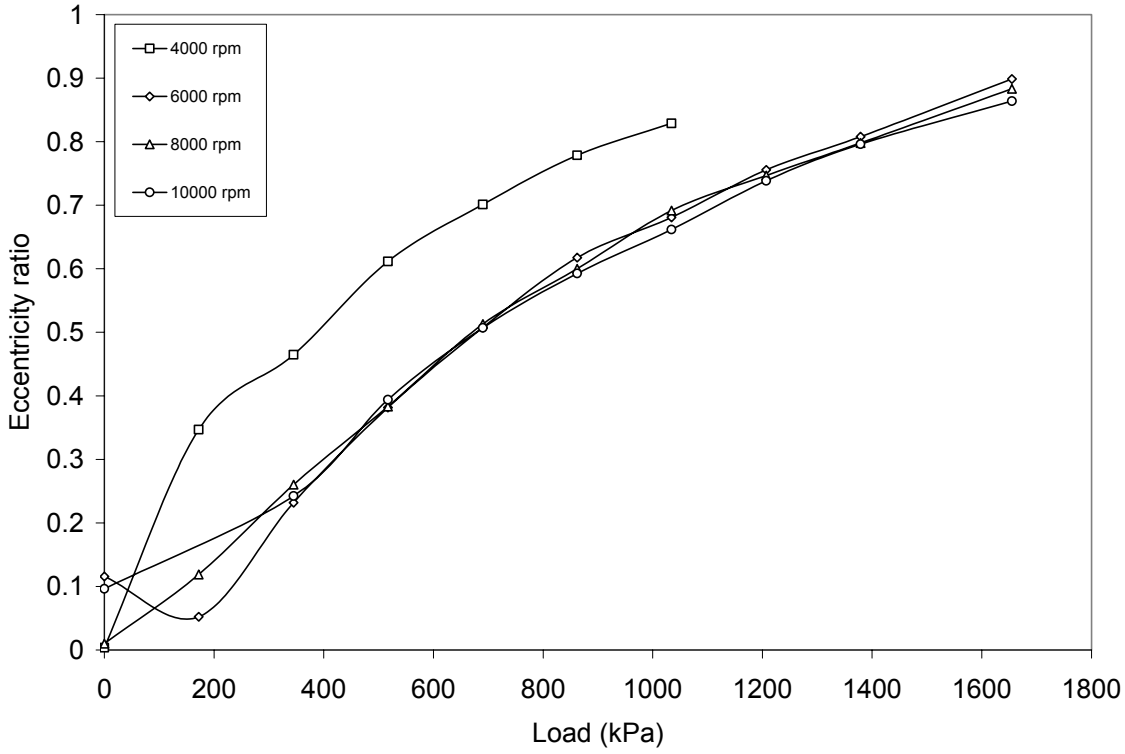

Fig. 10 Axial groove bearing eccentricity ratio vs. unit load

The effect of both applied load and rotor speed on the bearing eccentricity is presented on the dimensionless Sommerfeld number given in equation (16) above. The equation shows that as applied load increases, Sommerfeld number decreases. Also, as rotor speed increases, Sommerfeld number increases. This means that the effect of load and speed on Sommerfeld number is directly opposite to the effect of load and speed on bearing eccentricity. Fig. 11 shows the relationship between eccentricity ratio and Sommerfeld number. As Sommerfeld number increases (high speed, low load), bearing

eccentricity decreases. The numerical results plotted in Fig. 11 shows that any two bearings with the same Sommerfeld number operates at the same eccentricity ratio even if rotor speed or applied load are different. The experimental results show this especially at low Sommerfeld number. Neglecting the data for S>1, the largest deviation between the experimental eccentricity ratios for a fixed Sommerfeld number is 0.10. A possible reason for this deviation is an increase in the bearing clearance due to thermal growth. Fig. 11 also shows that the bearing has operated at higher eccentricity ratio than predicted. This indicates that the bearing has lower direct stiffness K_{yy} than predicted. This result will also be shown in the dynamic test. The higher eccentricity ratio could be related to the reduction in the direct stiffness K_{yy} as a result of an increase in the bearing clearance due to thermal growth. Moreover, since the numerical solution assumes an isothermal process[1], it neglects the reduction in oil viscosity due to oil film temperature rise. Therefore, it predicts lower eccentricity ratios.

[1] Static and dynamic performance from Someya [25] is calculated at the average of the inlet and exit oil temperatures.

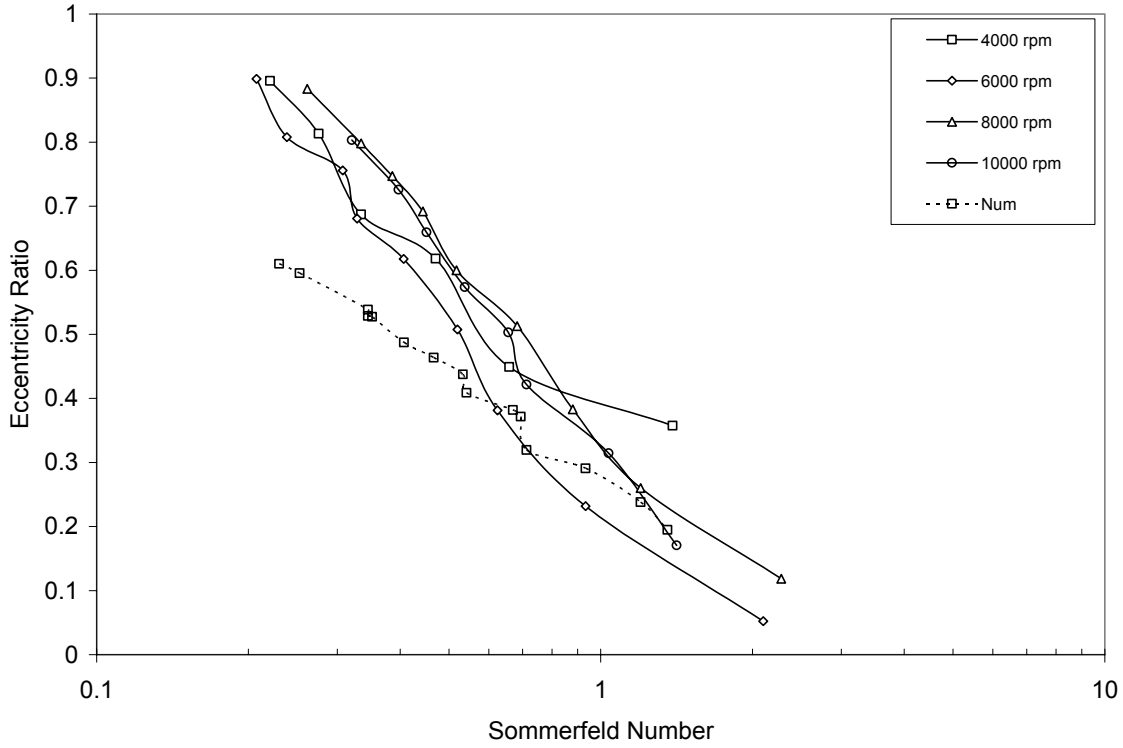

Fig. 11 Axial groove bearing eccentricity ratio vs. Sommerfeld number

Attitude Angle

The bearing attitude angle ψ represents the bearing displacement in *x*-direction due to the load applied in the *y*-direction. Hence, attitude angle is related to the cross-coupled stiffness K_{xy}. Fig. 12 shows the bearing locus plot. The plot shows that as the applied load increases, the bearing moves in both *x* and *y* directions. The *x*-eccentricity increases as load increases until it reaches a maximum value at about 0.33 then, it decreases slightly.

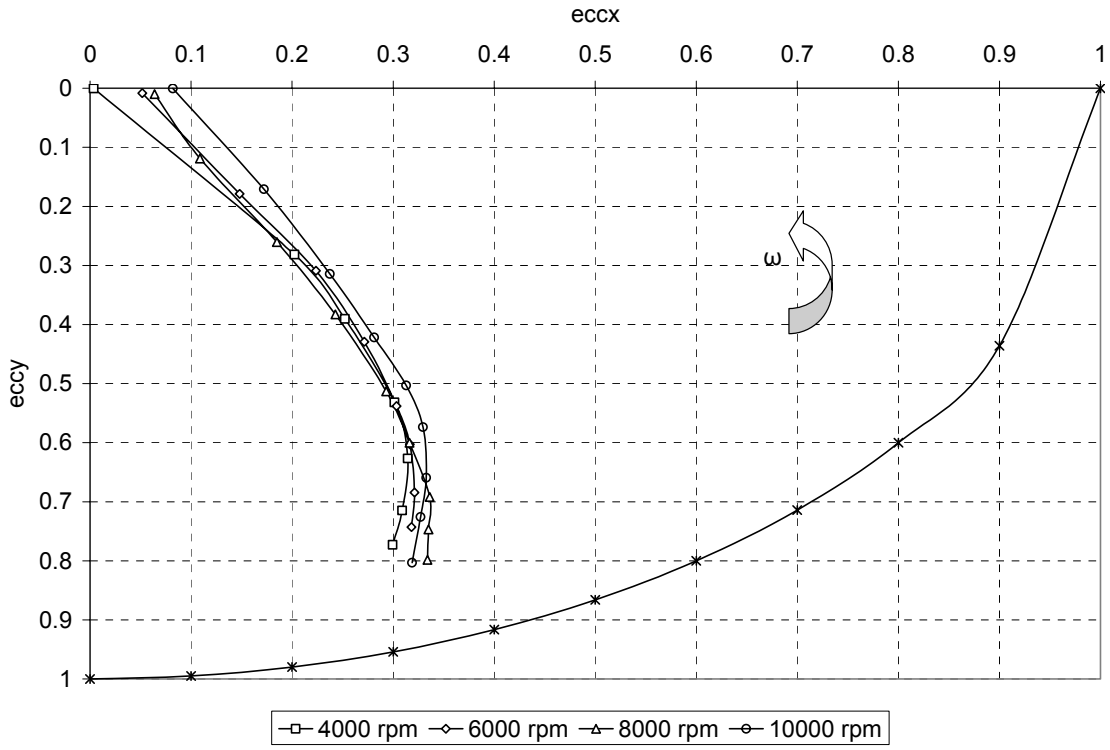

Fig. 12 Axial groove bearing locus plot

Knowing the bearing *x* and *y* displacements, the attitude angle is calculated using equation (18) and is plotted versus unit load in Fig. 13. The figure shows that for all rotor speeds as the applied load increases, the attitude angle decreases. At no-load, the bearing has the highest attitude angle. Also, for a fixed load, the attitude angle increases as the rotor speed increases. This is explained by the fact that as the rotor speed increases, the bearing reaction force in the lateral direction increases also.

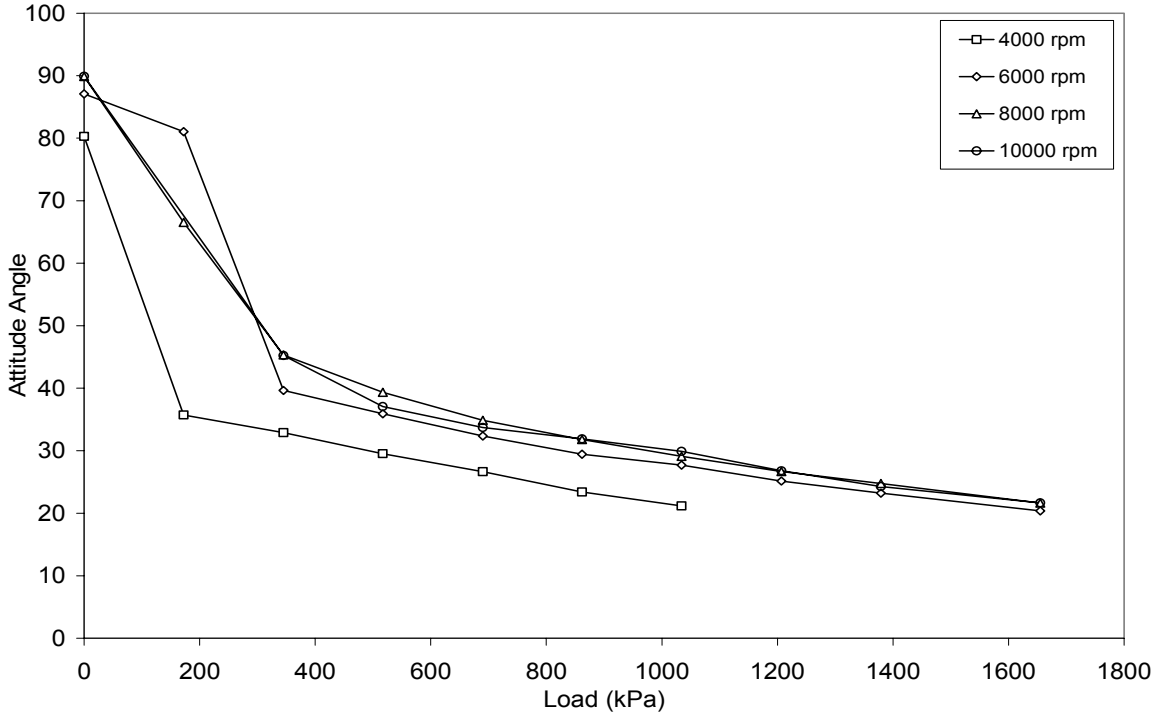

Fig. 13 Axial groove bearing attitude angle vs. unit load

Similar to eccentricity ratio, bearing attitude angle is plotted against Sommerfeld number in Fig. 14. The figure shows that the bearing attitude angle increases as Sommerfeld number increases (high speed, low load). The figure also shows the predicted attitude angles. Also, similar to eccentricity ratio, the bearing attitude angle can be determined once the Sommerfeld number is known regardless of speed and load. Neglecting the attitude angle values for S>0.8, the maximum deviation between the experimental attitude angles for a fixed Sommerfeld number is 8˚. Fig. 14 also shows that the predicted attitude angle is much larger than the experimental ones. This difference can be also partially contributed to the assumption of an isothermal process in the numerical solution. Equation 16 shows that reducing the oil viscosity while keeping all other parameters fixed results in lower Sommerfeld number, thus higher eccentricity and lower attitude angle.

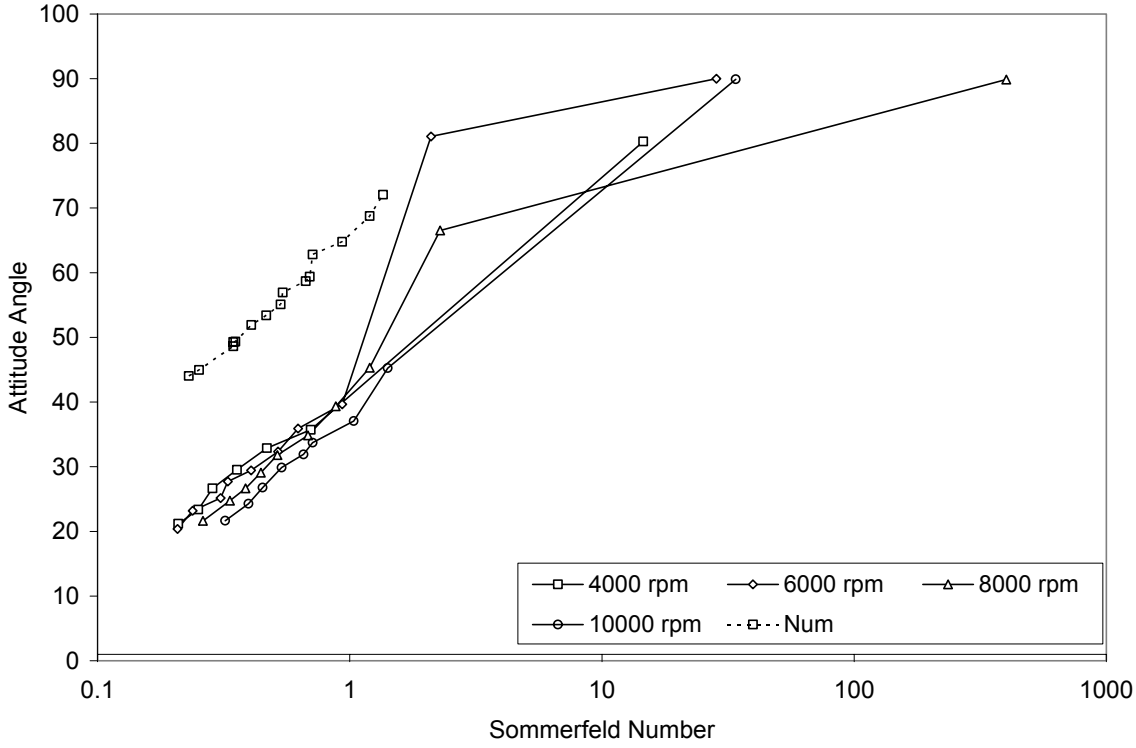

Fig. 14 Axial groove bearing attitude angle vs. Sommerfeld number

Since both eccentricity ratio and attitude angle are functions of Sommerfeld number, once one is known, the other one can be determined. Fig. 15 shows the experimental and theoretical values of eccentricity ratio versus attitude angle. As eccentricity ratio increases (high load, low speed i.e. low Sommerfeld number), attitude angle increases. Also, as eccentricity ratio decreases (high speed, low load i.e. high Sommerfeld number), attitude angle increases.

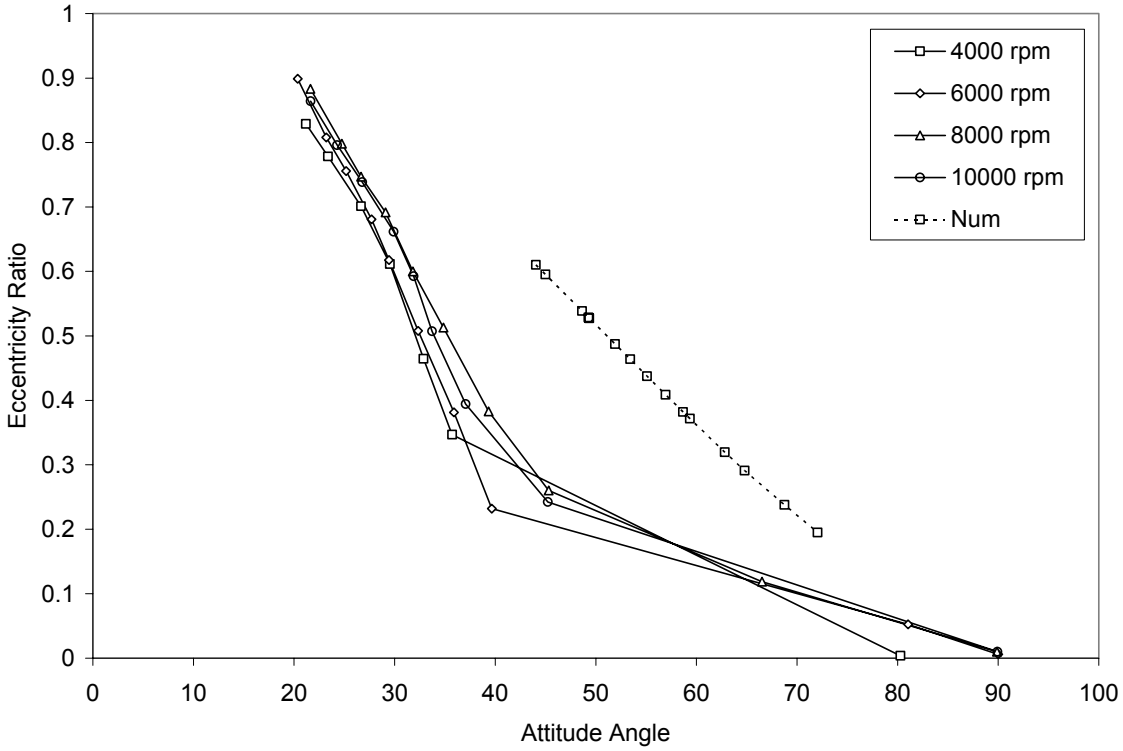

Fig. 15 Axial groove bearing eccentricity ratio versus attitude angle

Power Losses

The power loss is estimated using equations (19, 20, 21 and 22) given above. The main reason for this power loss is the shear stress between the oil film and the rotor. For a Newtonian, inertialess, and isoviscous fluid within thin film geometry, the local shear stress is given by [26]:

$$\tau = \mu \frac{U}{h} + \frac{1}{2}\frac{\partial P}{\partial x}(2y - h) \tag{39}$$

Equation (39) shows that the shear stress is composed of two terms. The first term is due to the shear driven flow (Couette flow) while the second term is due to the flow driven by the pressure gradient (Poiseuille flow). Shear stress increases by increasing the rotor speed and the pressure gradient. Shear stress due to Couette flow increases in the bearing converging region by increasing the load. However, it decreases

in the diverging region. Also, since power loss is proportional to both speed and shear stress, power loss is proportional to the square of speed. Therefore, increasing the speed has more effect on the power loss than increasing the load. Figs. 16 and 17 show the estimated power loss versus bearing unit load and rotor speed respectively. Numerical analysis does not solve the energy equation for the bearing. Therefore, power losses are not numerically estimated.

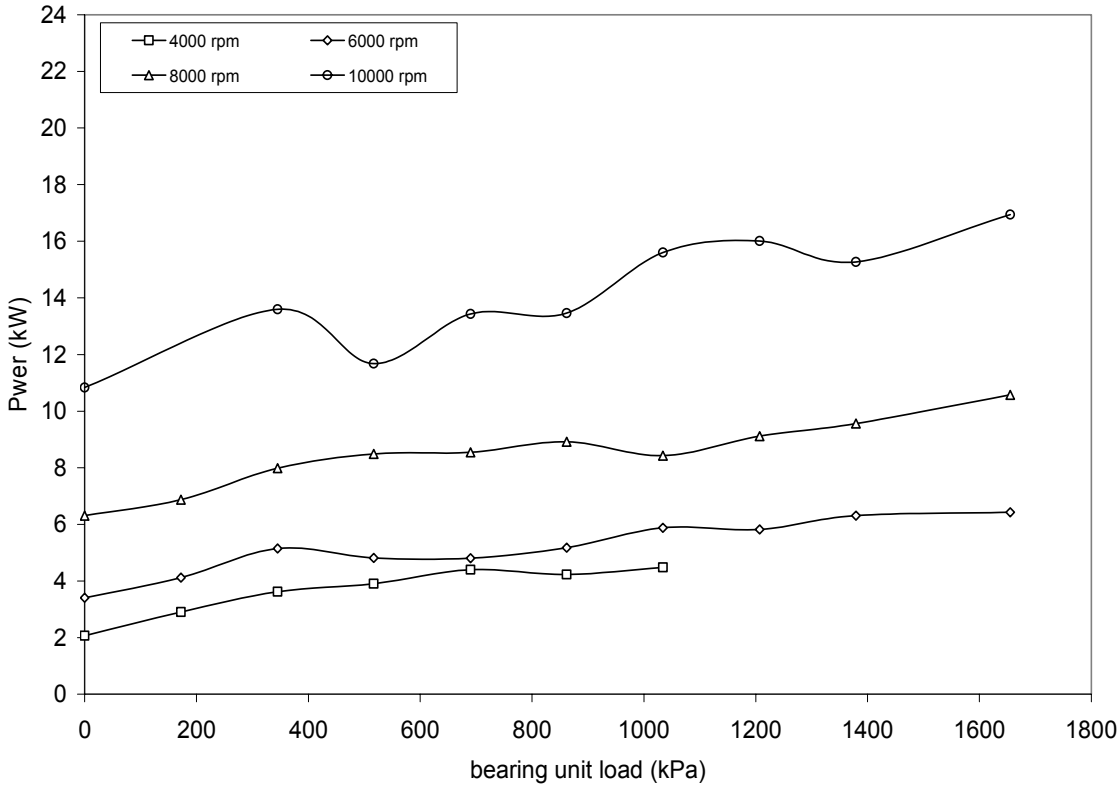

Fig. 16 Axial groove bearing estimated power loss vs. unit load

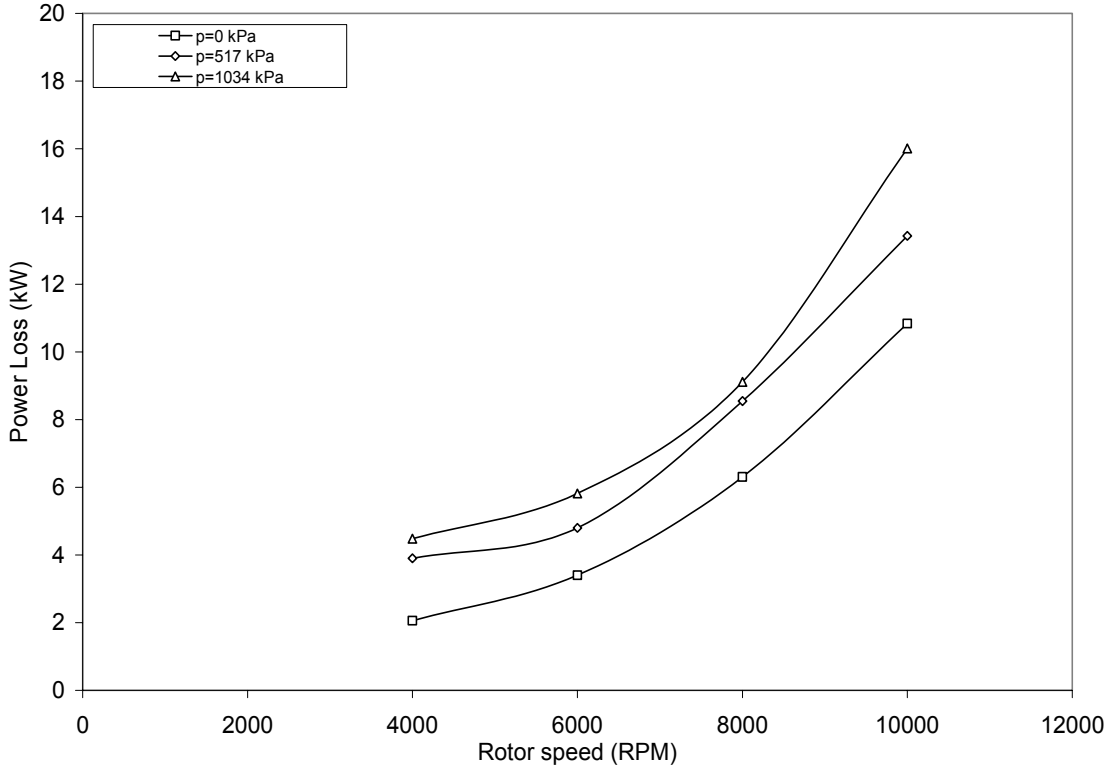

Fig. 17 Axial groove bearing power loss vs. speed

Dynamic Test Results

This section presents dynamic test results for the two-axial-groove bearing. The results discussed include the bearing baseline stiffness and damping coefficients, a comparison between the bearing experimental and theoretical force coefficients, and whirl-frequency ratio.

Table 5 shows the calculated Reynolds number for the test rotor speeds. The Reynolds number (*Re*) is given by the following equation:

$$Re = \frac{\rho \omega R C_r}{\mu} \tag{40}$$

The calculated test Reynolds numbers indicate that the flow is in the laminar flow regime. However, they are greater than 100. Therefore, it is a range in which Lund

and Reinhardt [10] anticipate a possible effect of fluid inertia on the bearing force coefficients.

Table 5. Reynolds number at test speeds for axial groove bearing

Speed (RPM)	4000	6000	8000	10,000
Re	135	213	302	399

Baseline Dynamic Stiffness

The tests aim to measure rotordynamic coefficients of the test bearing. However, the measurement procedure also measures stiffness and damping introduced by the pitch stabilizers, hose connections, etc. To account for these additional elements, a baseline test was conducted at zero rotor speed and with no oil supplied to the bearing (dry shakes). Figs. 18, 19 and 20 show the real and the imaginary parts of the direct and cross-coupled baseline dynamic stiffness. As explained in the dynamic test procedure section above, the four dynamic stiffness $\boldsymbol{H_{xx}}$, $\boldsymbol{H_{yy}}$, $\boldsymbol{H_{xy}}$ **and** $\boldsymbol{H_{yx}}$ are given in the following equations:

$$\boldsymbol{H}_{xx} = K_{xx} - M_{xx}\Omega^2 + \boldsymbol{i}\Omega C_{xx} \tag{41}$$

$$\boldsymbol{H}_{yy} = K_{yy} - M_{yy}\Omega^2 + \boldsymbol{i}\Omega C_{yy} \tag{42}$$

$$\boldsymbol{H}_{xy} = K_{xy} - M_{xy}\Omega^2 + \boldsymbol{i}\Omega C_{xy} \tag{43}$$

$$\boldsymbol{H}_{yx} = K_{yx} - M_{yx}\Omega^2 + \boldsymbol{i}\Omega C_{yx} \tag{44}$$

The uncertainty of the force coefficients is calculated using equations (36 and 37) given above in the dynamic test procedure section. Table 6 summarizes the baseline force coefficients and their uncertainties. Fig. 18 shows that both $\boldsymbol{H_{xx}}$ and $\boldsymbol{H_{yy}}$ real part curves are almost flat which indicates no significant added mass as would be expected

because there is no oil film. Fig. 19 shows that K_{xy} and K_{yx} are very small as expected also because unlike journal bearings, structures movements in x and y directions are not coupled. Fig. 20 shows some structural damping C_{xx} and C_{yy} with no cross-coupled damping C_{xy} and C_{yx} as expected.

Table 6. Baseline dynamic force coefficients

K_{xx} (MN/m)	2.83±0.202
K_{xy} (MN/m)	0.13±0.144
K_{yx} (MN/m)	-0.05±0.118
K_{yy} (MN/m)	2.62±0.320
C_{xx} (kN.s/m)	2..33±0.134
C_{xy} (KN.s/m)	0.34±0.231
C_{yx} (kN.s/m)	0.36±0.230
C_{yy} (kN.s/m)	2.84±0.580
M_{xx} (kg)	-0.87±0.235
M_{xy} (kg)	0.36±0.168
M_{yx} (kg)	0.07±0.137
M_{yy} (kg)	0.10±0.372

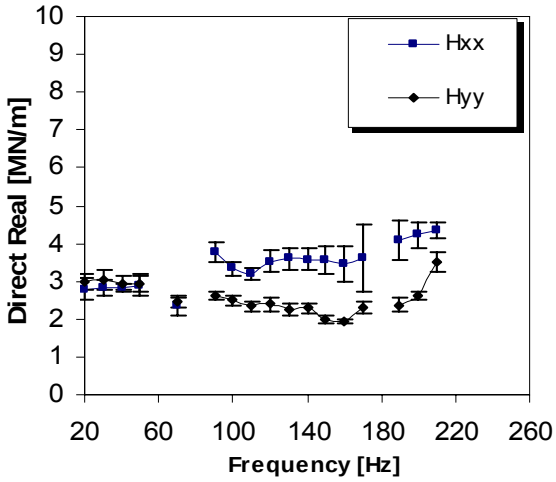

Fig. 18 Baseline real direct dynamic stiffness

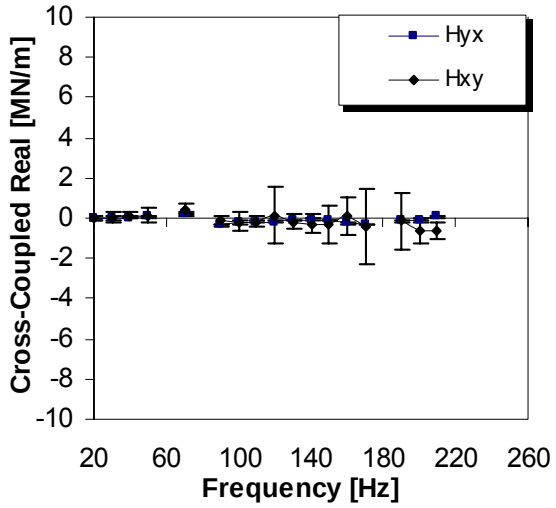

Fig. 19 Baseline cross-coupled direct dynamic stiffness

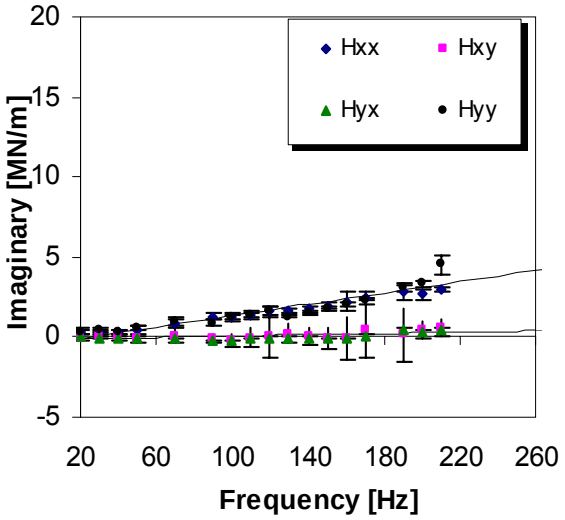

Fig. 20 Baseline imaginary dynamic stiffness

Example of Bearing Dynamic Stiffness

This section provides an example of how the bearing rotordynamic coefficients and their associated uncertainties are extracted from the measured dynamic stiffness. The following example includes a condition at 6000 rpm and a static unit load of 345 kPa (50 psi). Referring to Fig. 21, the real part of the direct dynamic stiffness (Re($\boldsymbol{H}_{xx}$)) and (Re($\boldsymbol{H}_{yy}$)) is fitted to a line whose slope and intercept are estimates of the opposite sign of the direct added-mass ($-M_{xx}$ and $-M_{yy}$) and stiffness (K_{xx} and K_{yy}). Evaluating equations 27 and equations 29 through 37 results in the values given in table 7 for these four parameters.

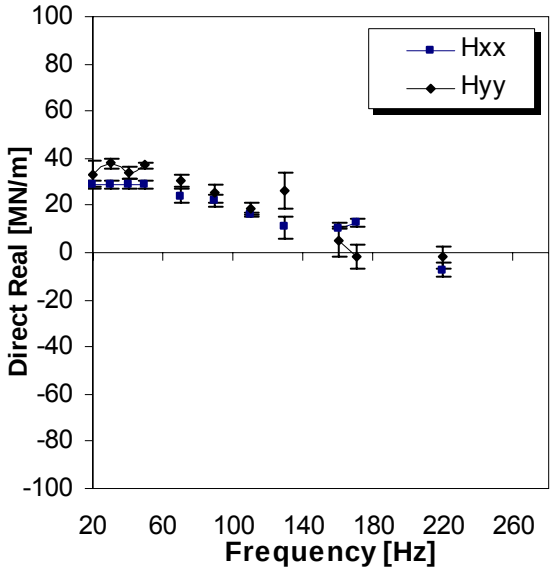

Fig. 21 Dynamic stiffness at 6000 rpm and 345kPa

Fig. 22 presents the real part of the cross-coupled dynamic stiffness. Unlike the real part direct dynamic stiffness, the real part of the cross-coupled dynamic stiffness is almost frequency independent. This means that the inertia effect on the cross-coupled stiffness can be neglected. Actually, if the curves are fitted using the outlined procedure above, the result shows high uncertainty of the added mass up to 65%. Therefore, the effect of inertia on cross-coupled stiffness of this bearing is neglected. An average stiffness is calculated instead. The uncertainty is calculated using:

$$\Delta K = \pm t \frac{\sigma}{\sqrt{N}} \tag{45}$$

$$\sigma = \sqrt{\frac{\sum_{i=1}^{N} (y_i - \hat{y}_i)^2}{N-1}} \tag{46}$$

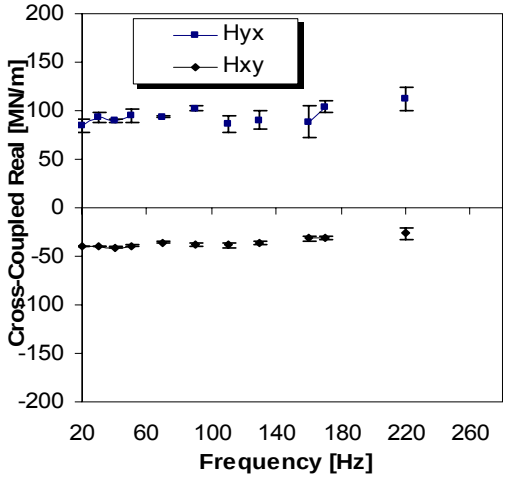

Fig. 22 Real cross-coupled dynamic stiffness at 6000 rpm and 345 kPa

Fig. 23 presents the real and cross-coupled imaginary part of the impedance function. The damping coefficients (C_{xx}, C_{yy}, C_{xy}, *and* Cyx) are identified from the slope of the imaginary part of the dynamic stiffness. Evaluating equations (27) and equations (29) through (37) results in the values given in table 7 for the damping coefficients.

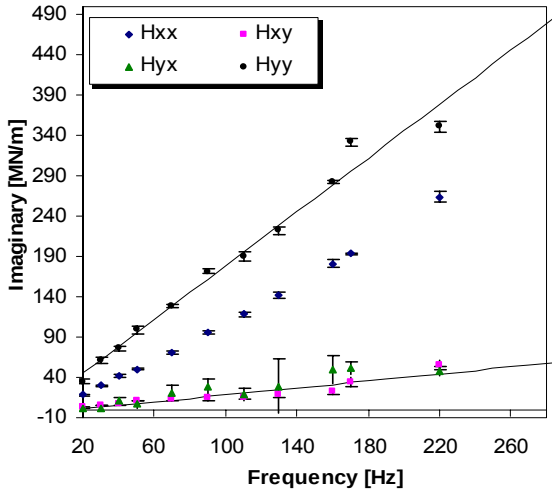

Fig. 23 Direct and cross-coupled imaginary part at 6000 rpm and 345 kPa

Table 7. Bearing force coefficients at 6000 rpm and 345 kPa (50 psi)

K_{xx} (MN/m)	28.56±2.233
K_{xy} (MN/m)	-36.01±2.449
K_{yx} (MN/m)	94.30±4.668
K_{yy} (MN/m)	34.77±4.811
C_{xx} (kN.s/m)	191.33±6.902
C_{xy} (KN.s/m)	34.44±9.014
C_{yx} (kN.s/m)	42.68±10.062
C_{yy} (kN.s/m)	265.35±24.849
M_{xx} (kg)	18.42±3.142
M_{xy} (kg)	0
M_{yx} (kg)	0
M_{yy} (kg)	23.54±5.898

Stiffness Coefficients

Figs. 24 (a), (b), (c), (d) and (e) show the experimental direct and cross-coupled bearing stiffness versus rotor speed at 0 kPa, 345 kPa, 690 kPa, 1034 kPa, and 1379 kPa respectively. For all figures except 24 (a), the experimental results are compared to the stiffness values obtained by the numerical solutions. The numerical solution is undefined at the no-load conditions. The uncertainties of the experimental results are given by the error bars of the data and they are below ±15% in most cases. Generally, the experimental stiffness coefficients follow the same trend as the numerical values except for K_{xx}. While the experimental results show that K_{xx} decreases as speed increases at a fixed load (Sommerfeld number increases), the numerical results show that K_{xx}

increases. The figures also show that the bearing stiffness K_{yy} increases as load increases at a fixed speed or as speed decreases at a fixed load, i.e., as Sommerfeld number decreases. The bearing develops no direct stiffness if the rotor is centered in the bearing clearance, i.e., at no-load or at high speed conditions (high Sommerfeld number). Furthermore, the figures show that at all test conditions, the bearing experimental direct stiffness K_{yy} is lower than the predicted values. The maximum difference between predicted and estimated K_{yy} is 40% at 4000 rpm and 690 kPa. This result is consistent with the finding from Fig. 11 which shows that the bearing operates at higher eccentricity than predicted. Also, the figures show that the bearing measured cross-coupled stiffness K_{xy} is lower than predicted especially at high speeds. The difference between predicted and experimental values increases from 2% at 4000 rpm to about 100% at 10000 rpm. This result is also consistent with findings from Fig. 14 which shows that the bearing operates at lower attitude angle than predicted. Fig. 24 shows reasonable agreement between predictions and experimental results at low speeds.

Figs. 25 (a) and (b) show the bearing non-dimensional stiffness coefficients versus Sommerfeld number. The bearing stiffness coefficients are non-dimensioned using:

$$k_{ij} = K_{ij}\left(\frac{C_r}{W}\right) \tag{47}$$

The figure shows that both measured and predicted values of k_{yy} decrease as Sommerfeld number increases. However, the figure shows that the measured and predicted values of k_{xx} diverge as Sommerfeld number increases. A slight increase in k_{xx} is predicted as Sommerfeld number increases, while the measured values show that k_{xx} slightly decreases as Sommerfeld number increases. The figure also shows that both measured and predicted k_{xy} and k_{yx} increase as Sommerfeld number increases. The figure also shows that measured values of k_{xy} and k_{yx} are less than predicted at high Sommerfeld numbers. Also, k_{xy} and k_{yx} have opposite signs, which means that they act

to destabilize the rotor. Also, the figure shows that the maximum difference between k_{xy} and k_{yx} values is at high Sommerfeld number. This result explains why rotors supported on journal bearings become unstable if operated above a certain Sommerfeld number.

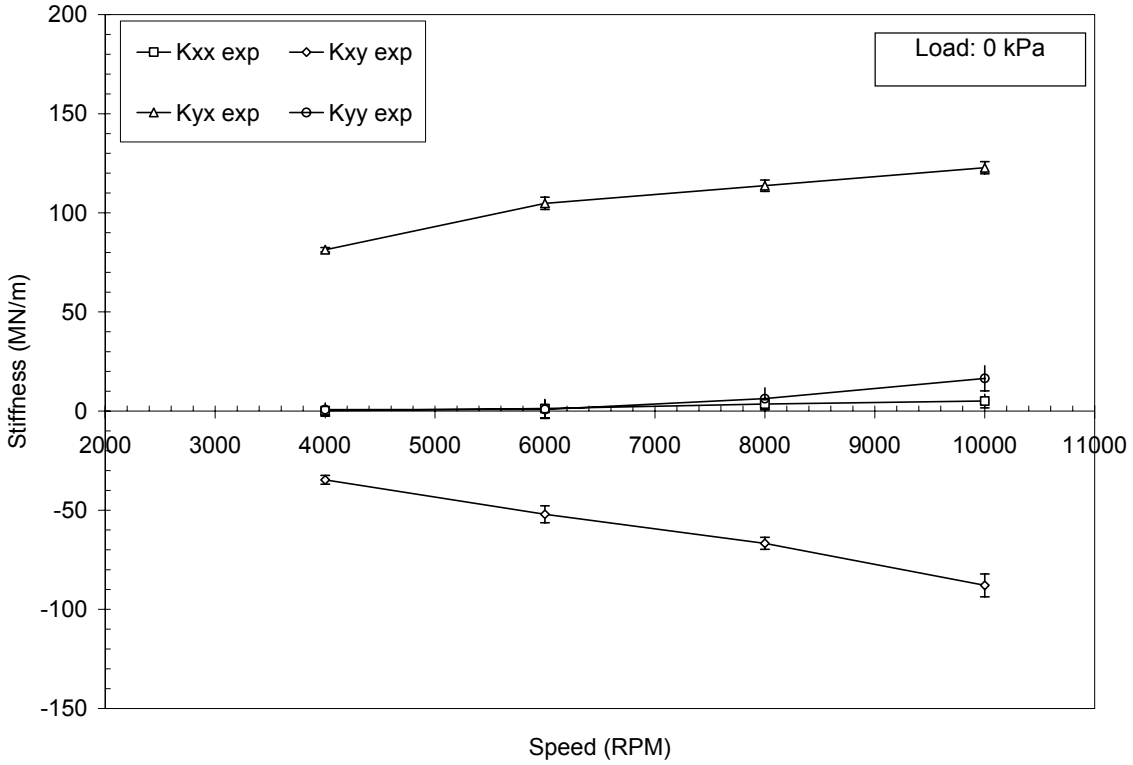

(a) 0 kPa

Fig. 24 Axial groove bearing stiffness coefficients vs. rotor speed

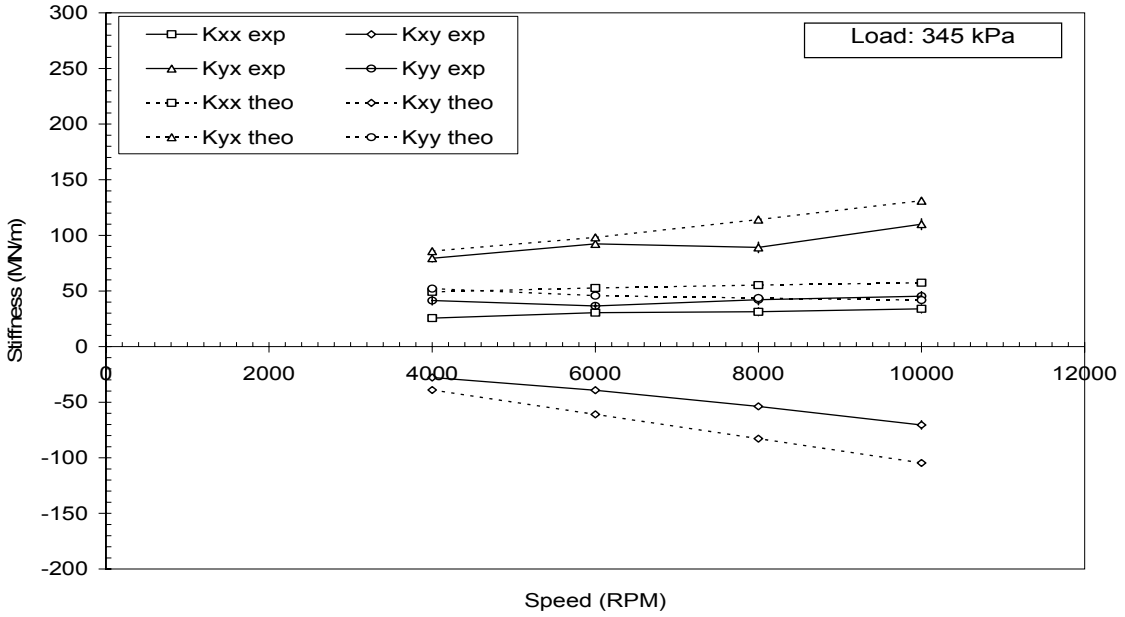

(b) 345 kPa

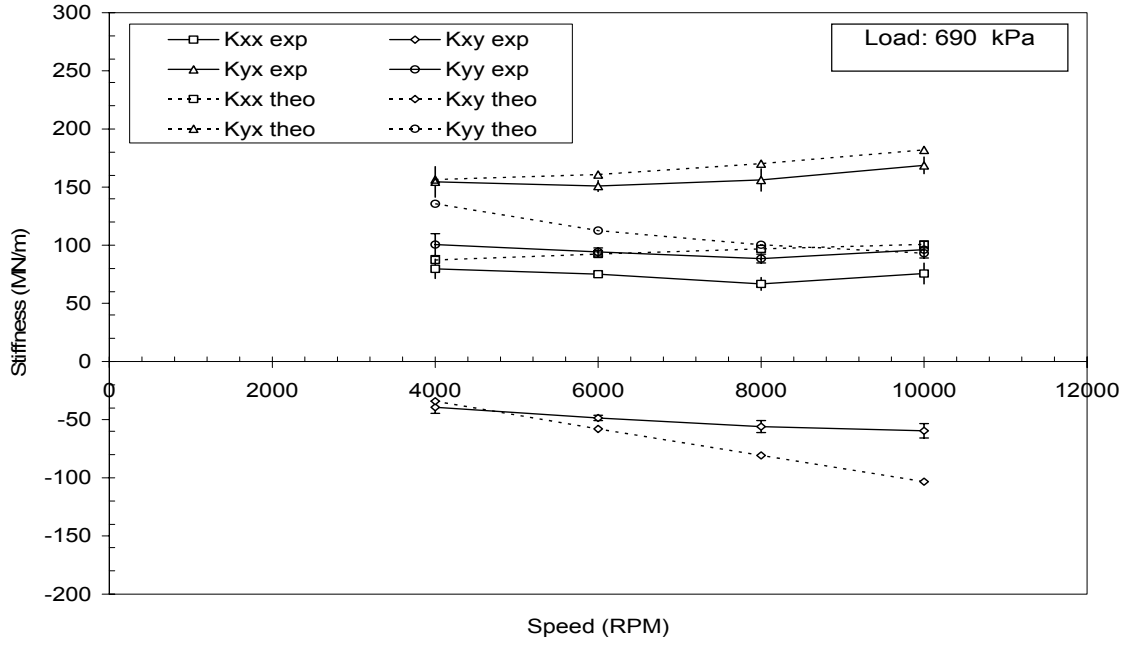

(c) 690 kPa

Fig. 24 “Continued”

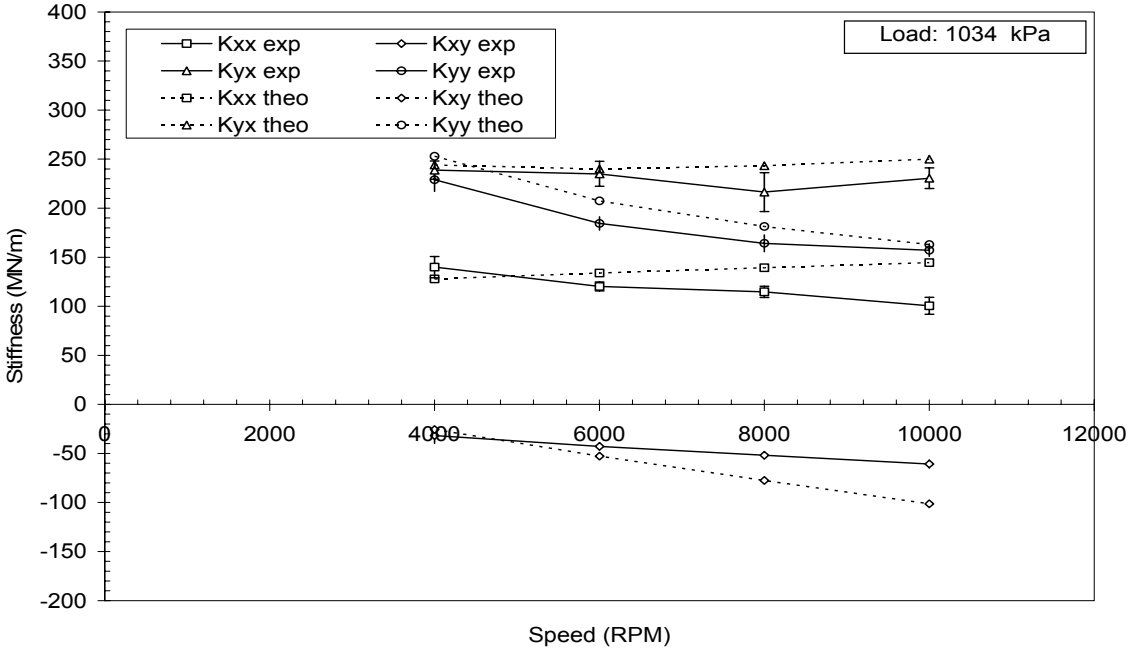

(d) 1034 kPa

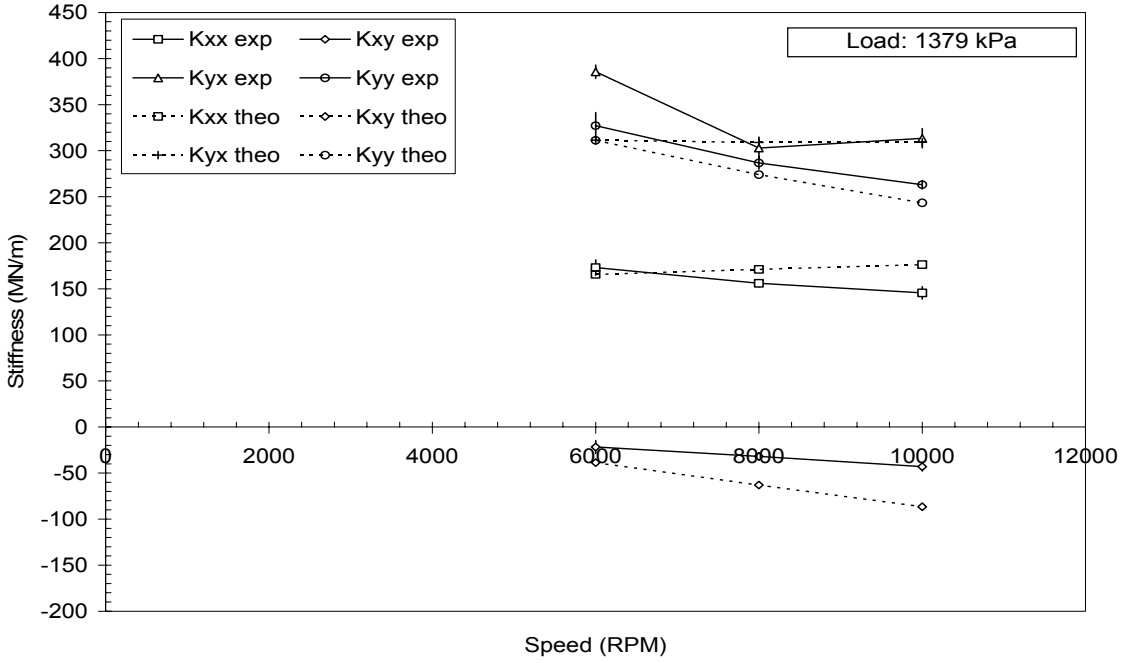

(e) 1379 kPa

Fig. 24 “Continued”

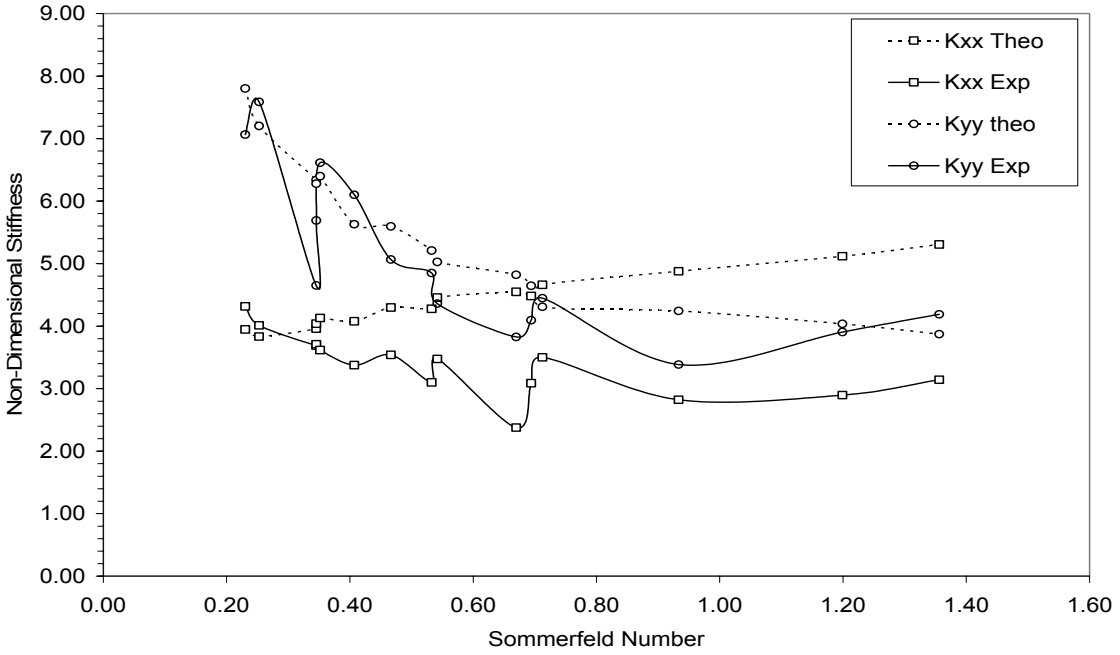

(a) Direct Stiffness

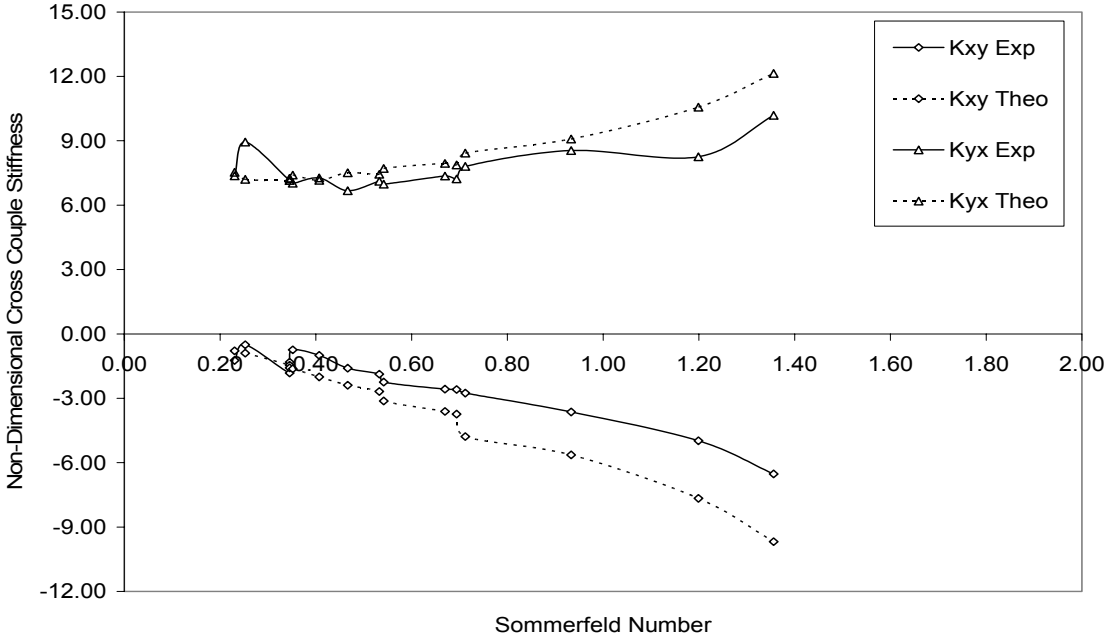

(b) Cross-coupled Stiffness

Fig. 25 Axial groove bearing dimensionless stiffness vs. Sommerfeld number

Figs. 26 (a), (b), (c), and (d) compare the bearing static stiffness determined as the local slope of the force-displacement curve to the dynamic stiffness at zero frequency. The bearing stiffness and flexibility coefficients are related by the following equation:

$$\left[K_{ij}\right]^{-1} = \frac{1}{(K_{xx}K_{yy} - K_{yx}K_{xy})}\begin{bmatrix} K_{yy} & -K_{xy} \\ -K_{yx} & K_{xx} \end{bmatrix} = \begin{bmatrix} \frac{\partial x}{\partial f_x} & \frac{\partial x}{\partial f_y} \\ \frac{\partial y}{\partial f_x} & \frac{\partial y}{\partial f_y} \end{bmatrix} \tag{48}$$

Thus,

$$\frac{\partial f_y}{\partial y} = K_{yy} - \frac{K_{xy}K_{yx}}{K_{xx}} \tag{49}$$

The figures show that the bearing stiffness as estimated from the static test is lower than that obtained from the dynamic test. The figures also show a sharp increase in the stiffness estimated from the dynamic test as load increases.

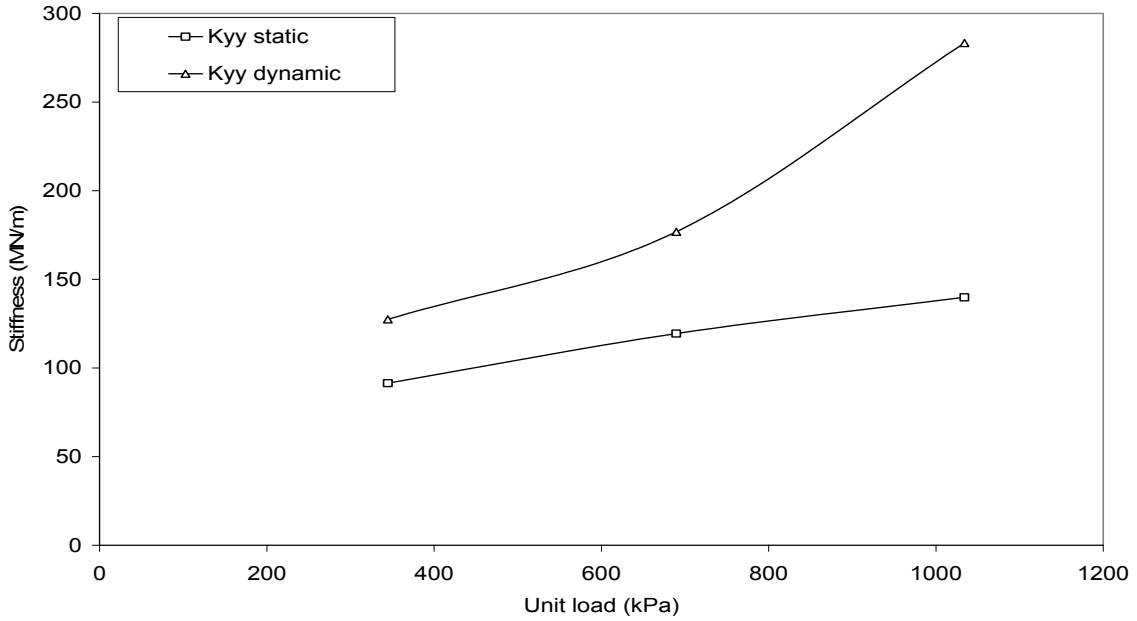

(a) 4000 rpm

Fig. 26 Axial groove bearing direct stiffness from static and dynamic tests

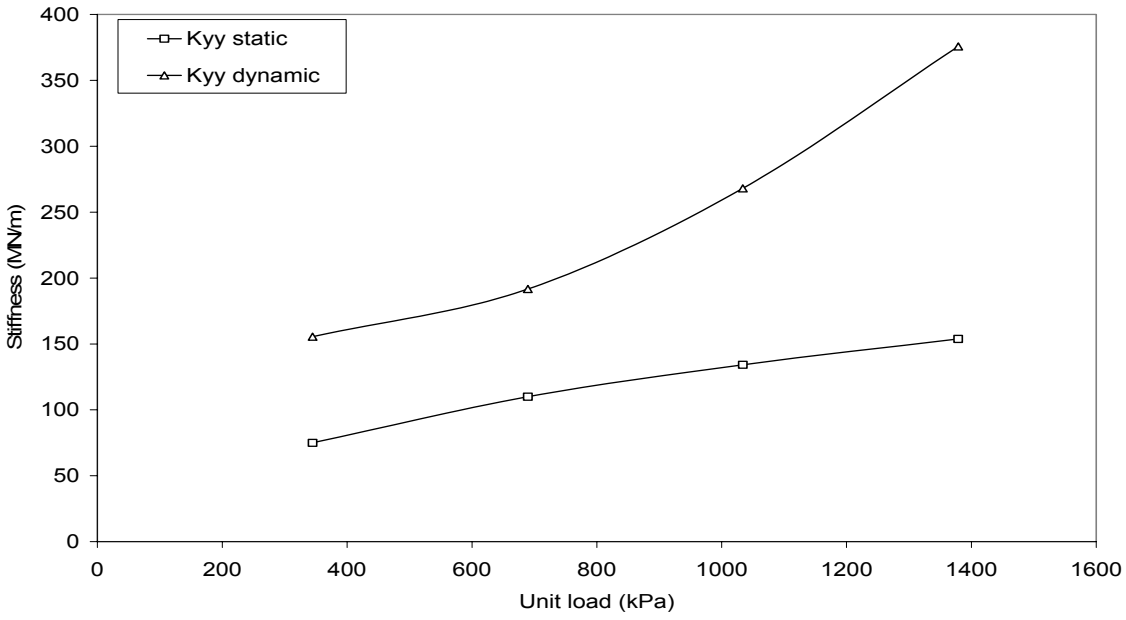

(b) 6000 rpm

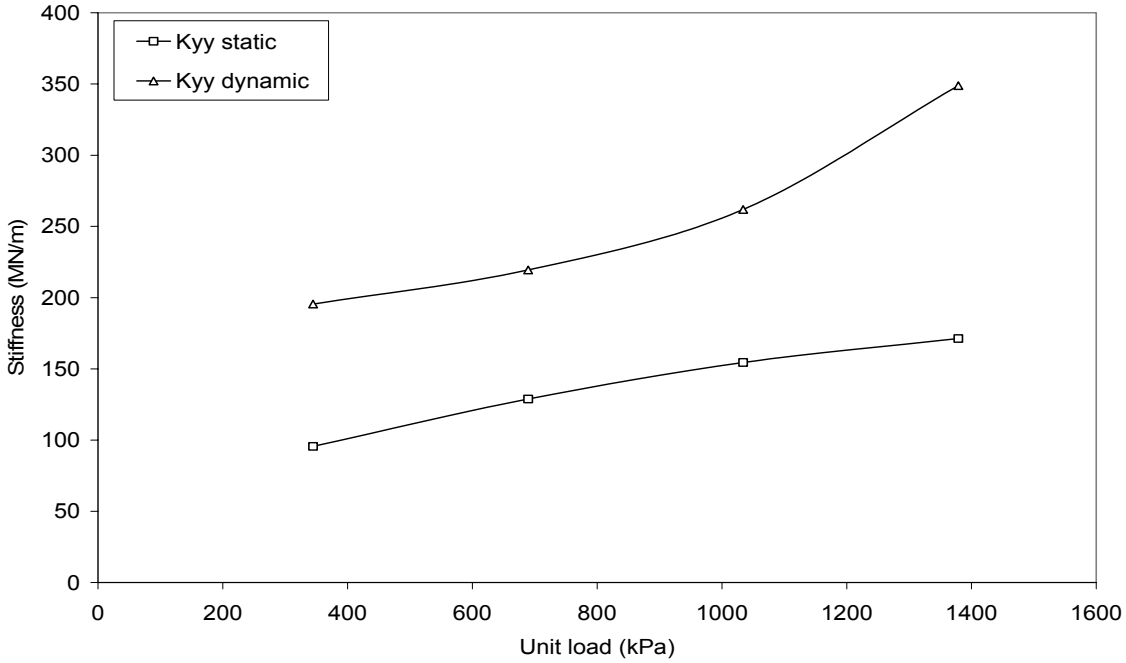

(c) 8000 rpm

Fig. 26 “Continued”

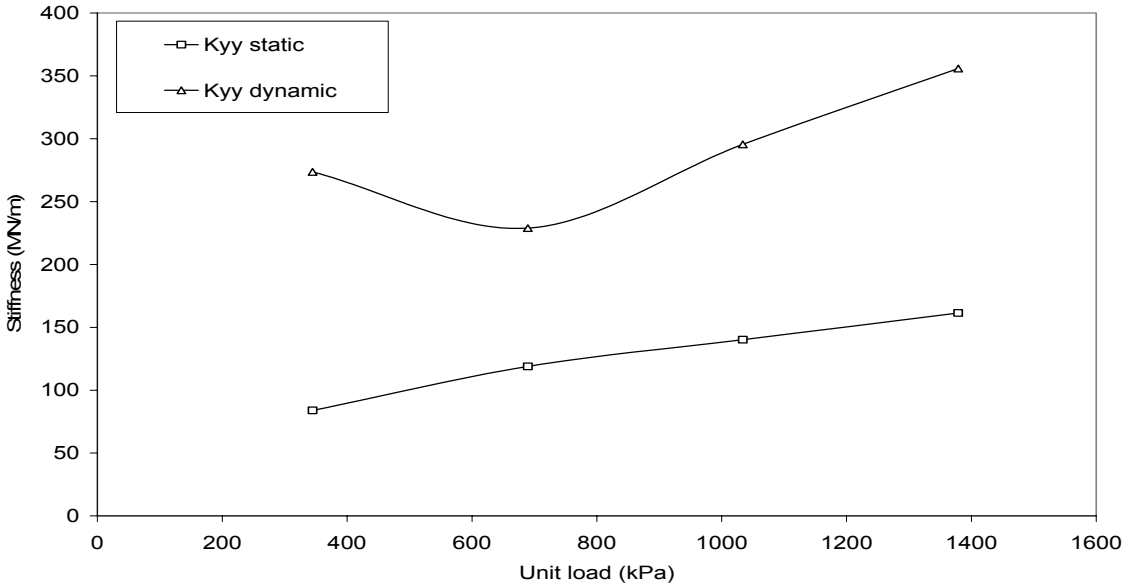

(d) 10,000 rpm

Fig. 26 "Continued"

Damping Coefficients

Figs. 27 (a), (b), (c), (d) and (e) show the bearing experimental direct and cross-coupled damping versus rotor speed at 0 kPa, 345 kPa, 690 kPa, 1034 kPa and 1379 kPa respectively. The bearing damping coefficients are direct measures of the bearing's capability to dissipate energy. The damping coefficients C_{xx} , C_{yy} , C_{xy} , and C_{yx} are related to the bearing reaction force by equation (8).

For all figures except 27 (a), the experimental results are compared to predicted values. The numerical solution is undefined at no-load conditions. The uncertainties of the experimental results are given by the error bars of the data and they are below ±15% in most cases. The experimental direct damping coefficients follow predicted trend. Although, the experimental values are less than predictions at most conditions, the difference between experimental and predicted direct damping coefficients is less than 20% at most conditions. The maximum difference between experimental and numerical

direct damping results is 26% for C_{yy} at 6000 rpm and 1379 kPa. The direct damping coefficients increase as load increases or speed decreases, i.e. as Sommerfeld number decreases.

The figures also show that predicted cross-coupled damping coefficients C_{xy}, and C_{yx} are equal at all test conditions. However, the experimental values of the cross-coupled damping coefficients C_{xy}, and C_{yx} are lower than predicted. Both numerical and experimental results of C_{xy}, and C_{yx} show a decrease as speed increases at fixed load.

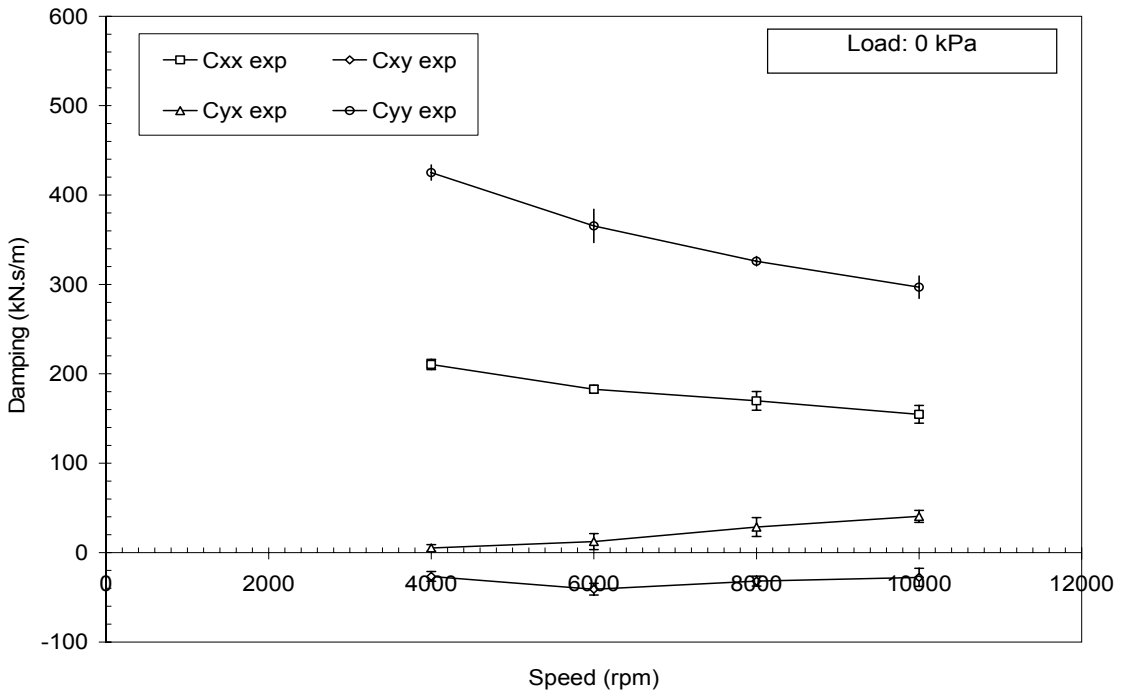

(a) 0 kPa

Fig. 27 Axial groove bearing damping coefficients vs. speed at various load condition

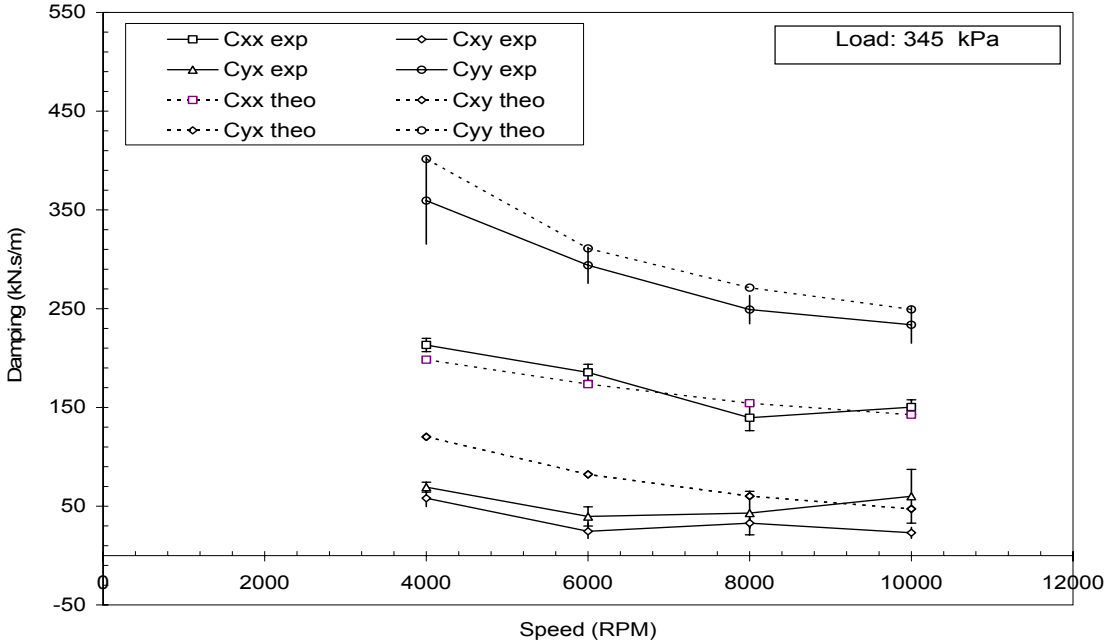

(b) 345 kPa

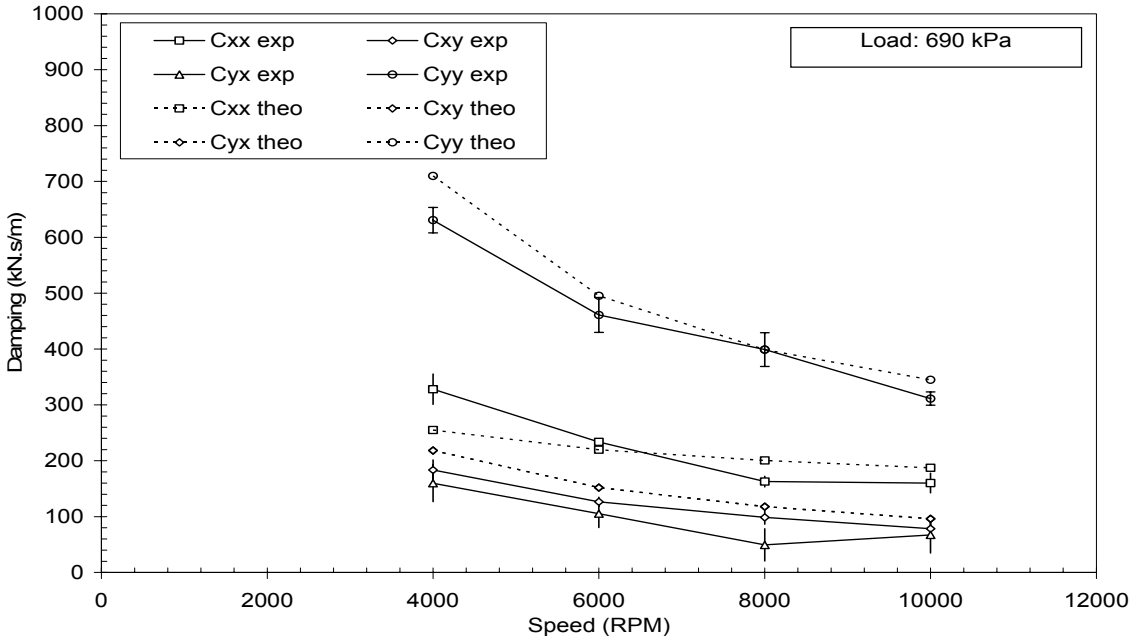

(c) 690 kPa

Fig. 27 “Continued”

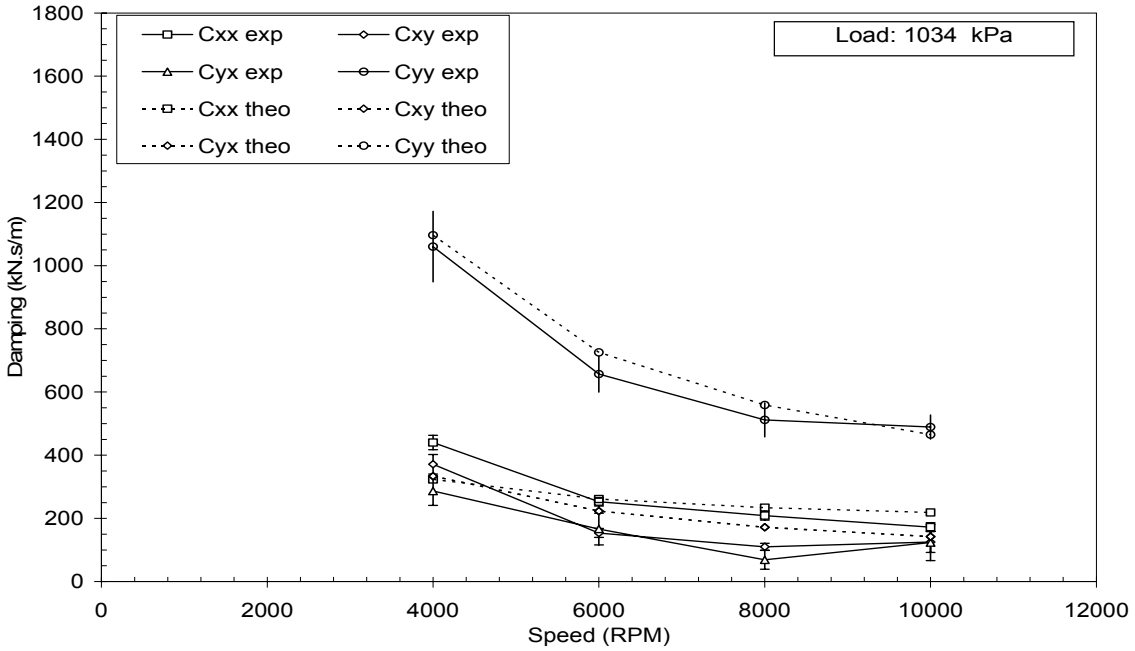

(d) 1034 kPa

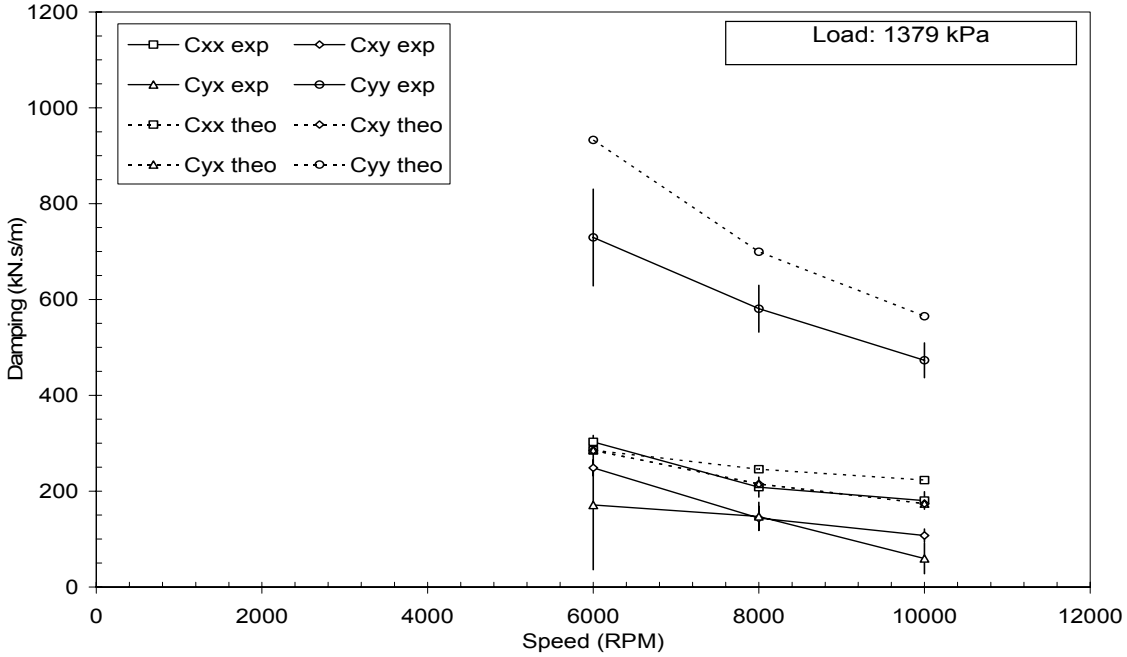

(e) 1379 kPa

Fig. 27 “Continued”

Figs. 28 (a) and (b) shows the non-dimensional bearing damping coefficients versus Sommerfeld number. The bearing damping coefficients are non dimensioned using the following equation:

$$c_{ij} = C_{ij}\left(\frac{C_r \omega}{W}\right) \tag{50}$$

Fig. 28 (a) shows that both the experimental and numerical non-dimensional direct damping increase as Sommerfeld number increases. This result should not be confused with the result obtained from Fig. 26 about the relationship between direct damping and Sommerfeld number. Dimensional direct damping decreases as Sommerfeld number increases. However, non-dimensional direct damping increases as Sommerfeld number increases. Fig. 28 (b) shows that the predicted cross-coupled damping is constant for all Sommerfeld numbers. However, the experimental values fluctuate within 25%-75% below the numerical results.

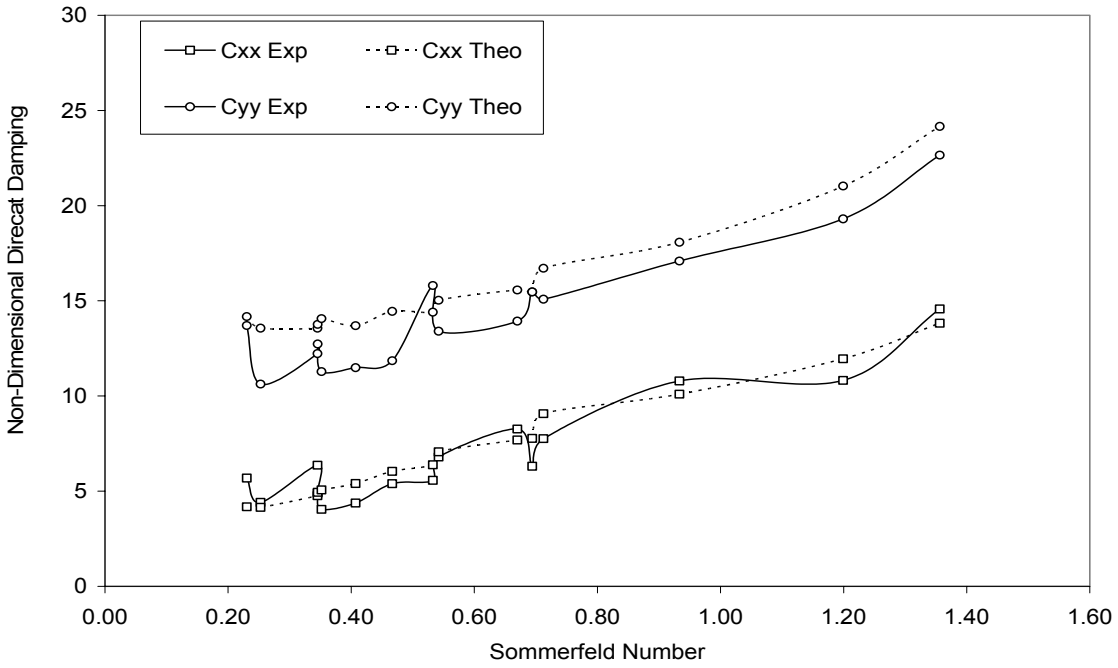

(a) Direct damping

Fig. 28 Axial groove bearing non-dimensional damping versus Sommerfeld number

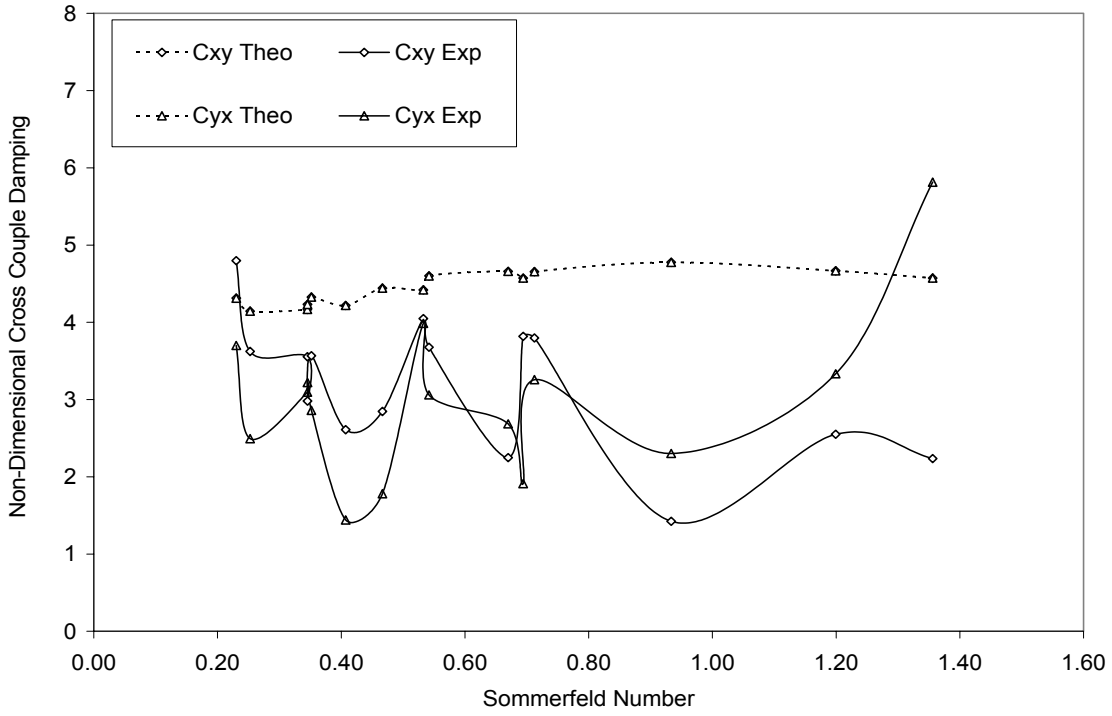

(b) Cross-coupled damping

Fig.28 "Continued"

Added Mass Coefficients

Figs. 29 (a), (b), (c), (d) and (e) show the bearing direct added mass coefficients versus rotor speed at various load condition. The cross-coupled mass terms are disregarded because of their high uncertainties. Fig. 29 (a) shows the added mass coefficients at no-load conditions. The figure shows that the direct added mass M_{yy} increases with speed from 60 kg at 4000 rpm to 75 kg at 10000 rpm. However, the direct added mass M_{xx} decreases slightly from 44 kg at 4000 rpm to 36 kg at 10000 rpm. Fig. 28 (b) shows the added mass coefficients at 345 kPa. The figure shows that both M_{xx} and M_{yy} values are lower compared to the no-load condition. Fig. 29 (c) shows that both

M_{xx} and M_{yy} values at 690 kPa are zero at all speeds except at 10000 rpm. Figs. 29 (d) and (e) show that both M_{xx} and M_{yy} values are zero at all speeds for unit load of 1034 kPa and 1379 kPa. The uncertainties of the added mass terms are given by the error bars of the data and they are below ±25% in most cases. Note that the uncertainty of the mass terms increases as load increases i.e. as Sommerfeld number decreases. The reason for this is that at low Sommerfeld number, the dynamic stiffness can not be fitted using the quadratic equation $(K - m\Omega^2)$. In these cases, the mass term is set to zero and an average stiffness is reported.

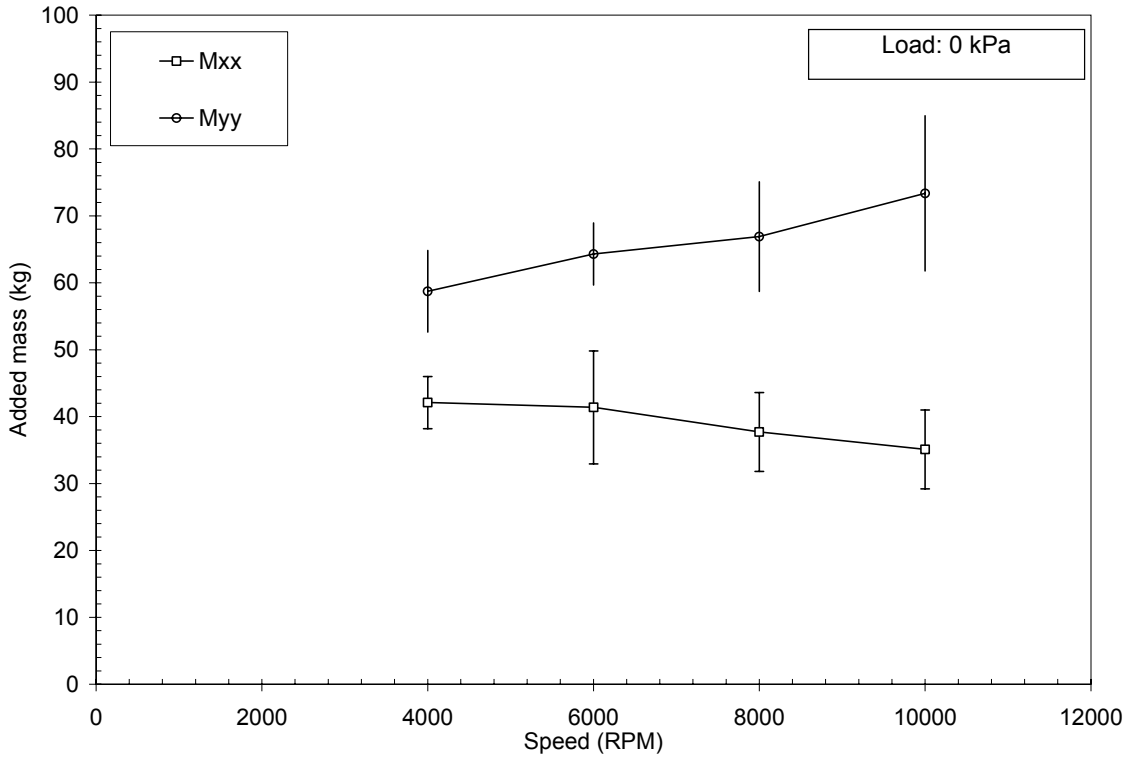

(a) 0 kPa

Fig. 29 Axial groove bearing added mass coefficients vs. speed

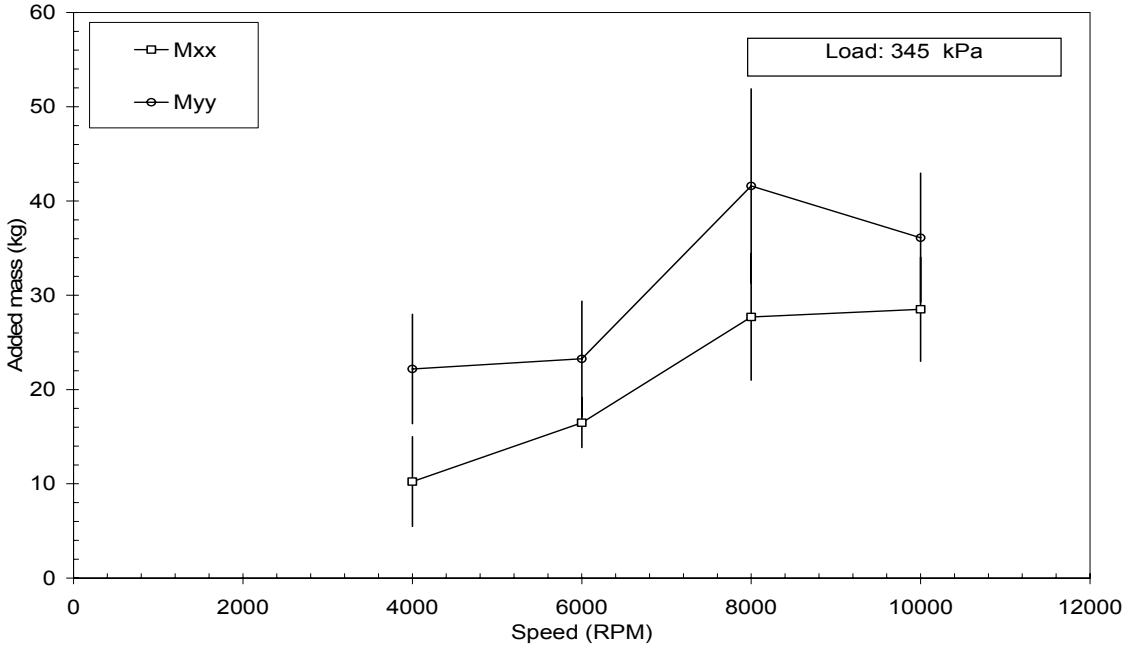

(b) 345 kPa

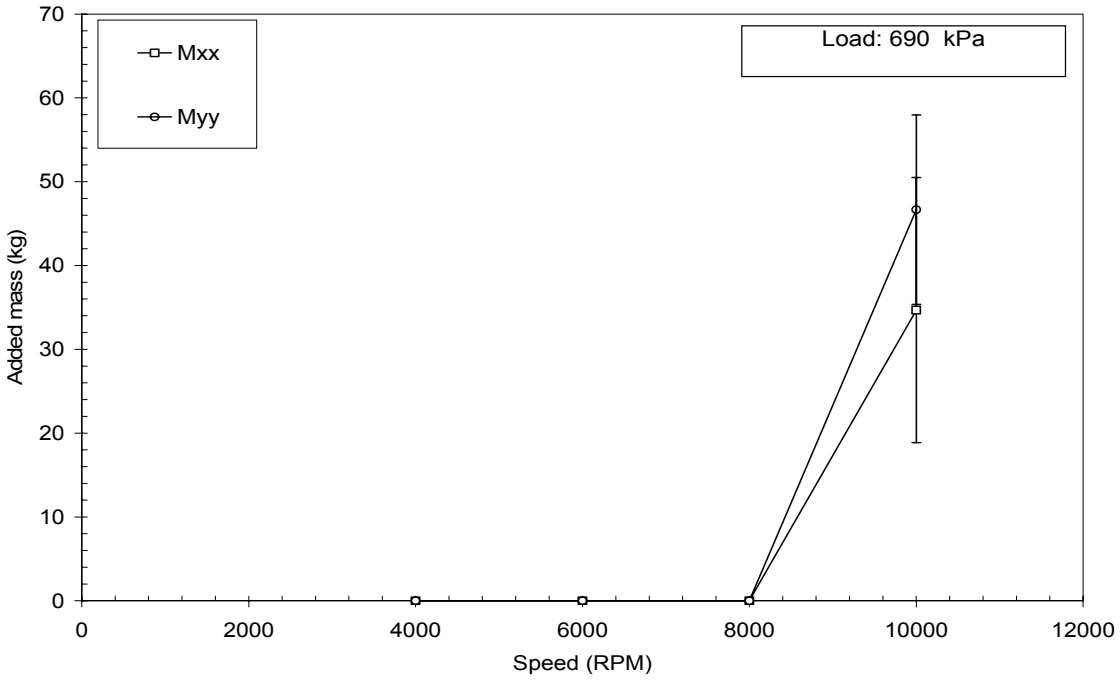

(c) 690 kPa

Fig. 29 “Continued”

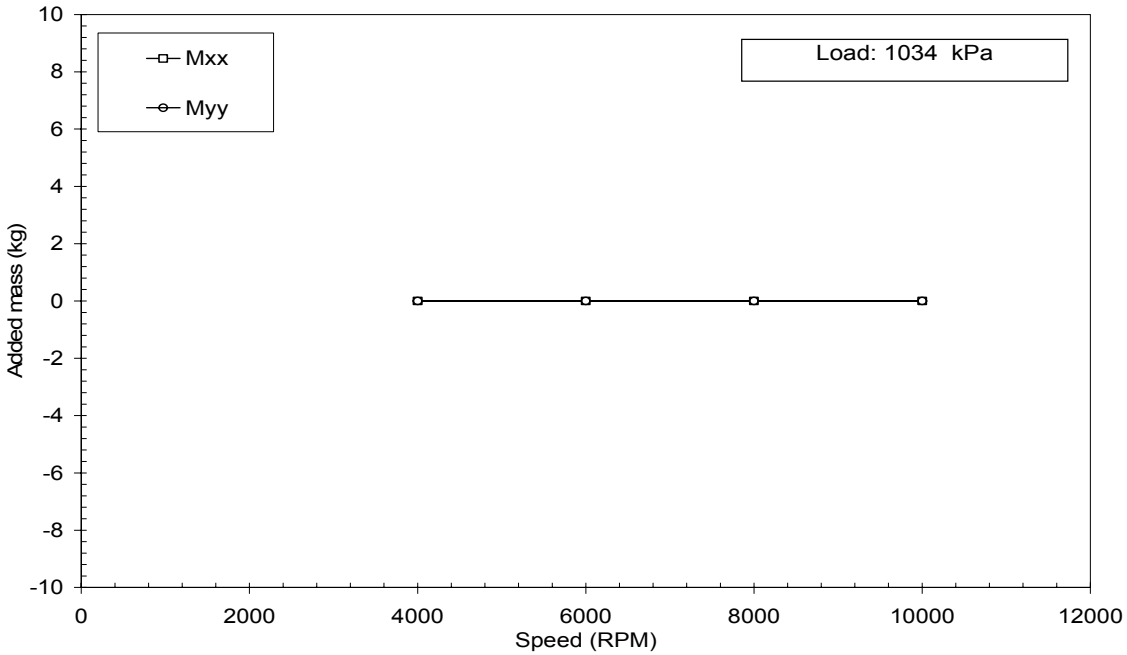

(d) 1034 kPa

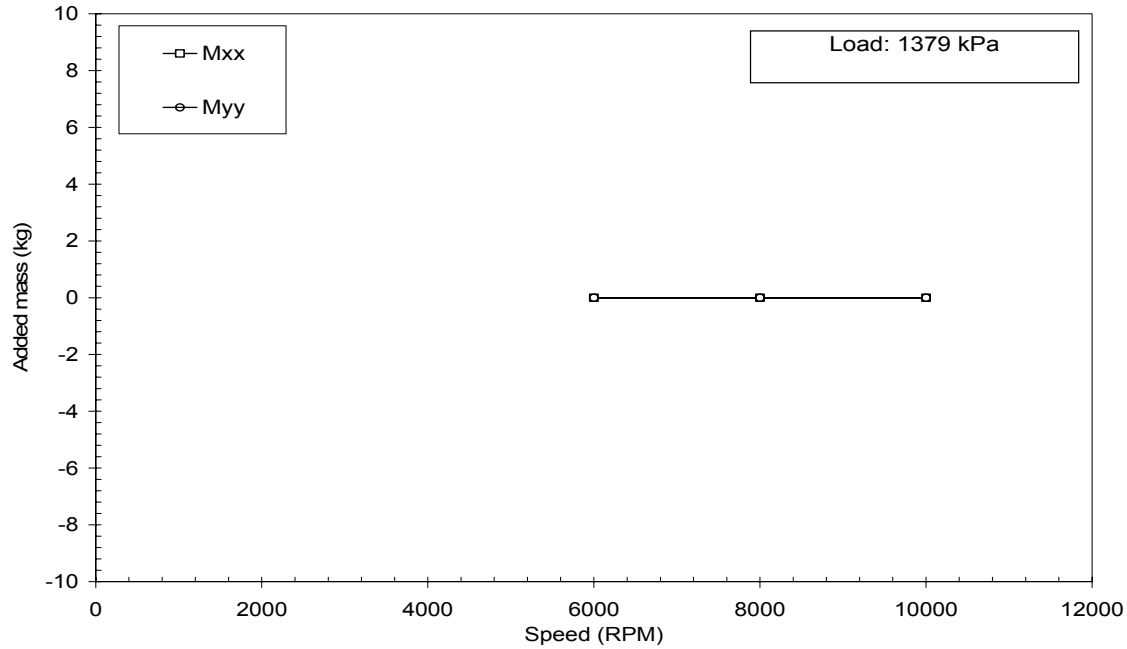

(e) 1379 kPa

Fig. 29 “Continued”

Figs. 30 (a) and (b) shows the direct added mass terms in dimensionless form versus Sommerfeld number and eccentricity ratio respectively. The added mass terms are non-dimensioned using the following equation:

$$m_{ij} = \frac{M_{ij}}{\rho \pi R^2 L (R / C_r)} \tag{51}$$

Fig. 30 (a) shows significant amount of direct added mass for Sommerfeld number greater than 0.60. Using equation (51), the direct added mass for Sommerfeld number > 0.6 is in the range of 20-70 kg. However, there is no direct added mass for *S* <0.60. Fig. 30 (b) shows both experimental and numerical M_{xx} and M_{yy} predicted by Reinhardt and Lund [10] versus ε_0. The figure shows that Lund and Reinhardt [10] under predicted the added mass at zero eccentricity. However, their analysis showed that if the unloaded pad is considered to contribute then, the predicted added mass coefficients at zero eccentricity ratio is twice the value shown in Fig. 30 (b). The figure also shows that both experimental M_{xx} and M_{yy} decreases with ε_0. The figure shows no added mass for $\varepsilon_0 >$ 0.50. On the other hand, the figure shows that predicted M_{yy} increases with increasing ε_0 while M_{xx} decreases slightly.

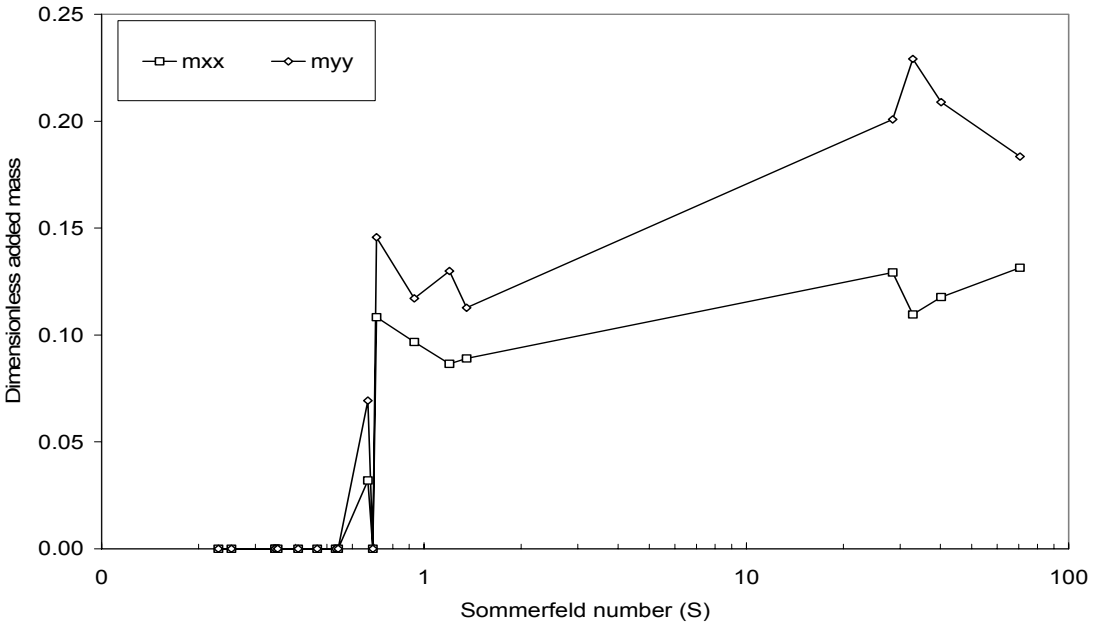

(a) Added mass vs. S

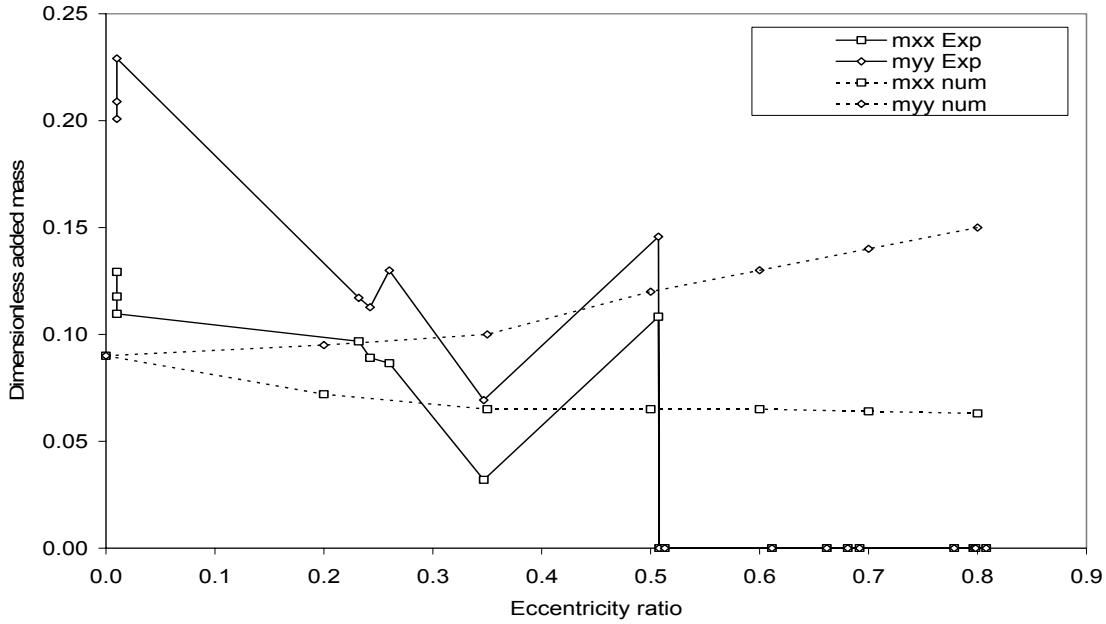

(b) Added mass vs. ε_0

Fig. 30 Axial groove bearing non-dimensional added mass vs. S and ε_0

Whirl-frequency Ratio (WFR)

Experimental *WFR* ignoring inertia effect is determined from the measured dynamic coefficients using equations (12) and (13). To account for the effects of fluid inertia on the *WFR* an analysis following San Andres [27] is carried out. The *WFR* is given by:

$$a + b(WFR)^2 + c(WFR)^4 = 0 \tag{52}$$

Where,

$$a = k_{xx}k_{yy} - k_{xy}k_{yx} + k_{eq}^2 - (k_{xx} + k_{yy})k_{eq} \tag{53}$$

$$b = (k_{xx} + k_{yy})k_{eqm} + (m_{xx} + m_{yy})k_{eq} - 2k_{eq}k_{eqm} - Term \tag{54}$$

$$Term = k_{xx}m_{yy} + k_{yy}m_{xx} + c_{xx}c_{yy} - k_{xy}m_{yx} - k_{yx}m_{xy} - c_{xy}c_{yx} \tag{55}$$

$$k_{eqm} = \frac{c_{yy}m_{xx} + c_{xx}m_{yy} - c_{xy}m_{yx} - c_{yx}m_{xy}}{c_{xx} + c_{yy}} \tag{56}$$

The dimensionless added mass coefficients from San Andres [27] are given as:

$$m_{ij} = \frac{C_r\omega^2}{W}M_{ij} \tag{57}$$

After obtaining the coefficients *a*, *b* and *c*, Equation (52) can be solved for the *WFR*.

Fig. 31 shows a comparison between the numerical and experimental whirl-frequency ratio. The figure shows good agreement between the theoretical and experimental whirl-frequency ratio for Sommerfeld number less than 0.80. For example, the figure shows that the bearing whirl-frequency ratio ignoring inertia effect is 0.45 at 0.20 Sommerfeld number and 0.48 at 0.62 Sommerfeld number which are 4% from the numerical values. The largest difference between numerical and experimental *WFR* for Sommerfeld number $S< 0.8$ is 20% at 0.60 Sommerfeld number. Theoretically, *WFR* increases with Sommerfeld number. However, the experimental results do not show this trend clearly. The large difference between numerical and experimental *WFR* for Sommerfeld number $S>0.80$ is contributed to the inaccuracy of the measured dynamic coefficients due to the bearing whirling action at high Sommerfeld number test conditions. Fig. 31 also shows that *WFR* considering inertia effect is slightly less than *WFR*

without considering inertia effect. This means that inertia helps stabilize the bearing. However, this difference is very small and can be ignored.

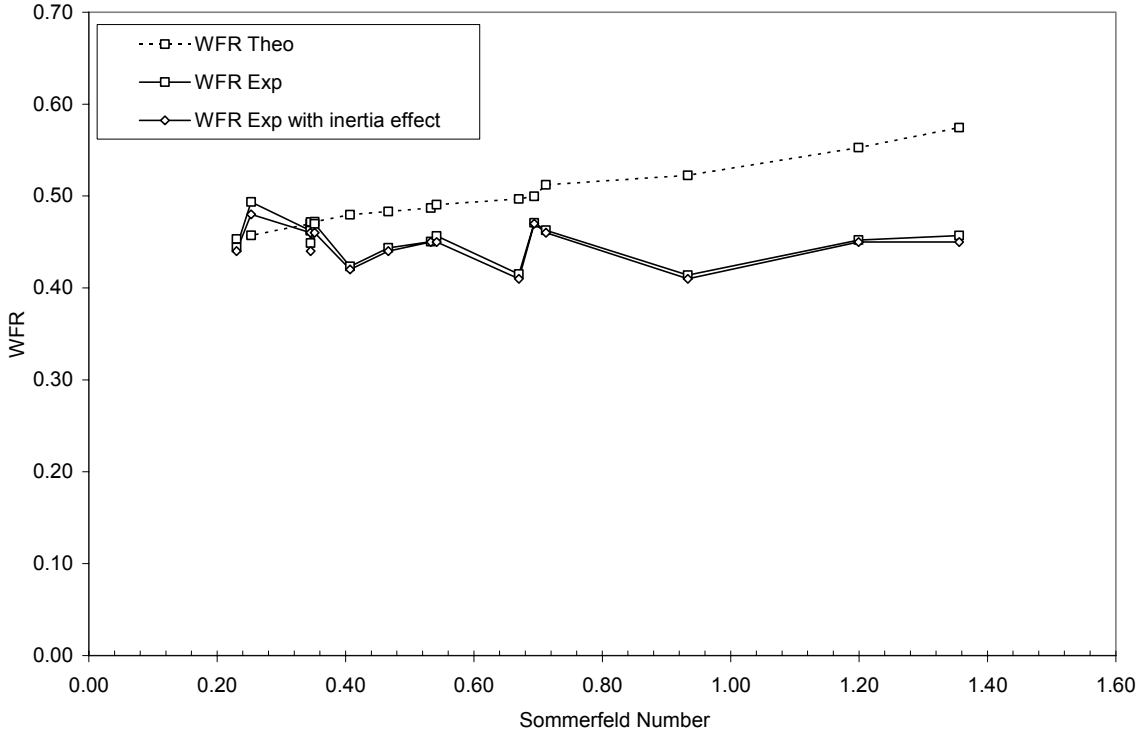

Fig. 31 Axial groove bearing experimental and theoretical whirl-frequency ratio vs. Sommerfeld number

PRESSURE-DAM BEARING TEST RESULTS

Static Test Results

As in the axial-groove bearing test results section above, this section discusses the static performance of the pressure-dam bearing. Data presented in this section includes bearing eccentricity ratio ε_0, attitude angle ψ and estimated power losses E. Experimental eccentricity ratio, attitude angle and power loss values will be compared to numerical values as obtained from $XLTRC^{2}$[2]. The bearing measured cold radial clearance was 0.119~0.131 mm (4.68~5.15 mils). The bearing clearance was measured again after the test was completed and found to be increased by about 0.005 mm (0.2 mils). The oil flow rate was maintained at 32 liter/min (8.5 GPM). Oil inlet temperate varied within 37.8°C-48.8°C (100°F-120°F) while the supply pressure was fixed at around 172 kPa (25 psi). Oil outlet temperatures are given in appendix B (page 102). Table 8 gives the Reynolds number for the test rotor speeds as calculated using equation (38). Because of the increase clearance in the pocket, Reynolds number in this region is expected to be three to four times higher than the values in table 8. Table 9 summarizes the test conditions for the pressure-dam bearing in terms of rotor speed and static load. Table 9 shows that, unlike the axial-groove bearing, the pressure-dam bearing was tested at 12,000 rpm because no vibration problem was encountered. Figs. 32 (a), (b) and (c) show the frequency spectrum at 11,000 rpm, 12,000 rpm, and 13,000. The figure shows a sharp increase in the 1X frequency response as speed is increased. Therefore, the test was stopped at 12,000 rpm. Table 9 also shows more static test points at 10,000 rpm compared to the axial-groove bearing. The reason for this is explained later.

[2] XLPresDm™ Spreadsheet is used for this analysis. The code assumes isothermal and laminar flow

Table 8. Reynolds number at test speeds for pressure-dam bearing

RPM	4000	6000	8000	10,000	12,000
Re	133	214	302	401	479

Table 9. Test Matrix for pressure-dam bearing

kPa (psi) RPM	0 (0)	172 (25)	345 (50)	517 (75)	690 (100)	862 (125)	1034 (150)	1207 (175)	1379 (200)	1517 (220)	1655 (240)	1793 (260)	1930 (280)
4000	S,D	S	S,D	S	S,D	S	S,D	S					
6000	S,D	S	S,D	S	S,D	S	S,D	S	S,D				
8000	S,D	S	S,D	S	S,D	S	S,D	S	S,D	S	S		
10000	S,D	S	S,D	S	S,D	S	S,D	S	S,D	S	S,D	S	S
12000	S,D	S	S,D	S	S,D	S	S,D	S	S,D	S	S,D	S	S

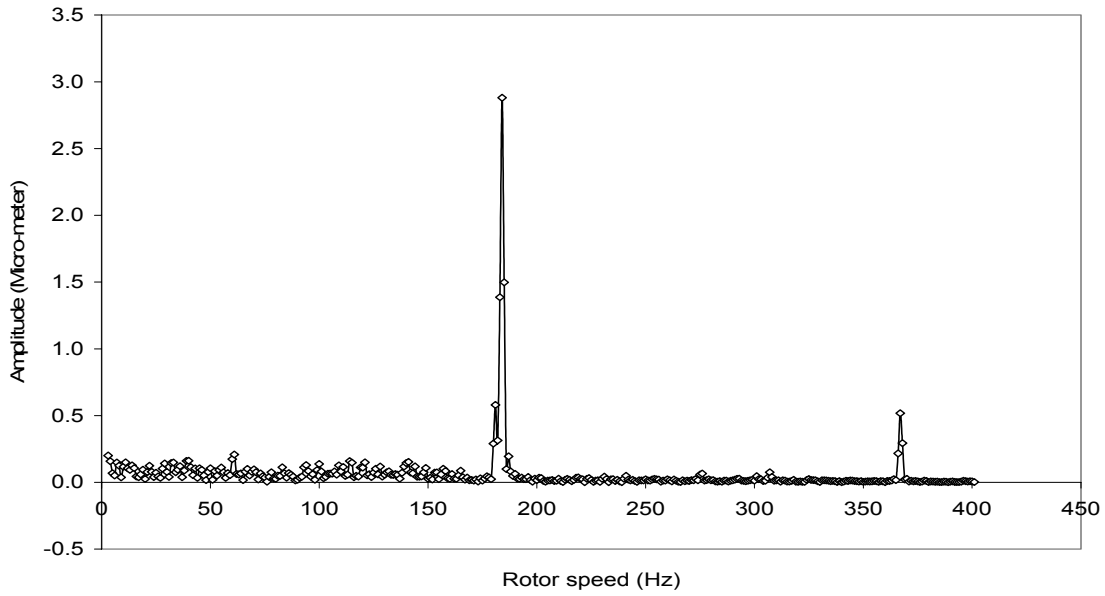

(a) 11,000 rpm

Fig. 32 Rotor frequency spectrum at 11,000 rpm, 12,000 rpm and 13,000 rpm with pressure-dam bearing

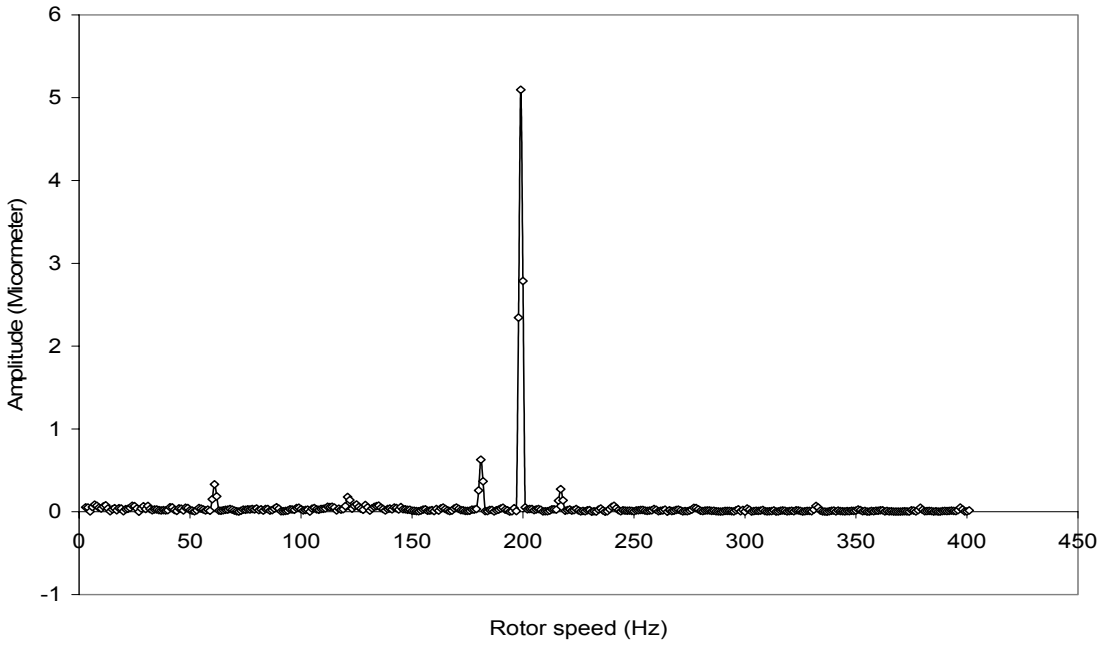

(b) 12,000 rpm

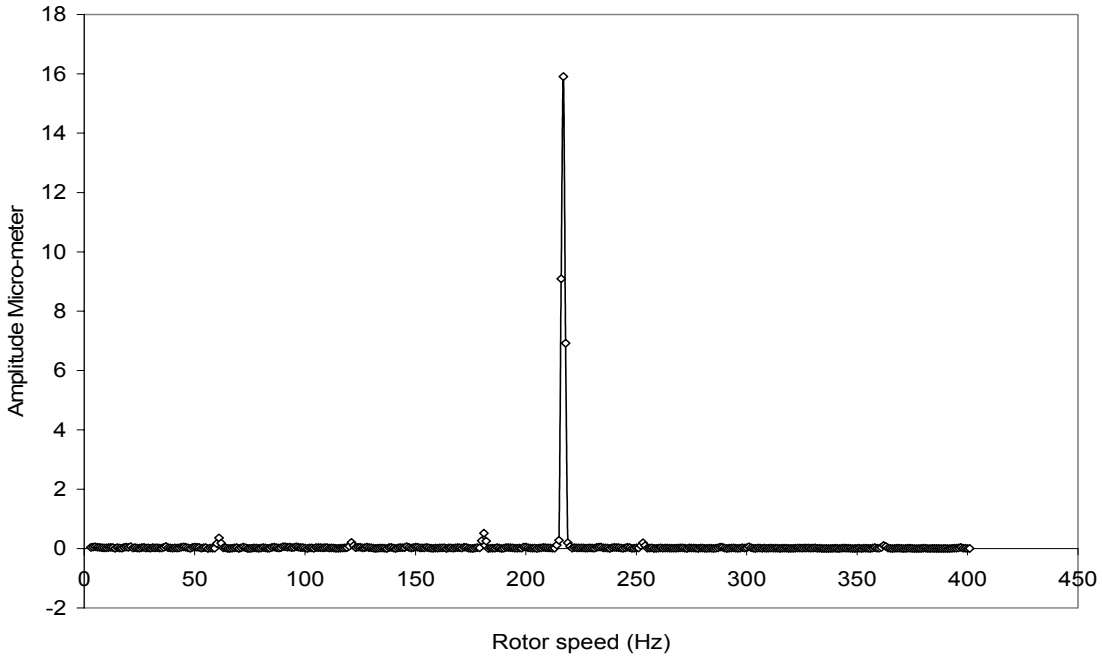

(c) 13,000 rpm

Fig. 32 “Continued”

Eccentricity

Fig. 33 shows the bearing eccentricity ratio at different rotor speeds versus Sommerfeld number. The figure also compares experimental results to $XLTRC^2$ predictions. The figure shows that, as expected, the bearing operates more eccentrically at low Sommerfeld numbers. Also, the figure shows that the bearing operates at moderate eccentricity ratios at high Sommerfeld numbers, except for 4000 rpm. This indicates that the dam is less effective at low speeds. Moreover, the figure shows that for S<0.60, the experimental eccentricity ratio is a function of Sommerfeld number. However, as Sommerfeld number increases, load decreases, eccentricity ratio increases with speed even for the same Sommerfeld number. For example, at 1.2 Sommerfeld number, the bearing eccentricity ratios are 0.41 at 6000 rpm, 0.5 at 10,000 rpm and 0.54 at 12,000 rpm. This also indicates that the dam is more effective at high speeds. Fig. 32 also shows that the bearing operates more eccentrically than predicted except for 4000 rpm at high Sommerfeld number. As explained earlier, the higher experimental eccentricity ratios compared to predictions can be contributed to an increase in the clearance due to thermal growth and the assumption of an isothermal process in the numerical solution.

Fig. 34 shows the effect of clearance on predicted eccentricity. The eccentricity ratio at the hot clearance refers to predictions at the measured clearance after the test was completed. The figure shows about a 5% increase in the predicted eccentricity ratio for low Sommerfeld numbers.

Fig. 35 compares the experimental and numerical eccentricity ratios for both the axial-groove bearing and the pressure-dam bearing. The figure shows that numerical analysis predicts that the pressure-dam bearing operates at higher eccentricity ratio. However, experimental results show that for S<0.2, both bearings operated at almost the same eccentricity ratio. For 0.2 <S<0.5, the axial-groove bearing operated slightly more eccentrically. The reason for this will be explained later. For S>0.5, the pressure-dam bearing eccentricity ratio stays almost constant at 0.50. However, the axial-groove

bearing eccentricity ratio decreased sharply. This result indicates that the pressure-dam bearing is more favorable at high Sommerfeld numbers.

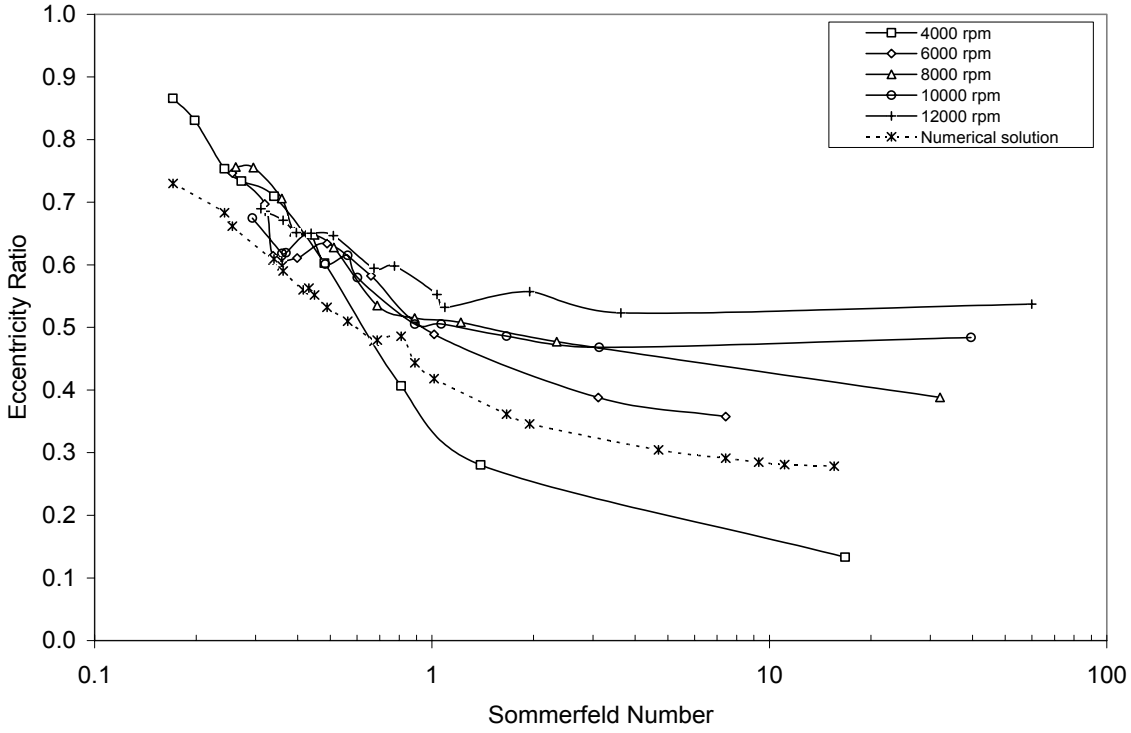

Fig. 33 Pressure-dam bearing eccentricity ratio vs. Sommerfeld number

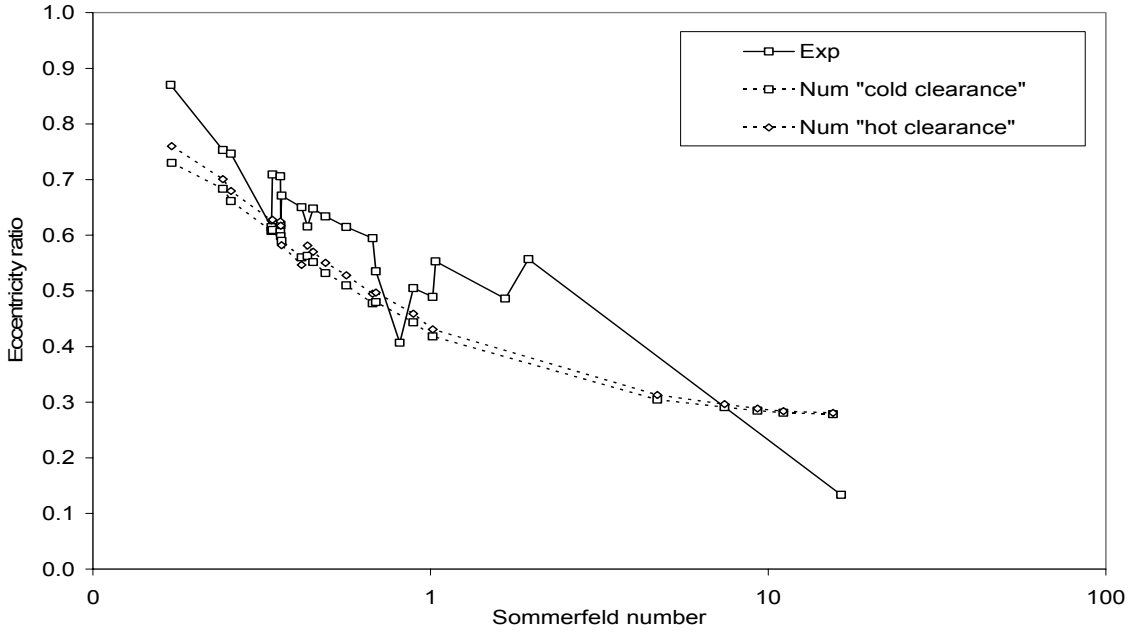

Fig. 34 Pressure-dam bearing eccentricity ratio vs. Sommerfeld number at cold and hot clearances

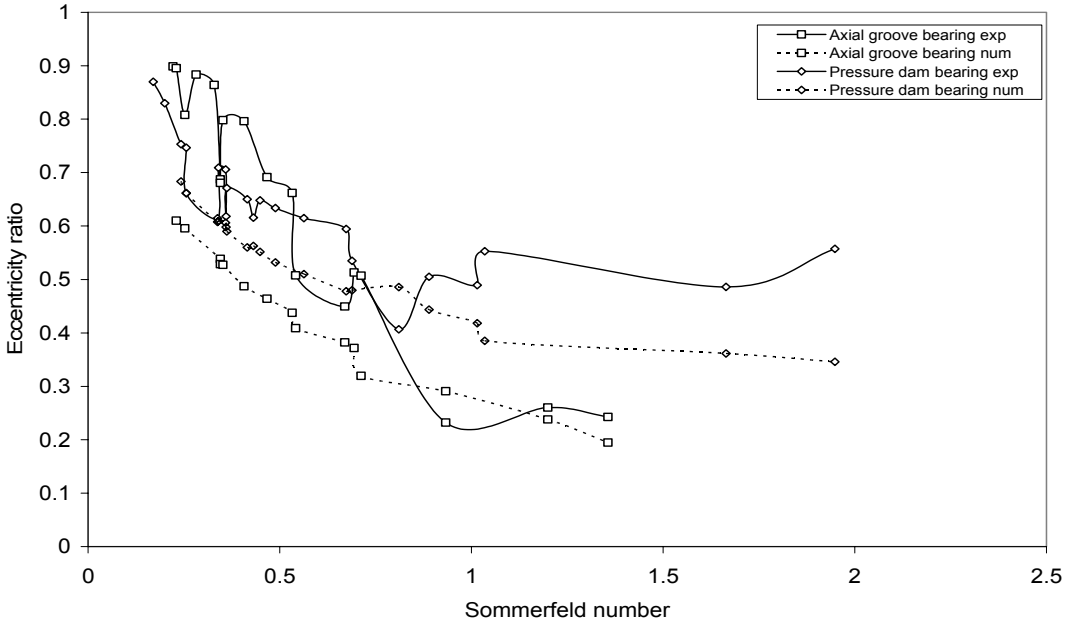

Fig. 35 Axial-groove bearing and pressure-dam bearing eccentricity ratios vs. Sommerfeld number

Attitude Angle

The attitude angle as defined in Fig. 1 is calculated from the bearing equilibrium position (e_x, e_y) using equation (18). Fig. 36 shows the bearing equilibrium position as a fraction of the bearing clearance for different test speeds at different load conditions. The figure shows that at no-load conditions, the bearing moves in the positive *x*-direction. Also, the bearing experiences higher eccentricity in the positive *x*-direction as speed increases. This displacement is mainly a result of the *x*-component of the force generated by the dam and the lateral force due to fluid rotation. Moreover, the figure shows that at all speeds, except 4000 rpm, and no-load, the bearing undergoes an eccentricity in the negative *y*-direction that increases with speed. This means that the bearing attitude angle at these conditions is higher than 90˚. This also means that the bearing needs to be loaded to be brought back to zero eccentricity in the *y*-direction which explains why the pressure-dam bearing was tested at higher loads than the axial-groove bearing at 10,000 rpm. This also explains why the pressure-dam bearing has lower eccentricity ratio for $0.2<S<0.5$. The reason for the high attitude angle is that at no-load conditions, the only acting force is the loading from the step. The direction of this force is in the fourth quadrant causing the attitude angle to be over 90˚ [12]. The figure also shows that as load is applied the bearing moves in both positive x and y direction. The displacement in the x-direction reaches maximum at moderate loads then decreases as more load is applied. The maximum x-displacement for all speeds is about 0.50-0.60.

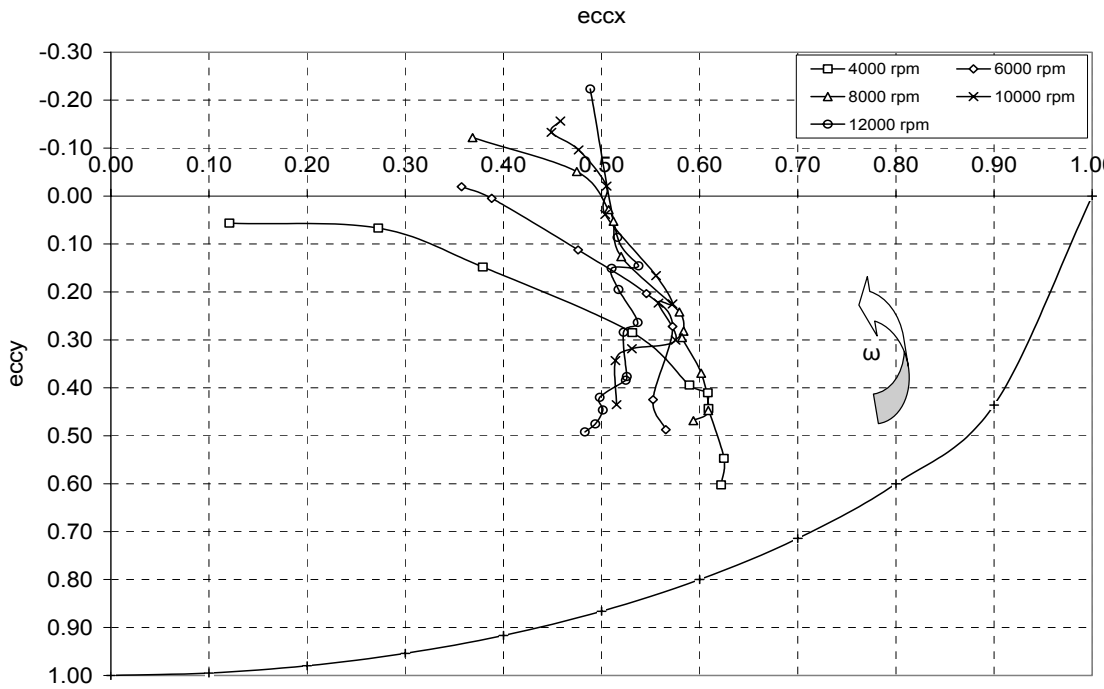

Fig. 36 Pressure-dam bearing locus plot

Fig. 37 shows the bearing attitude angle at various test conditions versus Sommerfeld number. The plot also compares calculated attitude angles to predictions. The figure shows that the attitude angle increases as the Sommerfeld number increases. Also, for S<0.80, experimental attitude angles can be considered functions of Sommerfeld number. However, for S>0.80, attitude angle depends also on the running speed. Fig. 37 also shows that the bearing attitude angles are higher than predicted. Possible reason for this is that the code under predicts the displacement in the x-direction due to step load. The x-component of the step force increases as the step angle increases [12]. Therefore, attitude angle is expected to increase as the step angle increases. Fig. 38 compares the experimental attitude angle to predictions for θ_s=130, and θ_s= 150. The figure shows that the attitude angles are more than 90º is higher for θ_s=150 at high Sommerfeld numbers.

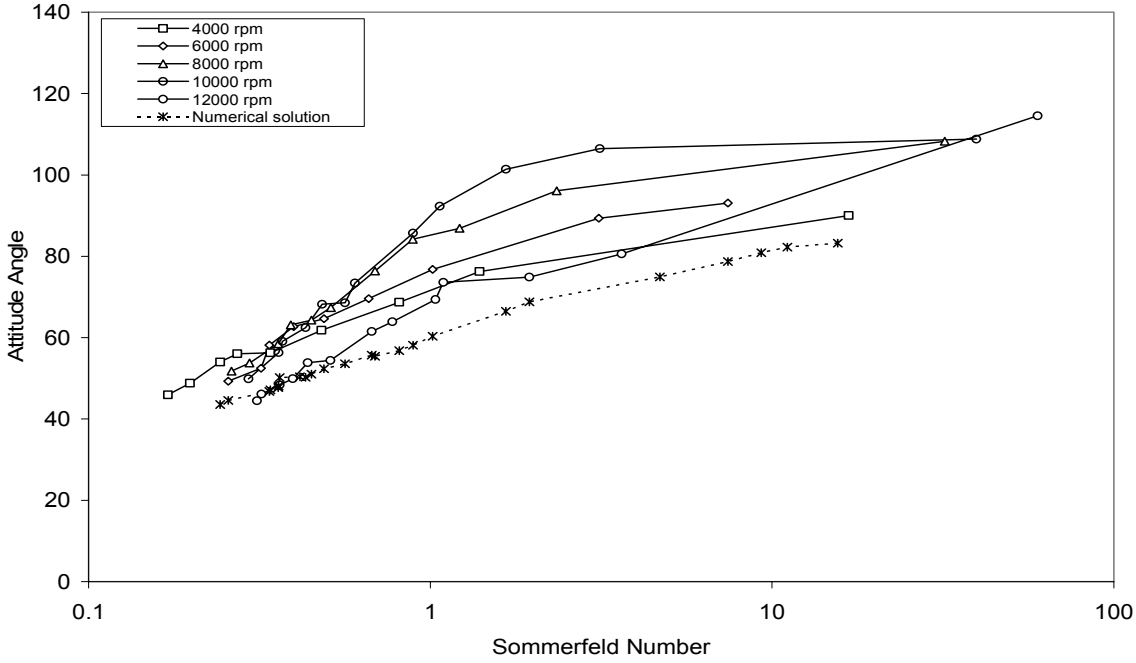

Fig. 37 Pressure-dam bearing attitude angle vs. Sommerfeld number

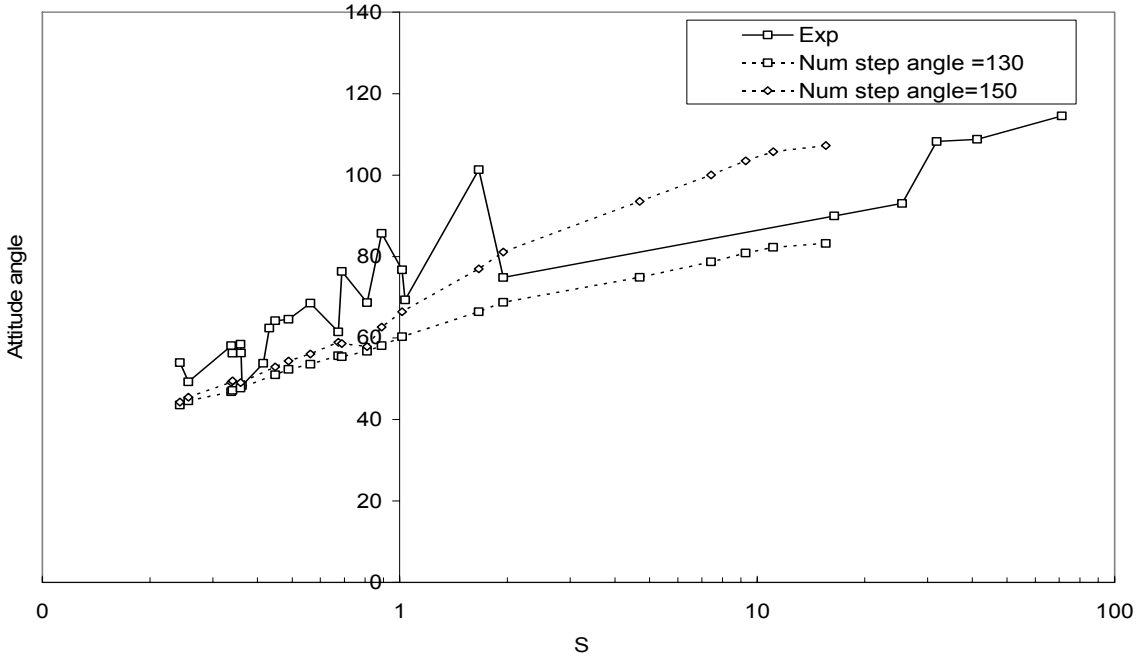

Fig. 38 Pressure-dam bearing attitude angle vs. Sommerfeld number at different step locations

Power Losses

Figs. 39 (a), (b), (c), and (d) compare the calculated power loss at different loads and speeds to predictions. Power losses are estimated using equations (19, 20, 21 and 22). Generally, numerical solution under predicts the power loss at low speeds by more than 100% at some test conditions. However, it predicts well the power loss at high speeds. The figure also shows increasing the speed increases the power loss sharply. The figure also shows that pressure-dam bearing has lower power losses than the axial-groove bearing given in Fig. 17. This is expected since the pressure-dam bearing has lower shear stress in the dam location due to the increase clearance.

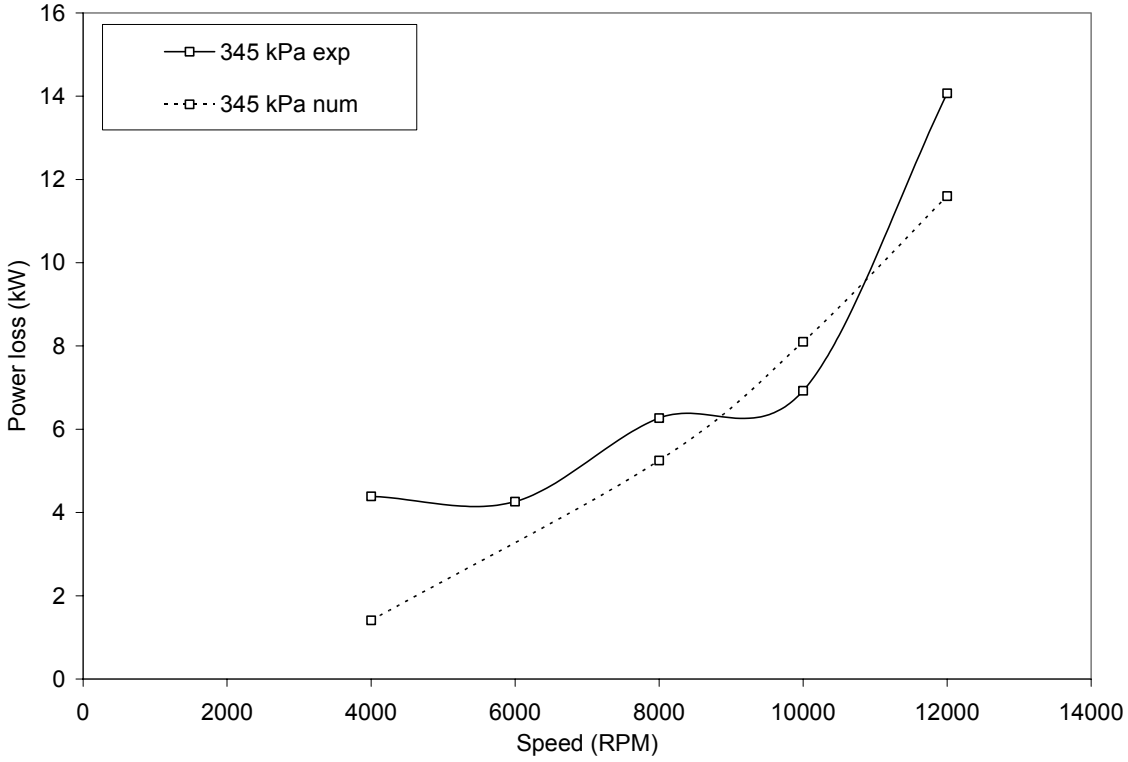

(a) 345 kPa

Fig. 39 Pressure-dam bearing power loss vs. rotor speed

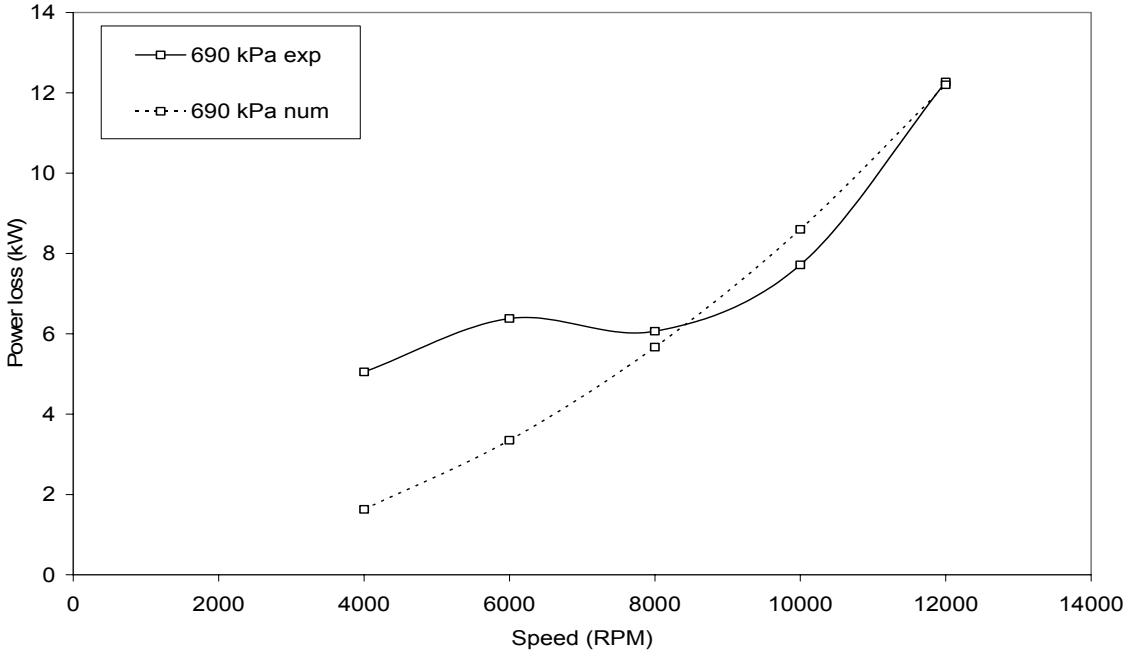

(b) 690 kPa

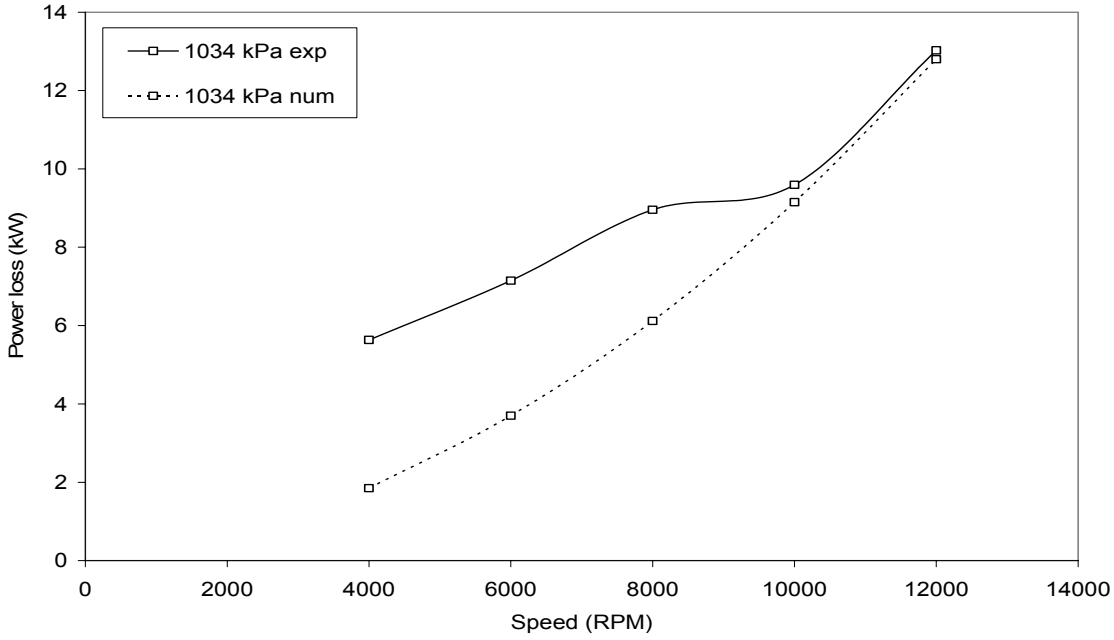

(c) 1034 kPa

Fig. 39 “Continued”

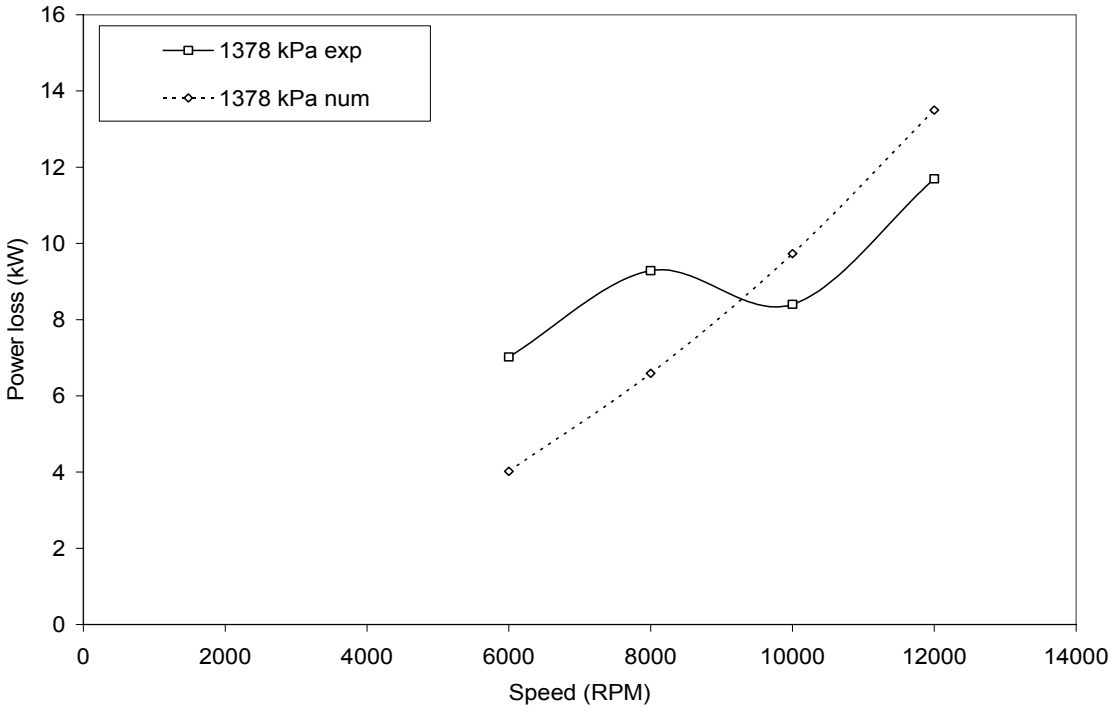

(d) 1378 kPa

Fig. 39 "Continued"

Dynamic Test Results

This section presents the results of the dynamic test for the pressure-dam bearing. The results discussed in this section include the bearing experimental and numerical force coefficients, and whirl-frequency ratio.

Stiffness Coefficients

Figs. 40 (a), (b), (c), (d), (e), and (f) show the experimental direct and cross-coupled bearing stiffness versus rotor speed at 0 kPa, 345 kPa, 690 kPa, 1034 kPa, 1379 kPa, and 1655 kPa respectively. For all figures except 40 (a), the experimental results are compared to the stiffness values obtained by the numerical solutions. The numerical solution is undefined at the no-load condition. Therefore, in Fig. 40 (a), the numerical solution at 33 kPa is shown. The uncertainties of the experimental results are given by

the error bars of the data and they are below ±15% in most cases. Generally, the experimental stiffness coefficients follow the same trend as predicted values except for K_{yy} at 12,000 rpm, high load conditions. While the numerical results show that K_{yy} decreases as speed increases at 1034 kPa, 1379 kPa, and 1655 kPa , the experimental results show that K_{yy} decreases up to 10,000 rpm; then, it increases sharply. This increase causes the bearing whirl-frequency ratio to decrease at 12,000 rpm as will be shown later. The figures also show that the bearing stiffnesses K_{yy} and K_{xx} increase as speed increases at no and low-load conditions (0 kPa, 345 kPa, and 690 kPa). This increase is caused by the increase in the step load as speed increases which results in higher eccentric operation. Furthermore, the figures show that at all test conditions, the bearing experimental direct stiffness K_{yy} and K_{xx} values are lower than predicted. The minimum difference between predicted and measured direct stiffness is less than 1% for K_{yy} at 10,000 rpm and 12,000 rpm with 345 kPa unit load. However, the maximum difference between predicted and measured direct stiffness is about 100% for K_{yy} at 4000 rpm with 345 kPa. This result is attributed to the result from Fig. 33 which shows that the bearing operated at lower eccentricity ratio than predicted at this condition. This also indicates that the dam is less effective at low speeds.

Moreover, the figures show that the bearing cross-coupled stiffness K_{xy} and K_{yx} increase as speed increases at light load. However, it tends to level off at high loads. The figures also show good agreement between experimental and predicted K_{xy} values. However, the numerical solution over predicts K_{yx} values at all test conditions. The maximum difference is 48% at 10,000 rpm and 1034 kPa. As discussed in the axial-groove bearing test results section above, the difference between the experimental and predicted stiffness values can be attributed to the increase in the bearing clearance due to thermal growth.

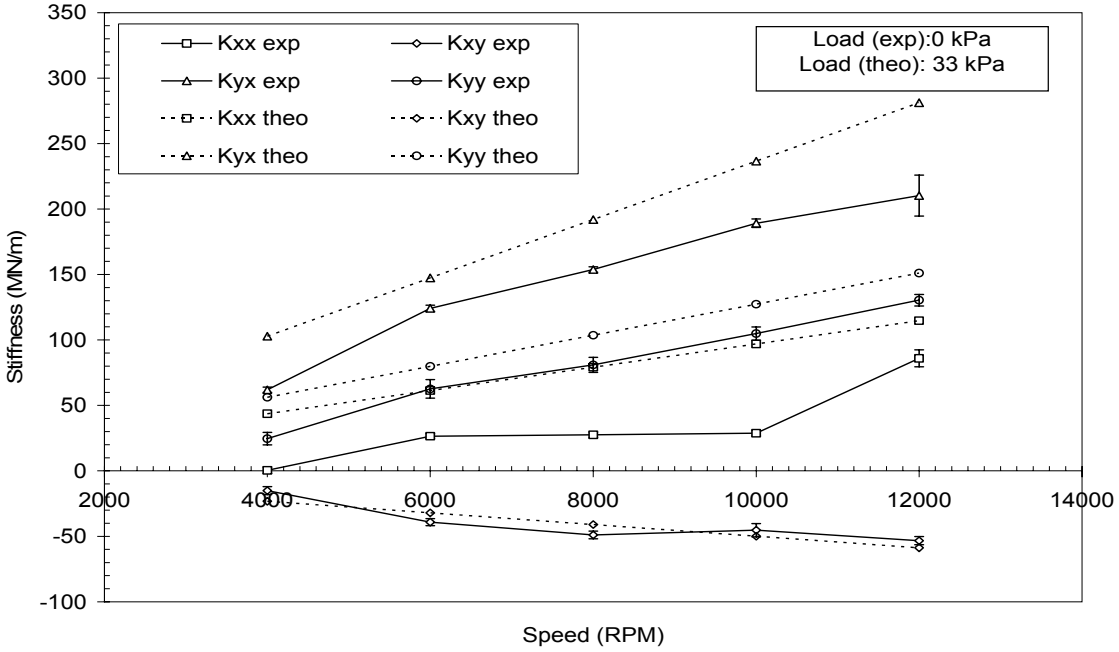

(a) 0 kPa

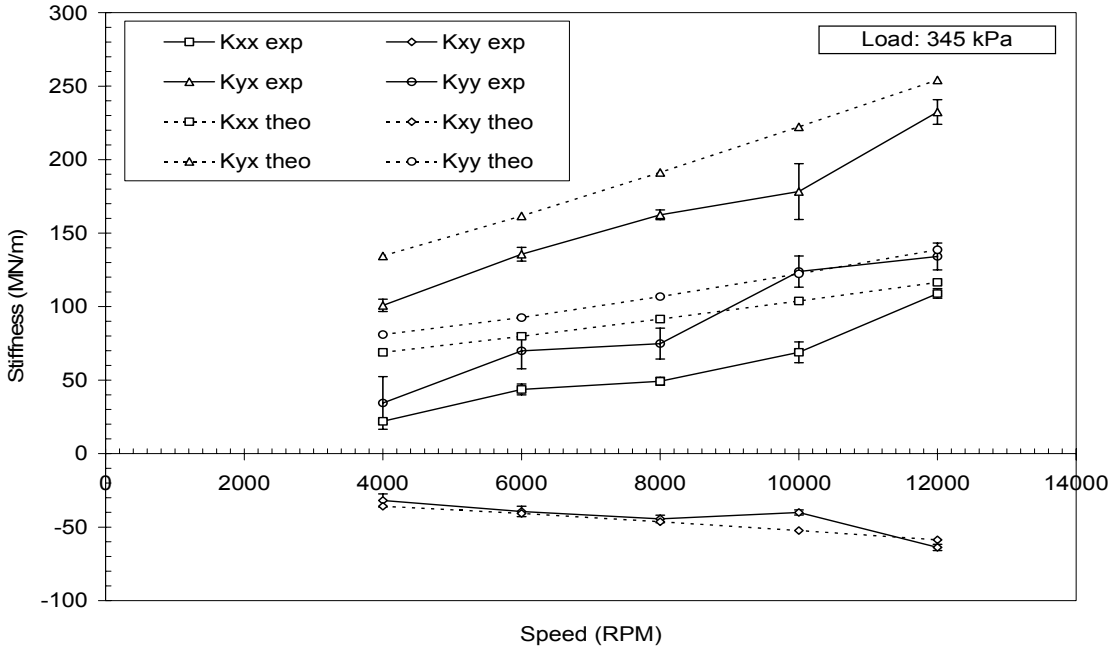

(b) 345 kPa

Fig. 40 Pressure-dam bearing stiffness coefficients

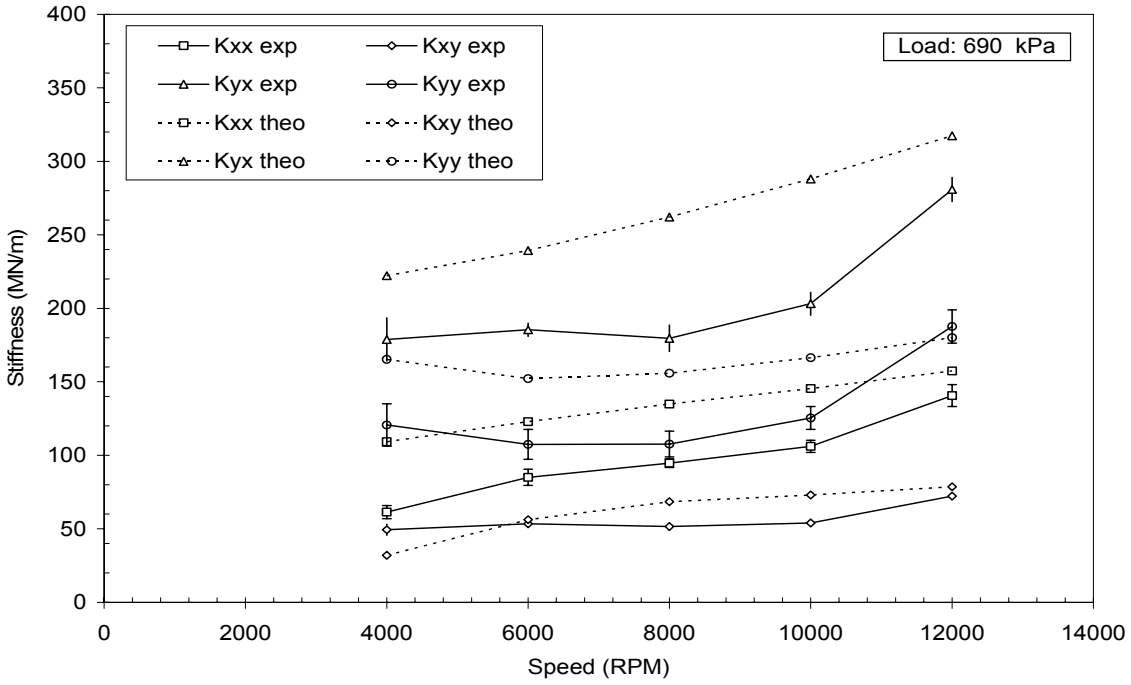

(c) 690 kPa

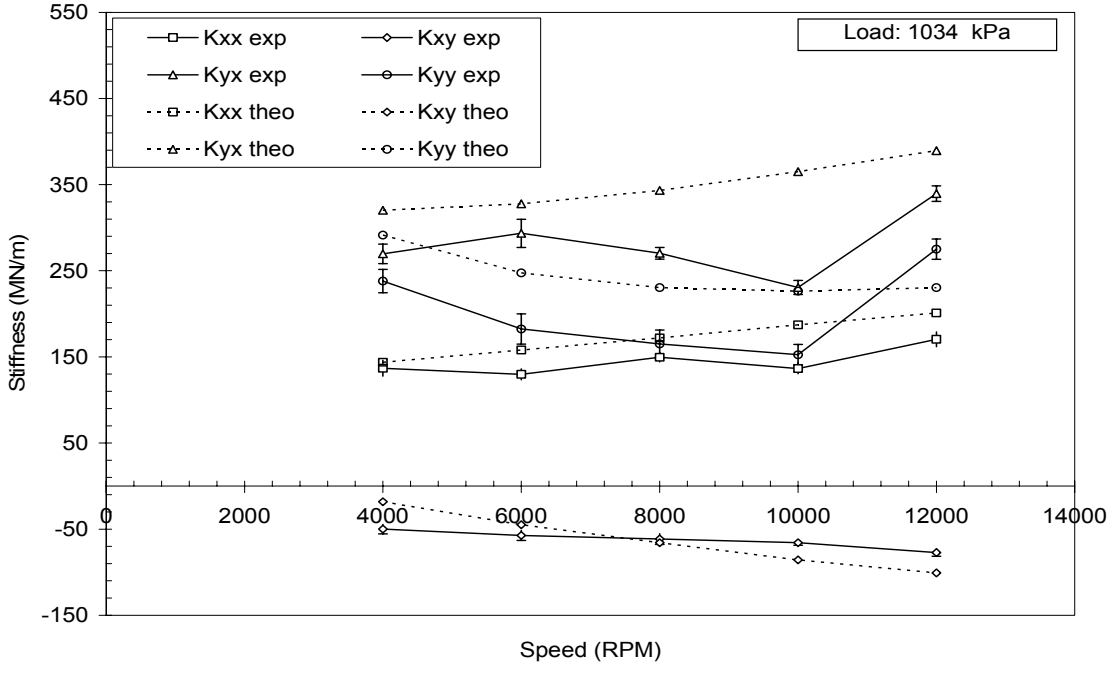

(d) 1034 kPa

Fig. 40 “Continued”

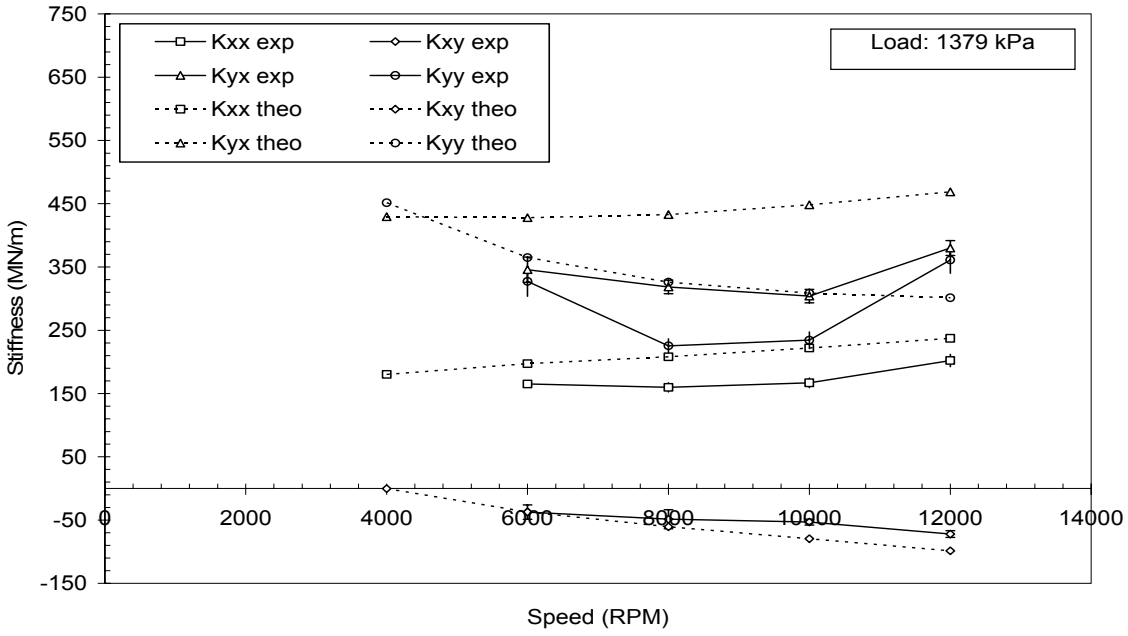

(e) 1379 kPa

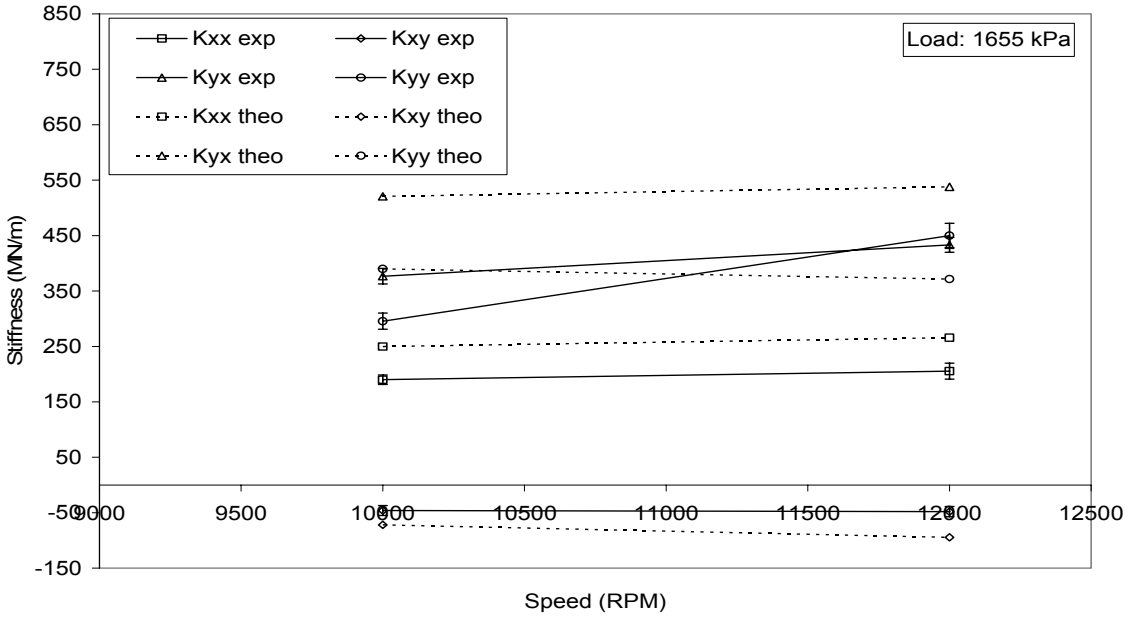

(f) 1655 kPa

Fig. 40 “Continued”

Figs. 41 (a), (b), (c), and (d) show the effect of clearance increase on the bearing stiffness coefficients at 690 kPa. The figures show that increasing the clearance decreases all four stiffness coefficients by about 10% at high speeds. Thus, it reduces the difference between experimental values and predictions by 25% at some points.

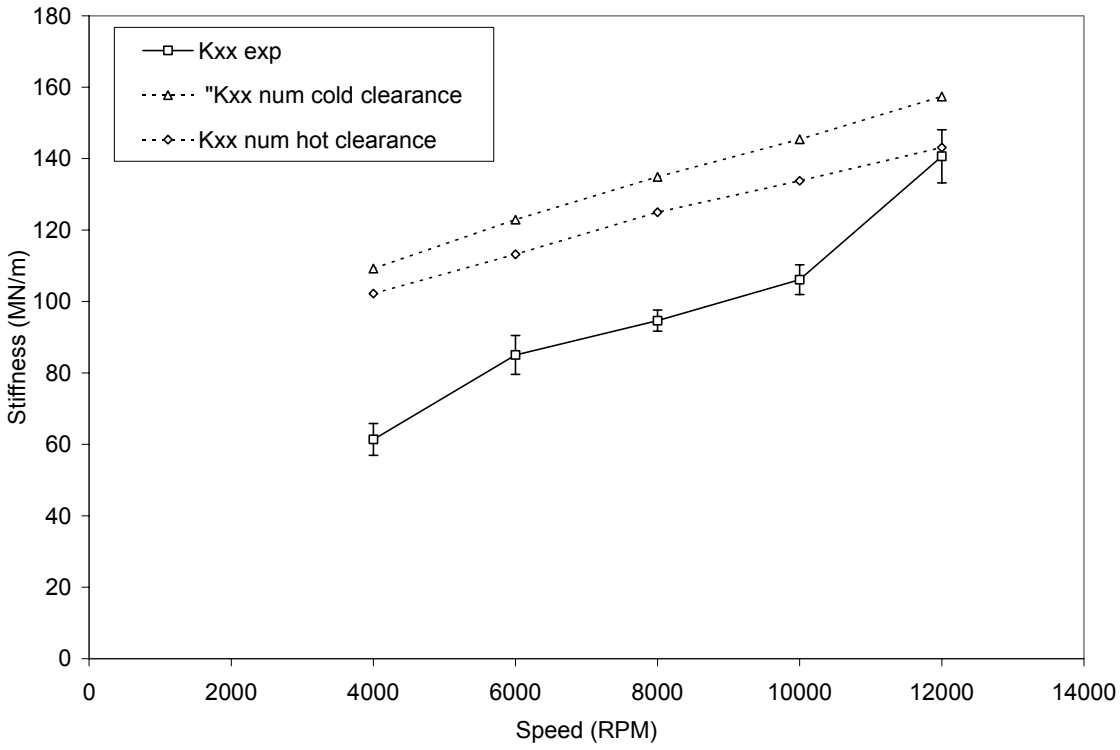

(a) K_{xx}

Fig. 41 Pressure-dam bearing stiffness coefficients at different bearing clearances

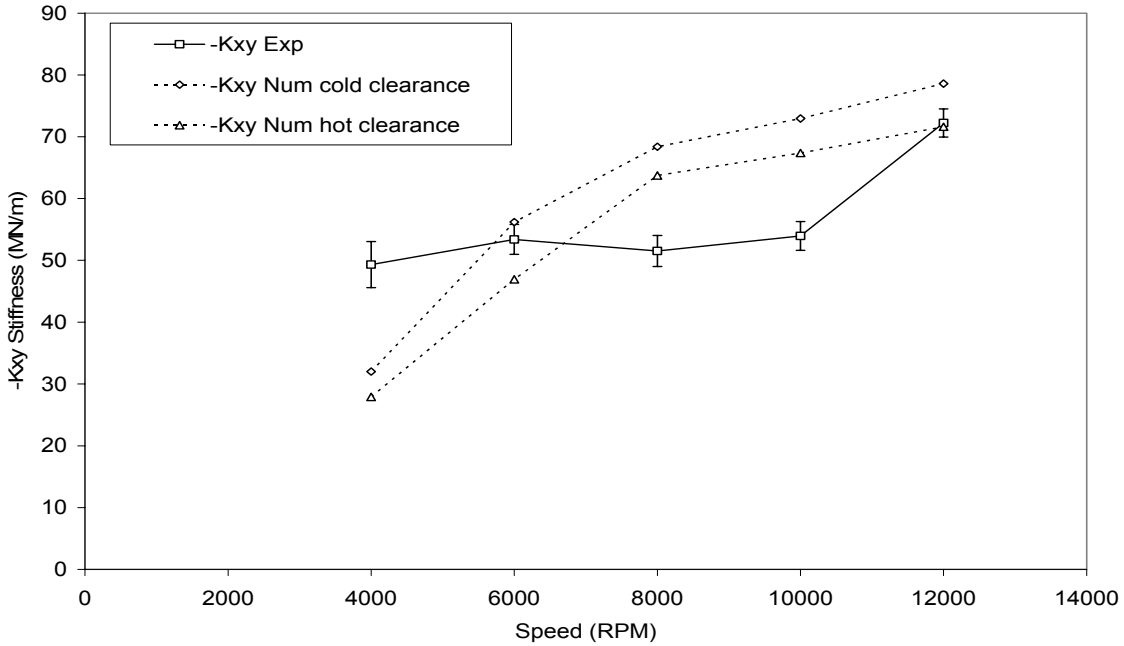

(b) $-K_{xy}$

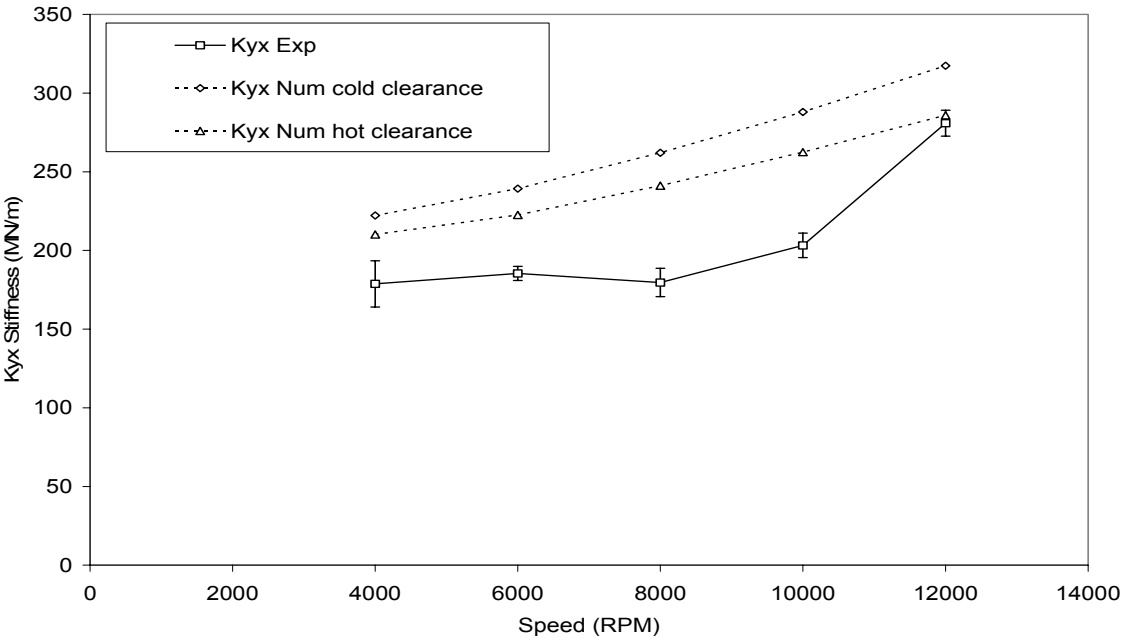

(c) K_{yx}

Fig. 41 “Continued”

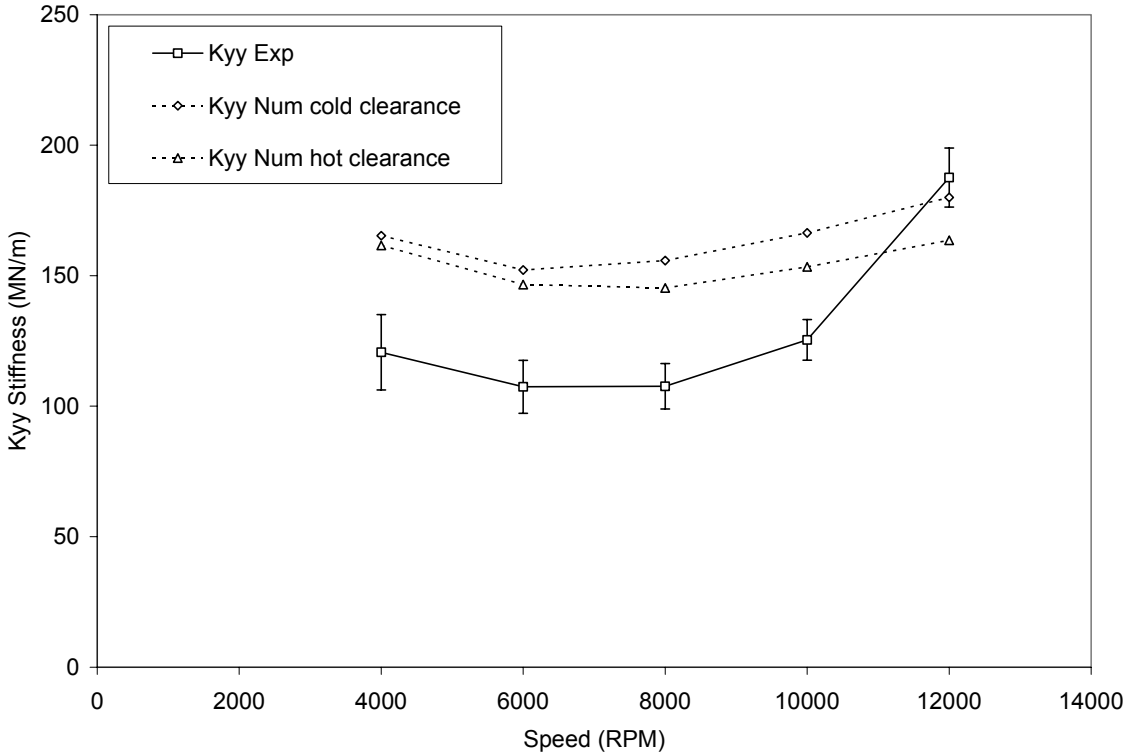

(d) K_{yy}

Fig. 41 "Continued"

Figs. 42 (a), and (b) compare the non-dimensional experimental and numerical direct and cross stiffness coefficients as predicted at the cold clearance versus Sommerfeld number. Fig. 42 (a) shows that experimental k_{xx} is almost constant up to S =1.0 (except for 0.34 and 0.81 Sommerfeld number which corresponds to 4000 rpm with 345 kPa, and 690 kPa); then, it increases. On the other hand numerical k_{xx} increases as Sommerfeld number increases. Fig. 42 (a) also shows that k_{yy} decreases as Sommerfeld number increases up to S=0.90 then, it increases. (The three points that shows high k_{yy} at 0.36, 0.41, and 0.67 Sommerfeld number corresponds to the 12,000 rpm high load conditions which were discussed above). Numerical k_{yy} values show the same trend as experimental values except for the 12,000 rpm with high load conditions. The figure also shows that the difference between numerical and experimental and experimental k_{xx} and

k_{yy} is within 1-185%. Fig. 42 (b) shows that both experimental and numerical k_{xy} and k_{yx} values increases as Sommerfeld number increases. The figure also shows that the difference between experimental and numerical values is within 1-48%.

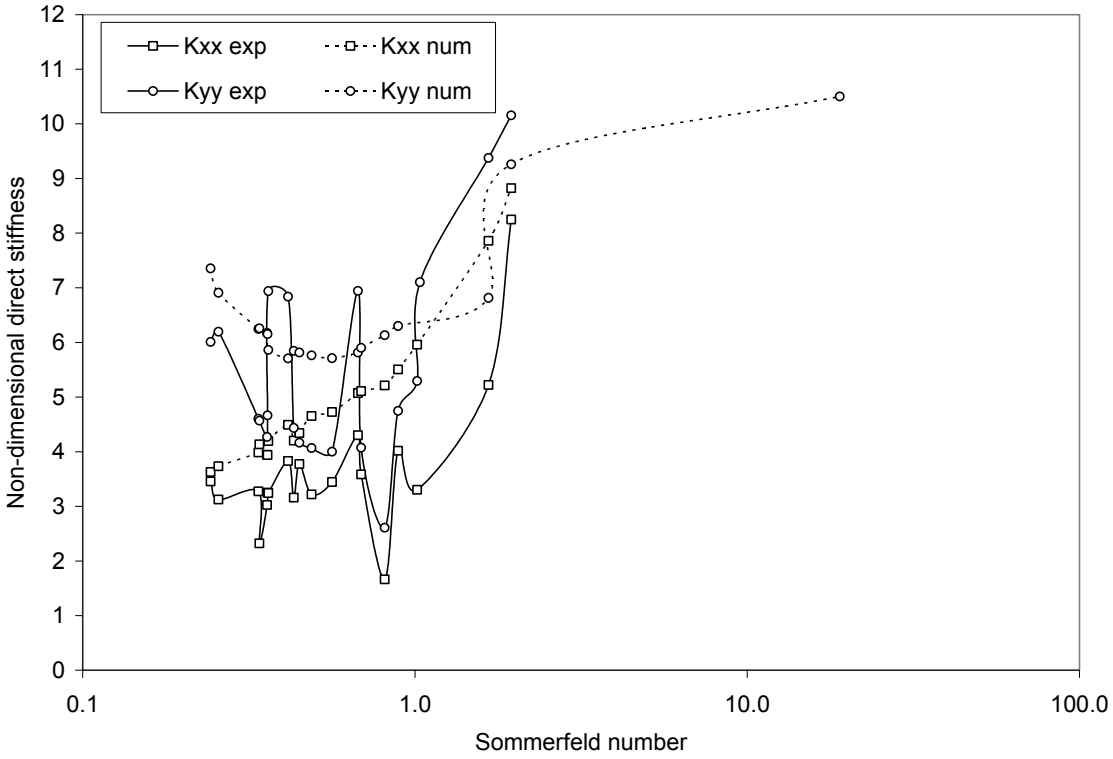

(a) Direct stiffness

Fig. 42 Pressure-dam bearing non-dimensional stiffness vs. Sommerfeld number

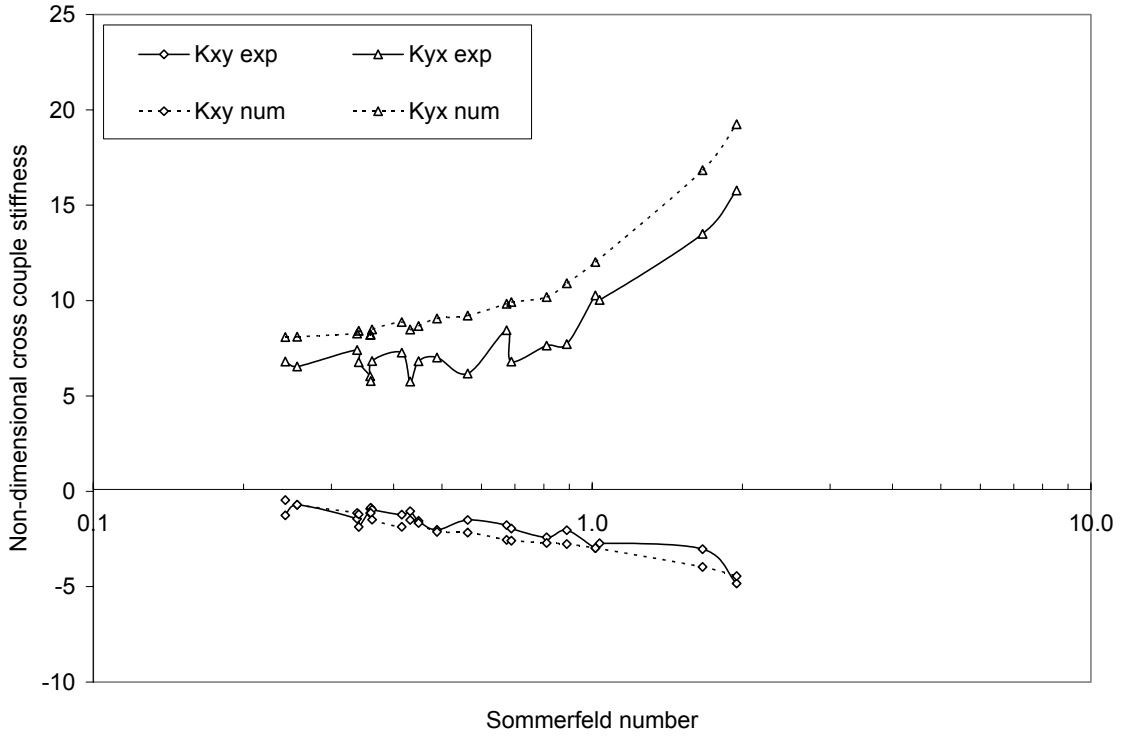

(b) Cross-coupled stiffness

Fig. 42 "Continued"

Figs. 43 (a), (b), (c), (d), and (e) compare the bearing stiffness as estimated using equation (49). Similar to the axial groove bearing results in Figs. 26, Figs. 43 show that the static stiffness determined from the force-displacement curve is lower than the stiffness estimated from the bearing force coefficients at zero frequency. However, the figures show better agreement at low load conditions except for 4000 rpm.

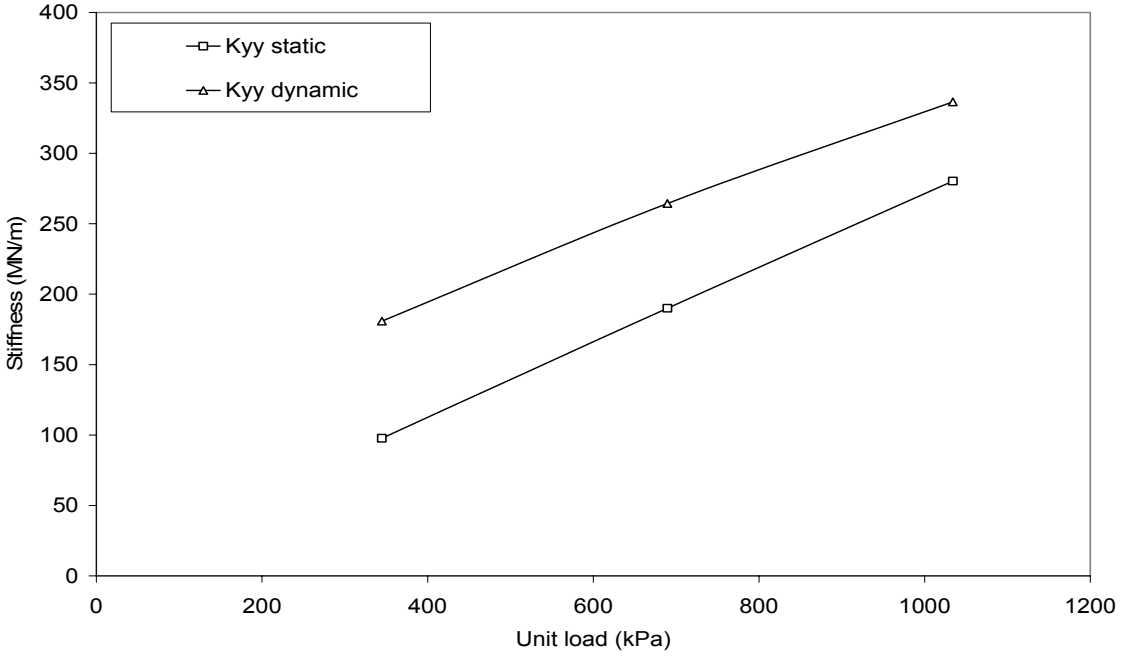

(a) 4000 rpm

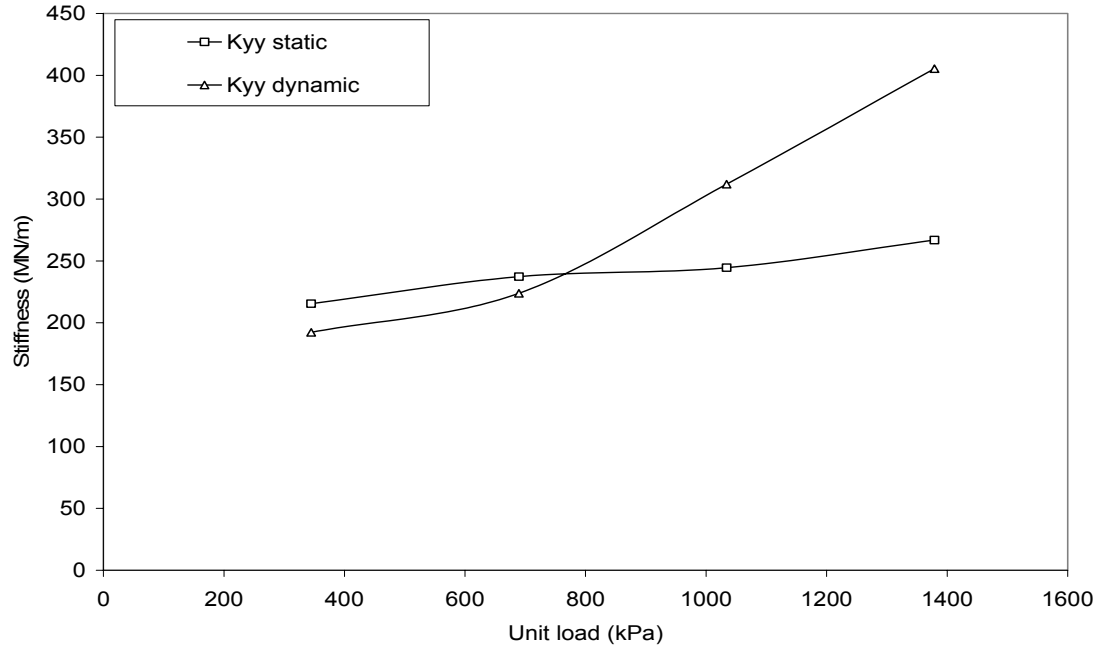

(b) 6000 rpm

Fig. 43 Pressure-dam bearing direct stiffness from static and dynamic tests

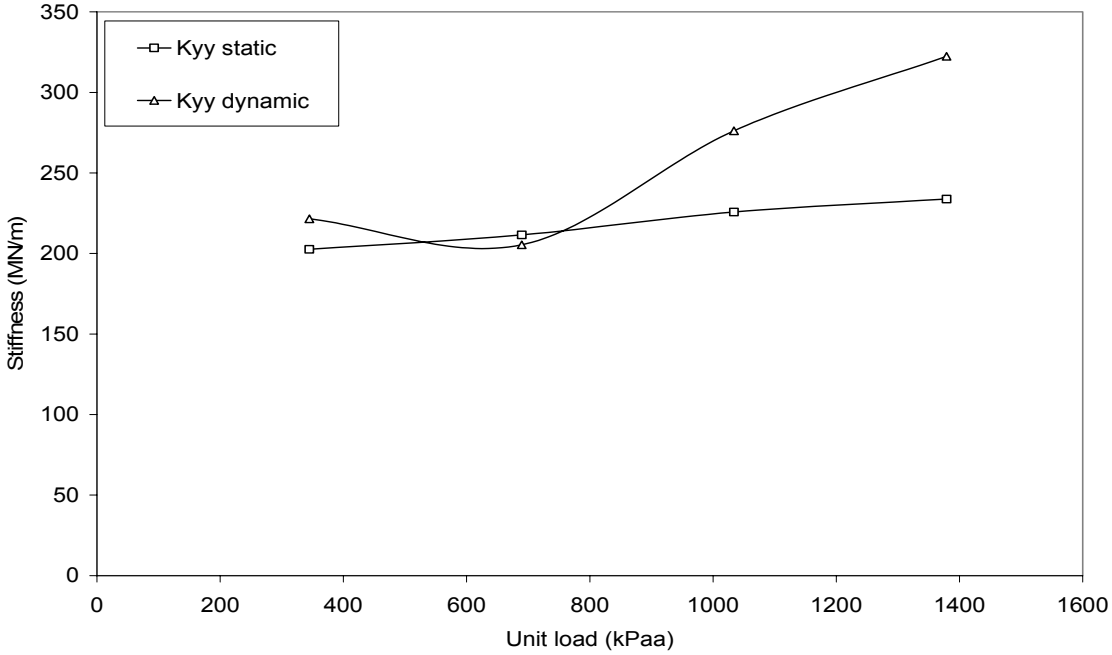

(c) 8000 rpm

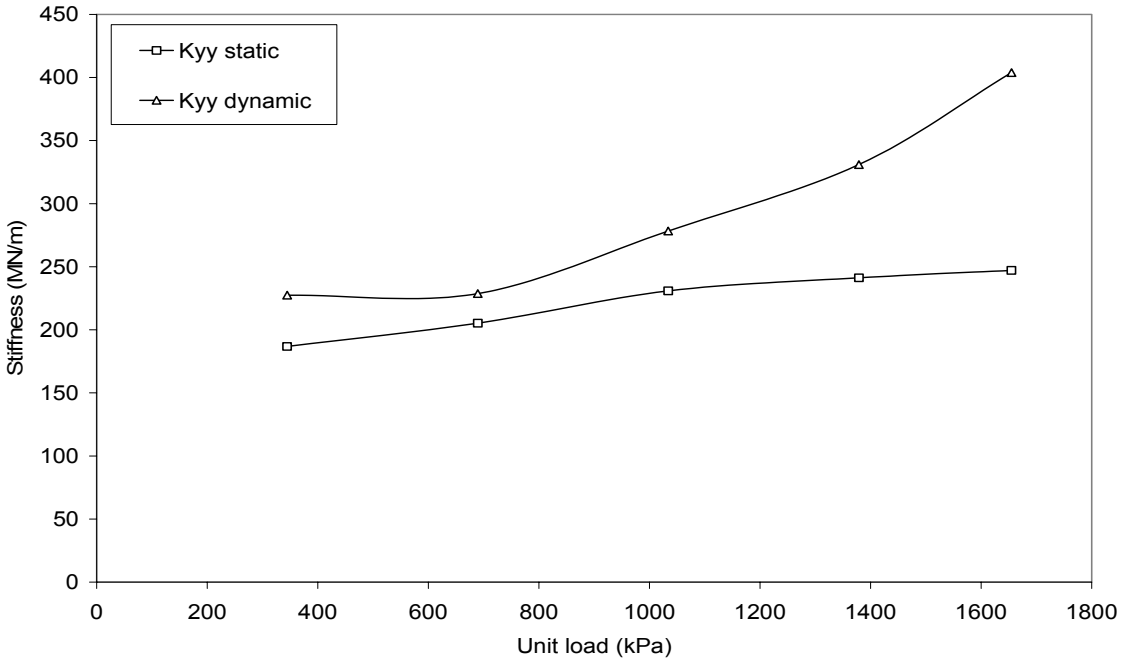

(d) 10,000 rpm

Fig. 43 “Continued”

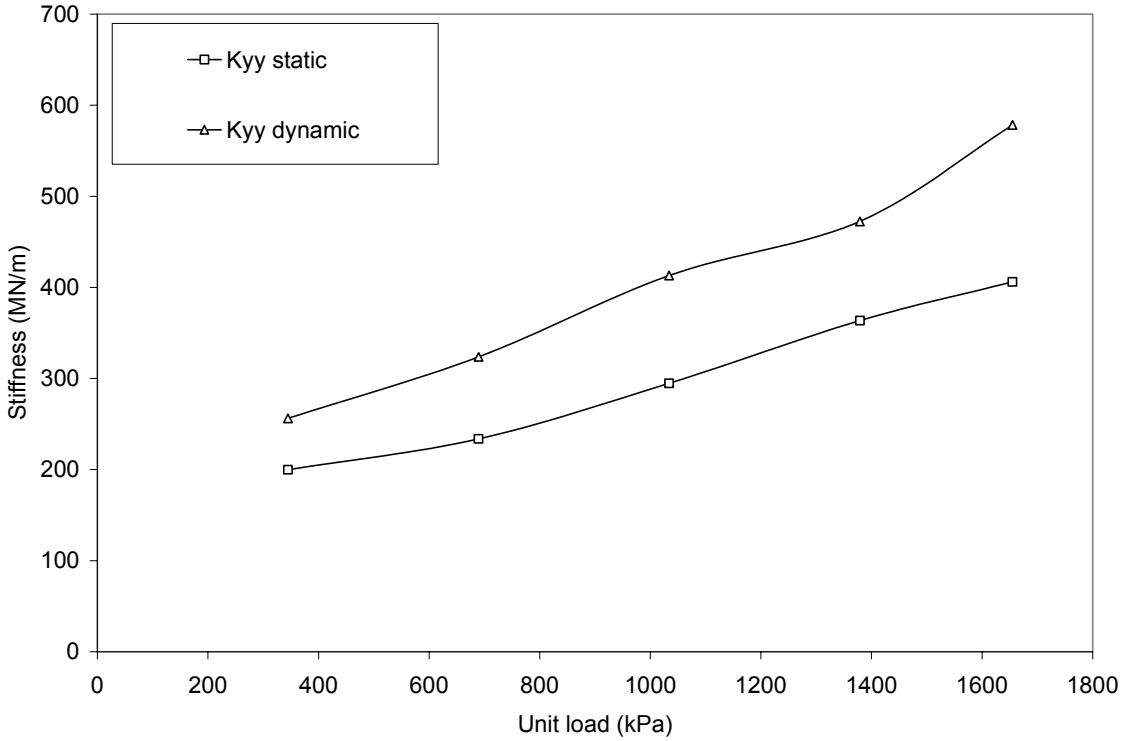

(e) 12,000 rpm

Fig. 43 "Continued"

Figs. 44 (a), (b), (c), and (d) compare experimental stiffness coefficients for both the pressure-dam bearing and the axial-groove bearing at 345 kPa and 1379 kPa. Unlike the axial-groove bearing, Fig. 44 (a) shows that the pressure-dam bearing develops significant direct stiffness at high speeds even at low load conditions because of its eccentric operation at these conditions. However, the figure also shows that the pressure-dam bearing has almost equivalent stiffness to the axial-groove bearing at 4000 rpm because of its low eccentricity. Fig. 44 (b) shows that both bearings have equivalent K_{xy} at low speeds. However, the pressure-dam bearing has lower K_{xy} at high speeds. The figure also shows that pressure-dam bearing has higher K_{yx} at all speeds. Figs 44 (c) and (b) show that as load increases, the difference between the bearings' experimental

stiffness coefficients K_{xx} and K_{yy} diminish although higher stiffness coefficients are predicted for the pressure-dam bearing.

The figure also shows that the pressure-dam bearing has lower K_{yy} at 8000 rpm and 10,000 rpm. The reason for this is that the pressure-dam bearing operates at lower eccentricity ratio at these speeds. The reason for the low eccentricity is that, at no-load the bearing moves in the negative y-direction. Fig. 44 (c) also shows that both bearings have almost equal cross-coupled stiffness coefficients K_{xy} and K_{yx} even higher values are predicted especially for the pressure-dam bearing K_{yx}

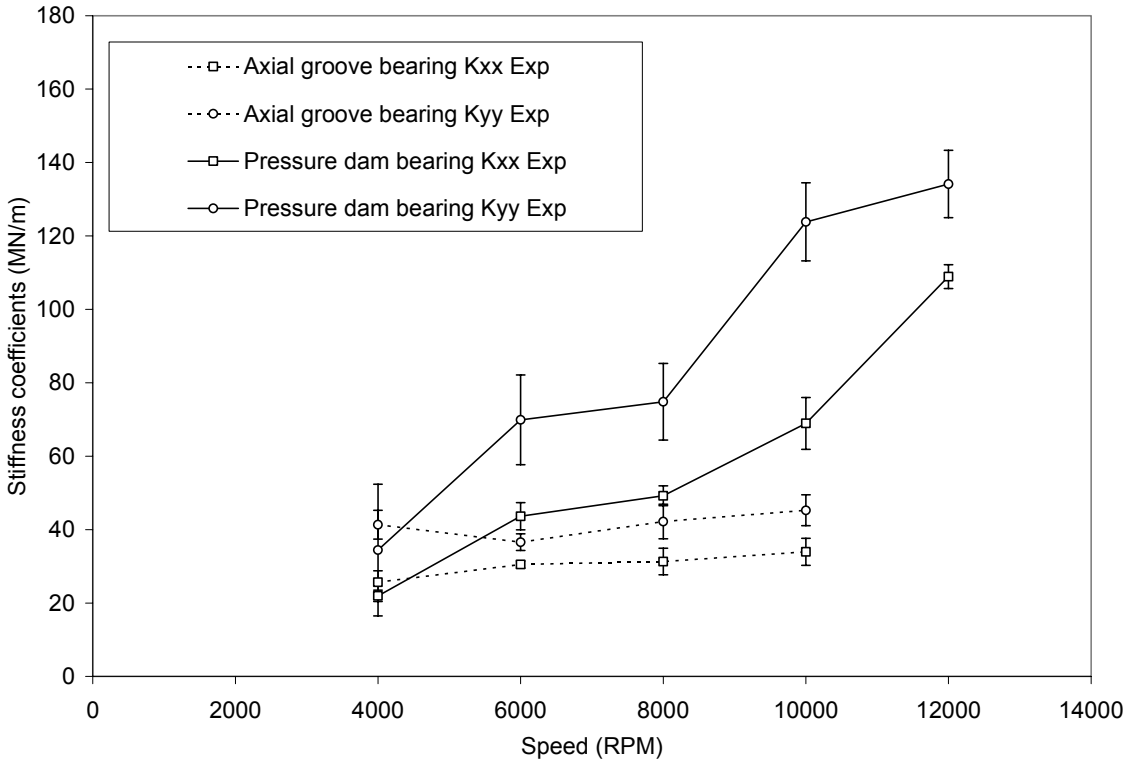

(a) K_{xx} & K_{yy} at 345 kPa

Fig. 44 Axial-groove bearing and pressure-dam bearing stiffness comparison

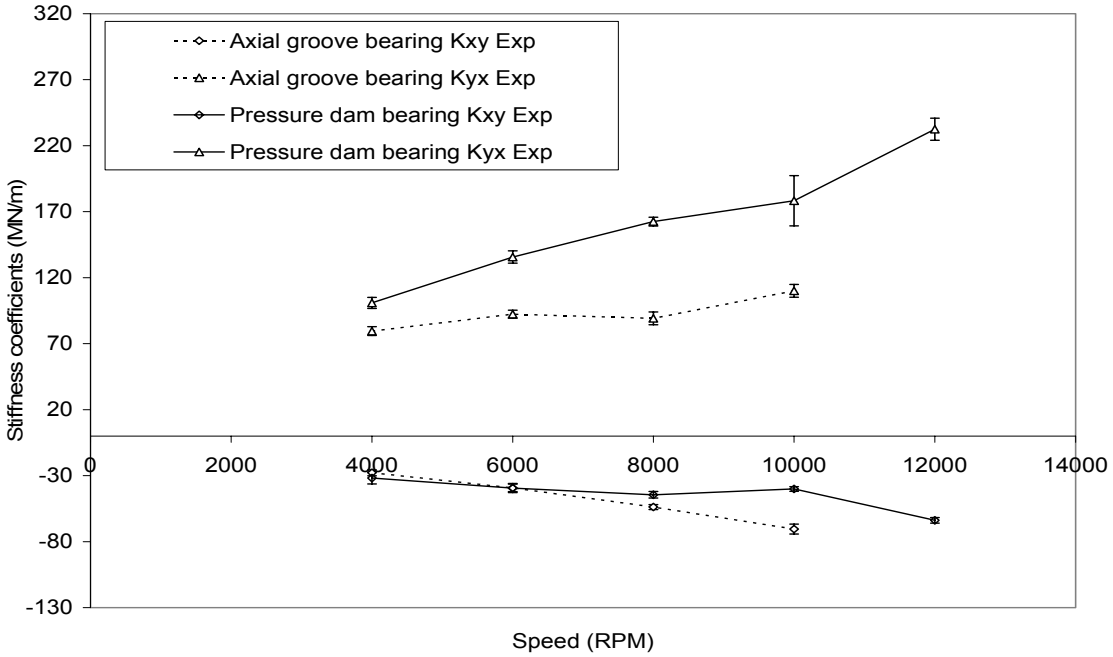

(b) K_{xy} & K_{yx} at 345 kPa

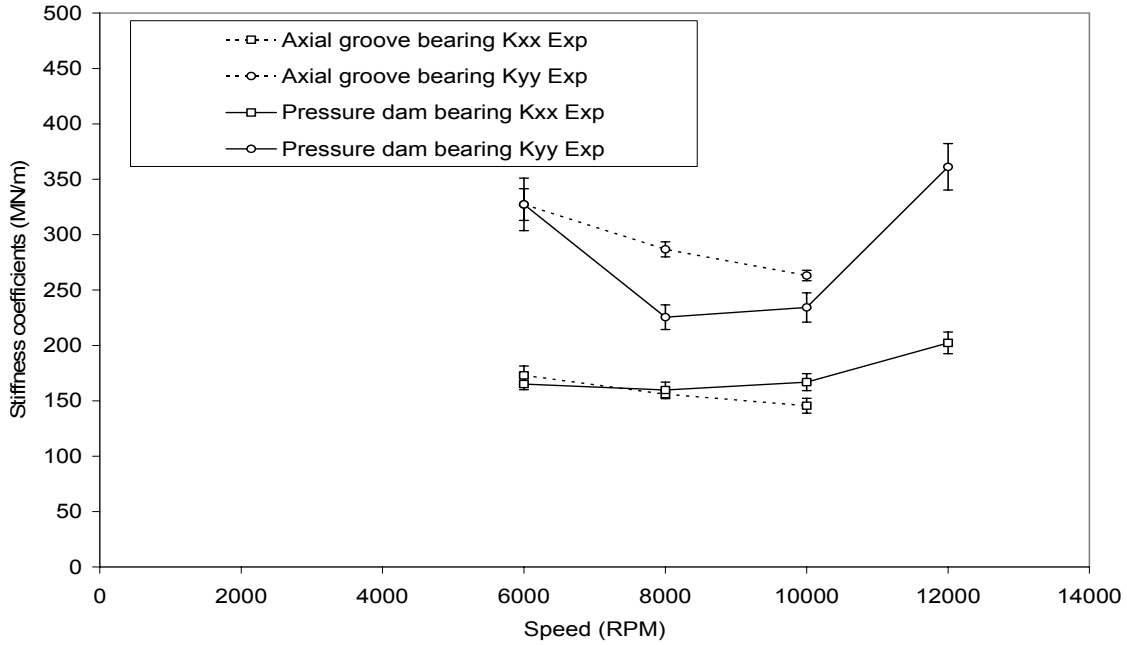

(c) K_{xx} & K_{yy} at 1379 kPa

Fig. 44 “Continued”

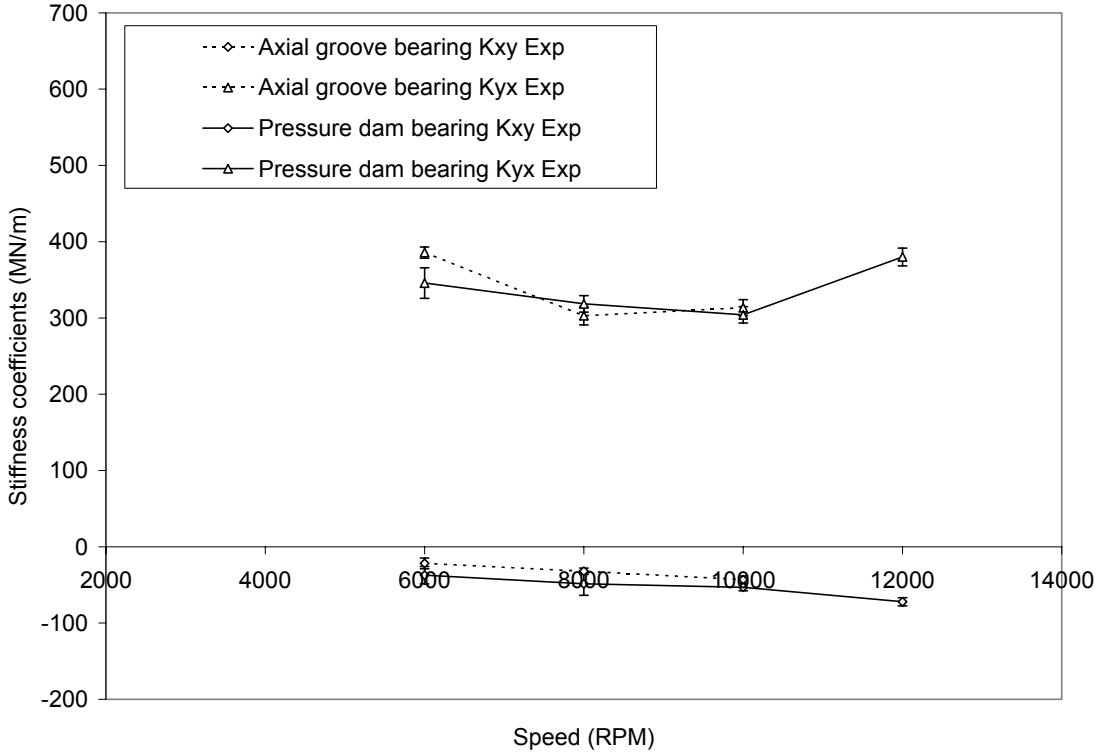

(d) K_{xy} & K_{yx} at 1379 kPa

Fig. 44 "Continued"

Damping Coefficients

Figs. 45 (a), (b), (c), (d), (e), and (f) show the experimental direct and cross-coupled bearing damping versus rotor speed at 0 kPa, 345 kPa, 690 kPa, 1034 kPa, 1379 kPa, and 1655 kPa respectively. For all figures except 45 (a), the experimental results are compared to the damping values obtained by the numerical solutions. The numerical solution is undefined at the no-load conditions. Therefore, in Fig. 45 (a), the numerical solution at 33 kPa is shown. The uncertainties of the experimental results are given by the error bars of the data and they are about ±10% in most cases.

Generally, the experimental damping coefficients decrease as speed increases; as predicted. However, as in the case of the experimental direct stiffness K_{yy}, the

experimental direct damping C_{yy} decreases as speed increases up to 10,000 rpm then, it increases at 12,000 rpm. This also helped reduce the *WFR* at 12,000 rpm as will be shown later. The code over predicts the damping coefficients at all test conditions. However, it better predicts the damping coefficients at low load conditions.

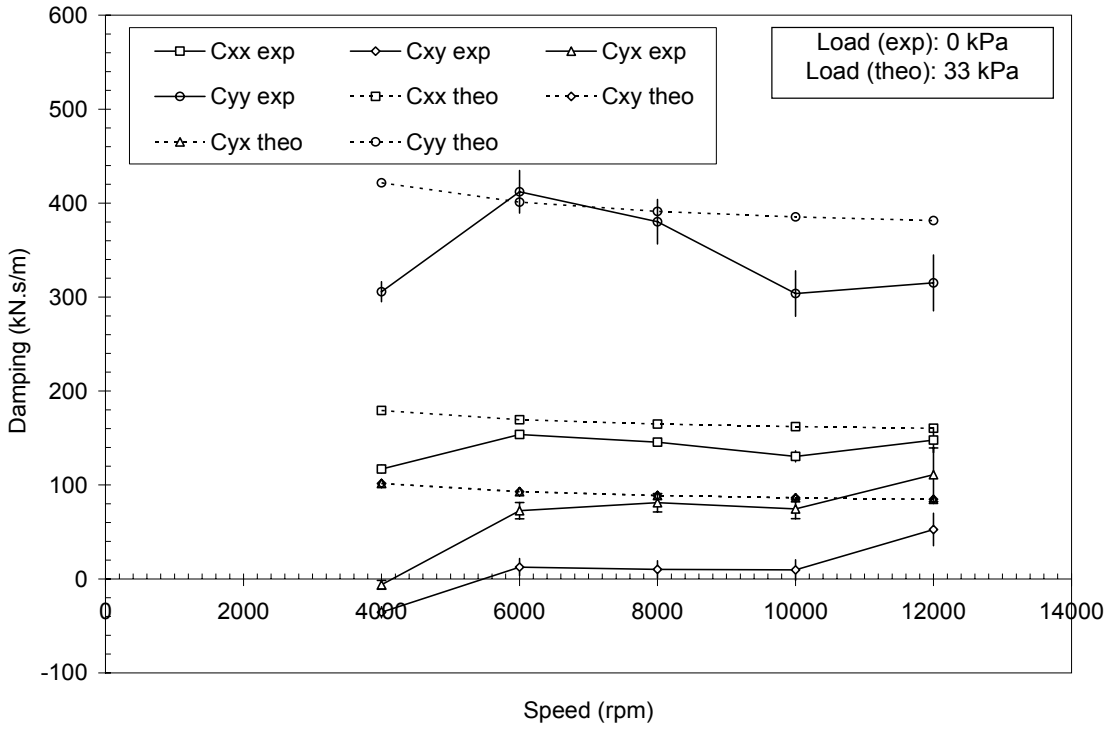

(a) 0 kPa

Fig. 45 Pressure-dam bearing damping coefficients

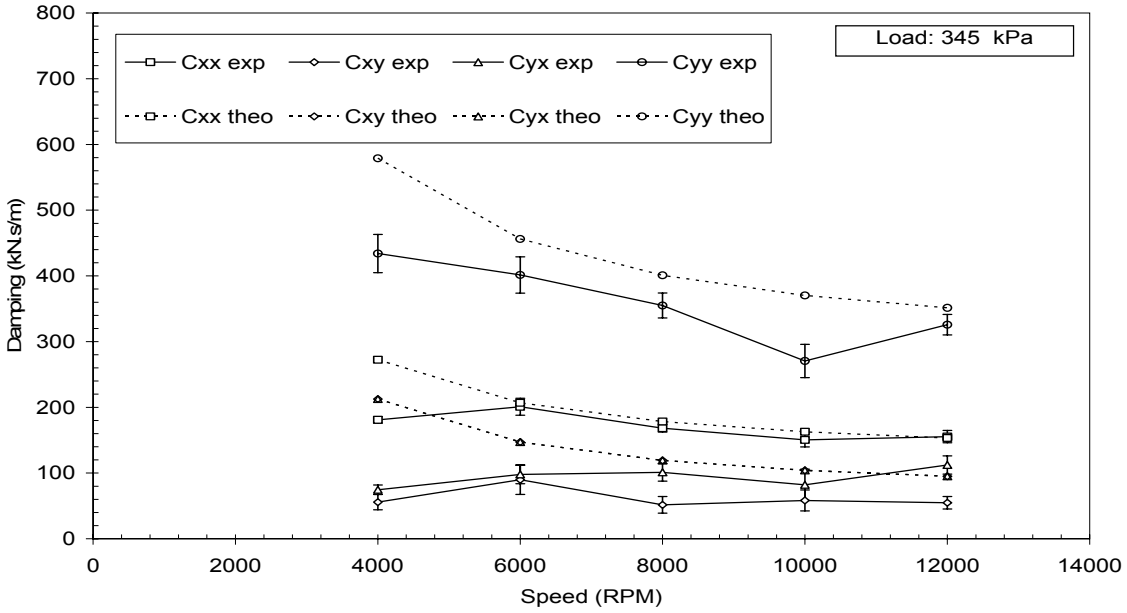

(b) 345 kPa

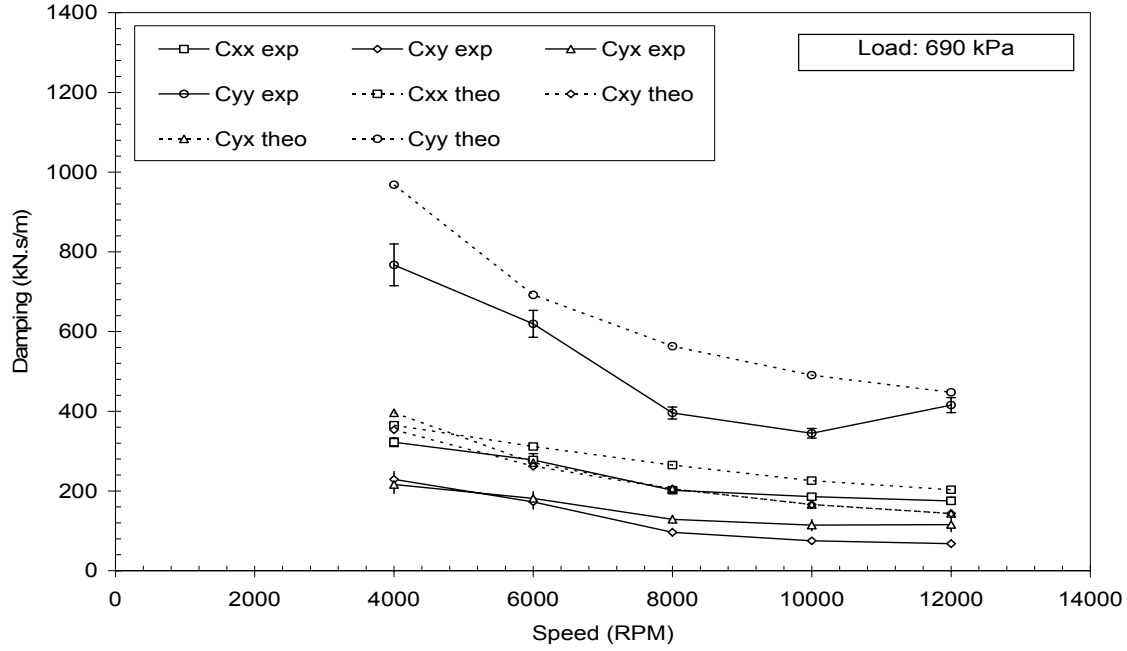

(c) 690 kPa

Fig. 45 “Continued”

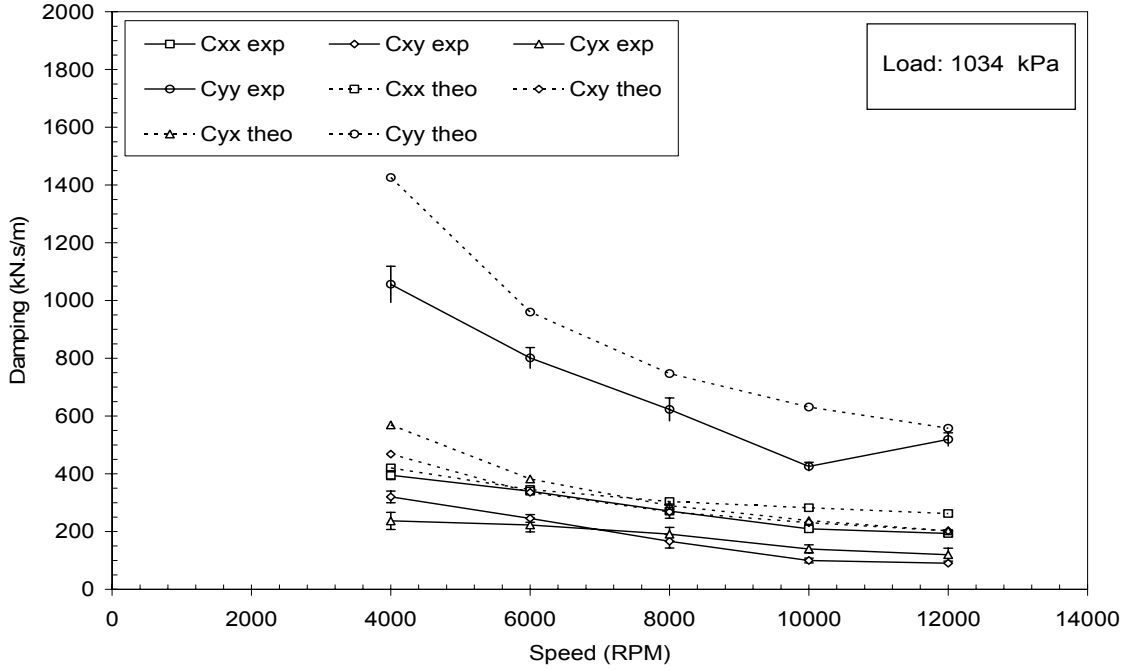

(d) 1034 kPa

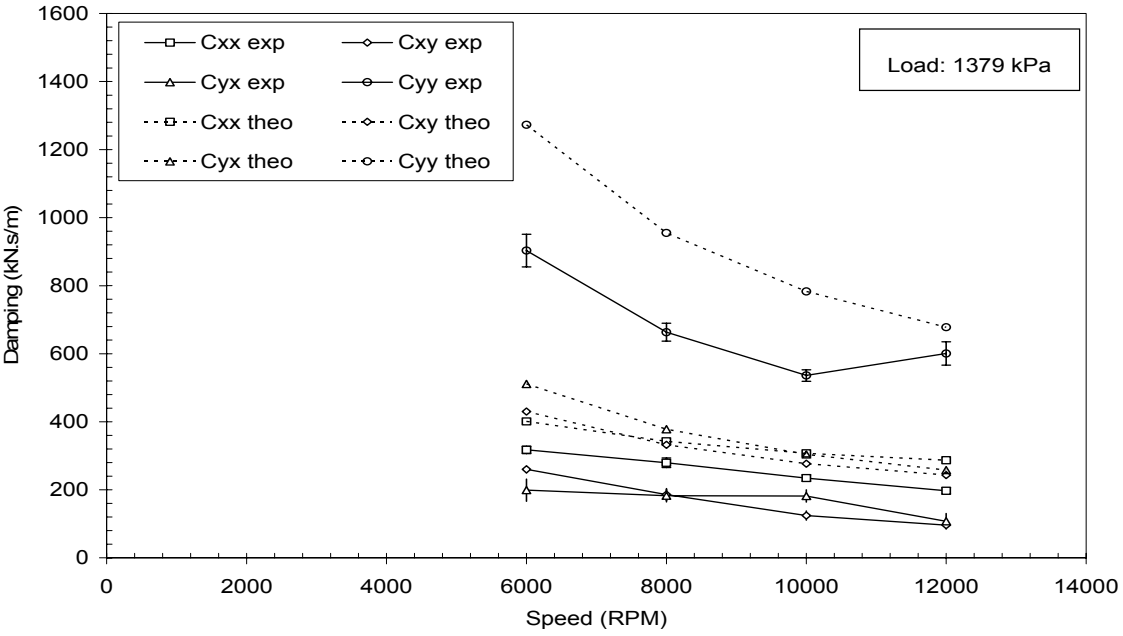

(e) 1379 kPa

Fig. 45 “Continued

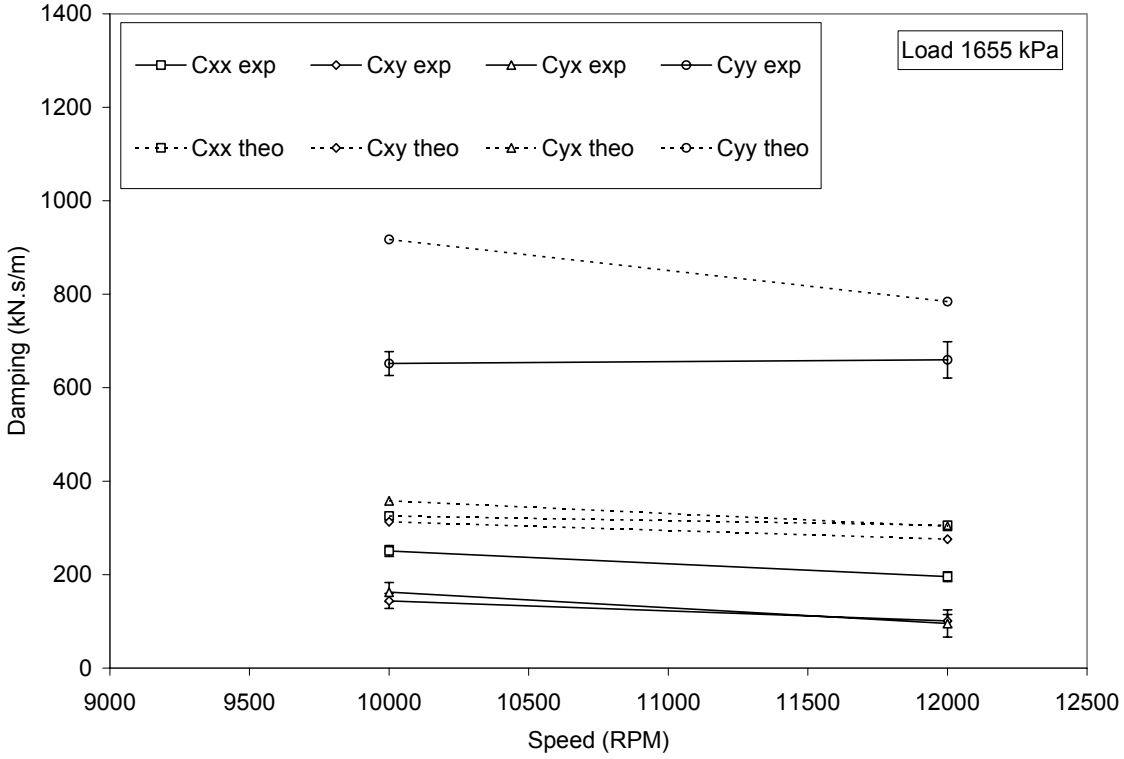

(f) 1655 kPa

Fig. 45 "Continued"

Figs. 46 (a), (b), (c), and (d) compare the predicted bearing damping coefficients at both the cold and hot clearances to experimental results at 1379 kPa. Fig. 46 (a) shows that the increase in the clearance significantly reduces the difference between C_{xx} predicted and experimental values. The difference reduces from about 32% to 23% at 12,000 rpm. However, Figs. 46 (b), (c), and (d) show smaller reduction in the damping coefficients C_{xy}, C_{yx} and C_{yy}.

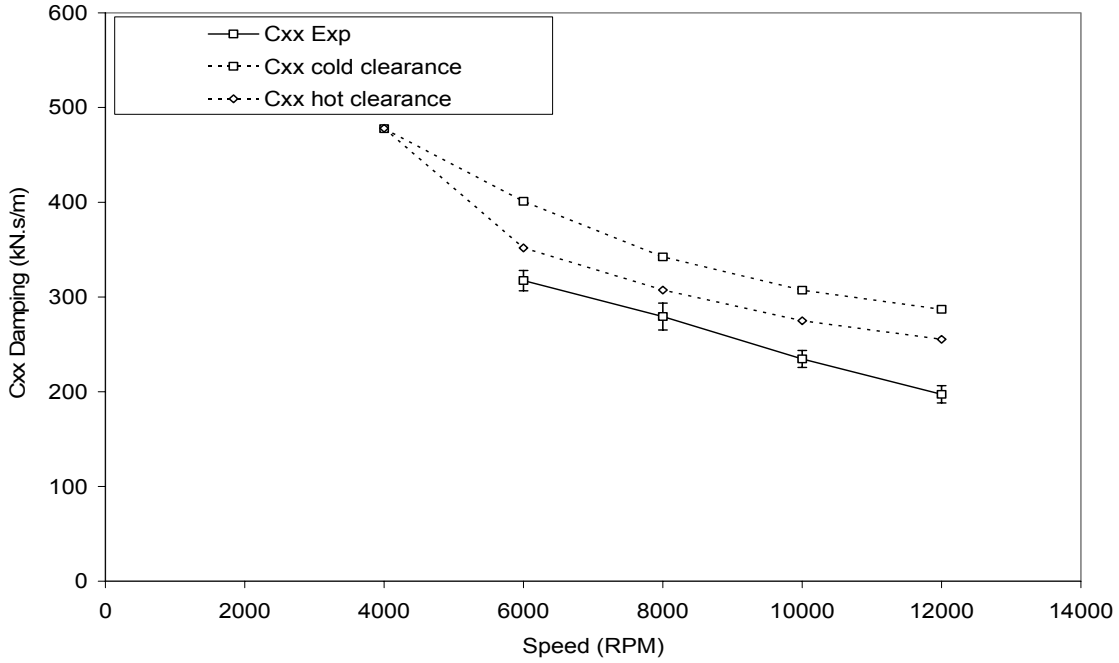

(a) C_{xx}

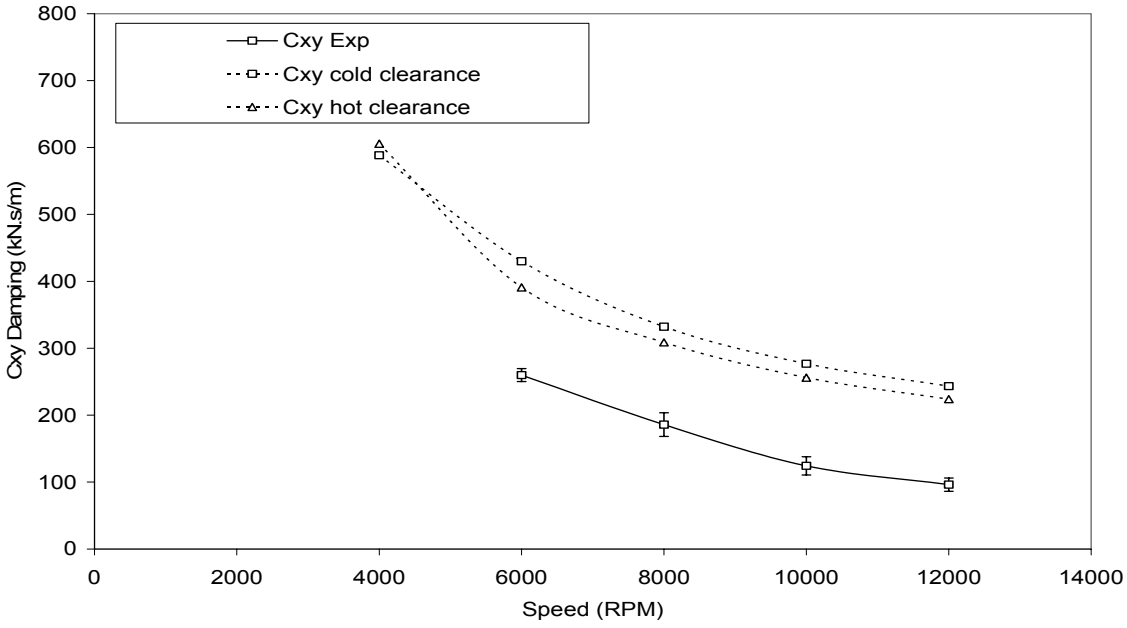

(b) C_{xy}

Fig. 46 Pressure-dam bearing damping coefficient at difference clearances

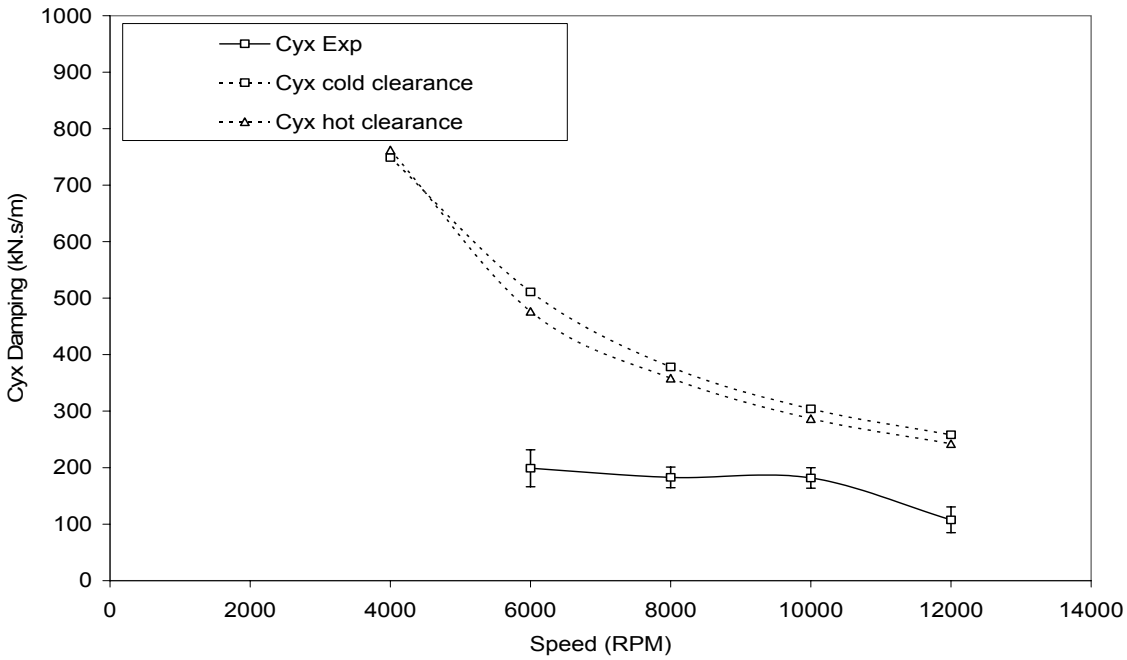

(c) C_{yx}

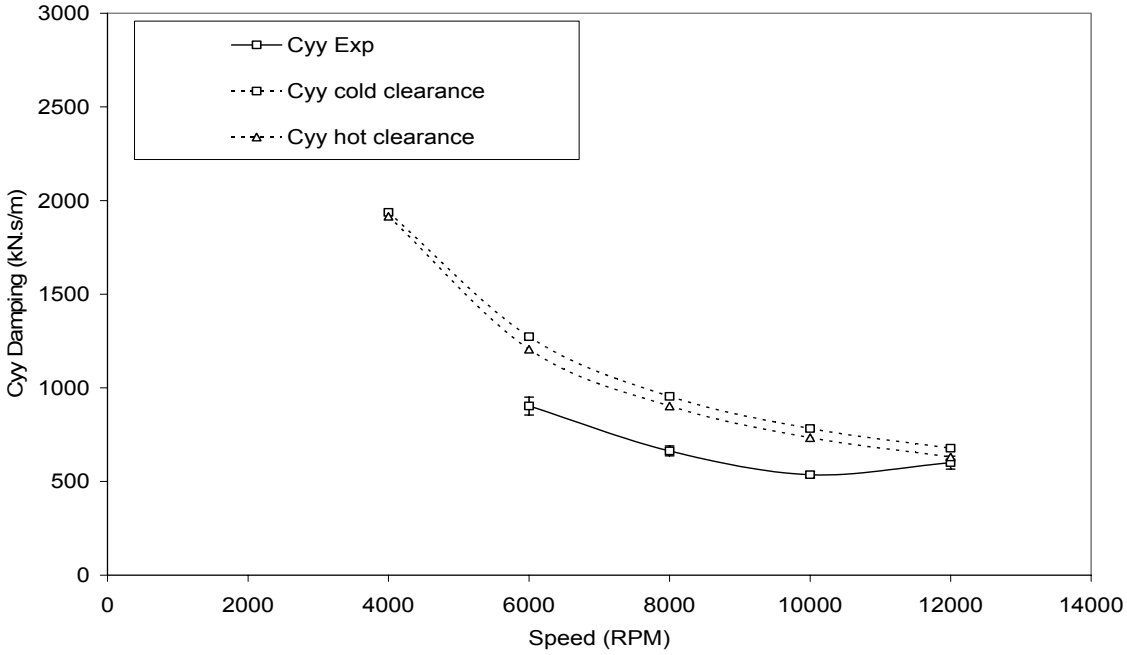

(d) C_{yy}

Fig. 46 “Continued”

Figs. 47 (a), and (b) show the non-dimensional damping coefficients versus Sommerfeld number. As predicted, these coefficients increase as Sommerfeld number increases. Fig. 47 (a) shows that numerical analysis over predict direct damping coefficients by 5-50% with better agreement for C_{xx}. Fig. 47 (b) shows that numerical analysis over predicts cross-coupled damping coefficients by 25-200%.

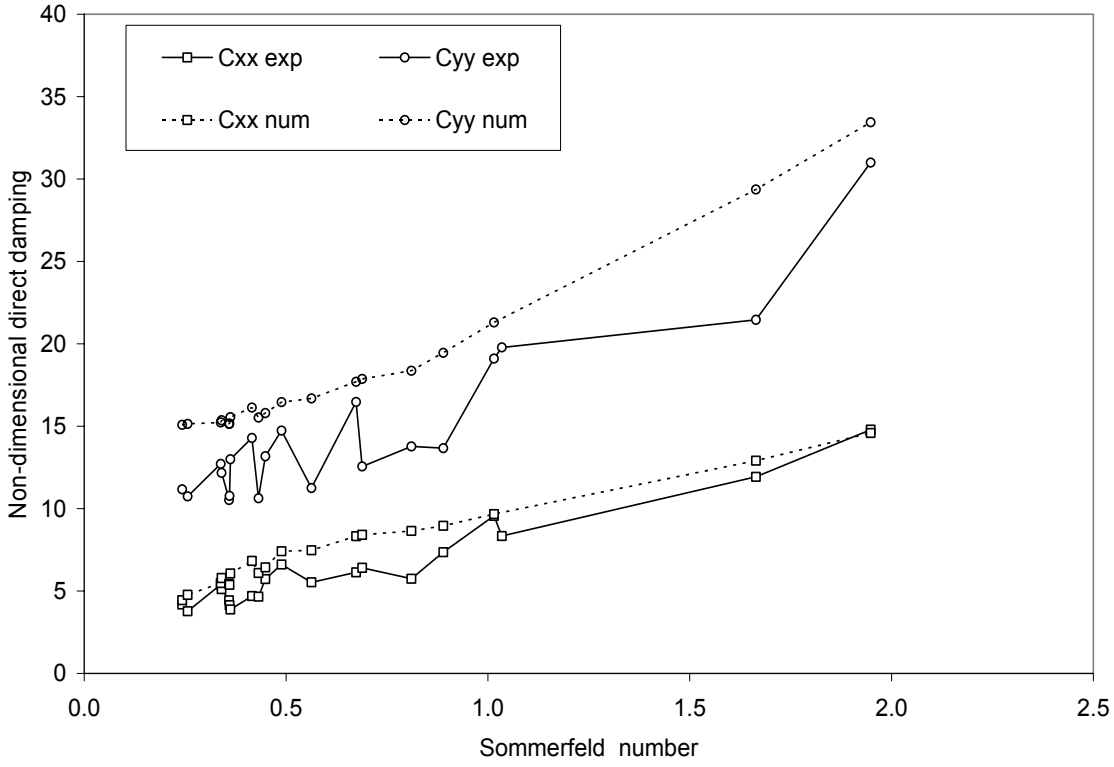

(a) Direct damping

Fig. 47 Pressure-dam bearing non-dimensional damping vs. Sommerfeld number

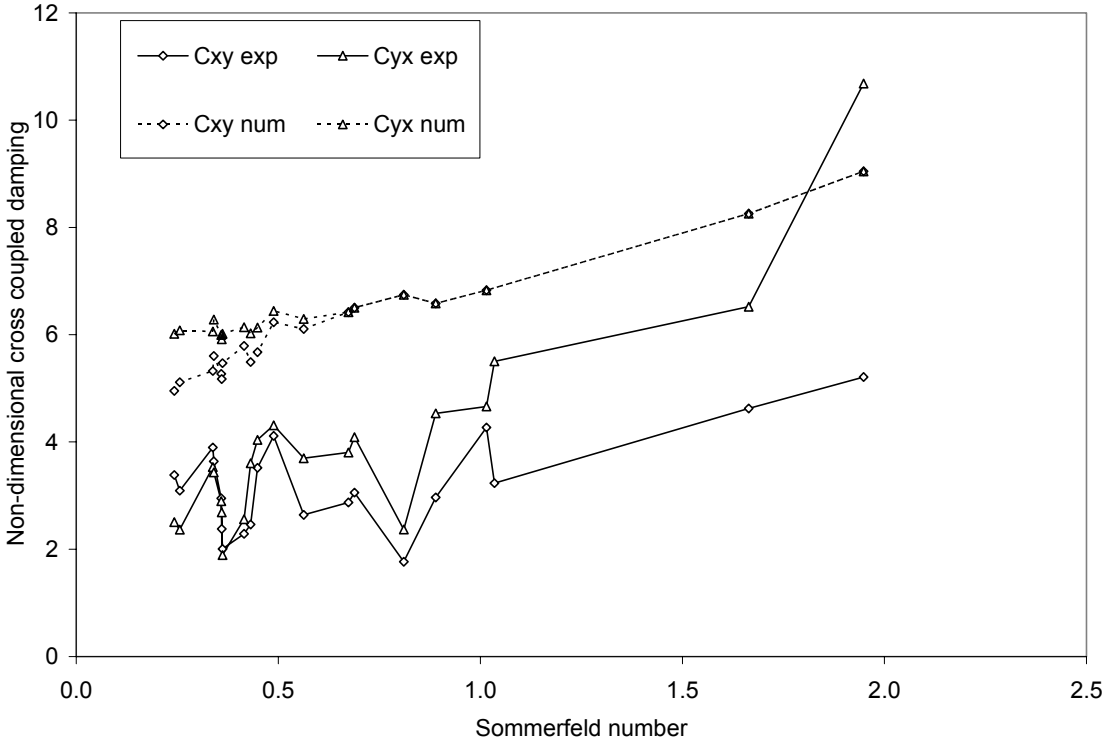

(b) Cross-coupled damping

Fig. 47 “Continued”

Figs. 48 (a), (b), (c), and (d) compare the experimental damping coefficients for both the axial-groove bearing and the pressure-dam bearing at 345 kPa, and 1379 kPa. The figures show that the pressure-dam bearing has higher damping coefficients than the axial-groove bearing.

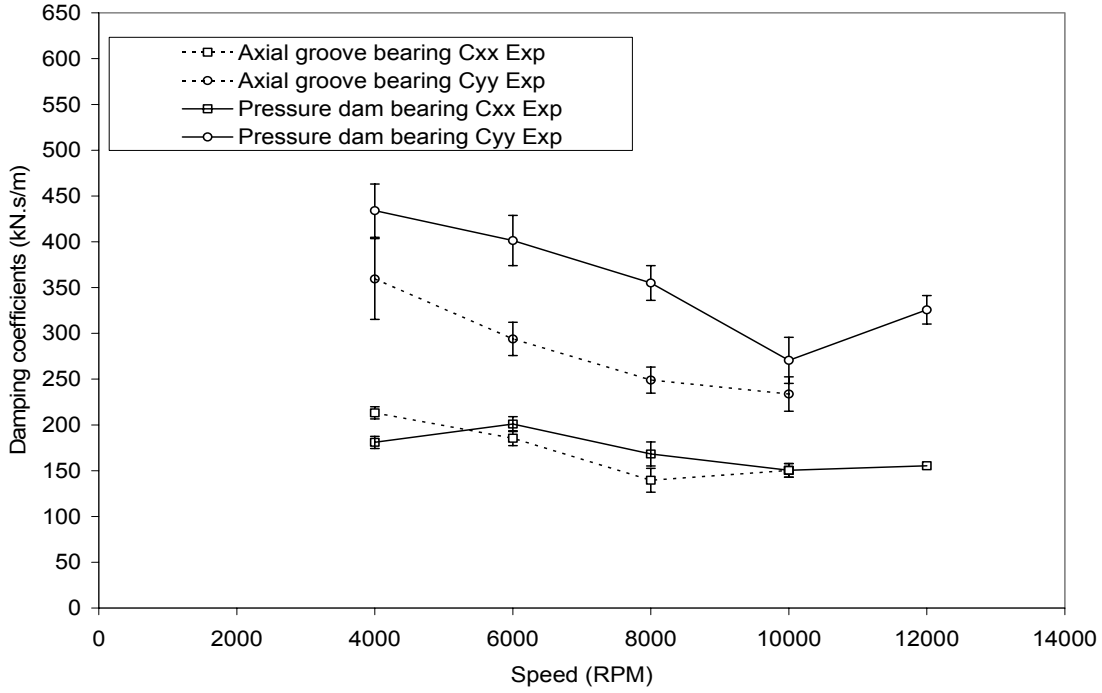

(a) Cxx & Cyy at 345 kPa

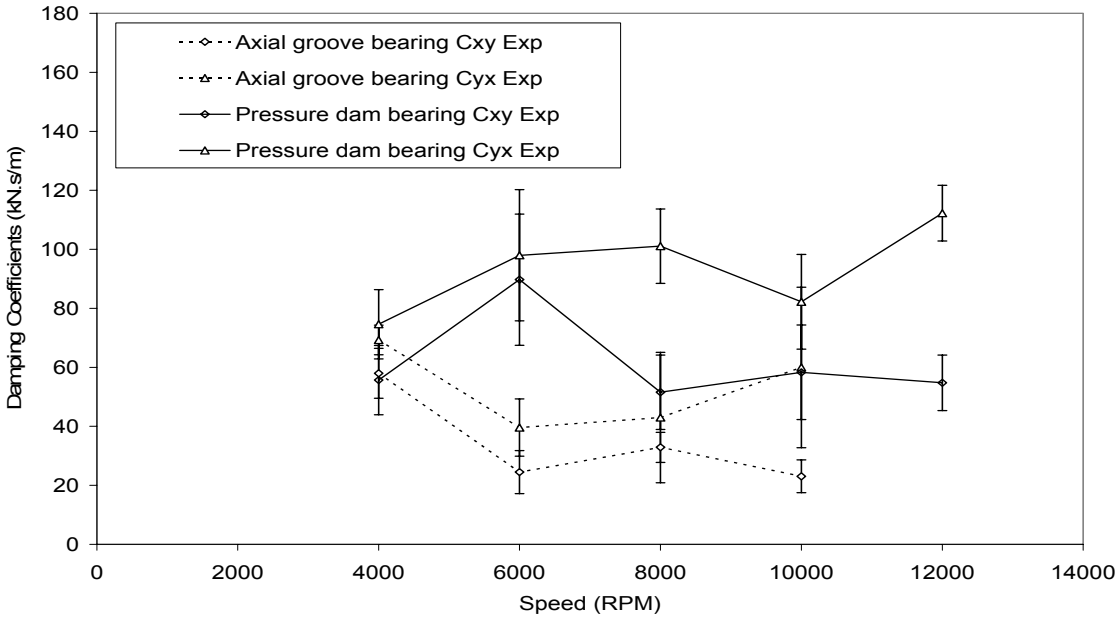

(b) Cxy & Cyx at 345 kPa

Fig. 48 Axial-groove bearing and pressure-dam bearing damping comparison

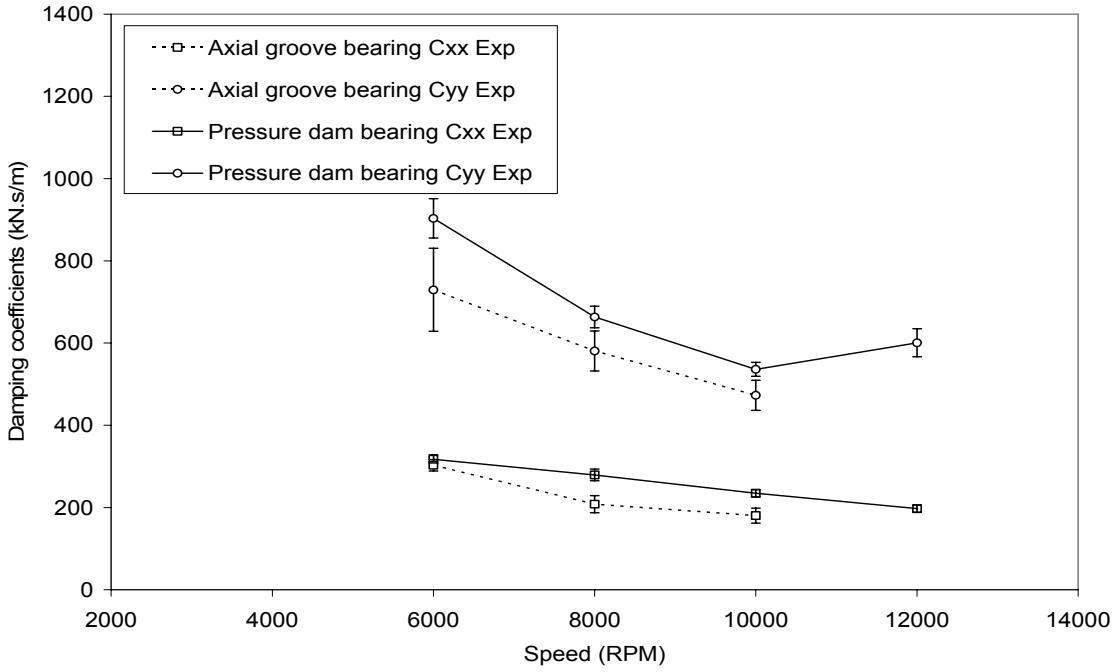

(c) Cxx & Cyy at 1379 kPa

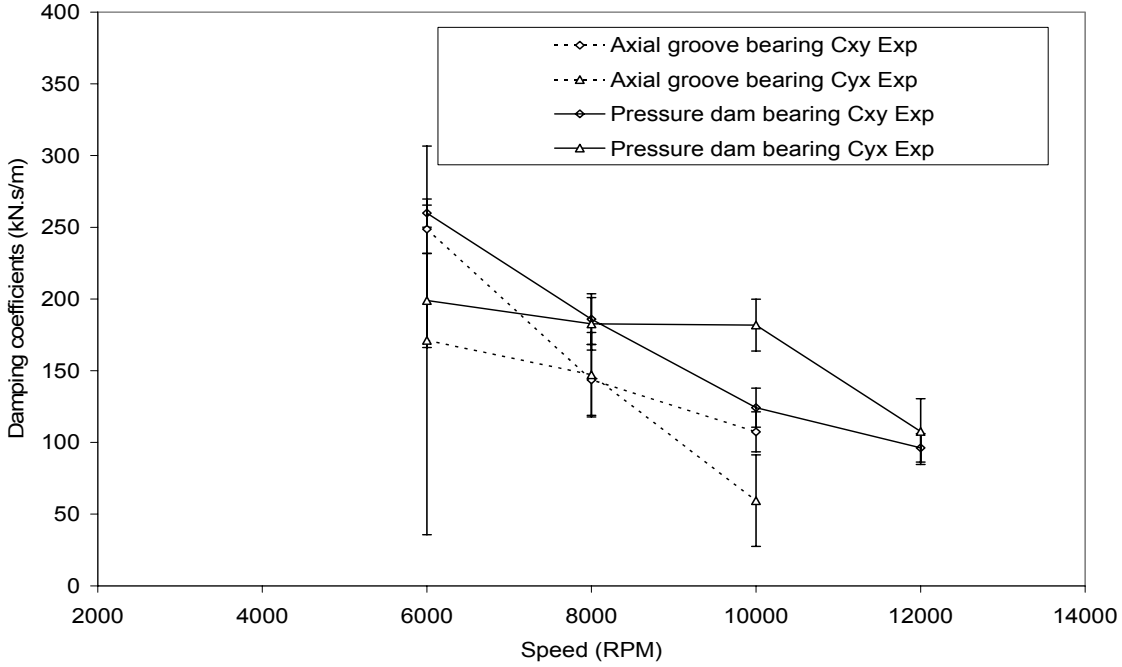

(d) Cxy & Cyx at 1379 kPa

Fig. 48 “Continued”

Added Mass Coefficients

Figs. 49 (a), (b), (c), (d), and (e) show the bearing direct added mass coefficients versus rotor speed at various load conditions. As in the axial-groove bearing, the cross-coupled mass terms are neglected because of their high uncertainties. The figures show significant added mass (30-80) kg that increases as load decreases. The figures also show that the uncertainties of these coefficients are within ±20% in most conditions. Moreover, the figures show higher uncertainties at high loads i.e. as these coefficients decreases.

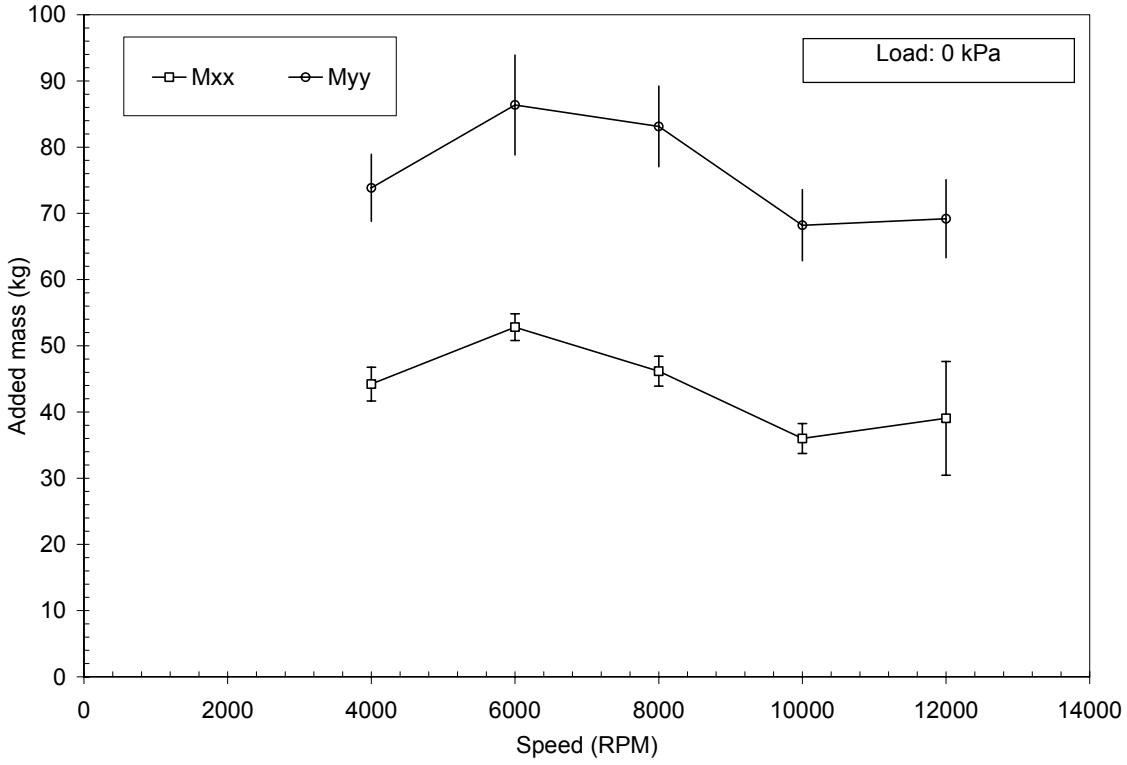

(a) 0 kPa

Fig. 49 Pressure-dam bearing added mass coefficients

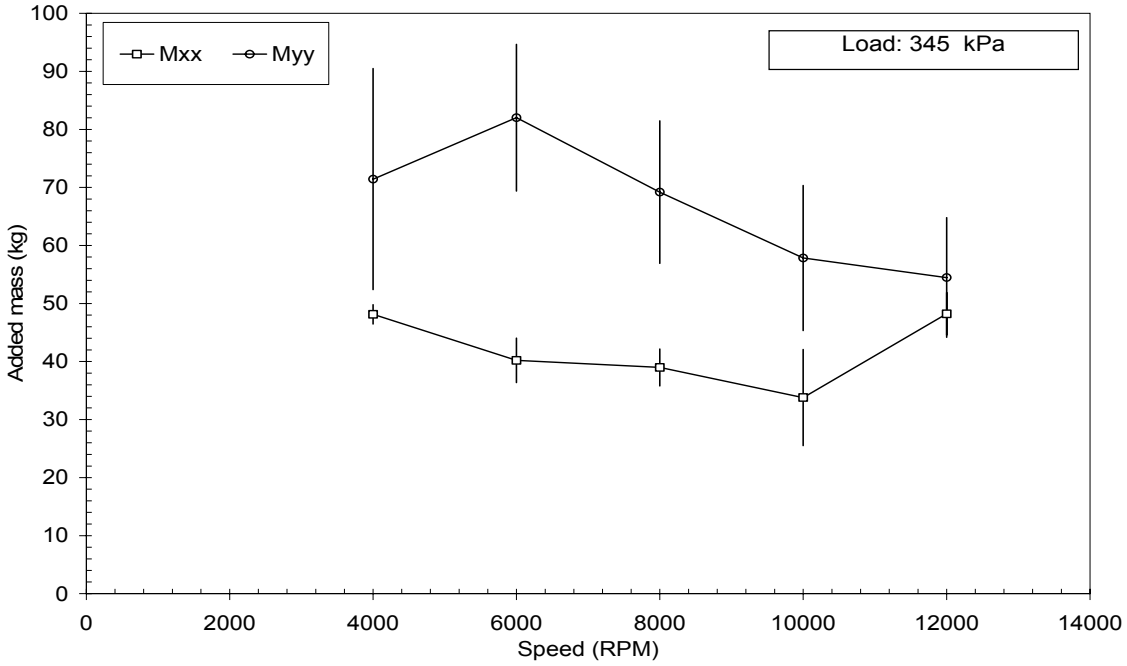

(b) 345 kPa

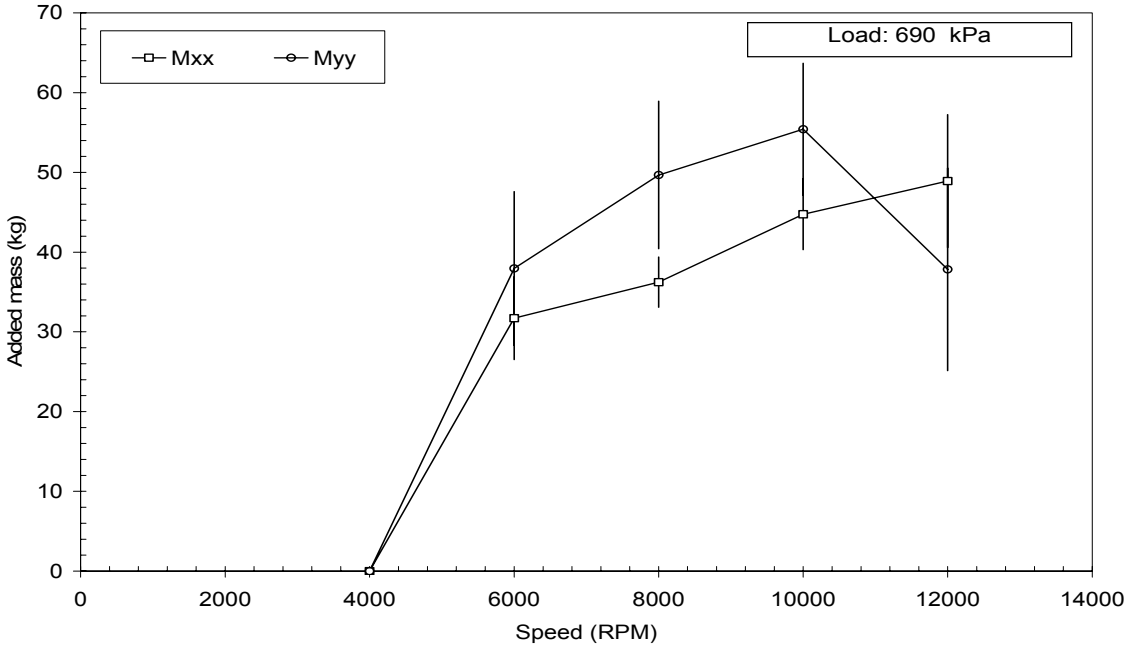

(c) 690 kPa

Fig. 49 “Continued”

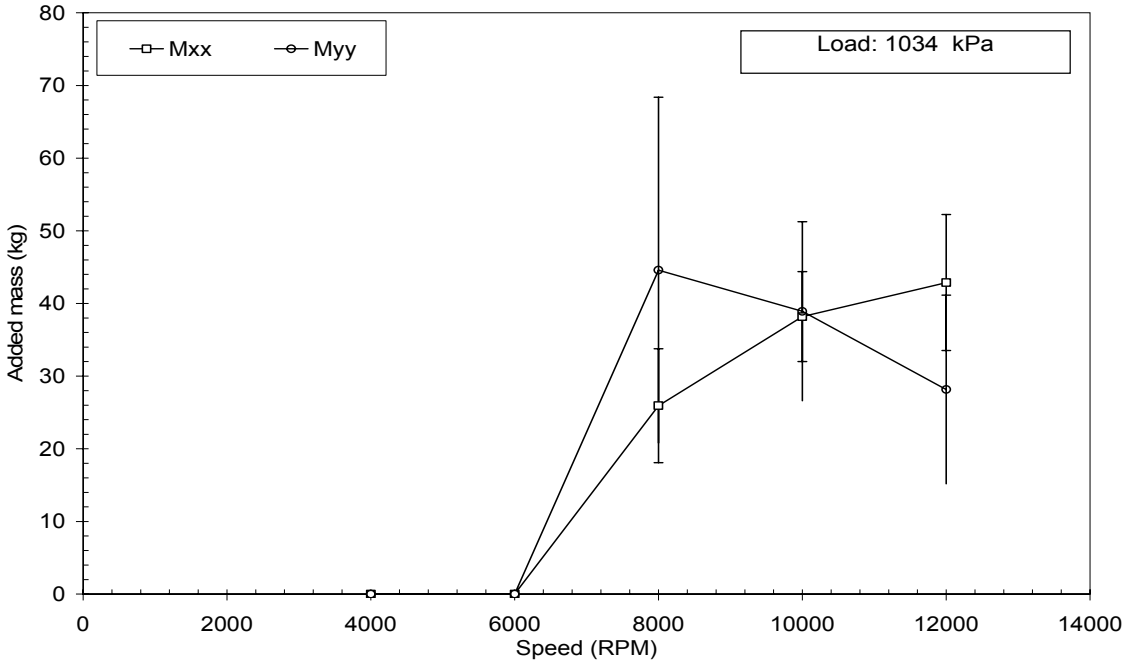

(d) 1034 kPa

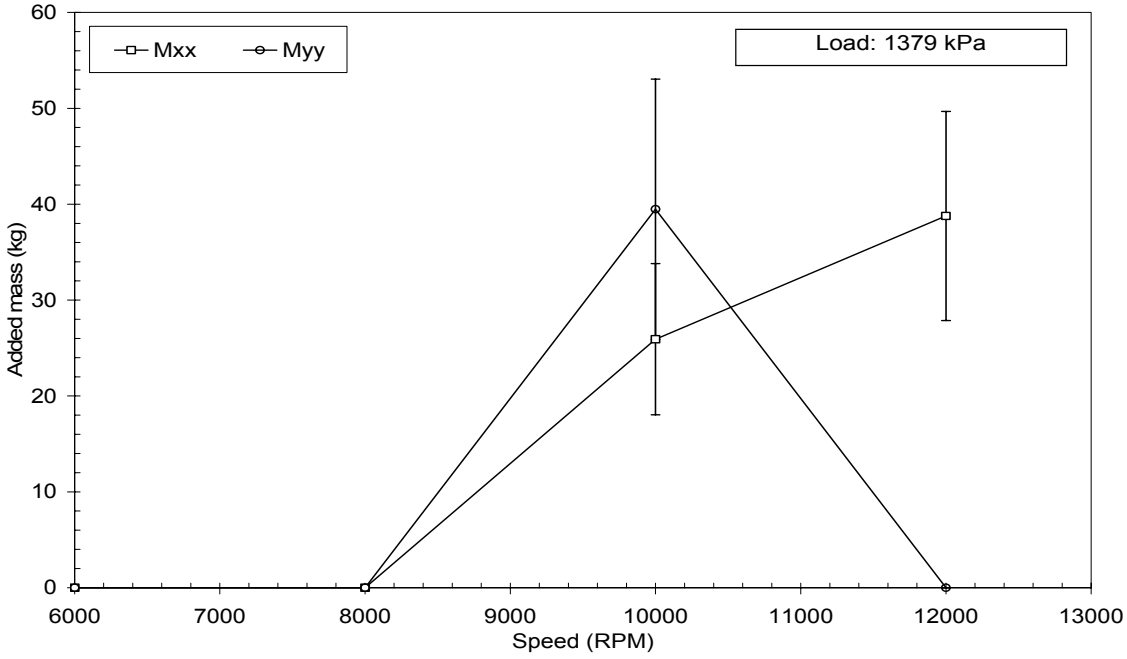

(e) 1379 kPa

Fig. 49 “Continued”

Fig. 50 compares the axial-groove bearing and pressure-dam bearing added mass coefficients. The figure shows that added mass coefficients for both bearings decrease as eccentricity increases. Moreover, the figure shows that the pressure-dam bearing has higher added mass coefficients than the axial-groove bearing. This result show that the fluid film inertia effect diminishes as eccentricity ratio increases. However, fluid film inertia effect is higher for the pressure-dam bearing than the axial-groove bearing as it extends to higher eccentricity ratios. This result is attributed to the pressure drop at the bearing step and the high Reynolds number in the pocket.

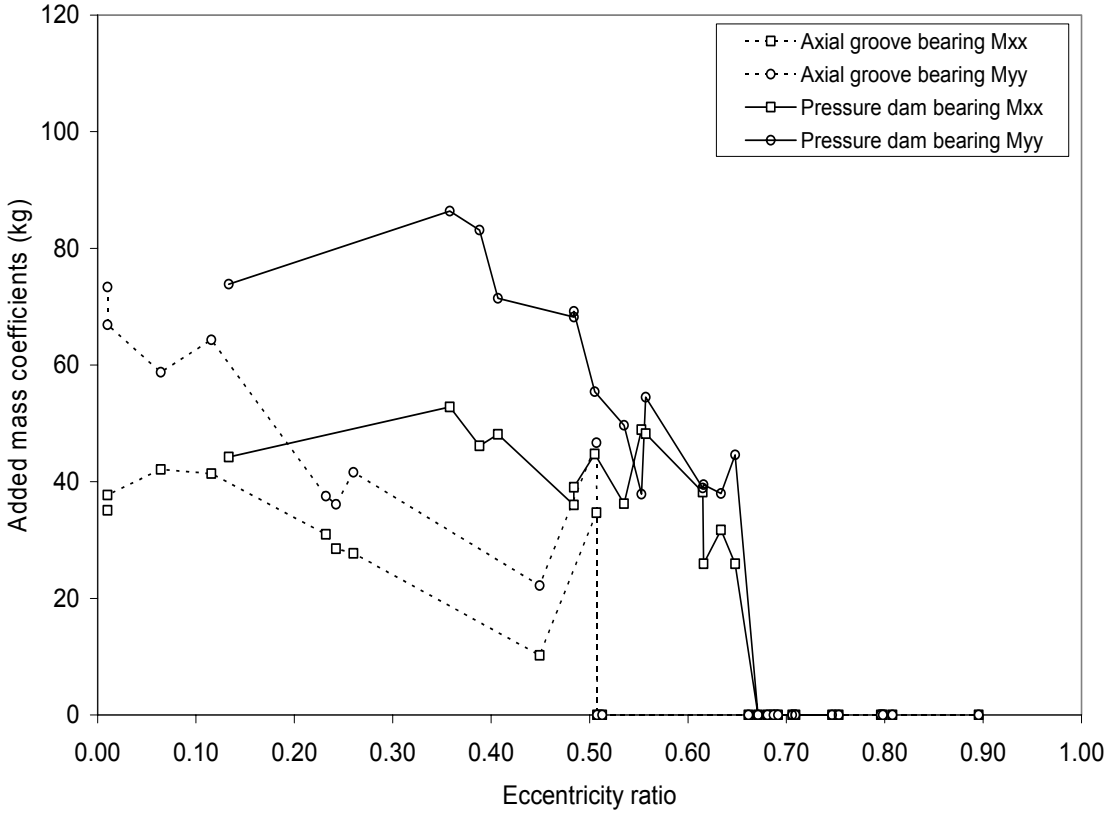

Fig. 50 Axial-groove bearing and pressure-dam bearing added mass coefficients comparison

Whirl-frequency Ratio (WFR)

Fig. 51 compares experimental and predicted *WFR* for the pressure-dam bearing. The figure shows that the bearing is slightly more stable than predicted. Numerical analysis predicts that *WFR* increases from 0.50 at low Sommerfeld number, S<0.50, to 0.53 at moderate Sommerfeld number, S=0.80. Then, it decreases to 0.46 at higher Sommerfeld number. Experimental results show that the bearing *WFR* is between 0.50 at low Sommerfeld number and 0.41 at high Sommerfeld number. The three points that shows *WFR* lower than 0.40 correspond to the 12,000 and 10,000 rpm high load conditions at which the bearing experimental direct stiffness K_{yy} and damping C_{yy} increased significantly.

Fig. 52 compares experimental *WFR* for both axial-groove bearing and pressure-dam bearing. Experimental results show that both bearings has almost equal *WFR* for S<1. However, pressure-dam bearing as predicted has about 8% lower *WFR* for S>1.

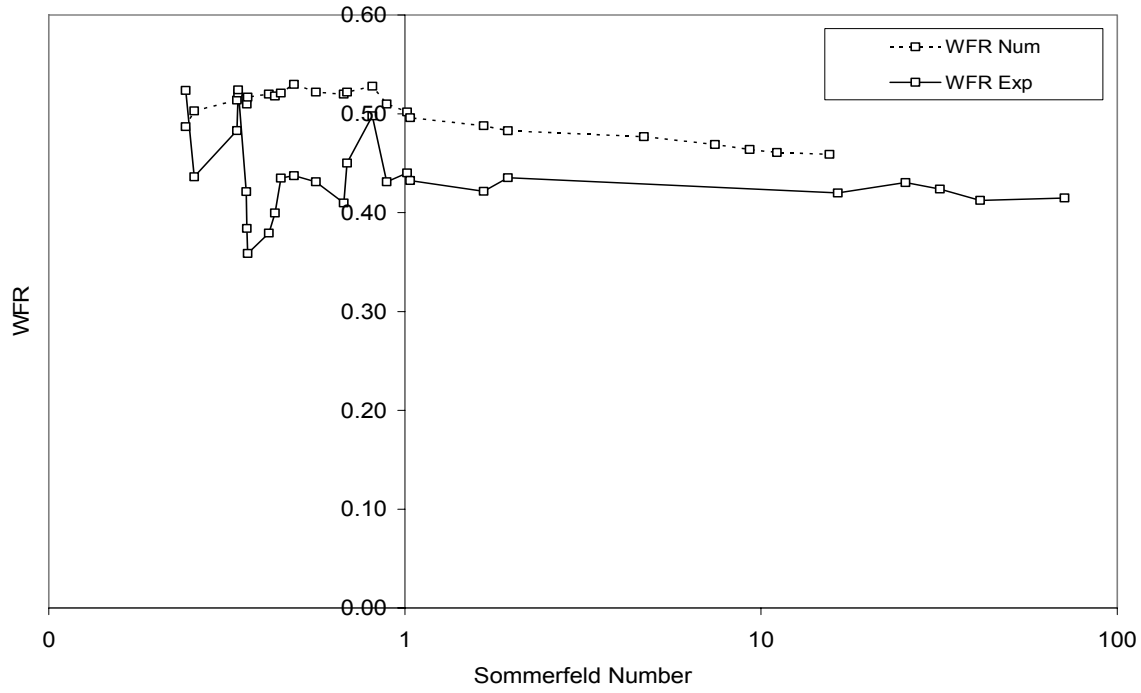

Fig. 51 Pressure-dam bearing whirl-frequency ratio

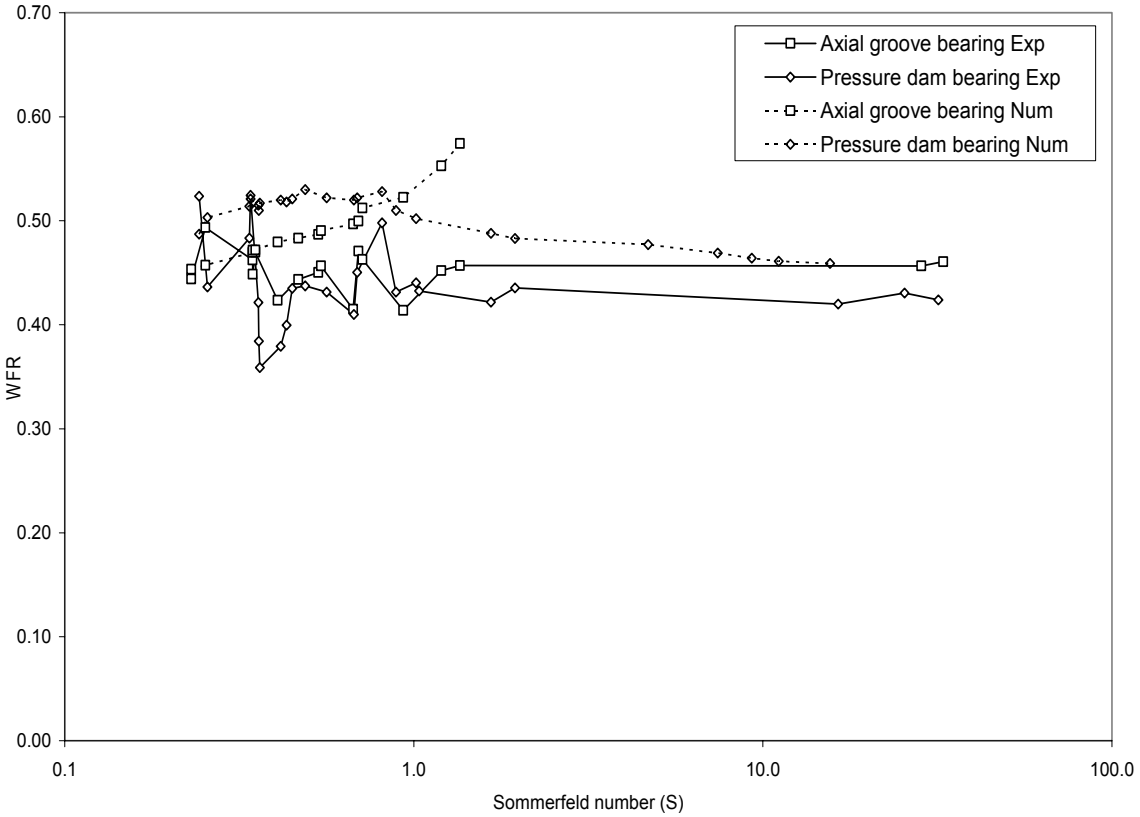

Fig. 52 Axial-groove bearing and pressure-dam bearing *WFR* comparison

Fig. 53 shows the predicted effect of the step location on *WFR*. The figure shows significant reduction in the *WFR* as Sommerfeld number increases, $S>1$, for $\theta_s=150^\circ$. The *WFR* reduces from 0.46 for $\theta_s=130$ to 0.35 for $\theta_s=150^\circ$ at $S=10$. However, the figure also shows no significant reduction in the *WFR* for low Sommerfeld number. However, most machines do not operate at such a high Sommerfeld number. Therefore, the pressure-dam bearing is frequently modified to include a relief track at the loaded pad. This track removes part of the bearing load-carrying surface thus forcing the bearing to operate at higher eccentricity ratio [12].

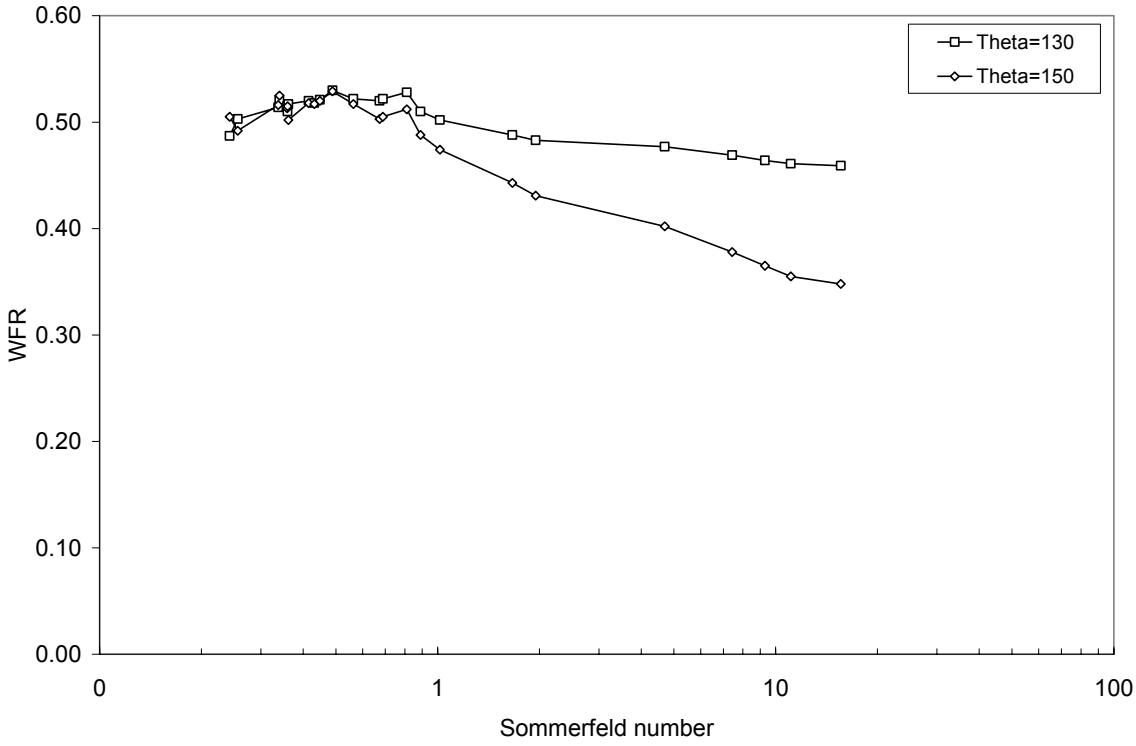

Fig. 53 Predicted *WFR* vs. Sommerfeld number at different step angles

Fig. 54 shows the predicted *WFR* of the tested pressure-dam bearing with and without a relief track. The relief track length ratio is $\bar{L}_t = 0.25$ while the groove depth is 0.04". The figure also shows the bearing predicted eccentricity ratio on the secondary axis. The figure shows that the bearing is always stable for $S<0.90$. However, as Sommerfeld number increases, the *WFR* for the both bearings approaches each other. The figure also shows that the minimum eccentricity ratio increases from 0.3 to 0.6 at high Sommerfeld number due to the relief track. Also, the bearing operates at very high eccentricity ratio for $S<1$ which is not favorable. Thus, the best operating region for this bearing is for $1<S<2$. Within this range, the predicted bearing *WFR* is 0.3-0.35 and the bearing eccentricity is 0.75-0.7.

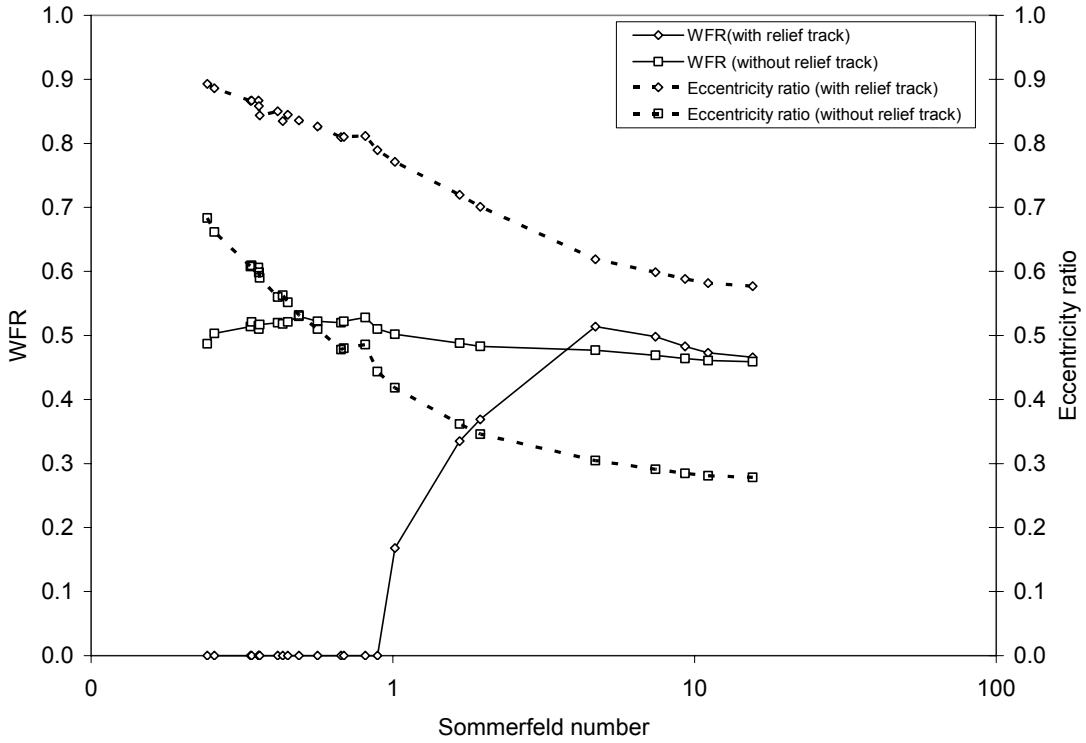

Fig. 54 Predicted *WFR* and eccentricity ratio vs. Sommerfeld number for pressure-dam bearing with/without relief track

SUMMARY AND CONCLUSIONS

The purpose of this project is to experimentally validate the predicted advantages of pressure-dam bearings over two-axial-groove bearings. Both bearings' static and dynamic characteristics were discussed and compared to predictions.

The following points summarize the most important findings from the two-axial-groove bearing tests:

- Axial-groove bearing static tests show that the bearing eccentricity increases as load increases. In case of no-load, the bearing has zero eccentricity. Static test results also show higher eccentricity and lower attitude angle than predicted.
- Dynamic tests show that the bearing direct stiffness increases as the eccentricity ratio increases.
- Dynamic tests also show that the bearing has lower direct stiffness than predicted
- The axial-groove bearing cross-coupled stiffness coefficients have opposite signs, which mean that they are destabilizing. Also, their values increase as speed increases. Also, good agreement between experimental results and predictions is found especially at low Sommerfeld numbers.
- The axial-groove bearing direct damping coefficients increases as eccentricity increases while, the cross-coupled damping is constant. Damping coefficients are also lower than predicted with reasonable agreement between experimental and numerical direct damping coefficients.
- The dynamic tests show that the axial-groove bearing has significant direct added mass as predicted by Reinhardt and Lund [10] that increases as eccentricity ratio decreases. The bearing estimated added mass is 20-70 kg for eccentricity ratio lower than 0.50. This added mass can alter the natural frequency for short rotors.
- Cross-coupled mass coefficients were ignored because of their high uncertainties.

- The two axial-groove bearing has *WFR*≈0.45. The bearing is more stable than predicted especially at high Sommerfeld number.
- Fluid inertia has no significant effect on the tested bearing *WFR*.

The following points summarize the most important findings from the pressure-dam bearing tests:

- The pressure-dam bearing static test shows that the dam is more effective at high speeds. The bearing operates at higher eccentricity as speeds increases at low loads. The bearing eccentricity versus Sommerfeld number curve flattens at about 0.50 eccentricity ratio for high speeds conditions.
- The pressure-dam bearing attitude angles are higher than 90˚ at high Sommerfeld number.
- The pressure-dam bearing develops significant stiffness even at no-load conditions due to its high eccentric operation.
- The pressure-dam bearing has lower direct stiffness coefficients than predicted especially at low speeds.
- The pressure-dam bearing cross-coupled stiffness coefficients are of opposite signs. Numerical analysis predicts cross-coupled stiffness coefficients reasonably.
- The pressure-dam bearing damping coefficients increases as eccentricity increases. Numerical analysis predicts direct damping coefficients reasonably however, it over predicts the cross-coupled damping coefficients significantly.
- The pressure-dam bearing has significant added mass 85-25 kg for eccentricity ratio lower than 0.66.
- The pressure-dam bearing has *WFR* ≈0.45 at low Sommerfeld number except for 10,000 and 12,000 rpm high load conditions. At these conditions *WFR* reduces to about 0.35.
- The pressure-dam bearing has *WFR*≈0.41 at high Sommerfeld numbers.
- Numerical analysis predicts that the pressure-dam bearing *WFR* can be reduced to 0.35 for *S*>1 by increasing the dam arc length to 150˚.

- Numerical analysis predicts that adding a relief track with $\bar{L}_t$=0.25 increases the bearing eccentricity thus, improves the stability significantly for S<1.

The following points compare the most important findings for both bearings:

- At high Sommerfeld number, the pressure-dam bearing has higher eccentricity ratio and direct stiffness than the axial-groove bearing. The pressure-dam has also lower K_{xy} but higher K_{yx}.
- At low Sommerfeld numbers, the pressure-dam bearing has about the same eccentricity and stiffness coefficients as the axial-groove bearing.
- The pressure-dam bearing has higher damping coefficients than the axial-groove bearing.
- The pressure-dam bearing has higher added mass than the axial-groove bearing. The increase in the added mass is believed to be due to the step inertia.
- Both bearings have almost equal *WFR* at low Sommerfeld number except for 10,000 and 12,000 rpm high load conditions.
- The pressure-dam bearing is slightly more stable than the two axial-groove bearing at high Sommerfeld numbers.
- Part of the difference between prediction and experimental results is caused by an increase in the bearing clearance due to thermal growth. Also, since the numerical analysis assumes an isothermal process, the reduction in the lubricant viscosity that results in lower eccentricity predictions is neglected.

REFERENCES

1) Pinkus, O., 1987, "The Reynolds Centennial: A Brief History of the Theory of Hydrodynamic Lubrication," Journal of Tribology, **109**, pp. 2-20.

2) Vance, J., 1988, *Rotordynamics of Turbomachinery*, John Wiley & Sons, New York.

3) Rayleigh, L., 1918, "Notes on the Theory of Lubrication," Philosophical Magazine, **35**, pp. 1-13.

4) Nicholas, J., 1994, "Stabilizing Turbomachinery with Pressure-dam Bearings," Encyclopedia of Fluid Mechanics, **2**, Gulf Publishing Company, Houston, TX.

5) Al-Ghasim, A., 2004, "Measurements of Rotordynamic Coefficients for a High Speed Flexure-Pivot Tilting Pad Bearing, Between Pad Configuration," Master's Thesis, Texas A&M University, College Station, TX.

6) Biezeno, C., and Grammel, R., 1954, *Engineering Dynamics, Vol III, Steam Turbines,* D. Van Nostrand, New York.

7) Newkirk, B., and Taylor, H., 1925, "Shaft Whipping Due to Oil Action in Journal Bearing," General Electric Review, **8**, pp. 559-568.

8) Lund, J., 1965, "The Stability of an Elastic Rotor in Journal Bearings with Flexible, Damped Supports," Journal of Applied Mechanics, pp. 911-920.

9) Lund, J., 1987, "Review of the Concept of Dynamic Coefficients for Fluid Film Journal Bearings," Journal of Tribology, **109**, pp. 37-41.

10) Reinhardt, E., and Lund, J., 1975, "The Influence of Fluid Inertia on the Dynamic Properties of Journal Bearings," Journal of Lubrication Technology, **97**, pp. 159-167.

11) Allaire, P., Nicholas, J., and Barrett, L., 1979, "Analysis of Step Journal Bearings-Infinite Length, Inertia Effects," ASLE Transactions, **22**, pp. 333-341.

12) Nicholas, J., and Allaire, P., 1980, "Analysis of Step Journal Bearings-Finite Length and Stability," ASLE Transactions, **22**, pp. 197-207.

13) Nicholas, J., Allaire, P., and Lewis, D., 1980, "Stiffness and Damping Coefficients for Finite Length Step Journal Bearings," ASLE Transactions, **23**, pp. 353-362.

14) Leader, M., Flack, R. and Allaire, P. 1980, "Experimental Study of Three Journal Bearings with a Flexible Rotor," ASLE Transactions, **23**, pp. 363-369.

15) Lanes, R., Flack, R., and Lewis, D. 1982, "Experiments on the Stability and Response of a Flexible Rotor in Three Types of Journal Bearings," ASLE Transactions, **25**, pp. 289-298.

16) Mehta, N., and Singh, A., 1986, "Stability Analysis of Finite Offset-Halves Pressure-dam Bearing," Journal of Tribology, **108**, pp. 270-274.

17) Flack, R., Leader, M., and Allaire, P., 1981, "Experimental and Theoretical Pressures in Step Journal Bearings," ASLE Transactions, **24**, pp. 316-322.

18) He, M., Allaire, P., Cloud, C. and Nicholas, J, 2004, "A Pressure-dam Bearing Analysis with Adiabatic Thermal Effects," STLE Transactions, **47**, pp. 70-76.

19) Miller, R., 1995, "A Test Rig for the Identification of Rotordynamic Coefficients of Fluid Film Bearings," Master's Thesis, Texas A&M University, College Station, TX.

20) De Santiago, O., 2002, "Identification of Bearing Supports' Force Coefficients From Rotor Responses Due to Imbalances and Impact Loads," Ph.D. Dissertation, Texas A&M University, College Station, TX.

21) Kostrzewsky, G., Taylor, D., and Flack, R., 1994, "Experimental Determination of the Dynamic Characteristics of a Two-Axial Groove Journal Bearing," Tribology Transactions, **37**, pp. 534-542.

22) Kaul, A., 1999, "Design and Development of a Test Setup for the Experimental Determination of the Rotordynamic and Leakage Characteristics of Annular

Bushing Oil Seals," Master's Thesis, Texas A&M University, College Station, TX.

23) Childs, D., and Hale, K., 1994, "A Test Apparatus and Facility to Identify the Rotordynamic Coefficients of High-Speed Hydrostatic Bearings," Journal of Tribology, **116**, pp. 337-343.

24) Rodriguez, L., 2004, "Experimental Frequency-Dependent Rotordynamic Coefficients for a Load-on-Pad, High Speed, Flexible-Pivot Tilting-Pad Bearing," Master's Thesis, Mechanical Engineering, Texas A&M University, College Station, TX.

25) Someya, T., Mitsui, J., Esaki, J., Saito, S., Kanemitsy, Y., Iwatsubo, T., Tanaka, M., Hisa, S., Fujikawa, T., and Kanki, H., 1989, *Journal-Bearing Databook*, Springer, New York.

26) San Andrés, L., 2002, "Modern Lubrication and its Applications", Class notes for MEEN 626, Mechanical Engineering Department, Texas A&M University, College Station, TX.

27) San Andrés, L., 1991, "Effect of Eccentricity on the Force Response of a Hybrid Bearing," STLE Tribology Transactions, **34** (4), pp. 537- 544.

APPENDIX A: AXIAL-GROOVE BEARING DATA

Table 10. Static test data

RPM	kPa	e_x (μm)	e_y (μm)	ε_0	T_{in} (˚C)	T_{out}(˚C)
4000	0	0.00	0.00	0.00	43.3	45.6
4000	172	28.19	39.11	0.34	42.2	45.4
4000	345	35.05	54.36	0.46	43.8	47.9
4000	517	41.91	74.17	0.61	42.2	46.5
4000	690	43.67	87.38	0.70	41.1	46.1
4000	862	42.93	99.82	0.77	40.2	44.7
4000	1034	41.66	107.95	0.82	41.1	46.1
6000	0	0.813	-1.52	0.11	46.1	49.7
6000	172	7.21	1.14	0.05	41.6	46.1
6000	345	20.65	25.35	0.23	45.0	50.6
6000	517	30.98	42.93	0.38	47.2	52.4
6000	690	37.84	59.69	0.50	42.2	47.4
6000	862	42.16	74.93	0.61	43.3	48.9
6000	1034	41.66	84.07	0.68	44.4	50.8
6000	1207	44.70	95.50	0.75	41.1	47.5
6000	1379	44.19	103.63	0.80	44.4	51.2
6000	1655	43.43	117.60	0.89	42.7	49.8
8000	0	8.89	0.00	0.01	44.4	51.3
8000	172	15.24	6.60	0.12	45.5	53.1
8000	345	25.41	25.44	0.26	45.0	53.7
8000	517	33.78	41.40	0.38	43.3	52.6
8000	690	40.89	58.92	0.51	40.5	50.0
8000	862	44.19	71.37	0.60	42.7	52.6
8000	1034	46.99	84.33	0.69	42.7	52.0
8000	1207	46.74	93.22	0.75	41.1	51.1
8000	1379	46.74	100.63	0.80	41.1	51.6
8000	1655	45.57	114.81	0.88	42.7	54.3
10000	0	12.6	0.254	0.01	43.8	55.6
10000	345	25.1	23.88	0.24	43.3	58.1
10000	517	33.02	43.94	0.39	43.3	56.1
10000	690	39.11	58.93	0.51	44.4	59.1
10000	862	43.69	70.10	0.59	40.0	54.5
10000	1034	45.97	8.00	0.66	40.0	57.1
10000	1207	46.22	91.95	0.73	39.4	57.1
10000	1379	45.46	101.60	0.79	39.4	56.2
10000	1655	44.45	112.01	0.86	39.4	58.1

Table 11. Force coefficients

RPM	kPa	*Kxx*	*Kxy*	*Kyx*	*Kyy*	*Cxx*	*Cxy*	*Cyx*	*Cyy*	*Mxx*	*Myy*
		(MN/m)				(kN.s/m)				(kg)	
4000	0	0.2	-34.6	81.4	0.7	210.5	-26.6	5.2	425.1	42.1	58.7
4000	345	25.6	-27.8	79.4	41.3	213.2	57.9	69.2	359.	10.2	22.1
4000	690	79.7	-39.3	154.5	100.5	328.1	183.4	159.7	630.6	0	0
4000	1034	139.9	-31.8	238.8	229.0	440.2	371.3	286.4	1060.3	0	0
6000	0	1.2	-52.0	104.8	0.8	182.7	-40.9	12.3	365.5	41.3	64.3
6000	345.1	30.4	-39.2	92.3	36.5	185.5	24.5	39.6	293.9	16.4	23.2
6000	690	75.0	-48.5	150.9	94.2	233.6	126.4	105.2	460.9	0	0
6000	1034	120.2	-42.8	235.0	184.4	252.6	153.8	166.1	656.8	0	0
6000	1379	173.0	-21.7	385.7	327.2	302.8	248.7	171.2	729.4	0	0
8000	0	3.6	-66.7	113.7	6.3	169.8	-31.9	28.6	326.0	37.7	66.9
8000	345	31.3	-53.8	89.2	42.2	139.5	32.9	43.1	249.2	27.7	41.6
8000	690	66.7	-55.9	156.1	88.5	162.7	98.5	49.3	399.0	0	0
8000	1034	114.7	-51.8	216.4	164.2	208.7	110.1	68.8	511.7	0	0
8000	1379	155.9	-31.9	302.8	286.7	208.2	143.6	147.2	580.8	0	0
10000	0	5.0	-87.9	122.7	16.5	154.6	-27.7	40.5	296.9	35.1	73.3
10000	345	33.9	-70.4	110.0	45.2	150.3	23.1	59.9	233.7	28.5	36.1
10000	690	75.6	-59.5	168.6	96.1	160.1	78.3	67.2	311.2	34.6	46.6
10000	1034	100.4	-60.8	228.6	157.2	172.4	125.3	123.4	489.2	0	0
10000	1379	145.5	-43.0	313.4	263.1	180.4	107.4	59.4	473.0	0	0

Table 12. Uncertainty of force coefficients

RPM	kPa	*Kxx*	*Kxy*	*Kyx*	*Kyy*	*Cxx*	*Cxy*	*Cyx*	*Cyy*	*Mxx*	*Myy*
		(MN/m)				(kN.s/m)				(kg)	
4000	0	2.10	2.20	1.10	3.30	5.80	5.40	3.70	8.50	3.90	6.10
4000	345	3.12	2.24	3.36	3.92	6.66	8.45	5.02	44.10	4.76	5.81
4000	690	8.30	5.23	13.10	9.42	27.20	18.20	32.90	22.80	16.29	0
4000	1034	10.80	7.90	9.27	11.80	23.10	30.90	45.10	111.60	0	0
6000	0	4.65	4.27	3.08	4.52	4.40	6.50	9.00	18.60	8.43	4.64
6000	345	0.97	2.86	3.06	2.28	8.11	7.30	9.70	18.20	2.63	6.12
6000	690	2.23	2.27	4.73	3.55	5.50	8.10	24.70	31.10	0	0
6000	1034	4.55	3.71	12.70	6.85	13.60	14.20	50.20	57.10	0	0
6000	1379	8.37	7.07	7.35	14.27	13.80	16.80	135.50	101.00	0	0
8000	0	2.90	3.00	2.90	5.40	10.50	5.50	10.50	5.40	5.90	8.20
8000	345	3.60	1.87	4.79	4.70	13.10	5.10	22.10	14.30	6.70	10.30
8000	690	5.49	5.13	9.58	3.77	9.60	12.20	28.80	30.10	0	0
8000	1034	5.71	3.50	19.80	8.60	14.00	11.10	29.90	54.10	0	0
8000	1379	4.07	4.14	12.01	6.76	20.86	24.70	29.45	48.80	0	0
10000	0	3.42	5.77	3.03	6.30	9.84	10.10	6.70	12.50	5.46	11.60
10000	345	3.70	3.81	4.90	4.20	7.40	5.56	27.20	18.77	5.52	6.86
10000	690	8.93	6.24	6.35	7.15	17.90	17.70	32.44	11.75	15.81	11.30
10000	1034	8.63	4.09	10.55	6.34	13.91	33.20	57.10	38.10	0	0
10000	1379	6.77	4.82	10.47	4.71	18.30	13.89	31.90	36.50	0	0

Table 13. Dynamic stiffness real and imaginary parts at 4000 rpm 0 kPa (MN/m)

f	$R(H_{xx})$	$I(H_{xx})$	$R(H_{xy})$	$I(H_{xy})$	$R(H_{yx})$	$I(H_{yx})$	$R(H_{yy})$	$I(H_{yy})$	$\Delta R(H_{xx})$	$\Delta I(H_{xx})$	$\Delta R(H_{xy})$	$\Delta I(H_{xy})$	$\Delta R(H_{yx})$	$\Delta I(H_{yx})$	$\Delta R(H_{yy})$	$\Delta I(H_{yy})$
20	-1.1	24.6	-35.5	-5.0	80.6	-0.7	3.3	54.1	0.63	0.69	1.09	0.41	2.11	0.65	0.61	1.42
30	-1.0	38.3	-36.0	-6.9	80.5	0.9	1.8	79.2	0.39	0.72	1.29	0.37	1.68	0.56	0.70	1.90
40	-1.3	50.8	-35.1	-8.3	82.8	0.1	-1.7	106.2	0.61	1.10	1.32	0.75	1.71	0.68	0.52	2.72
50	-3.2	62.8	-33.2	-10.4	84.5	0.1	-5.4	133.6	0.66	1.47	1.31	0.42	1.49	1.24	0.74	3.46
60	-11.3	71.5	-33.3	-18.2	88.3	-0.5	-6.2	162.4	55.18	36.06	25.99	36.11	5.39	5.59	4.20	4.12
70	-5.2	86.2	-28.9	-13.1	87.8	0	-17.0	193.9	1.75	1.60	2.25	1.31	2.80	3.14	8.82	4.39
80	-10.2	98.4	-27.6	-18.5	87.3	1.4	-14.0	217.2	1.31	2.60	1.84	1.13	2.20	1.86	1.05	5.64
90	-14.1	112.4	-24.8	-20.3	89.9	-0.6	-18.6	240.2	1.54	2.99	1.15	1.42	2.95	1.99	1.96	5.78
100	-17.5	125.9	-22.6	-22.4	91.4	0.4	-22.7	268.9	2.17	3.66	2.45	2.31	1.51	3.52	3.18	5.87
110	-20.8	139.1	-17.9	-22.1	91.7	-0.6	-22.5	292.8	1.84	4.37	3.03	2.25	2.37	2.79	3.24	9.69
120	-23.3	156.0	-17.7	-28.2	93.0	-0.3	-40.5	333.2	5.91	5.07	11.94	8.80	9.04	14.09	19.16	21.41
130	-18.4	173.0	-9.5	-31.3	72.3	-29.1	-46.1	355.8	40.17	23.26	12.65	10.84	73.32	46.52	29.30	16.26
140	-39.0	188.0	-13.0	-28.8	100.4	1.2	-47.3	370.0	3.24	4.90	3.42	4.45	6.60	4.47	6.45	13.73
150	-20.6	231.5	-20.4	-24.2	115.4	1.1	-55.5	404.3	22.13	15.61	4.50	4.99	15.09	22.89	7.45	11.52
160	-40.6	205.6	-5.8	-24.7	102.9	4.8	-54.3	424.9	3.67	4.97	3.21	4.18	2.43	2.38	4.70	16.15
170	-44.5	223.1	-10.2	-28.6	108.8	7.8	-65.2	456.4	2.18	4.10	7.45	6.08	3.06	4.66	4.52	6.90
180	-61.6	256.5	11.7	-3.1	108.0	16.3	-73.9	474.0	89.79	99.07	146.24	229.38	29.33	24.03	38.11	25.12
190	-69.3	228.3	8.3	-26.8	116.1	9.8	-71.0	485.9	23.55	21.04	24.80	19.31	45.21	54.74	33.73	56.97
200	-69.5	250.4	4.5	-29.9	116.4	13.5	-79.1	514.3	12.73	5.90	5.63	22.05	17.35	18.13	38.27	17.75
210	-399.6	266.0	21.6	-58.6	70.8	19.5	-81.1	557.0	172.46	71.97	19.14	22.80	50.97	71.64	18.66	22.29
220	-108.1	287.7	-2.2	-5.3	125.1	12.9	-117.8	589.1	8.06	9.95	9.91	10.42	11.33	9.55	20.15	16.50
230	-106.6	302.3	6.5	-12.5	128.8	19.5	-85.8	624.3	6.38	2.69	11.41	7.25	4.99	6.06	19.87	8.11
240	-63.4	261.4	2.4	-2.3	128.0	20.1	-76.9	654.3	13.21	10.75	7.22	10.26	16.46	11.14	38.09	35.46
250	-57.3	298.6	-9.2	-9.1	141.2	14.8	-106.1	682.9	9.98	13.27	7.06	13.25	16.26	25.60	26.00	24.99
260	4.7	227.5	10.3	23.5	135.9	7.9	-82.3	715.0	38.07	11.37	8.77	11.84	14.07	31.56	41.99	29.99
270	-297.3	234.6	14.4	4.9	132.7	-5.1	-65.3	790.3	23.75	18.32	10.83	19.21	21.79	19.99	72.52	25.36
280	-79.8	332.6	22.9	36.3	150.8	28.3	28.4	875.0	17.61	7.13	8.09	21.02	4.31	4.82	81.71	21.91
290	-97.9	315.0	48.7	36.0	146.3	17.7	100.1	842.8	21.59	6.29	9.62	13.27	7.43	10.40	94.68	43.42
300	-52.1	339.7	61.0	74.4	167.4	40.9	90.1	982.8	27.44	8.16	19.48	26.98	8.10	7.86	100.94	32.99

Table 14. Dynamic stiffness real and imaginary parts at 4000 rpm 345 kPa (MN/m)

f	$R(H_{xx})$	$I(H_{xx})$	$R(H_{xy})$	$I(H_{xy})$	$R(H_{yx})$	$I(H_{yx})$	$R(H_{yy})$	$I(H_{yy})$	$\Delta R(H_{xx})$	$\Delta I(H_{xx})$	$\Delta R(H_{xy})$	$\Delta I(H_{xy})$	$\Delta R(H_{yx})$	$\Delta I(H_{yx})$	$\Delta R(H_{yy})$	$\Delta I(H_{yy})$
20	29.2	20.0	-28.3	7.4	76.9	5.9	38.8	45.6	2.95	0.68	0.81	0.52	2.32	0.85	2.02	2.27
30	28.4	32.2	-27.9	12.3	83.0	11.7	40.9	72.4	3.02	1.04	0.91	0.90	2.61	0.96	2.46	2.74
40	27.7	46.0	-27.7	15.4	80.7	15.5	37.9	93.8	3.66	1.60	0.94	1.12	2.57	0.58	2.58	3.14
50	24.2	57.0	-25.9	18.6	84.7	18.4	39.0	120.7	3.02	1.62	1.39	1.61	2.24	0.97	2.20	3.88
60	18.8	75.3	-32.3	21.2	84.3	21.4	42.7	142.4	53.75	46.08	31.55	44.52	7.32	5.31	3.30	7.60
70	20.4	84.9	-26.8	24.1	79.3	29.1	31.6	157.9	1.95	4.02	1.81	1.85	2.76	1.10	2.34	6.51
80	23.3	99.0	-21.1	29.2	72.1	43.0	-43.5	225.1	2.85	3.78	2.07	1.56	4.05	2.64	9.89	18.84
90	22.6	114.3	-25.9	33.5	82.4	38.5	24.9	213.3	2.83	3.86	1.49	2.81	1.83	3.41	1.29	6.59
100	22.9	127.1	-24.4	39.2	91.5	35.4	25.4	239.2	3.18	3.83	2.03	3.75	1.83	2.47	2.49	8.04
110	20.4	138.4	-26.3	35.3	84.2	42.6	11.6	240.2	2.21	4.08	2.55	2.29	1.85	1.52	3.20	8.83
120	29.5	151.5	-20.8	45.8	85.0	51.7	7.3	284.8	8.53	7.75	5.41	8.02	9.32	7.90	11.37	16.68
130	22.2	175.3	-16.8	46.6	67.6	5.7	3.9	271.6	26.28	35.26	16.08	6.20	58.29	91.71	40.55	12.77
140	15.6	183.6	-16.5	55.0	113.8	60.4	4.9	352.2	7.14	7.14	13.92	2.75	12.12	15.17	31.23	6.17
150	50.8	204.9	-3.4	59.7	74.5	13.4	55.1	323.7	18.33	11.16	8.48	8.14	21.27	15.11	5.91	9.50
160	15.0	200.6	-13.1	49.8	93.5	55.6	18.0	358.5	1.42	7.04	5.71	6.43	1.37	5.23	4.09	12.17
170	19.7	215.3	-12.9	67.1	105.5	81.5	13.8	413.5	3.65	7.75	3.48	9.29	2.40	3.91	3.20	12.64
180	3.4	236.6	-15.9	48.1	96.3	79.7	5.1	382.4	88.96	99.03	166.94	180.45	13.30	11.77	7.72	12.59
190	3.7	221.4	-5.8	69.7	113.1	68.7	47.8	419.4	18.33	18.35	14.80	15.90	31.20	23.14	15.95	14.88
200	11.3	249.4	-12.3	62.0	88.0	77.9	-1.8	402.9	9.06	19.43	25.32	19.17	25.24	11.29	45.28	25.55
210	-448.8	796.4	-186.9	221.4	400.0	251.2	92.4	573.2	695.98	735.26	219.58	248.70	534.91	624.59	174.30	197.41
220	-8.1	301.7	-5.3	100.2	121.2	70.5	21.0	446.4	6.69	8.12	6.83	9.28	6.69	7.70	5.75	10.11
230	-20.9	283.2	-2.8	85.8	140.1	110.4	19.2	535.9	4.63	8.50	5.93	5.24	6.75	4.36	3.26	14.79
240	-12.9	247.5	-2.9	80.5	121.2	104.2	9.3	505.7	7.33	6.61	6.64	8.57	11.43	7.86	9.53	20.64
250	6.4	279.5	-4.99	91.6	147.4	105.4	20.5	564.0	3.82	8.90	6.91	7.04	8.34	5.81	8.30	17.22
260	15.0	214.9	-0.2	77.2	105.6	126.9	16.6	558.1	8.10	25.55	6.89	11.11	15.86	49.00	11.02	27.17
270	-165.4	200.4	-35.8	80.3	82.6	73.9	-6.4	515.9	49.92	373.32	66.11	124.76	404.56	503.12	69.67	242.41
280	-20.6	325.7	-10.4	128.3	155.5	148.8	-22.6	702.4	11.51	9.33	10.43	9.07	5.21	11.64	13.30	19.63
290	-53.3	317.1	-23.5	106.1	135.8	123.6	3.0	581.7	9.09	12.11	10.78	10.59	4.93	4.52	4.89	13.64
300	-7.8	336.5	2.0	137.3	151.6	183.2	7.9	830.9	9.56	13.21	11.81	15.68	4.20	10.65	14.37	17.66

Table 15. Dynamic stiffness real and imaginary parts at 4000 rpm 690 kPa (MN/m)

f	$R(H_{xx})$	$I(H_{xx})$	$R(H_{xy})$	$I(H_{xy})$	$R(H_{yx})$	$I(H_{yx})$	$R(H_{yy})$	$I(H_{yy})$	$\Delta R(H_{xx})$	$\Delta I(H_{xx})$	$\Delta R(H_{xy})$	$\Delta I(H_{xy})$	$\Delta R(H_{yx})$	$\Delta I(H_{yx})$	$\Delta R(H_{yy})$	$\Delta I(H_{yy})$
20	70.2	38.1	-41.0	25.8	150.6	23.6	102.7	82.1	3.97	2.18	1.60	1.97	7.22	1.92	5.79	3.04
30	75.2	61.0	-37.5	43.2	150.1	25.5	107.0	116.5	4.93	2.58	2.83	2.62	6.04	3.67	4.59	5.40
40	75.0	79.3	-32.0	54.5	152.9	45.0	102.3	167.4	4.58	2.74	2.73	2.88	7.02	1.71	6.15	5.11
50	76.5	96.4	-23.1	69.4	162.3	32.1	125.1	199.6	4.99	2.72	2.02	4.14	7.86	2.54	8.12	8.46
60	71.3	125.4	-35.1	79.0	152.0	67.6	99.9	247.1	33.12	33.97	37.42	31.55	13.39	7.86	13.64	11.68
70	69.4	150.3	-26.3	91.1	162.9	88.5	100.3	290.7	4.20	4.43	2.67	4.10	7.05	3.29	6.90	9.29
80	78.1	158.5	-11.1	95.6	143.1	89.9	74.4	339.2	5.56	4.93	2.36	4.41	12.05	2.97	10.41	19.13
90	75.6	182.8	-10.8	116.4	164.2	116.0	83.6	405.5	5.72	6.32	2.39	8.01	8.02	6.98	5.49	16.03
100	92.4	212.9	-1.1	133.9	193.2	104.3	102.1	423.3	6.47	4.71	4.50	7.65	7.17	6.95	8.13	15.49
110	82.9	230.1	-6.0	129.9	155.1	96.0	76.9	388.3	6.86	6.05	2.73	8.15	8.97	5.43	9.59	15.54
120	88.8	233.5	13.1	139.0	171.6	114.9	103.8	484.6	11.10	10.56	9.01	13.81	21.07	12.33	21.02	25.15
130	91.0	275.4	20.0	164.0	198.0	148.9	107.3	508.7	28.85	24.46	23.29	22.45	79.51	49.87	75.19	42.60
140	131.6	310.8	43.2	189.2	271.6	165.9	132.2	624.8	12.20	8.81	8.55	10.10	11.47	12.74	10.94	25.25
150	122.0	316.2	50.1	177.1	296.7	86.6	261.5	529.9	10.21	11.53	7.51	12.36	18.41	10.53	17.56	19.04
160	60.0	306.5	17.7	163.7	163.0	149.4	83.0	606.7	14.97	19.50	9.53	17.42	9.55	8.41	7.73	18.80
170	90.0	324.8	34.8	185.6	214.5	175.5	114.2	694.4	10.57	11.77	11.79	12.00	12.03	7.83	16.43	21.01
180	164.3	539.2	62.9	284.7	259.2	162.2	155.6	666.9	413.69	228.99	696.77	578.88	24.13	11.34	26.33	33.29
190	111.6	359.7	78.9	195.6	267.2	133.8	245.9	654.8	14.19	9.88	19.22	16.62	13.32	12.88	16.43	25.44
200	77.1	395.2	47.9	205.2	196.8	179.6	104.7	674.7	57.94	93.18	38.65	44.14	160.01	87.38	76.50	75.84
210	125.8	438.2	73.1	246.0	338.9	232.1	208.5	836.1	15.39	9.19	14.32	10.96	14.25	10.75	21.94	26.77
220	113.9	431.0	90.0	237.1	237.9	119.8	133.8	615.4	15.81	9.11	9.72	11.17	11.37	6.08	13.91	15.51
230	106.6	410.2	98.5	216.7	323.7	204.0	208.1	863.0	18.25	15.94	23.09	24.68	15.25	5.96	16.11	25.64
240	104.8	465.8	101.2	253.6	305.1	197.7	251.5	823.7	13.06	9.02	17.24	14.32	17.60	10.23	27.80	19.85
250	97.4	459.8	74.6	258.9	297.8	225.2	164.0	923.9	12.33	13.37	11.90	14.59	19.91	8.75	31.67	32.41
260	57.1	481.3	76.5	278.6	345.7	265.6	267.6	938.6	39.92	32.79	38.44	29.34	71.90	39.91	64.22	30.74
270	94.3	445.3	101.8	241.6	307.6	172.1	273.5	777.1	24.79	15.68	17.35	13.89	21.86	19.83	31.84	29.09
280	137.5	557.2	162.3	327.0	379.0	266.5	323.9	1115.2	14.90	9.84	17.84	10.52	17.48	10.52	30.21	32.38
290	72.2	591.3	85.8	333.5	308.2	224.1	219.7	893.6	15.64	9.06	13.63	12.06	17.13	7.59	29.41	31.37
300	97.6	592.1	87.5	374.8	154.3	244.3	-202.0	840.7	29.75	23.00	47.62	35.83	23.73	10.01	52.14	21.73

Table 16. Dynamic stiffness real and imaginary parts at4000 rpm and 1034 kPa (MN/m)

f	$R(H_{xx})$	$I(H_{xx})$	$R(H_{xy})$	$I(H_{xy})$	$R(H_{yx})$	$I(H_{yx})$	$R(H_{yy})$	$I(H_{yy})$	$\Delta R(H_{xx})$	$\Delta I(H_{xx})$	$\Delta R(H_{xy})$	$\Delta I(H_{xy})$	$\Delta R(H_{yx})$	$\Delta I(H_{yx})$	$\Delta R(H_{yy})$	$\Delta I(H_{yy})$
20	121.8	51.5	-36.7	38.4	230.8	33.7	212.7	115.2	3.72	2.19	1.37	2.52	1.96	1.76	1.82	5.16
30	120.1	77.4	-33.9	60.5	231.3	39.7	213.6	168.4	2.33	4.49	2.84	4.12	2.21	3.56	1.79	8.90
40	121.0	103.8	-31.1	84.2	239.1	65.5	212.5	246.1	2.43	3.61	1.46	3.22	2.33	2.58	3.71	10.73
50	125.2	119.8	-15.5	107.9	252.2	49.4	244.6	290.8	2.15	5.12	2.07	5.55	4.35	1.82	7.12	12.39
60	120.0	163.7	-23.1	135.8	248.4	95.8	222.6	369.8	57.55	48.77	65.16	57.19	8.81	14.32	13.10	15.78
70	128.7	197.8	-13.9	158.6	261.4	124.9	227.3	432.3	3.73	7.62	3.30	7.21	3.77	6.71	4.39	19.50
80	147.7	211.6	17.6	171.9	246.6	91.5	198.8	419.5	4.22	9.78	5.12	8.49	4.14	4.10	5.70	14.67
90	143.3	238.9	16.5	198.2	272.8	153.2	230.0	583.5	3.68	6.78	6.27	8.37	6.58	5.11	10.31	23.39
100	168.8	262.1	41.7	218.8	311.2	132.5	265.4	600.0	5.24	9.30	6.32	9.16	7.17	3.30	10.20	22.06
110	158.4	290.1	36.1	225.0	268.1	127.5	232.2	573.9	4.50	9.50	6.24	12.28	8.82	5.96	11.26	25.27
120	167.2	296.1	62.4	237.1	288.5	138.5	267.4	673.6	15.38	27.66	19.18	36.47	30.95	34.08	35.53	61.90
130	185.0	348.1	100.1	271.9	329.3	154.1	315.9	751.9	35.46	36.07	42.64	52.68	111.41	135.35	172.53	162.44
140	240.0	355.2	141.3	290.0	437.0	195.6	356.7	860.8	11.58	6.50	15.09	9.75	33.14	17.69	48.26	33.11
150	233.9	372.6	150.2	271.5	462.4	85.4	511.4	725.5	17.16	11.34	20.22	10.26	16.10	9.30	19.33	25.60
160	165.9	391.7	99.3	291.2	293.8	208.1	250.9	892.7	14.75	11.87	14.73	11.36	15.46	9.04	13.16	34.06
170	199.7	390.2	138.0	288.9	368.5	198.0	336.8	942.4	8.50	10.32	17.39	12.19	12.38	7.68	20.52	24.72
180	261.6	701.8	82.4	609.6	407.2	155.6	389.4	854.9	410.76	169.20	570.98	724.13	19.74	15.48	25.85	44.16
190	225.2	425.5	181.5	291.4	416.7	140.1	464.8	863.0	26.87	24.06	30.21	26.15	36.97	32.72	31.79	64.57
200	219.2	485.6	184.9	331.2	404.0	181.5	387.6	879.1	13.42	82.63	27.16	41.49	121.68	84.51	85.44	39.45
210	261.3	482.3	217.2	324.1	528.8	203.6	520.9	1035.2	17.68	11.46	21.45	9.66	24.22	17.53	36.11	19.27
220	215.0	486.4	190.7	326.5	361.1	93.9	380.8	754.8	24.93	19.68	24.14	14.17	16.11	6.73	22.00	18.28
230	240.6	472.1	237.9	320.2	504.7	197.2	496.4	1107.0	10.55	18.45	25.84	15.15	20.61	9.09	30.23	41.23
240	244.4	507.5	246.5	338.6	489.1	183.0	566.5	1051.8	15.83	19.66	23.99	12.92	20.85	8.55	31.78	30.16
250	233.9	511.2	235.6	350.6	461.5	187.3	478.1	1088.4	11.41	18.89	20.56	15.71	18.64	15.71	38.56	25.64
260	210.1	525.8	242.9	353.8	525.5	216.7	604.6	1094.9	51.76	47.08	51.72	33.47	87.36	80.36	89.81	76.15
270	218.2	475.0	237.5	296.2	478.1	132.5	581.8	925.0	52.30	24.57	57.33	19.39	81.02	24.52	91.45	43.36
280	277.1	573.0	326.6	387.0	542.7	269.5	589.4	1408.7	14.18	12.40	18.47	10.56	15.39	5.67	22.93	51.71
290	241.3	625.7	281.2	405.2	477.5	180.2	552.3	1066.8	12.88	11.77	17.08	8.28	11.36	4.38	21.99	27.61
300	235.5	603.4	270.7	394.4	429.1	183.4	496.1	1014.6	15.22	21.00	21.29	13.16	16.89	7.95	42.11	26.58

Table 17. Dynamic stiffness real and imaginary parts at 6000 rpm and 0 kPa (MN/m)

f	$R(H_{xx})$	$I(H_{xx})$	$R(H_{xy})$	$I(H_{xy})$	$R(H_{yx})$	$I(H_{yx})$	$R(H_{yy})$	$I(H_{yy})$	$\Delta R(H_{xx})$	$\Delta I(H_{xx})$	$\Delta R(H_{xy})$	$\Delta I(H_{xy})$	$\Delta R(H_{yx})$	$\Delta I(H_{yx})$	$\Delta R(H_{yy})$	$\Delta I(H_{yy})$
20	-2.7	22.4	-49.3	-6.8	104.5	0.4	2.8	51.5	0.66	1.08	2.86	0.83	6.59	2.27	3.30	6.69
30	-3.5	35.7	-50.1	-11.3	103.4	0.3	5.0	73.4	0.44	1.44	3.22	0.82	7.76	1.86	1.33	7.54
40	-2.8	49.2	-51.9	-14.3	100.0	3.6	4.9	89.1	0.59	2.09	3.68	0.95	4.81	1.38	2.46	3.16
50	-2.4	60.4	-52.8	-15.3	103.9	6.4	-2.3	110.0	0.70	2.47	3.88	1.39	5.62	2.62	2.79	4.55
60	-14.8	71.1	-56.2	-21.7	104.2	7.5	-9.2	129.9	50.42	21.48	27.83	40.95	7.51	5.18	5.28	7.22
70	-4.0	80.1	-45.1	-15.0	116.5	9.1	-25.9	173.0	1.12	4.04	3.65	1.72	8.81	3.26	5.54	6.18
80	-10.0	93.0	-42.3	-21.3	117.9	4.2	-19.0	189.1	1.03	3.18	4.44	1.00	12.64	8.78	2.45	8.76
90	-11.3	104.4	-39.0	-23.6	115.5	8.4	-25.0	209.2	2.68	4.63	3.86	1.83	7.66	3.98	1.75	7.32
100	-13.8	120.6	-50.9	-23.5	105.9	2.4	-19.5	212.7	3.70	6.62	5.65	2.58	4.39	11.63	7.61	4.37
110	-16.0	127.8	-34.1	-29.8	105.7	4.8	-28.0	255.3	2.41	5.97	4.02	3.93	2.79	4.65	1.81	8.28
120	-18.7	138.2	-28.8	-31.5	112.0	4.6	-32.0	284.4	3.81	3.71	3.63	6.69	7.10	9.13	8.87	6.97
130	-30.1	149.7	-27.0	-34.8	108.5	17.5	-42.8	300.7	4.23	4.12	1.18	6.45	4.25	3.54	2.77	10.96
140	-37.9	162.9	-23.7	-42.5	114.6	10.7	-47.4	322.3	5.45	7.79	3.10	4.30	7.94	19.99	6.76	10.91
150	-26.1	198.5	-33.9	-37.1	119.2	26.8	-60.9	341.2	12.54	15.13	9.02	7.90	16.91	11.62	5.27	6.86
160	-37.5	179.1	-15.6	-31.4	113.6	24.7	-62.3	370.9	6.01	6.94	3.98	7.29	7.81	10.99	6.35	5.10
170	-44.3	193.3	-20.8	-41.5	119.2	18.8	-64.0	393.2	2.98	8.97	6.10	7.09	8.53	5.92	1.09	12.77
180	23.1	217.6	144.4	308.9	127.0	35.1	-89.8	430.8	83.78	140.24	141.27	136.71	30.58	13.05	4.65	19.69
190	-58.5	191.0	-7.2	-36.2	119.1	35.3	-90.4	434.7	17.82	17.59	8.07	12.11	34.17	20.37	4.97	16.23
200	-70.8	216.8	14.2	-35.3	127.4	46.4	-113.7	437.5	4.72	20.40	10.50	12.60	15.70	34.77	11.11	18.41
210	449.5	448.4	-111.0	-14.6	36.4	200.2	-107.4	438.1	337.70	118.83	52.35	51.72	171.17	53.83	28.28	14.51
220	-116.9	265.4	3.1	-33.9	132.5	33.2	-118.8	500.2	10.02	12.98	5.13	3.17	26.31	20.34	6.38	7.64
230	-112.4	269.0	11.5	-37.2	138.3	43.3	-116.6	539.8	6.36	9.23	3.62	5.91	18.99	10.90	9.26	12.95
240	-67.3	219.0	5.6	-21.2	127.2	42.5	-112.0	551.3	5.60	17.58	9.99	10.19	9.32	13.27	9.35	12.96
250	-77.0	254.4	2.2	-41.3	138.3	38.7	-120.0	574.8	3.52	3.84	13.25	4.54	5.21	5.62	3.97	11.95
260	13.4	168.2	6.0	-8.5	152.2	26.0	-122.8	601.7	12.05	16.33	5.61	5.04	47.55	17.64	15.01	18.67
270	-423.8	48.3	75.0	-20.6	124.5	28.6	-133.9	640.1	39.63	54.27	3.53	4.62	21.77	79.13	12.01	24.06
280	-106.4	287.7	16.1	-22.0	156.6	55.0	-113.5	692.3	4.73	13.06	4.33	7.38	14.69	3.26	15.20	14.67
290	-140.3	256.0	43.2	-11.4	152.4	64.8	-103.5	735.9	6.26	16.79	7.83	6.66	17.34	41.34	30.61	24.25
300	-96.1	280.8	31.7	0.5	172.8	66.6	-123.0	770.1	14.17	12.88	32.72	27.43	35.23	30.55	14.36	23.52

Table 18. Dynamic stiffness real and imaginary parts at 6000 rpm and 345 kPa (MN/m)

f	$R(H_{xx})$	$I(H_{xx})$	$R(H_{xy})$	$I(H_{xy})$	$R(H_{yx})$	$I(H_{yx})$	$R(H_{yy})$	$I(H_{yy})$	$\Delta R(H_{xx})$	$\Delta I(H_{xx})$	$\Delta R(H_{xy})$	$\Delta I(H_{xy})$	$\Delta R(H_{yx})$	$\Delta I(H_{yx})$	$\Delta R(H_{yy})$	$\Delta I(H_{yy})$
20	29.0	18.2	-39.5	2.8	84.0	2.5	33.4	35.1	1.80	0.48	0.32	0.76	6.98	0.38	5.21	2.77
30	29.1	29.9	-39.5	5.9	93.1	2.0	37.9	61.1	1.63	0.74	0.68	0.61	4.46	2.49	2.15	3.36
40	29.0	42.4	-40.7	6.5	89.4	11.5	33.9	76.1	2.21	1.43	0.56	1.40	1.96	3.42	2.26	2.53
50	28.7	50.6	-39.5	10.8	94.9	6.6	37.1	99.0	1.45	0.65	0.99	0.57	6.98	5.14	1.42	5.32
60	36.6	63.5	-29.3	18.6	87.9	12.1	39.8	111.5	13.44	43.63	40.08	13.17	2.83	3.63	4.62	2.84
70	24.1	71.0	-35.4	13.0	93.2	21.1	30.2	128.2	2.73	1.96	0.72	1.79	0.97	8.88	2.47	2.23
80	22.2	82.3	-32.8	10.0	91.0	33.6	-24.6	196.5	2.11	2.57	2.05	2.36	4.39	9.04	13.37	6.46
90	21.8	96.2	-38.1	14.9	102.0	27.6	25.0	171.6	2.69	2.52	1.38	3.25	2.57	10.69	3.45	2.47
100	16.8	102.9	-42.3	19.2	108.6	17.5	26.8	180.7	13.26	23.20	13.90	8.35	23.57	28.08	15.56	15.35
110	16.1	118.2	-38.4	14.9	85.9	19.5	18.8	190.0	0.98	2.47	2.60	1.60	8.99	7.63	2.71	5.03
120	23.3	135.7	-40.0	25.7	97.0	31.5	8.1	225.9	1.71	1.86	1.93	3.94	10.47	15.64	3.25	7.43
130	10.8	141.7	-35.9	18.3	89.9	29.1	26.4	222.4	4.85	4.48	1.38	3.34	9.44	33.49	7.75	5.07
140	5.8	160.2	-38.3	28.7	116.4	44.5	0.9	277.4	6.84	3.20	1.21	3.22	18.10	7.86	3.93	7.00
150	41.3	175.3	-20.6	35.5	92.3	24.5	44.1	279.4	10.74	4.71	2.38	2.65	25.13	17.69	9.83	2.97
160	10.6	181.0	-31.5	21.8	88.3	49.3	5.5	282.7	0.76	4.92	2.72	3.06	16.09	17.94	7.13	1.77
170	12.9	193.2	-31.0	34.4	104.1	51.6	-1.9	332.1	1.82	1.08	2.17	5.17	5.73	6.79	4.89	5.00
180	-6.2	225.0	-47.2	11.2	89.0	54.5	-5.7	307.3	50.65	23.56	30.45	66.22	23.38	8.69	5.60	10.55
190	0.5	192.4	-22.8	34.3	118.2	52.2	35.5	339.5	5.01	4.40	5.49	5.38	24.73	23.60	11.44	8.98
200	13.2	199.9	-3.9	51.1	93.7	105.5	-56.5	291.1	37.81	109.05	12.52	55.77	51.15	201.48	29.79	109.93
210	758.1	308.1	130.2	174.8	-37.9	-141.6	1.6	348.2	581.77	241.79	146.82	86.00	218.21	342.33	64.83	95.55
220	-7.3	263.7	-26.6	55.5	112.4	47.7	-1.8	351.0	3.03	6.87	5.42	5.06	12.14	5.74	4.71	6.00
230	-22.3	254.7	-28.3	43.8	126.5	76.9	-5.4	431.5	2.76	5.68	2.88	6.84	9.99	2.76	5.59	3.78
240	-5.6	207.0	-18.1	36.7	104.4	64.9	7.2	413.7	3.41	6.14	2.15	3.49	6.83	15.55	5.22	9.80
250	-0.9	237.7	-26.1	50.4	134.3	82.7	-7.0	469.9	2.47	5.02	2.63	3.44	24.83	6.86	4.95	4.86
260	44.8	167.2	-11.9	38.1	109.8	96.0	-9.0	457.9	18.96	5.65	3.98	6.07	14.01	6.78	2.28	7.12
270	-257.1	136.5	-56.3	25.9	139.3	146.2	0.7	465.2	56.09	20.45	5.89	7.45	23.77	39.89	10.74	11.93
280	-26.9	273.9	-30.3	68.3	134.9	107.0	1.7	580.0	4.70	4.53	2.42	10.72	9.60	14.26	3.98	17.81
290	-66.9	261.7	-31.6	52.9	102.2	96.4	-50.9	459.0	5.88	5.31	3.44	9.92	8.12	15.58	16.11	11.92
300	-24.6	264.3	-44.4	60.9	100.7	131.4	-116.1	685.6	62.91	72.24	18.50	13.31	200.30	116.42	28.95	27.87

Table 19. Dynamic stiffness real and imaginary parts at 6000 rpm and 690 kPa (MN/m)

f	$R(H_{xx})$	$I(H_{xx})$	$R(H_{xy})$	$I(H_{xy})$	$R(H_{yx})$	$I(H_{yx})$	$R(H_{yy})$	$I(H_{yy})$	$\Delta R(H_{xx})$	$\Delta I(H_{xx})$	$\Delta R(H_{xy})$	$\Delta I(H_{xy})$	$\Delta R(H_{yx})$	$\Delta I(H_{yx})$	$\Delta R(H_{yy})$	$\Delta I(H_{yy})$
20	71.9	25.1	-46.0	13.9	141.9	16.7	91.4	54.5	1.93	0.85	1.18	1.20	16.50	8.29	5.24	7.79
30	72.3	45.0	-47.4	21.1	156.9	16.7	98.8	91.4	1.03	1.78	0.99	1.31	13.27	8.98	2.57	5.95
40	76.9	59.4	-47.3	30.4	146.3	37.3	91.5	117.3	2.68	2.10	1.04	2.03	13.66	12.98	3.77	7.23
50	74.3	70.0	-44.2	37.6	155.3	25.9	101.5	155.1	1.80	2.14	0.95	2.14	18.36	14.14	4.32	9.33
60	64.5	87.0	-47.0	32.6	149.9	40.6	104.7	177.6	75.54	73.71	62.67	59.44	9.43	14.97	9.48	6.62
70	71.9	96.3	-39.2	51.9	165.4	46.7	97.9	210.3	2.23	2.55	1.98	2.21	14.11	13.03	5.82	8.92
80	81.5	118.0	-41.5	62.0	166.1	75.7	88.8	277.2	2.46	3.06	3.00	2.82	12.13	10.14	6.57	7.37
90	75.5	134.5	-40.1	69.9	179.0	78.9	92.6	282.4	2.69	2.25	2.69	2.73	12.85	16.94	8.06	10.76
100	67.8	148.7	-50.7	78.6	167.5	30.5	105.6	270.8	11.33	6.40	8.38	7.42	9.28	13.52	8.82	8.92
110	75.5	158.4	-33.5	85.3	148.4	64.6	89.3	302.6	2.78	4.58	5.03	2.62	4.79	17.56	7.13	12.67
120	80.7	176.3	-29.4	98.6	180.5	77.3	85.8	357.0	10.00	9.43	13.10	9.59	19.50	27.28	21.61	20.71
130	81.0	185.3	-19.2	97.5	172.5	93.5	100.1	364.5	6.65	7.37	3.48	5.08	15.55	26.98	9.01	15.18
140	70.8	206.9	-19.3	108.8	175.4	93.0	78.6	426.1	5.53	8.01	6.04	6.80	23.27	16.95	13.40	15.39
150	106.3	225.4	0.5	119.3	222.2	22.6	168.7	418.5	23.01	13.28	13.84	12.43	44.99	32.42	23.40	13.72
160	75.5	237.6	-17.4	116.3	171.7	111.4	85.9	454.3	6.74	5.78	8.23	5.06	22.91	16.02	14.42	11.36
170	77.3	249.7	-9.9	127.6	196.2	110.1	93.8	510.8	5.06	3.98	6.87	7.25	14.80	18.27	4.01	16.36
180	62.4	300.8	-40.6	137.0	190.0	121.9	83.8	492.3	93.40	64.16	89.87	146.51	29.18	24.28	13.94	23.22
190	41.7	271.6	-18.7	128.9	201.0	129.3	136.4	536.9	13.85	8.83	9.34	10.75	30.71	36.33	15.98	21.64
200	89.8	312.3	22.0	183.9	156.4	96.9	-33.8	470.4	34.30	35.25	28.64	24.64	121.93	77.08	108.16	60.16
210	855.6	147.7	399.1	166.5	-68.5	282.4	-32.4	662.7	495.45	595.88	261.65	301.39	577.40	601.82	240.35	349.00
220	95.4	364.5	10.0	190.6	228.4	80.7	108.1	537.1	6.71	9.32	7.51	12.93	25.97	31.71	16.60	13.82
230	71.7	355.3	2.9	183.8	256.5	171.6	114.7	691.2	10.10	12.50	17.86	17.56	21.10	29.79	11.29	28.26
240	60.8	291.6	6.0	151.1	231.5	150.0	148.1	639.3	5.80	10.62	6.64	12.82	38.78	20.92	22.78	19.90
250	86.4	320.8	16.2	172.9	247.6	138.0	134.7	724.8	4.64	8.01	10.07	5.68	26.63	22.41	18.25	13.77
260	103.2	207.6	31.2	115.1	266.6	156.2	153.1	690.8	15.60	12.76	10.33	10.84	49.09	33.54	28.36	17.86
270	-334.9	292.5	-187.5	158.8	322.7	143.4	201.5	675.3	36.59	46.39	18.48	24.45	123.11	70.73	63.83	36.77
280	67.9	377.0	15.9	215.6	269.5	213.5	144.7	901.0	8.63	7.45	8.30	10.27	9.32	16.10	14.18	16.72
290	10.6	401.9	-17.9	222.8	240.7	195.5	157.7	741.2	15.35	11.70	8.26	8.81	29.35	26.43	14.51	23.39
300	80.7	398.6	12.2	267.3	148.0	253.7	-187.6	907.2	26.04	63.83	58.99	101.90	57.33	120.18	112.43	202.99

Table 20. Dynamic stiffness real and imaginary parts at 6000 rpm and 1034 kPa (MN/m)

f	$R(H_{xx})$	$I(H_{xx})$	$R(H_{xy})$	$I(H_{xy})$	$R(H_{yx})$	$I(H_{yx})$	$R(H_{yy})$	$I(H_{yy})$	$\Delta R(H_{xx})$	$\Delta I(H_{xx})$	$\Delta R(H_{xy})$	$\Delta I(H_{xy})$	$\Delta R(H_{yx})$	$\Delta I(H_{yx})$	$\Delta R(H_{yy})$	$\Delta I(H_{yy})$
20	113.0	45.0	-44.3	28.9	228.6	21.7	181.0	69.1	9.15	15.37	7.37	8.14	35.89	15.71	11.61	9.29
30	101.6	57.7	-41.6	30.5	239.1	6.2	192.4	114.8	8.03	6.83	5.28	7.66	36.90	21.17	3.93	16.72
40	115.3	81.4	-42.4	47.4	222.4	58.6	169.2	160.5	9.22	8.45	4.23	8.09	10.92	19.69	8.50	6.78
50	115.0	80.6	-33.8	58.8	256.9	19.2	197.2	215.8	5.76	6.43	3.60	7.99	48.80	15.19	10.85	25.29
60	123.5	88.0	-33.2	69.3	256.7	61.8	196.2	256.8	41.19	80.95	54.25	67.84	41.72	32.29	16.49	24.04
70	113.6	125.2	-34.1	83.7	220.9	76.0	183.7	282.3	6.62	12.41	2.77	10.12	14.52	16.30	5.40	15.04
80	138.8	135.3	-6.9	98.5	175.6	37.8	113.0	280.4	6.60	13.89	5.48	10.16	64.95	60.21	9.50	40.45
90	121.8	153.1	-21.0	106.9	281.6	76.8	202.3	392.0	4.67	11.13	6.33	9.20	61.79	27.21	27.42	26.41
100	120.7	162.9	-25.4	120.4	248.7	33.5	201.7	370.7	18.60	18.49	16.82	15.39	17.28	50.71	38.72	26.58
110	117.2	185.7	-17.8	126.1	229.9	93.7	172.4	410.7	8.04	13.77	8.93	13.63	12.29	46.69	15.71	27.22
120	126.0	197.9	-3.4	135.8	215.4	104.6	156.2	470.7	15.76	18.32	13.14	16.00	46.62	23.52	30.62	19.08
130	135.2	231.2	-1.1	150.2	206.8	144.3	175.0	472.9	17.72	17.08	13.93	15.89	83.37	107.03	64.71	39.32
140	146.4	230.0	22.1	157.3	316.9	205.3	180.8	644.3	13.50	19.15	15.83	11.62	25.46	131.88	24.80	81.57
150	169.1	260.9	36.0	169.8	279.0	30.6	314.3	540.4	31.13	33.67	23.02	20.14	168.14	46.56	81.99	44.49
160	116.3	270.0	7.9	158.2	263.5	150.1	183.9	605.6	14.80	18.08	19.36	15.99	81.78	57.40	33.03	50.50
170	125.6	275.7	19.8	170.9	279.7	180.6	186.8	714.5	8.20	23.20	16.17	10.65	11.65	84.30	15.92	52.47
180	203.5	386.4	-8.0	286.2	344.4	145.7	226.4	649.9	210.91	153.48	330.78	181.25	90.08	34.31	48.39	32.37
190	126.1	320.1	33.7	199.4	380.1	89.8	333.2	657.8	11.16	24.29	14.62	24.17	141.22	41.00	78.54	21.84
200	132.1	353.7	10.4	235.5	234.9	124.1	145.3	543.8	86.82	70.57	228.03	161.10	284.41	317.52	221.88	924.40
210	147.6	409.6	38.8	267.9	316.9	239.4	278.6	862.6	21.65	26.26	11.76	31.43	162.81	100.48	118.18	56.54
220	160.8	387.9	68.8	249.0	247.6	192.7	221.8	700.9	16.36	24.78	16.46	18.88	98.18	197.88	72.54	127.69
230	158.7	371.4	62.8	231.6	335.7	140.8	232.1	873.1	21.93	23.44	27.43	29.52	73.22	62.09	41.03	42.15
240	136.3	385.7	61.2	243.2	322.0	125.2	303.8	802.9	10.25	20.62	17.08	19.68	22.98	88.35	18.23	61.77
250	147.0	371.1	69.2	239.6	261.2	243.7	105.4	934.7	13.87	29.13	28.53	32.53	68.31	94.21	41.99	66.31
260	96.4	349.9	42.9	228.6	357.6	317.2	307.9	981.9	15.93	15.95	18.00	15.29	98.90	148.96	69.61	98.16
270	21.6	314.6	4.0	210.1	478.0	40.6	428.5	764.5	14.17	29.01	10.71	24.97	177.18	222.47	99.65	143.99
280	164.6	442.2	96.7	296.3	364.8	317.2	223.5	1258.8	17.06	24.24	23.99	24.04	34.23	58.18	23.22	63.97
290	121.4	498.0	72.8	331.4	325.2	196.4	316.7	925.4	13.25	26.39	31.90	18.60	77.60	30.97	47.46	41.89
300	140.5	450.4	101.1	299.9	281.7	173.3	218.6	693.9	39.48	49.85	109.34	40.70	67.56	109.63	77.50	155.73

Table 21. Dynamic stiffness real and imaginary parts at 6000 rpm and 1379 kPa (MN/m)

f	$R(H_{xx})$	$I(H_{xx})$	$R(H_{xy})$	$I(H_{xy})$	$R(H_{yx})$	$I(H_{yx})$	$R(H_{yy})$	$I(H_{yy})$	$\Delta R(H_{xx})$	$\Delta I(H_{xx})$	$\Delta R(H_{xy})$	$\Delta I(H_{xy})$	$\Delta R(H_{yx})$	$\Delta I(H_{yx})$	$\Delta R(H_{yy})$	$\Delta I(H_{yy})$
20	162.0	30.9	-13.9	25.8	350.9	-20.8	329.6	95.1	12.76	6.72	3.89	7.10	35.19	45.44	10.11	8.77
30	150.4	61.9	-21.8	28.1	380.4	-10.6	331.9	149.5	11.05	11.88	6.76	6.28	40.85	27.08	12.84	9.55
40	168.1	78.1	-23.9	58.3	394.2	43.6	310.7	236.4	13.81	16.20	8.71	9.81	57.63	48.14	17.46	22.40
50	158.0	88.9	-16.6	69.6	402.1	9.2	344.1	292.5	9.52	7.74	3.67	7.91	64.09	25.90	17.50	27.53
60	167.2	102.5	-12.7	75.3	380.8	40.0	359.2	338.5	90.67	77.17	89.80	59.25	45.80	39.72	24.62	21.10
70	158.5	128.9	-16.1	98.7	246.3	116.7	296.1	348.3	11.50	15.46	8.97	16.63	54.67	40.44	22.29	24.40
80	183.9	149.3	9.2	125.4	274.3	-30.5	307.9	340.2	11.00	11.68	5.70	13.07	37.35	84.48	36.20	32.84
90	166.2	173.5	-7.2	133.7	382.7	2.3	384.9	480.6	15.92	12.41	11.56	19.31	25.02	65.56	32.66	25.79
100	166.5	191.5	-15.7	159.7	298.9	11.6	331.0	453.6	24.81	22.93	18.91	33.60	38.87	71.16	72.54	43.57
110	166.9	203.6	5.8	158.8	315.1	67.6	328.3	521.2	13.38	14.15	13.33	15.06	27.22	37.70	11.40	26.55
120	178.9	219.2	21.4	176.8	277.7	174.7	276.5	642.4	21.51	16.88	22.04	29.16	75.22	66.31	55.19	48.79
130	188.9	251.8	33.4	190.6	236.5	105.0	307.5	576.9	14.82	20.32	19.76	25.21	140.24	66.18	71.43	51.29
140	208.6	249.8	62.4	207.8	529.4	108.0	452.6	780.1	20.61	29.83	12.90	28.12	117.30	48.72	90.84	38.14
150	230.2	294.2	87.1	225.6	245.9	-106.9	429.7	567.9	34.51	41.69	30.46	36.41	238.75	117.41	126.67	111.15
160	176.6	303.3	38.3	218.2	253.6	243.2	259.5	860.3	16.66	20.71	14.41	25.44	123.69	98.98	88.77	54.29
170	195.3	303.7	67.1	227.7	464.8	191.1	424.0	911.3	19.01	19.57	20.56	23.02	86.85	67.93	60.13	57.11
180	254.6	446.0	43.2	383.9	533.4	257.0	449.9	912.1	90.70	164.18	203.38	284.16	107.20	125.28	60.13	103.19
190	200.2	340.3	89.5	245.8	445.7	7.2	528.6	775.1	24.61	19.97	32.25	19.63	103.93	84.29	74.58	59.39
200	203.2	374.2	105.5	264.7	294.3	241.0	290.2	973.2	58.20	36.72	67.72	37.04	143.84	292.28	175.11	300.63
210	218.4	406.9	108.3	288.4	343.0	-19.6	339.8	799.3	24.72	13.37	18.67	17.29	157.93	226.39	167.11	168.18
220	231.2	415.9	130.1	300.9	345.4	407.6	398.8	1022.5	14.50	27.34	20.22	21.64	100.05	265.60	73.81	190.87
230	234.5	408.6	131.8	313.0	602.2	30.8	561.9	1043.8	17.65	27.28	26.71	42.56	148.48	85.09	124.24	68.52
240	224.7	401.2	142.8	292.1	416.2	95.4	509.7	994.5	18.98	17.49	27.76	14.92	66.58	97.30	57.91	89.32
250	223.8	393.6	142.4	292.6	313.9	303.7	392.1	1154.2	22.84	19.38	34.51	19.99	109.17	102.06	77.56	82.73
260	166.5	375.5	116.3	278.8	493.1	179.5	578.1	1099.0	26.05	20.36	26.20	18.34	93.37	203.31	79.83	144.51
270	67.9	341.2	49.3	253.5	773.5	-230.6	782.8	714.9	28.24	25.02	30.93	21.73	158.47	261.03	96.89	209.28
280	226.2	466.0	152.9	340.5	358.7	319.7	129.3	1418.2	17.40	27.73	23.21	23.56	52.50	39.67	39.10	31.02
290	214.0	532.9	171.3	384.3	414.9	256.4	577.0	1143.0	21.55	43.04	24.36	35.74	107.36	96.87	104.04	76.63
300	213.2	472.2	178.1	326.3	445.7	260.4	598.4	964.0	43.12	33.39	33.93	23.51	42.97	115.16	45.41	66.88

Table 22. Dynamic stiffness real and imaginary parts at 8000 rpm and 0 kPa (MN/m)

f	$R(H_{xx})$	$I(H_{xx})$	$R(H_{xy})$	$I(H_{xy})$	$R(H_{yx})$	$I(H_{yx})$	$R(H_{yy})$	$I(H_{yy})$	$\Delta R(H_{xx})$	$\Delta I(H_{xx})$	$\Delta R(H_{xy})$	$\Delta I(H_{xy})$	$\Delta R(H_{yx})$	$\Delta I(H_{yx})$	$\Delta R(H_{yy})$	$\Delta I(H_{yy})$
20.0	1.5	17.2	-61.4	-7.2	114.9	-1.1	7.2	42.9	0.76	0.64	1.10	0.71	1.02	0.82	0.96	1.24
30.0	-0.9	29.9	-60.8	-12.6	113.3	-0.3	9.5	64.9	0.84	0.89	0.67	0.58	0.92	0.76	0.79	1.19
40.0	-2.5	43.7	-62.3	-18.2	110.7	1.4	12.0	82.1	0.87	1.10	0.78	0.94	0.74	0.55	0.89	1.55
50.0	-3.2	57.4	-65.6	-22.5	109.1	5.6	9.4	97.0	0.85	1.14	0.95	1.00	1.14	1.03	1.33	1.55
60.0	-5.9	77.2	-75.5	-36.2	110.6	10.7	5.9	116.3	46.59	51.77	55.44	54.42	4.96	6.43	7.12	6.70
70.0	0.0	78.8	-67.9	-19.3	113.4	15.6	-8.3	133.2	1.75	1.91	1.37	2.23	1.06	1.26	1.92	3.47
80.0	-4.2	87.9	-63.8	-20.5	119.8	16.8	-16.7	157.6	2.05	1.85	3.17	1.50	2.95	2.28	2.36	5.87
90.0	-6.3	99.0	-58.4	-19.6	124.7	16.4	-24.3	182.3	3.37	2.40	2.29	3.79	3.26	4.33	5.38	5.56
100.0	-11.4	111.0	-53.1	-24.3	124.1	12.5	-27.4	205.9	2.52	2.16	3.09	2.48	2.55	3.36	3.24	7.12
110.0	-11.4	122.5	-49.7	-26.3	122.3	14.9	-33.6	226.2	1.97	2.65	2.54	3.45	2.54	2.74	4.34	7.00
120.0	-14.5	135.6	-47.2	-31.6	121.2	16.4	-38.4	247.4	2.54	3.30	6.00	3.56	6.37	9.27	11.93	9.70
130.0	7.3	63.9	-24.2	8.3	189.8	124.0	-121.1	241.1	184.69	136.02	114.27	127.05	318.61	168.13	97.86	251.41
140.0	-27.2	160.1	-47.7	-38.2	121.1	17.0	-43.3	275.7	2.38	2.63	9.64	4.12	5.77	4.91	5.94	21.71
150.0	-26.0	201.9	-52.5	-47.3	127.5	9.3	-49.2	307.5	16.55	10.19	4.91	6.60	9.42	24.68	10.24	11.15
160.0	-31.2	174.9	-33.6	-39.8	125.1	24.4	-60.4	330.1	3.23	3.46	3.27	4.38	3.64	3.73	4.04	10.50
170.0	-35.3	187.4	-31.4	-43.6	125.9	25.0	-65.1	349.2	1.94	3.55	3.14	4.00	2.12	1.12	4.33	9.14
180.0	-73.6	213.2	-48.5	-75.1	121.0	29.7	-76.1	361.9	62.21	51.12	78.93	83.65	15.35	14.14	23.65	23.03
190.0	-57.8	187.4	-20.6	-41.4	132.9	35.6	-85.4	388.4	4.85	6.66	4.40	4.42	4.99	5.54	3.70	10.18
200.0	-60.3	208.2	-15.6	-47.2	131.4	33.5	-87.4	409.7	3.68	2.64	5.59	5.29	4.97	3.96	8.11	14.54
210.0	-325.0	1042.0	-119.1	-242.5	147.2	46.2	-103.8	428.9	1434.04	1037.45	435.04	117.33	134.12	143.84	33.84	36.09
220.0	-101.5	241.4	-11.2	-47.6	136.3	41.6	-107.3	446.2	4.15	5.92	5.46	4.17	4.90	6.17	5.45	11.34
230.0	-105.6	249.5	-6.3	-48.9	136.6	50.3	-123.4	465.8	3.98	6.01	5.20	4.81	4.70	3.22	7.62	7.55
240.0	-71.9	206.8	-1.4	-34.0	143.7	52.3	-121.6	498.4	4.98	7.43	4.58	5.88	9.02	9.30	10.84	17.02
250.0	-69.6	241.3	-5.9	-38.1	145.5	52.9	-125.8	518.0	5.82	4.97	8.59	6.17	7.04	5.29	18.19	9.98
260.0	-32.4	192.1	-1.3	-5.0	200.9	-14.9	-128.2	512.4	44.16	43.92	30.72	25.53	181.87	120.55	87.20	93.20
270.0	-339.5	83.6	40.6	-29.8	206.8	87.8	-152.5	584.0	74.66	136.61	16.60	18.80	189.81	106.98	30.87	28.87
280.0	-103.2	273.9	1.7	-29.8	157.4	73.3	-140.7	622.7	5.46	7.18	5.85	6.31	5.72	6.23	9.81	17.60
290.0	-124.3	259.3	16.9	-12.9	159.7	93.1	-165.7	669.9	7.30	5.60	7.80	5.97	6.95	3.98	11.78	15.58
300.0	-96.8	277.2	12.1	-11.5	178.5	91.5	-159.1	717.2	9.18	7.53	8.31	8.15	8.28	4.42	9.00	17.25

Table 23. Dynamic stiffness real and imaginary parts at 8000 rpm and 345 kPa (MN/m)

f	$R(H_{xx})$	$I(H_{xx})$	$R(H_{xy})$	$I(H_{xy})$	$R(H_{yx})$	$I(H_{yx})$	$R(H_{yy})$	$I(H_{yy})$	$\Delta R(H_{xx})$	$\Delta I(H_{xx})$	$\Delta R(H_{xy})$	$\Delta I(H_{xy})$	$\Delta R(H_{yx})$	$\Delta I(H_{yx})$	$\Delta R(H_{yy})$	$\Delta I(H_{yy})$
20	28.5	14.2	-50.6	1.5	89.5	-8.5	39.6	28.1	1.44	1.50	1.65	1.27	2.88	1.79	2.41	1.78
30	26.7	28.8	-50.9	2.0	86.6	0.4	42.9	45.7	0.54	1.85	1.32	0.64	1.57	2.10	1.41	1.34
40	31.7	41.5	-53.9	4.2	90.6	10.0	37.7	63.0	0.78	1.35	1.65	0.69	2.51	2.53	3.69	2.49
50	33.7	49.9	-54.0	7.2	99.9	14.9	35.3	83.7	1.25	1.22	2.13	1.28	1.43	1.09	1.57	1.68
60	33.2	71.8	-64.5	9.7	101.7	3.4	50.0	98.2	40.36	44.12	43.08	49.76	5.29	4.80	5.07	4.53
70	28.9	60.7	-47.1	9.2	95.8	6.8	44.2	105.8	2.24	2.91	1.86	2.28	4.64	3.41	3.32	3.90
80	35.1	76.6	-54.3	16.0	88.9	35.7	-4.7	117.6	4.80	3.88	4.37	5.49	8.36	4.21	3.43	9.03
90	30.0	77.6	-46.7	17.9	110.0	24.1	27.5	145.7	1.80	1.11	3.53	1.92	1.75	2.08	2.11	3.27
100	23.6	89.2	-45.9	16.9	107.5	18.6	27.8	156.8	1.31	1.92	2.63	2.14	3.74	2.15	2.21	4.39
110	20.6	99.8	-43.9	18.4	107.1	19.3	23.9	167.4	1.68	2.34	2.68	1.60	1.79	2.30	2.74	4.21
120	17.6	113.6	-44.2	18.1	109.3	23.7	12.1	190.1	3.21	4.38	3.32	3.79	4.08	5.91	6.87	6.09
130	8.3	71.3	-23.0	16.2	137.5	-2.9	33.8	194.7	20.59	45.96	25.75	12.36	35.90	15.89	11.32	18.03
140	7.6	141.1	-51.5	20.5	114.5	23.5	9.9	218.7	3.32	5.67	14.98	4.45	5.31	4.62	4.12	19.88
150	25.8	172.7	-37.9	35.6	109.7	-13.1	42.0	237.2	14.42	13.67	11.87	3.89	11.79	18.99	7.05	10.75
160	3.3	159.7	-28.1	19.4	90.5	14.5	-18.3	221.9	4.06	3.89	2.49	4.93	3.50	4.34	3.96	4.40
170	5.6	169.9	-31.1	25.7	112.1	30.9	2.9	291.3	3.28	2.99	6.82	3.71	3.19	2.01	6.07	11.55
180	-17.1	196.0	-24.6	-6.5	97.9	28.7	2.2	263.9	41.61	53.97	41.61	40.28	12.98	13.30	7.24	8.67
190	-11.8	178.8	-22.1	16.3	111.6	19.4	37.5	287.5	4.49	4.14	3.22	4.27	6.64	5.79	4.62	6.31
200	-6.2	205.4	-24.7	10.1	99.3	31.7	2.7	283.5	4.37	6.40	4.12	5.83	2.41	3.10	3.47	6.24
210	-475.5	437.3	-105.6	1.3	302.3	71.3	41.3	370.7	442.14	424.40	72.30	68.83	123.80	162.90	24.78	26.35
220	-37.0	260.8	-25.4	21.4	112.4	28.8	2.0	306.0	9.20	8.57	4.69	6.83	5.19	4.56	3.09	5.63
230	-32.5	253.9	-24.5	10.6	124.7	55.2	0.2	375.4	6.31	5.74	4.98	3.32	4.93	4.24	5.80	10.13
240	-20.3	207.8	-19.6	10.6	117.2	45.0	9.3	357.8	7.96	5.86	3.20	4.31	4.77	6.45	4.85	9.92
250	-1.0	242.5	-25.8	17.9	135.3	57.1	-3.3	411.7	7.88	5.47	3.16	5.50	5.09	5.03	8.08	9.50
260	13.6	197.9	-14.2	23.8	183.5	-21.2	-11.3	360.7	17.78	33.80	9.28	12.58	94.66	93.37	37.29	37.68
270	-223.3	181.3	-45.4	22.3	170.3	4.9	-43.8	328.2	78.60	57.47	58.48	25.97	113.39	80.58	30.63	116.58
280	-13.8	267.9	-38.7	23.3	133.4	71.4	1.6	479.7	7.36	3.15	6.52	8.00	8.33	4.98	11.92	15.38
290	-36.7	270.5	-30.1	13.9	119.6	46.0	-45.5	404.9	11.26	4.89	9.06	8.41	3.63	5.16	8.81	7.24
300	3.0	277.1	-36.1	36.1	99.0	56.5	-88.7	447.8	10.79	6.27	5.59	10.46	3.89	5.11	7.14	6.84

Table 24. Dynamic stiffness real and imaginary parts at 8000 rpm and 690 kPa (MN/m)

f	$R(H_{xx})$	$I(H_{xx})$	$R(H_{xy})$	$I(H_{xy})$	$R(H_{yx})$	$I(H_{yx})$	$R(H_{yy})$	$I(H_{yy})$	$\Delta R(H_{xx})$	$\Delta I(H_{xx})$	$\Delta R(H_{xy})$	$\Delta I(H_{xy})$	$\Delta R(H_{yx})$	$\Delta I(H_{yx})$	$\Delta R(H_{yy})$	$\Delta I(H_{yy})$
20	67.1	22.0	-56.2	7.4	131.5	14.8	93.6	36.9	1.50	1.63	0.91	1.70	7.52	4.66	2.97	2.89
30	61.9	40.1	-60.4	8.2	136.1	33.1	87.7	59.2	0.97	1.51	0.72	1.12	2.62	5.16	2.81	2.95
40	76.3	56.0	-63.3	22.5	158.7	32.5	91.9	102.6	2.03	1.81	1.82	1.89	7.65	4.22	3.74	4.85
50	79.2	62.0	-58.5	27.7	176.7	38.8	89.9	129.3	1.52	2.22	2.34	1.54	3.98	5.81	3.09	3.66
60	75.3	78.0	-75.4	36.9	172.2	21.4	105.4	143.7	93.91	88.53	46.63	73.69	12.17	8.48	6.43	7.08
70	75.6	74.5	-51.3	38.6	169.7	27.4	94.6	169.7	3.55	2.84	3.35	2.37	7.41	4.97	4.73	5.46
80	73.1	92.7	-52.2	40.1	152.7	33.2	64.5	189.1	4.61	5.44	3.32	2.48	10.64	5.53	4.13	12.48
90	76.0	102.2	-52.7	48.3	173.6	54.8	91.3	225.4	5.96	2.70	1.90	4.48	4.57	11.21	8.28	5.38
100	71.0	108.8	-47.7	54.3	181.9	40.2	91.5	248.8	4.05	1.95	2.77	3.73	5.71	3.87	4.13	3.56
110	67.5	119.6	-43.7	59.4	172.6	41.7	90.9	258.0	3.38	3.30	2.84	4.45	4.34	3.11	3.54	5.31
120	75.2	137.6	-39.9	70.3	171.2	52.2	75.9	287.0	9.09	6.62	11.09	10.01	19.97	13.14	14.18	28.55
130	39.7	95.0	-29.0	49.1	160.8	-10.1	101.7	251.6	31.46	42.03	22.71	29.58	28.34	49.10	28.94	25.73
140	53.8	172.4	-52.9	71.1	179.3	59.6	74.3	333.2	9.23	6.31	21.93	6.56	8.14	19.90	14.54	24.97
150	78.7	165.5	-25.2	76.2	193.8	20.6	129.4	348.5	9.82	14.10	10.47	7.01	20.89	11.63	6.29	14.03
160	64.1	186.2	-17.8	72.6	129.0	69.7	-36.1	344.8	4.21	5.44	6.20	4.39	6.64	9.40	14.54	25.92
170	58.8	205.5	-32.4	81.9	189.7	75.2	82.9	416.4	5.40	2.63	5.83	7.43	4.33	6.56	8.66	9.39
180	43.4	230.6	-37.3	66.7	177.4	76.4	76.7	403.8	84.45	74.04	99.37	97.88	22.63	21.34	25.81	23.39
190	35.2	226.1	-28.7	84.8	197.0	72.3	119.8	428.8	6.20	7.55	7.92	6.90	12.87	9.05	8.04	5.57
200	48.7	254.2	-31.8	91.8	184.8	74.9	84.2	428.2	7.09	4.69	5.64	8.71	3.29	7.72	10.51	7.24
210	-714.0	584.1	-327.4	97.9	459.5	207.4	178.3	570.3	1049.35	1293.27	262.96	581.59	203.98	253.25	89.16	82.61
220	53.9	321.6	-23.0	123.1	207.3	64.0	96.4	448.6	14.89	5.03	8.11	4.68	5.21	9.01	6.13	6.15
230	44.3	304.5	-22.5	109.3	211.6	110.2	61.4	559.9	9.09	11.83	9.69	11.59	7.61	8.17	4.71	14.10
240	31.0	261.0	-23.7	90.3	199.2	92.0	100.9	529.1	6.42	9.34	11.45	8.89	6.11	16.03	10.22	9.21
250	68.8	287.6	-10.8	108.8	205.0	115.4	54.8	608.4	5.39	3.48	7.28	10.73	10.83	7.65	16.72	17.36
260	65.3	219.0	8.5	98.6	244.7	-12.9	41.2	498.9	32.99	27.09	15.65	26.51	120.20	211.04	112.56	130.77
270	-182.4	192.4	-95.9	94.5	393.0	131.8	64.5	584.2	144.22	169.09	139.09	37.32	380.64	396.37	95.60	358.36
280	56.9	335.1	-30.0	136.6	210.7	154.3	85.7	744.9	6.43	7.80	10.20	11.24	11.05	15.99	16.26	23.17
290	37.0	346.5	-38.3	141.1	210.7	118.7	122.3	612.7	12.06	6.35	9.16	11.38	5.39	9.35	6.61	6.96
300	78.7	335.1	-14.8	156.8	194.4	101.2	98.6	571.5	5.95	4.41	8.24	10.06	4.94	6.37	6.17	9.31

Table 25. Dynamic stiffness real and imaginary parts at 8000 rpm and 1034 kPa (MN/m)

f	$R(H_{xx})$	$I(H_{xx})$	$R(H_{xy})$	$I(H_{xy})$	$R(H_{yx})$	$I(H_{yx})$	$R(H_{yy})$	$I(H_{yy})$	$\Delta R(H_{xx})$	$\Delta I(H_{xx})$	$\Delta R(H_{xy})$	$\Delta I(H_{xy})$	$\Delta R(H_{yx})$	$\Delta I(H_{yx})$	$\Delta R(H_{yy})$	$\Delta I(H_{yy})$
20	100.2	28.2	-53.9	11.7	178.2	-6.3	165.6	39.5	8.33	3.50	1.32	1.45	19.15	11.54	7.39	7.24
30	103.5	52.4	-57.6	17.8	182.8	35.1	156.7	67.2	9.63	5.80	1.80	1.71	19.18	13.37	4.33	6.87
40	119.3	63.6	-57.4	32.4	216.5	48.5	149.3	131.3	12.25	5.31	2.12	1.41	25.28	11.64	7.17	3.76
50	120.4	68.8	-52.1	40.1	261.7	49.6	160.5	177.3	10.72	7.23	2.55	1.83	24.73	11.03	4.09	4.97
60	136.6	70.6	-33.3	44.3	245.9	44.1	176.5	193.8	88.97	112.25	86.91	58.00	30.67	14.10	11.44	18.47
70	103.8	79.2	-42.0	47.0	227.1	22.7	178.4	208.6	9.63	5.95	3.10	2.12	22.25	6.55	5.87	6.28
80	120.7	112.2	-45.5	65.6	234.7	60.6	141.8	248.7	9.74	8.38	3.60	4.50	22.77	8.20	7.94	6.14
90	119.4	116.5	-43.6	73.7	249.7	67.1	155.1	293.6	9.13	10.36	4.06	3.21	21.05	9.77	9.08	5.02
100	114.0	130.0	-39.1	79.7	249.9	56.7	160.5	323.1	14.79	13.97	4.95	4.70	26.07	12.79	7.55	5.18
110	109.3	136.3	-31.1	81.3	235.4	56.9	161.3	336.1	12.04	7.81	4.81	6.26	27.01	6.73	6.83	7.25
120	94.5	176.2	-62.2	76.7	229.1	121.8	104.1	390.5	224.99	245.81	332.81	63.43	87.76	440.46	410.48	205.18
130	62.7	101.2	-22.6	60.1	242.8	-52.3	199.5	332.0	47.45	43.52	28.01	30.84	43.94	66.81	58.43	37.14
140	95.5	205.4	-44.6	100.6	257.8	81.1	149.3	449.2	14.99	20.73	24.17	17.08	14.97	12.19	24.51	36.05
150	133.9	214.2	-12.9	116.6	257.5	18.6	235.8	431.0	26.94	20.74	14.02	12.64	36.93	19.38	14.83	12.18
160	133.4	211.6	-2.8	107.6	199.2	104.8	51.7	466.8	12.86	19.17	7.32	11.39	28.88	17.48	27.34	20.00
170	129.4	225.4	-4.1	123.8	285.9	100.9	186.6	534.4	10.78	22.80	13.53	9.52	23.73	6.38	11.63	15.33
180	116.6	243.7	-11.2	114.3	272.7	85.4	172.7	505.0	104.09	84.48	107.91	86.12	41.04	14.72	27.62	17.27
190	78.3	257.1	-14.7	122.1	281.9	79.5	216.8	543.6	14.67	27.84	10.43	8.18	26.39	11.22	6.37	14.03
200	110.9	275.1	-0.6	132.7	268.5	87.0	172.6	536.5	15.10	15.65	16.06	9.89	28.01	7.44	15.20	9.23
210	14.3	889.5	-117.6	396.9	417.3	178.9	261.4	666.7	396.39	423.25	163.03	239.17	142.66	139.69	80.72	59.43
220	112.5	348.7	3.8	171.6	300.0	71.7	199.0	559.6	13.30	21.28	9.15	11.27	19.67	9.51	11.48	10.33
230	99.3	339.5	0.3	159.2	313.0	139.8	167.9	726.4	13.83	21.80	12.56	10.11	26.37	9.74	11.20	19.53
240	107.5	292.9	25.4	152.0	303.8	74.3	251.1	641.0	118.13	47.87	116.58	54.67	93.94	84.76	115.88	60.66
250	111.9	309.3	10.2	143.7	255.5	118.6	130.1	681.2	13.23	13.52	13.00	26.88	13.13	23.14	29.87	17.12
260	97.4	249.3	19.7	131.3	178.9	-95.3	17.1	653.3	36.28	49.41	25.75	32.07	215.81	279.17	203.26	148.63
270	-212.5	272.5	-160.4	150.7	396.7	-101.2	194.5	597.2	85.89	92.45	37.71	51.09	231.07	364.42	162.65	175.54
280	112.5	371.5	6.8	187.5	279.3	220.7	64.5	981.6	11.44	31.28	11.76	11.33	23.82	25.89	28.82	28.13
290	97.0	401.6	-5.5	212.4	303.0	134.7	241.7	738.0	8.42	28.08	4.52	8.29	26.91	22.49	14.45	18.27
300	137.0	379.1	23.6	215.6	274.7	109.1	185.5	661.3	9.17	31.85	10.83	7.28	23.72	11.80	14.26	12.90

Table 26. Dynamic stiffness real and imaginary parts at 8000 rpm and 1379 kPa (MN/m)

f	$R(H_{xx})$	$I(H_{xx})$	$R(H_{xy})$	$I(H_{xy})$	$R(H_{yx})$	$I(H_{yx})$	$R(H_{yy})$	$I(H_{yy})$	$\Delta R(H_{xx})$	$\Delta I(H_{xx})$	$\Delta R(H_{xy})$	$\Delta I(H_{xy})$	$\Delta R(H_{yx})$	$\Delta I(H_{yx})$	$\Delta R(H_{yy})$	$\Delta I(H_{yy})$
20	151.9	32.7	-32.5	17.5	274.3	21.5	292.1	62.5	2.67	2.95	2.20	1.84	12.46	4.70	5.97	2.77
30	150.1	46.6	-30.1	20.6	295.8	25.0	288.5	101.3	1.31	2.24	3.31	2.10	13.01	18.01	8.50	7.46
40	157.3	53.2	-34.3	35.8	301.5	47.6	277.6	158.8	2.88	3.44	4.25	2.36	15.94	11.78	6.50	7.97
50	150.5	63.9	-26.4	40.9	325.6	15.3	298.5	193.1	4.35	4.67	3.44	3.01	11.93	10.74	7.06	6.96
60	152.4	79.1	-33.7	47.6	313.3	41.1	290.1	242.7	87.05	59.65	61.77	62.10	22.25	9.54	11.77	9.53
70	150.0	104.0	-30.2	64.2	308.7	61.7	278.5	284.1	2.58	2.61	3.65	2.14	9.97	9.70	6.89	9.36
80	166.5	102.1	-15.8	75.1	316.0	44.7	281.4	331.9	3.80	4.13	3.09	2.48	14.04	5.54	6.39	5.66
90	160.8	117.8	-20.5	89.2	330.3	72.9	277.8	405.8	1.76	5.49	7.12	5.67	12.03	20.52	17.08	7.48
100	162.2	123.2	-13.0	94.8	328.5	54.9	286.1	422.7	3.87	3.58	5.17	5.69	11.24	9.05	14.75	14.65
110	145.7	139.1	-13.5	90.6	295.5	49.7	275.8	408.4	4.11	7.32	11.84	8.04	8.48	7.10	10.87	10.82
120	149.9	139.6	0.5	99.6	316.6	48.8	292.5	485.5	9.20	8.28	13.33	8.14	23.94	20.04	30.24	21.42
130	171.2	204.0	-30.7	145.8	307.4	60.1	259.9	462.4	7.59	10.66	14.13	13.74	11.75	14.80	24.41	8.91
140	171.9	170.8	13.1	126.7	378.8	91.6	283.2	590.0	9.06	12.68	20.85	14.18	20.24	24.64	27.11	26.66
150	211.3	196.4	40.5	134.5	444.1	-9.8	440.4	557.7	15.81	17.99	22.96	14.61	16.02	24.62	16.70	12.19
160	147.4	225.9	14.6	136.0	251.7	55.3	184.1	452.7	10.75	8.02	13.15	13.39	19.22	17.17	7.91	18.25
170	145.3	215.4	9.3	138.5	349.7	66.5	310.6	673.8	7.69	7.78	12.75	14.10	3.59	18.09	9.61	15.86
180	112.2	301.5	-28.8	137.8	370.3	64.1	317.6	641.7	334.26	303.50	455.27	462.13	20.29	11.44	27.95	19.04
190	165.1	255.1	35.2	157.8	391.0	43.7	400.6	658.1	7.24	7.13	14.88	15.67	26.42	8.99	16.83	13.53
200	156.4	282.6	26.9	165.8	341.2	73.7	297.0	666.0	6.74	12.34	18.19	14.29	14.18	16.69	10.68	11.51
210	174.3	295.7	43.3	172.3	432.3	110.4	376.0	781.0	16.96	11.78	23.01	21.02	20.89	8.67	13.89	16.51
220	170.2	336.5	46.4	195.7	358.1	39.7	324.2	635.7	17.71	13.28	14.16	20.75	45.71	39.08	34.34	23.07
230	168.4	300.5	51.7	166.4	457.3	116.9	331.4	953.9	5.96	11.68	14.45	20.85	28.91	13.91	11.39	24.39
240	168.3	337.0	50.4	190.2	417.8	78.5	433.1	852.2	6.95	9.19	11.78	11.15	13.63	21.56	13.89	28.53
250	165.1	325.5	47.1	199.3	400.9	75.2	391.4	893.4	11.08	8.80	15.31	25.53	15.06	32.90	11.58	23.71
260	115.4	330.7	28.6	200.5	385.4	92.4	402.7	897.7	18.77	10.19	13.55	25.64	76.09	49.95	82.33	53.44
270	132.1	299.6	54.4	188.3	350.8	0.6	380.4	812.6	15.52	19.17	12.89	22.97	73.50	62.59	138.61	67.78
280	180.8	369.7	61.4	194.9	264.2	159.2	-9.7	924.5	6.43	5.73	15.20	13.27	9.44	26.31	17.25	33.43
290	175.1	425.1	55.9	268.9	386.5	108.8	444.3	894.5	6.32	8.68	16.74	12.98	18.69	14.25	14.37	12.32
300	170.9	383.7	67.9	245.6	360.6	59.8	423.2	782.6	9.95	12.18	14.57	12.59	20.72	22.23	12.31	24.18

Table 27. Dynamic stiffness real and imaginary parts at 10000 rpm and 0 kPa (MN/m)

f	$R(H_{xx})$	$I(H_{xx})$	$R(H_{xy})$	$I(H_{xy})$	$R(H_{yx})$	$I(H_{yx})$	$R(H_{yy})$	$I(H_{yy})$	$\Delta R(H_{xx})$	$\Delta I(H_{xx})$	$\Delta R(H_{xy})$	$\Delta I(H_{xy})$	$\Delta R(H_{yx})$	$\Delta I(H_{yx})$	$\Delta R(H_{yy})$	$\Delta I(H_{yy})$
20	2.8	13.0	-78.2	-9.5	125.0	0.1	14.3	34.9	0.91	0.75	2.95	0.89	2.29	1.17	2.28	2.28
30	-0.6	26.2	-77.5	-15.1	124.6	0.3	15.9	56.7	0.64	0.45	3.11	0.64	2.41	1.09	2.15	2.24
40	-2.3	39.6	-79.0	-20.5	121.4	1.5	17.1	74.4	1.48	1.03	3.06	1.56	2.52	1.19	1.14	2.76
50	-4.3	52.9	-81.0	-27.4	119.6	3.9	18.4	89.6	0.92	1.00	3.15	0.86	2.56	1.27	2.02	3.41
60	-6.7	62.5	-79.9	-35.5	117.7	7.9	18.2	102.7	21.73	37.42	44.11	27.64	3.47	5.61	7.02	5.00
70	0.2	77.5	-88.1	-28.9	118.7	17.9	1.1	122.9	1.31	0.84	2.11	1.06	2.67	2.43	2.86	4.52
80	-0.1	88.0	-89.9	-31.4	125.6	20.4	2.0	137.8	1.62	1.80	3.26	2.05	2.56	2.20	4.36	2.06
90	-2.0	95.7	-89.0	-24.4	125.4	24.3	-12.6	147.3	2.89	2.95	5.23	2.68	2.84	3.68	3.47	4.77
100	-5.5	102.4	-81.6	-23.4	131.2	25.0	-25.1	169.9	3.30	2.45	5.22	3.23	3.11	4.81	3.82	5.95
110	-6.3	111.0	-74.9	-20.6	134.6	25.4	-34.7	194.0	3.54	3.14	4.42	3.24	3.29	5.43	4.33	5.87
120	-12.6	120.4	-66.7	-26.1	132.7	28.0	-46.8	217.3	4.48	3.38	6.63	4.52	6.83	9.58	8.27	9.52
130	-22.6	125.4	-60.8	-27.7	137.1	28.2	-50.7	237.6	7.40	6.55	4.25	4.91	9.77	7.89	5.87	7.72
140	-30.7	144.6	-58.2	-39.5	136.2	26.9	-53.1	257.5	5.20	5.30	4.15	5.15	5.63	7.94	7.50	5.12
150	-27.3	185.4	-74.3	-44.2	143.8	30.8	-62.5	276.6	12.92	12.80	7.45	6.82	14.62	16.04	6.16	8.35
160	-32.4	163.1	-64.3	-37.6	130.7	29.5	-59.4	270.1	5.54	10.80	25.10	8.75	23.00	5.74	12.42	51.14
170	-33.4	190.4	-86.8	-39.3	110.4	22.6	-47.9	245.0	2.20	10.10	25.81	4.33	17.71	6.82	10.67	46.82
180	-61.2	213.5	-66.4	-69.3	133.4	39.0	-79.2	325.1	36.01	37.05	42.28	20.92	12.75	13.18	16.40	14.63
190	-47.1	177.4	-38.0	-41.7	137.7	41.8	-84.1	348.5	6.09	4.56	3.18	3.72	5.36	2.55	3.54	6.11
200	-55.9	198.0	-31.4	-52.3	143.0	43.6	-97.5	377.6	4.70	4.43	3.33	5.49	3.98	3.92	7.15	5.93
210	-258.7	609.4	-113.9	-176.1	106.3	18.5	-84.1	382.0	118.39	121.27	43.33	29.65	34.82	59.45	18.59	10.15
220	-94.1	232.9	-33.0	-51.6	137.7	50.1	-115.7	398.4	3.86	5.44	4.42	2.94	7.63	6.21	7.86	7.46
230	-97.4	237.5	-17.8	-57.7	143.8	67.9	-132.0	451.7	4.93	6.18	3.41	3.46	5.46	3.60	5.53	6.52
240	-59.9	203.1	-20.3	-38.5	145.0	58.6	-127.6	451.8	3.28	4.38	3.26	2.30	5.14	4.21	3.60	10.64
250	-68.2	229.4	-24.5	-45.9	145.4	64.2	-132.9	468.8	4.54	3.13	3.00	3.48	3.81	4.06	6.46	7.72
260	-11.2	156.4	-16.1	-10.5	157.0	61.3	-148.4	488.9	5.44	7.04	4.43	2.59	9.07	7.12	6.91	9.69
270	-339.0	-23.0	75.5	-28.2	99.6	56.2	-171.6	513.0	28.13	45.99	9.72	10.88	16.80	18.47	12.23	12.20
280	-96.8	258.4	-14.0	-37.8	151.7	84.9	-156.7	552.4	4.62	3.81	2.85	5.29	3.08	3.29	5.53	6.17
290	-115.8	250.5	4.2	-8.7	137.9	124.9	-218.0	622.0	4.27	5.81	4.91	5.13	8.98	9.05	9.88	13.59
300	-84.3	259.7	1.6	-10.0	174.7	117.2	-183.7	655.8	6.85	3.01	3.81	7.39	4.60	4.90	8.30	11.73

Table 28. Dynamic stiffness real and imaginary parts at 10000 rpm and 345 kPa (MN/m)

f	$R(H_{xx})$	$I(H_{xx})$	$R(H_{xy})$	$I(H_{xy})$	$R(H_{yx})$	$I(H_{yx})$	$R(H_{yy})$	$I(H_{yy})$	$\Delta R(H_{xx})$	$\Delta I(H_{xx})$	$\Delta R(H_{xy})$	$\Delta I(H_{xy})$	$\Delta R(H_{yx})$	$\Delta I(H_{yx})$	$\Delta R(H_{yy})$	$\Delta I(H_{yy})$
20	31.6	12.8	-63.9	-0.8	107.1	-9.2	42.4	22.0	0.80	0.90	1.25	0.81	2.82	2.08	2.24	2.83
30	27.6	24.5	-64.1	-1.8	100.3	-12.7	45.5	33.6	0.79	0.77	1.36	1.02	1.92	1.61	1.19	2.54
40	28.4	39.0	-67.1	-3.7	92.9	2.6	39.2	48.3	1.19	1.19	1.17	0.98	1.42	3.06	2.98	2.25
50	28.5	47.7	-66.2	-2.0	95.0	10.2	39.1	65.4	0.92	1.64	1.64	0.67	2.01	2.09	2.05	1.80
60	35.2	56.6	-64.7	4.3	106.7	10.6	47.4	82.6	36.56	36.09	42.72	43.26	4.61	4.43	5.00	3.73
70	27.9	62.7	-64.4	0.4	100.0	17.0	36.8	87.8	2.21	1.55	1.08	1.54	2.59	2.00	2.24	2.07
80	35.4	70.0	-62.0	7.3	101.6	25.4	4.1	117.1	2.12	3.98	2.96	1.20	2.07	2.54	1.95	2.40
90	29.6	80.7	-66.5	4.4	111.7	17.1	35.1	123.7	2.05	4.28	3.59	2.12	3.16	3.55	3.14	2.28
100	23.7	90.1	-65.5	2.3	106.0	13.2	36.0	131.9	2.05	3.43	2.78	2.23	1.59	3.27	3.04	2.23
110	27.3	101.4	-70.7	7.4	105.8	20.7	24.2	138.9	1.91	3.11	2.76	2.85	2.50	1.96	2.54	4.01
120	28.9	107.2	-65.2	13.5	115.8	30.1	11.2	171.3	3.08	3.78	2.20	2.30	5.81	4.19	4.35	6.20
130	20.3	97.9	-49.7	11.8	112.5	10.5	31.5	166.0	4.48	4.45	3.25	3.80	6.20	5.46	4.45	6.42
140	13.1	123.7	-63.4	14.8	132.1	35.6	0.8	206.3	3.74	4.26	3.55	2.66	4.70	4.01	3.74	4.87
150	40.8	160.3	-60.0	37.1	140.9	-13.2	48.0	218.4	22.75	18.71	7.82	12.12	11.83	23.76	11.40	5.27
160	3.7	139.5	-53.4	8.5	96.6	22.7	-35.5	191.7	3.99	5.28	4.06	3.79	4.98	4.53	4.10	5.33
170	3.2	163.3	-87.0	26.4	105.2	28.8	-11.4	199.1	4.23	3.89	7.27	5.55	4.32	5.78	7.76	9.53
180	-27.8	165.6	-58.5	3.0	123.0	25.4	-15.9	234.4	49.59	40.28	20.73	40.61	8.76	10.74	5.37	5.93
190	-20.7	149.6	-32.8	20.3	136.1	11.8	17.3	266.2	4.97	6.32	4.26	4.19	7.45	5.32	4.20	7.78
200	-18.0	180.6	-35.4	15.6	120.2	20.6	-16.0	263.8	3.49	5.74	5.42	3.39	5.95	3.29	4.33	8.70
210	-32.3	439.4	-55.6	76.8	229.9	-42.1	31.9	325.4	94.61	61.94	23.30	16.25	49.82	75.40	10.88	12.05
220	-43.1	225.5	-24.3	20.8	117.1	9.2	-9.1	293.2	6.03	8.12	6.39	3.29	5.98	7.80	3.68	7.33
230	-44.0	236.1	-26.9	15.4	121.6	33.2	4.5	352.8	5.65	13.56	6.52	4.97	8.26	5.19	6.34	7.24
240	-27.9	201.9	-21.0	8.6	113.2	26.1	14.7	340.2	4.06	8.14	3.08	2.86	7.77	4.61	4.10	5.93
250	-16.3	224.4	-21.0	18.8	125.1	46.2	9.3	394.1	4.94	5.67	4.83	5.21	4.66	3.91	6.79	13.64
260	19.8	144.9	-11.7	11.5	126.0	37.1	14.6	362.3	8.11	9.83	2.42	2.30	12.00	10.23	4.49	6.65
270	-252.5	68.0	0.1	-1.2	111.1	58.0	-43.4	357.3	50.06	29.09	5.38	11.81	14.07	20.66	6.32	10.02
280	-37.9	247.0	-25.9	4.1	131.2	62.2	24.8	421.2	3.62	7.39	4.12	3.45	3.18	4.93	7.94	11.75
290	-75.0	244.5	-16.9	-5.8	106.1	54.9	-62.6	371.8	4.79	7.47	5.75	2.61	6.09	7.21	2.57	5.80
300.00	-33.3	250.0	-25.4	14.7	101.0	80.1	-91.9	440.3	3.57	8.53	6.79	4.85	5.74	4.60	7.07	4.61

Table 29. Dynamic stiffness real and imaginary parts at 10000 rpm and 690 kPa (MN/m)

f	$R(H_{xx})$	$I(H_{xx})$	$R(H_{xy})$	$I(H_{xy})$	$R(H_{yx})$	$I(H_{yx})$	$R(H_{yy})$	$I(H_{yy})$	$\Delta R(H_{xx})$	$\Delta I(H_{xx})$	$\Delta R(H_{xy})$	$\Delta I(H_{xy})$	$\Delta R(H_{yx})$	$\Delta I(H_{yx})$	$\Delta R(H_{yy})$	$\Delta I(H_{yy})$
20	65.0	15.2	-62.5	1.5	146.3	-1.0	92.2	28.9	1.17	0.82	1.04	0.75	3.62	2.85	1.58	2.85
30	59.6	29.5	-63.7	0.8	147.7	-0.7	98.3	46.2	0.95	1.06	1.57	1.04	2.81	2.38	1.75	0.79
40	64.2	41.7	-69.3	2.9	145.5	16.9	86.0	71.1	1.61	1.50	1.32	0.91	3.11	0.72	4.07	1.37
50	53.5	58.2	-74.2	3.9	147.9	38.4	81.5	94.2	1.20	2.60	1.73	2.27	3.10	2.28	1.12	4.15
60	66.1	32.6	-58.3	15.3	164.8	35.4	93.2	113.7	20.40	49.51	50.77	29.51	1.46	6.06	4.20	4.13
70	72.0	70.9	-66.4	23.8	166.0	31.9	88.2	133.5	3.52	5.28	2.97	2.72	3.59	3.14	2.44	2.47
80	83.7	88.2	-73.4	35.5	171.7	45.7	73.7	171.8	3.04	3.76	2.04	1.76	4.21	4.26	3.49	3.64
90	73.9	91.8	-71.2	35.3	171.4	43.2	78.7	182.5	4.63	3.33	1.48	3.90	4.74	4.16	3.16	3.32
100	68.8	98.0	-65.3	35.6	166.0	38.0	76.7	196.9	3.05	3.43	2.40	2.42	4.24	3.45	3.26	3.89
110	68.0	104.5	-60.1	38.7	161.1	37.3	78.5	204.7	3.45	2.45	3.99	4.37	2.08	4.77	5.06	2.05
120	71.0	103.3	-50.8	41.9	176.1	43.5	76.2	239.3	5.12	4.16	5.39	2.34	9.53	8.52	14.94	8.32
130	53.2	115.8	-58.5	32.9	164.2	28.6	81.3	221.0	8.74	4.16	4.17	7.22	4.29	8.04	7.49	3.82
140	47.6	130.8	-62.2	46.3	188.7	54.9	55.0	287.5	3.95	4.21	2.77	3.93	3.60	6.49	5.18	6.56
150	86.7	137.8	-39.7	70.8	232.0	3.7	120.9	310.7	21.16	13.80	7.48	11.34	10.16	15.37	7.20	8.05
160	37.6	156.7	-75.5	50.3	152.7	61.1	27.2	294.4	4.02	8.18	12.43	11.46	14.45	5.11	15.77	8.92
170	28.0	184.4	-95.4	61.7	162.1	59.7	36.0	309.5	5.15	7.65	10.93	9.95	7.64	8.85	14.51	8.76
180	7.6	212.7	-92.7	47.6	180.9	58.1	48.9	330.8	51.42	45.69	17.63	45.51	13.51	16.33	6.45	7.81
190	0.0	180.6	-49.1	47.3	192.1	40.0	94.3	359.1	4.92	8.25	4.23	4.52	5.41	8.74	6.55	5.24
200	14.1	217.9	-51.6	57.2	167.7	44.0	50.5	353.5	9.21	3.10	4.60	9.88	4.09	5.77	7.48	5.72
210	-50.7	562.3	-125.9	154.6	373.9	-4.8	154.0	442.4	116.34	226.48	75.11	63.40	48.35	99.64	27.63	30.32
220	22.3	264.6	-42.4	82.9	177.2	36.6	70.0	378.6	9.21	3.49	3.32	3.87	6.86	6.29	5.47	5.12
230	12.9	265.0	-45.3	64.6	196.7	82.1	57.5	472.6	4.80	7.57	4.40	7.04	7.41	4.72	7.73	4.90
240	24.3	226.5	-25.8	63.0	175.5	77.7	79.0	439.1	2.25	6.08	3.97	5.80	7.20	8.85	6.90	12.04
250	35.0	250.0	-30.1	68.4	200.1	76.6	81.5	487.3	5.39	5.40	6.81	6.18	3.67	4.27	7.73	7.66
260	48.5	173.6	-17.0	49.8	180.8	86.4	74.3	466.3	7.04	14.88	3.33	3.61	4.41	8.25	6.96	3.53
270	-255.7	161.4	-80.9	24.0	194.3	98.4	80.5	469.1	42.28	15.82	12.21	9.44	14.12	26.24	8.03	10.07
280	20.7	284.3	-39.5	67.2	212.0	116.9	73.9	615.9	9.15	5.08	9.96	6.71	6.47	6.49	7.97	16.32
290	-26.6	293.2	-49.2	67.7	202.3	90.2	75.3	511.0	6.52	9.58	3.96	3.77	4.64	4.12	6.19	5.86
300	24.4	291.7	-39.0	83.7	215.6	84.6	89.3	546.7	9.33	4.56	4.29	4.77	2.42	8.77	7.71	5.20

Table 30. Dynamic stiffness real and imaginary parts at 10000 rpm and 1034 kPa (MN/m)

f	$R(H_{xx})$	$I(H_{xx})$	$R(H_{xy})$	$I(H_{xy})$	$R(H_{yx})$	$I(H_{yx})$	$R(H_{yy})$	$I(H_{yy})$	$\Delta R(H_{xx})$	$\Delta I(H_{xx})$	$\Delta R(H_{xy})$	$\Delta I(H_{xy})$	$\Delta R(H_{yx})$	$\Delta I(H_{yx})$	$\Delta R(H_{yy})$	$\Delta I(H_{yy})$
20	95.1	21.7	-59.9	5.7	205.2	9.7	162.7	42.3	2.72	2.62	1.19	1.43	4.92	8.72	6.65	3.32
30	96.1	35.2	-60.3	6.2	202.4	9.6	173.1	60.0	2.29	1.69	1.51	1.78	5.54	3.67	4.99	4.82
40	100.5	50.7	-69.9	6.6	207.9	36.3	145.8	90.3	4.24	3.15	1.89	3.46	4.53	4.63	5.89	2.47
50	82.2	71.8	-72.9	10.3	204.2	58.1	148.5	125.3	1.92	3.22	2.14	3.34	4.07	4.75	4.33	3.98
60	108.7	77.4	-65.9	32.8	233.2	57.9	155.3	154.9	89.68	76.81	76.65	70.51	9.93	11.28	9.33	7.56
70	115.1	87.0	-69.8	39.4	240.4	59.6	144.5	183.8	7.04	4.23	3.67	5.72	10.13	4.61	4.67	8.21
80	133.2	90.3	-60.8	61.3	252.6	51.6	136.1	231.5	7.89	5.39	4.31	5.26	8.49	6.69	5.50	6.18
90	116.1	102.3	-63.6	56.2	246.3	57.2	152.6	253.6	8.76	6.24	5.05	8.15	11.64	8.16	7.13	10.89
100	104.1	99.9	-52.4	50.6	236.9	36.7	167.6	264.2	5.87	4.61	3.44	7.09	8.07	6.54	7.00	8.58
110	103.4	107.9	-51.9	53.3	234.6	35.8	166.4	275.5	3.48	2.41	2.97	3.25	5.55	4.56	5.59	7.04
120	113.9	116.7	-46.6	65.8	245.7	47.2	161.7	315.6	6.22	5.41	6.97	6.08	15.76	18.20	19.88	20.38
130	94.4	135.8	-52.8	58.2	239.8	45.0	166.5	305.1	8.87	6.95	4.85	5.70	10.71	7.46	6.44	8.93
140	78.9	151.5	-54.6	67.3	255.5	52.2	155.3	372.8	6.76	8.65	9.60	6.00	13.67	13.58	14.70	15.01
150	114.0	160.7	-38.0	86.6	288.5	-19.9	220.1	365.5	18.45	14.98	10.87	10.79	22.62	25.12	16.61	14.14
160	84.8	180.8	-74.3	82.3	186.4	90.2	42.4	391.2	7.01	14.38	20.37	15.50	24.71	14.77	17.04	44.52
170	76.3	222.0	-106.5	115.9	189.6	70.4	67.6	353.5	6.11	10.04	21.66	9.05	19.43	5.13	26.68	29.17
180	66.8	246.6	-80.0	92.7	237.4	65.9	126.0	423.4	25.42	41.94	24.14	40.91	9.02	12.09	13.62	6.70
190	42.3	199.9	-42.4	76.6	256.1	47.5	183.3	455.6	7.36	7.63	7.80	7.19	10.26	8.18	10.97	8.46
200	73.2	229.6	-37.4	93.0	244.7	65.7	144.3	459.4	7.45	9.03	9.63	7.44	6.65	8.80	9.38	11.88
210	153.1	514.0	-64.0	220.7	353.9	15.7	228.3	516.5	125.08	66.73	55.96	34.12	71.04	55.00	29.73	28.97
220	84.4	281.2	-25.6	124.2	263.8	55.4	164.5	478.9	7.25	7.30	4.95	7.93	11.40	6.55	11.98	5.11
230	94.0	281.8	-20.2	116.7	289.6	109.3	150.3	618.9	10.47	9.88	13.26	11.13	14.07	10.82	16.93	15.68
240	73.1	244.9	-16.6	98.3	266.4	80.8	185.7	558.6	5.68	6.73	5.79	11.18	13.14	6.70	14.37	22.26
250	97.8	258.6	-9.2	109.5	282.9	71.8	174.9	589.0	5.20	3.85	5.15	5.78	7.53	6.31	9.08	8.30
260	90.1	183.7	-0.3	78.7	252.0	88.2	164.6	584.1	10.47	8.74	7.99	3.57	14.83	9.73	15.57	7.74
270	-173.9	200.2	-93.1	48.4	296.9	90.5	189.0	592.0	19.87	26.83	11.12	14.29	26.16	17.26	8.89	12.21
280	77.0	305.4	-24.7	108.1	270.3	185.4	48.3	841.5	3.84	5.85	10.26	8.75	5.21	5.34	11.74	11.21
290	47.4	325.7	-39.2	135.6	285.2	97.6	205.7	626.3	6.50	7.20	6.66	8.83	8.21	4.38	12.06	11.77
300	88.0	305.7	-13.2	143.7	245.8	69.0	145.3	551.4	5.33	5.25	3.77	4.86	6.43	10.55	28.47	11.36

Table 31. Dynamic stiffness real and imaginary parts at 10000 rpm and 1379 kPa (MN/m)

f	$R(H_{xx})$	$I(H_{xx})$	$R(H_{xy})$	$I(H_{xy})$	$R(H_{yx})$	$I(H_{yx})$	$R(H_{yy})$	$I(H_{yy})$	$\Delta R(H_{xx})$	$\Delta I(H_{xx})$	$\Delta R(H_{xy})$	$\Delta I(H_{xy})$	$\Delta R(H_{yx})$	$\Delta I(H_{yx})$	$\Delta R(H_{yy})$	$\Delta I(H_{yy})$
20	141.7	27.0	-49.8	10.2	290.2	-10.1	278.1	49.5	2.01	1.94	1.10	1.27	3.06	6.13	2.61	3.30
30	142.2	43.6	-49.9	11.5	281.1	18.7	268.8	72.1	1.11	1.87	0.95	0.83	3.00	4.52	2.96	4.37
40	148.9	45.5	-57.6	20.8	271.7	23.7	249.8	130.2	3.74	2.83	1.29	1.76	7.09	10.07	5.37	4.29
50	122.6	78.1	-57.4	31.3	305.5	54.7	268.8	174.6	3.06	3.78	2.14	4.25	8.83	3.90	6.22	4.76
60	161.8	82.2	-57.0	45.8	309.2	40.7	276.7	193.8	67.45	53.84	57.81	60.71	8.77	7.69	6.55	8.14
70	152.8	87.6	-48.8	50.4	313.0	44.8	268.1	232.9	3.24	4.01	1.41	2.13	3.58	6.30	1.65	3.51
80	174.8	83.7	-34.0	68.1	327.4	33.7	266.1	283.3	3.50	3.44	3.20	2.27	10.10	5.78	3.64	6.00
90	156.1	101.8	-38.8	70.4	320.5	72.8	260.6	335.7	3.74	4.34	4.33	3.67	8.15	7.75	7.38	6.91
100	156.8	95.2	-32.3	69.7	312.9	36.4	262.9	337.0	2.57	3.60	2.53	3.21	5.87	7.00	6.01	7.17
110	140.0	120.2	-40.7	66.6	291.5	41.1	247.8	330.1	4.43	4.33	4.62	4.22	5.89	8.18	8.78	7.82
120	139.1	114.7	-31.8	73.7	316.3	35.4	259.4	393.9	5.07	6.00	3.92	4.39	15.73	13.74	16.64	11.08
130	155.4	156.5	-37.4	92.5	317.6	40.2	263.5	381.6	5.04	3.56	6.22	6.27	5.64	9.02	6.02	8.12
140	146.1	152.1	-23.2	100.7	350.5	66.0	243.0	487.1	5.83	4.05	4.65	6.06	8.18	11.07	9.87	11.76
150	168.3	166.0	-3.3	106.1	425.7	-10.8	368.3	477.4	11.42	11.17	11.51	7.07	11.24	11.70	9.65	9.00
160	130.2	189.7	-15.6	101.6	218.9	51.5	75.2	368.8	9.73	9.56	7.84	8.16	11.68	7.60	7.78	13.88
170	120.2	197.7	-38.3	117.1	309.6	48.7	219.7	529.4	6.61	5.70	11.98	7.70	9.19	5.05	18.61	11.58
180	162.2	323.8	-42.5	179.5	344.9	59.1	254.8	549.1	157.68	128.73	122.58	170.61	8.58	13.15	10.36	12.90
190	133.1	232.8	-11.6	115.1	346.1	43.4	322.7	563.3	4.94	5.22	5.77	7.14	7.14	7.62	7.94	8.35
200	131.4	243.6	-15.4	120.5	317.0	68.5	249.2	572.1	8.10	5.75	9.02	10.57	5.73	8.84	9.70	10.62
210	167.7	251.8	8.1	139.6	422.6	75.2	336.6	675.3	12.89	7.62	9.51	9.27	6.66	9.25	9.07	11.95
220	140.6	278.8	4.0	155.1	342.6	8.3	310.3	559.1	6.66	9.19	6.06	3.13	5.27	3.91	5.09	4.57
230	149.2	262.7	17.8	136.8	391.3	118.2	255.5	802.8	5.85	6.12	8.85	5.03	9.66	8.13	8.90	12.59
240	151.9	282.3	27.4	137.8	366.7	75.0	347.3	701.5	5.59	6.21	8.59	9.35	8.78	6.05	6.87	10.98
250	143.8	273.0	16.7	138.7	366.0	56.3	319.6	728.4	3.77	6.43	5.62	9.16	10.37	5.64	9.40	8.37
260	111.2	269.9	5.7	134.2	372.9	87.0	331.7	737.5	9.67	7.01	6.17	6.60	5.86	9.84	3.93	7.82
270	97.5	243.2	7.5	122.5	370.0	30.8	363.4	681.3	8.87	10.72	6.51	5.21	6.11	7.03	13.23	5.21
280	151.3	316.0	21.3	141.7	245.0	145.6	-35.7	785.5	4.54	3.34	8.28	8.27	6.02	5.26	6.46	17.18
290	138.2	370.3	0.7	197.5	371.2	86.5	358.4	766.8	7.89	6.45	8.37	11.61	9.81	2.87	14.24	13.60
300	142.9	337.4	22.2	187.6	332.0	32.3	332.4	673.0	5.93	7.13	5.93	7.07	8.69	5.92	6.21	18.57

APPENDIX B: PRESSURE-DAM BEARING DATA

Table 32. Static test data for pressure-dam bearing

RPM	kPa	e_x (μm)	e_y (μm)	ε_0	T_{in} (˚C)	T_{out}(˚C)
4000	0	13.71	6.35	0.13	43.33	47.91
4000	172	31.24	7.62	0.28	42.78	46.93
4000	345	43.43	17.01	0.41	37.78	42.77
4000	517	60.70	32.51	0.60	41.11	46.81
4000	690	67.31	44.95	0.71	42.22	48.38
4000	862	69.59	46.99	0.73	41.67	47.23
4000	1034	69.59	50.54	0.75	38.89	45.27
4000	1206	71.37	62.48	0.83	42.22	49.00
4000	1379	71.12	68.83	0.87	42.22	49.01
6000	0	40.89	-2.28	0.36	41.11	46.57
6000	172	44.45	0.508	0.39	41.98	47.25
6000	345	54.35	12.95	0.49	42.78	47.96
6000	517	62.48	23.36	0.58	44.04	49.77
6000	690	65.53	30.98	0.63	42.78	50.52
6000	862	61.97	32.00	0.61	42.78	50.03
6000	1034	59.6	37.08	0.61	41.67	50.34
6000	1206	63.24	48.51	0.70	39.44	47.20
6000	1379	64.51	55.62	0.75	41.11	49.63
8000	0	42.16	-13.97	0.39	42.90	49.02
8000	172	54.35	-5.84	0.48	46.11	54.40
8000	345	57.91	3.30	0.51	45.56	52.56
8000	517	58.42	6.09	0.51	44.44	48.15
8000	690	59.43	14.47	0.54	42.22	49.05
8000	862	66.29	27.68	0.63	42.78	52.89
8000	1034	66.80	32.25	0.65	41.11	51.18
8000	1206	66.54	33.78	0.65	41.11	51.20

Table 32. Continued

RPM	kPa	e_x (μm)	e_y (μm)	ε_0	T_{in} (˚C)	T_{out}(˚C)
8000	1379	68.83	42.14	0.71	38.89	49.37
8000	1517	69.59	51.05	0.76	42.78	52.12
8000	1655	67.81	53.59	0.76	42.78	53.32
10000	0	52.32	-17.78	0.48	43.33	51.68
10000	172	51.30	-15.24	0.47	45.75	52.26
10000	345	54.35	-10.92	0.49	43.33	51.11
10000	517	57.65	-2.28	0.51	45.43	50.52
10000	690	57.65	4.31	0.51	40.56	49.25
10000	862	63.50	19.05	0.58	44.23	54.81
10000	1034	65.53	25.65	0.61	40.56	51.35
10000	1206	63.75	25.40	0.60	43.89	49.50
10000	1379	65.78	34.29	0.65	40.56	50.02
10000	1517	60.70	36.32	0.62	44.44	50.71
10000	1655	58.67	39.11	0.62	39.44	50.49
10000	1793	58.92	49.78	0.67	43.53	54.78
12000	0	55.88	-25.65	0.54	37.78	46.77
12000	172	58.92	9.91	0.52	42.78	55.28
12000	345	61.46	16.51	0.56	38.89	54.69
12000	517	58.42	17.27	0.53	44.44	61.51
12000	690	59.18	22.35	0.55	38.89	52.70
12000	862	61.46	30.22	0.60	38.89	56.27
12000	1034	59.69	32.51	0.59	38.89	53.54
12000	1206	60.19	42.92	0.65	44.44	56.95
12000	1379	59.94	43.94	0.65	44.44	57.48
12000	1517	56.89	48.01	0.65	48.89	53.03
12000	1655	57.40	51.05	0.67	48.89	53.28
12000	1793	56.38	54.35	0.69	48.89	55.98
12000	1931	55.118	56.134	0.69	48.89	53.15

Table 33. Bearing pad temperature measurements

RPM	Unit load (kPa)	loaded pad 5% arc length (°C)	Unloaded pad 5% arc length(°C)	Loaded pad 75% arc length(°C)
4000	0	48.3	44.6	54.0
4000	345	46.0	50.1	51.5
4000	690	50.2	44.6	56.9
4000	1034	46.3	43.2	58.3
4000	1379	52.0	45.4	63.6
6000	0	45.5	42.0	54.4
6000	345	50.9	44.0	59.3
6000	690	49.0	43.6	61.0
6000	1034	45.2	41.9	61.4
6000	1379	50.6	44.3	66.8
6000	1655	50.6	44.9	72.2
8000	0	47.6	42.9	59.6
8000	345	54.3	45.7	65.1
8000	690	50.3	44.2	64.5
8000	1034	47.2	43.0	65.4
8000	1379	50.0	44.5	69.5
10000	0	54.5	45.7	66.4
10000	345	52.9	45.4	67.0
10000	690	49.5	44.2	67.5
10000	1034	46.2	42.9	68.8
10000	1379	51.5	45.6	74.1
10000	1655	46.4	43.5	73.3
12000	0	50.7	44.8	70.6
12000	345	49.7	44.4	73.0
12000	690	51.1	45.3	76.0
12000	1034	51.7	46.3	79.1
12000	1379	48.5	45.0	79.9
12000	1655	50.8	45.6	82.4

Table 34. Force coefficients for pressure-dam bearing

RPM	kPa	*Kxx*	*Kxy*	*Kyx*	*Kyy*	*Cxx*	*Cxy*	*Cyx*	*Cyy*	*Mxx*	*Myy*
		MN/m				*kN.s/m*				*kg*	
4000	0	0.5	-15.1	61.9	24.6	116.9	-35.5	-6.3	305.7	44.2	73.8
4000	345	21.9	-31.8	100.8	34.4	180.9	55.6	74.6	434.0	48.1	71.4
4000	690	61.3	-49.3	178.7	120.6	322.3	229.4	216.4	767.2	0	0
4000	1034	136.8	-49.9	269.6	238.0	395.2	319.9	236.9	1056.1	0	0
6000	0	26.4	-39.1	124.1	62.6	153.7	12.6	72.6	412.0	52.8	86.4
6000	345	43.6	-39.3	135.6	69.9	200.8	89.7	97.9	401.4	40.2	82.0
6000	690	85.0	-53.3	185.4	107.3	277.7	172.8	181.2	619.3	31.7	37.9
6000	1034	129.7	-57.3	293.4	182.4	339.7	245.7	222.7	801.4	0	0
6000	1379	165.1	-37.2	345.7	327.3	317.3	259.9	198.9	903.2	0	0
8000	0	27.5	-48.9	153.8	81.0	145.4	10.1	81.1	380.1	46.1	83.1
8000	345	49.2	-44.4	162.4	74.8	168.3	51.5	101.1	355.0	38.9	69.1
8000	690	94.6	-51.5	179.6	107.6	202.0	96.3	128.9	395.7	36.2	49.6
8000	1034	149.5	-61.5	270.2	165.0	270.7	166.3	191.1	622.9	25.9	44.5
8000	1379	159.7	-48.6	318.4	225.5	279.4	185.9	182.7	663.4	0	0
10000	0	28.7	-45.3	189.1	104.9	130.4	9.5	74.5	303.7	36.0	68.2
10000	345	68.9	-40.1	178.2	123.8	150.4	58.3	82.2	270.5	33.8	57.8
10000	690	106.1	-53.9	203.2	125.4	185.5	74.8	114.3	344.7	44.7	55.4
10000	1034	136.4	-65.8	260.7	152.5	209.1	99.8	139.8	425.5	38.2	38.9
10000	1379	166.9	-53.1	304.0	234.3	234.6	124.4	181.8	536.1	25.9	39.4
10000	1655	206.6	-60.2	371.1	295.6	250.7	143.8	162.6	651.7	23.5	0
12000	0	85.9	-53.3	210.2	130.4	147.7	52.5	110.8	315.1	39.0	59.7
12000	345	108.9	-63.8	208.2	134.3	155.4	54.7	112.2	325.7	48.2	54.4
12000	690	140.6	-72.2	265.0	187.6	175.2	67.9	115.6	415.6	48.9	37.8
12000	1034	170.4	-70.2	334.5	275.1	193.3	90.5	119.9	519.2	42.8	28.1
12000	1379	202.2	-58.6	384.0	361.2	197.3	96.2	107.6	600.6	38.7	0
12000	1655	205.	-60.8	433.2	450.1	195.6	101.1	95.4	659.5	0	0

Table 35. Uncertainty of force coefficients for pressure-dam bearing

RPM	kPa	*Kxx*	*Kxy*	*Kyx*	*Kyy*	*Cxx*	*Cxy*	*Cyx*	*Cyy*	*Mxx*	*Myy*
		(MN/m)				(kN.s/m)				(kg)	
4000	0	2.39	3.06	2.05	4.77	4.35	5.90	4.62	10.66	2.54	5.06
4000	345	1.57	4.45	4.17	17.93	4.73	11.74	7.14	29.11	1.66	19.04
4000	690	4.44	3.73	14.71	14.43	10.89	19.54	22.71	52.49	0	0
4000	1034	9.22	5.53	11.38	13.56	15.37	20.35	29.62	62.48	0	0
6000	0	1.89	2.69	2.37	7.10	3.84	9.05	8.69	22.70	2.01	7.54
6000	345	3.70	3.52	4.67	12.22	12.97	22.24	14.36	27.52	3.83	12.63
6000	690	5.46	2.42	4.49	10.15	16.28	18.19	16.85	33.60	5.19	9.63
6000	1034	6.33	5.84	16.35	17.49	8.54	13.31	23.88	35.70	0	0
6000	1379	4.95	11.41	20.05	23.63	10.78	9.79	32.74	47.90	0	0
8000	0	2.13	2.89	2.05	5.74	3.72	9.26	9.72	23.66	2.26	6.09
8000	345	2.70	2.50	3.33	10.45	5.96	12.60	13.29	19.01	3.17	12.28
8000	690	2.96	2.52	9.00	8.71	8.32	9.99	9.93	15.02	3.14	9.24
8000	1034	5.33	6.26	6.70	16.16	24.736	23.05	23.35	39.62	7.85	23.78
8000	1379	7.13	15.07	10.75	11.06	14.22	17.69	18.29	26.25	0	0
10000	0	2.22	5.06	3.17	5.05	5.87	10.84	10.40	24.13	2.35	5.36
10000	345	7.05	1.72	19.04	10.64	10.74	16.04	23.66	25.23	8.29	12.50
10000	690	4.18	2.33	7.70	7.78	7.23	7.59	13.81	11.89	4.44	8.26
10000	1034	6.00	2.92	8.22	11.94	7.37	8.51	14.28	14.56	6.19	12.32
10000	1379	7.64	4.71	10.60	13.15	8.93	13.60	18.10	16.98	7.88	13.57
10000	1655	8.51	2.81	10.29	14.54	11.70	16.11	20.58	25.51	9.14	0
12000	0	6.47	3.13	15.66	4.43	13.30	17.29	28.53	29.66	8.59	5.88
12000	345	3.26	2.10	11.62	9.17	9.27	9.42	13.94	15.62	3.66	10.30
12000	690	7.42	2.28	8.24	11.30	8.91	10.18	17.38	18.89	8.34	12.70
12000	1034	8.50	4.32	8.98	11.80	8.97	11.70	22.46	22.83	9.35	12.98
12000	1379	9.71	5.32	11.66	20.91	9.15	9.94	22.89	34.12	10.91	0
12000	1655	14.40	7.59	13.32	21.93	10.34	13.37	29.10	38.87	0	0

Table 36. Dynamic stiffness real and imaginary parts at 4000 rpm and 0 kPa (MN/m)

f	$R(H_{xx})$	$I(H_{xx})$	$R(H_{xy})$	$I(H_{xy})$	$R(H_{yx})$	$I(H_{yx})$	$R(H_{yy})$	$I(H_{yy})$	$\Delta R(H_{xx})$	$\Delta I(H_{xx})$	$\Delta R(H_{xy})$	$\Delta I(H_{xy})$	$\Delta R(H_{yx})$	$\Delta I(H_{yx})$	$\Delta R(H_{yy})$	$\Delta I(H_{yy})$
20	-0.4	12.7	-20.8	-4.9	53.0	2.1	34.2	34.9	0.52	0.49	0.46	0.36	0.65	0.76	0.64	0.68
30	-0.8	20.2	-19.1	-7.5	53.2	3.6	31.3	51.4	1.12	1.11	2.08	1.24	1.25	1.38	2.74	2.03
40	-4.1	26.5	-16.0	-13.5	58.3	7.9	25.8	77.2	1.81	1.82	5.26	1.99	2.38	2.52	6.11	3.49
50	-7.6	36.2	-18.8	-15.1	58.9	6.1	20.4	89.8	1.20	0.85	2.00	1.97	1.49	0.64	2.32	2.42
60	-22.7	35.8	-5.4	-39.4	67.5	-4.1	26.3	124.3	72.05	106.40	167.51	118.99	74.19	69.87	109.03	119.30
70	-0.6	59.5	-35.4	-3.2	66.8	8.8	-6.8	131.4	5.69	13.22	21.10	8.18	6.86	12.82	19.72	12.78
80	-12.7	59.9	-18.7	-21.4	61.9	1.8	2.6	146.5	1.01	1.37	1.62	1.72	1.46	1.33	0.81	3.94
90	-15.9	68.0	-15.8	-23.6	59.2	0.3	-0.6	162.7	1.19	2.26	3.25	1.84	1.03	1.63	2.15	5.37
100	-20.6	76.1	-15.7	-25.9	65.2	-1.2	-8.5	187.8	1.20	1.94	2.95	1.69	1.19	1.61	1.63	4.32
110	-24.3	84.1	-13.6	-29.8	63.6	-0.4	-14.0	204.7	1.22	1.56	2.59	1.33	2.18	1.70	3.61	5.39
120	-23.8	93.1	-19.3	-27.3	72.5	-2.3	-27.6	236.5	14.45	10.36	22.85	27.27	33.65	42.43	65.47	85.44
130	-26.3	96.3	-12.6	-22.3	58.5	4.1	-25.8	230.8	7.26	3.04	8.14	28.64	14.00	6.26	11.44	49.91
140	-33.3	99.4	-14.5	-26.7	65.3	9.1	-36.9	254.9	2.31	4.15	3.33	5.58	3.72	5.82	6.75	15.40
150	-40.7	111.7	-14.9	-35.6	65.2	2.1	-43.7	282.3	1.76	2.42	3.21	3.51	1.65	2.26	3.54	5.99
160	-40.0	124.9	-15.2	-39.2	60.2	-3.5	-53.2	296.9	2.60	3.45	12.02	12.31	2.09	2.09	3.24	6.32
170	-48.9	130.1	-10.6	-41.9	60.4	-1.0	-64.0	314.0	2.40	3.52	9.04	7.21	2.11	2.42	6.46	7.35
180	203.2	537.3	-231.0	13.3	191.0	48.8	-110.4	381.2	458.76	612.81	620.37	472.02	120.36	161.30	97.35	128.64
190	-64.2	140.9	-9.9	-44.1	61.8	3.9	-77.6	360.5	4.11	4.17	8.06	13.25	2.35	2.98	7.52	6.06
200	-69.4	147.9	-4.6	-48.1	62.3	0.2	-79.8	369.9	3.73	8.31	29.01	20.62	7.01	5.72	23.05	24.83
210	-79.1	150.1	-14.9	-41.8	65.2	6.1	-100.7	419.4	2.29	3.02	8.12	6.28	3.61	5.33	11.18	16.87
220	-88.1	168.5	-11.1	-42.1	68.3	-6.3	-111.1	444.7	2.34	3.52	4.91	7.20	2.91	2.42	9.38	11.63
230	-91.7	172.7	8.6	-17.5	73.0	-4.4	-150.5	534.0	5.32	4.05	27.97	37.97	4.05	4.03	26.29	22.50
240	-102.0	193.7	-3.4	-46.0	53.5	-9.4	-112.1	516.6	4.02	5.21	8.92	11.33	14.30	5.47	17.37	26.32
250	-115.1	217.5	-1.5	-57.2	34.0	-33.6	-112.5	561.7	2.20	3.28	3.84	8.62	3.92	4.66	3.00	11.30
260	-112.0	239.7	-6.0	-74.9	-11.5	-42.3	-89.0	623.4	3.63	3.40	23.46	31.14	8.64	5.55	18.76	84.25
270	-126.3	302.1	-24.8	-83.1	-103.5	-52.7	-63.2	737.5	10.69	30.15	88.54	22.47	32.74	60.54	203.70	113.31
280	-41.5	330.1	-41.9	-105.1	-172.0	41.8	53.6	766.0	27.55	8.08	10.63	8.24	21.59	34.27	23.33	31.42
290	76.3	326.1	-123.1	-126.2	-137.0	338.9	195.2	721.6	7.46	31.53	13.81	16.51	55.41	15.13	26.60	45.67
300	-29.4	252.1	-150.4	-52.7	189.1	251.0	117.9	791.9	132.25	102.44	116.23	171.23	32.01	34.17	63.01	48.44

Table 37. Dynamic stiffness real and imaginary parts at 4000 rpm and 345 kPa (MN/m)

f	$R(H_{xx})$	$I(H_{xx})$	$R(H_{xy})$	$I(H_{xy})$	$R(H_{yx})$	$I(H_{yx})$	$R(H_{yy})$	$I(H_{yy})$	$\Delta R(H_{xx})$	$\Delta I(H_{xx})$	$\Delta R(H_{xy})$	$\Delta I(H_{xy})$	$\Delta R(H_{yx})$	$\Delta I(H_{yx})$	$\Delta R(H_{yy})$	$\Delta I(H_{yy})$
20	21.5	21.5	-34.8	2.5	91.7	7.6	50.3	59.0	1.80	1.59	1.43	0.85	6.28	1.59	3.58	2.68
30	22.6	31.9	-33.0	5.3	94.5	13.7	51.3	90.0	1.57	2.75	2.25	1.81	4.82	2.84	2.96	3.15
40	20.8	40.9	-30.7	4.9	98.7	22.4	47.0	128.8	3.51	2.66	2.59	3.59	6.72	2.91	7.45	5.65
50	17.7	52.5	-33.7	8.0	93.3	22.6	37.8	147.4	2.41	2.33	2.00	1.63	6.27	1.81	5.13	8.08
60	-0.4	75.2	-56.8	-2.7	68.8	1.6	40.0	137.8	74.98	64.69	63.69	151.20	86.80	121.48	226.64	94.95
70	13.2	74.4	-46.6	12.4	91.7	20.3	24.0	196.3	4.03	5.52	9.67	4.85	7.01	6.25	8.00	14.47
80	10.3	83.3	-29.5	13.2	85.0	48.7	-46.2	279.6	2.31	4.08	2.65	3.13	9.88	3.06	16.79	17.39
90	4.9	94.4	-31.9	13.6	98.9	34.0	29.9	263.7	3.96	5.56	6.52	6.94	6.43	3.99	5.11	13.01
100	1.6	105.4	-29.2	17.3	103.9	45.8	11.5	305.2	2.00	4.75	2.03	2.47	6.47	2.82	4.51	14.17
110	-3.6	117.1	-25.8	18.8	99.4	46.6	10.2	324.9	4.11	4.66	5.36	5.86	7.68	3.40	6.65	13.74
120	-2.2	136.5	-28.8	31.2	117.1	70.0	-10.2	376.3	60.66	59.68	130.22	97.41	139.81	162.74	362.10	206.76
130	-6.6	136.0	-9.2	34.2	102.8	62.4	-28.7	396.6	6.99	11.90	28.77	13.92	16.14	17.95	44.32	28.48
140	-18.3	152.4	-29.1	31.7	103.3	69.7	-39.6	414.8	5.42	8.33	14.47	10.06	8.79	8.75	21.54	25.95
150	-23.6	165.3	-31.4	32.3	96.5	70.7	-54.0	413.6	3.02	8.63	10.89	7.92	6.70	4.35	8.22	19.11
160	-30.0	175.7	-26.7	29.1	98.1	82.3	-62.9	494.7	7.82	7.12	16.55	21.58	8.81	5.82	9.88	25.11
170	-33.1	182.0	-25.0	37.0	102.6	78.1	-44.9	507.4	6.35	10.31	8.50	12.95	8.29	4.57	10.55	18.62
180	373.3	-214.1	196.2	-342.9	146.7	-173.0	-81.2	344.9	2041.47	1633.09	984.40	1072.29	888.50	786.53	512.27	371.55
190	-43.3	212.1	-28.2	51.0	117.2	92.6	-71.4	558.9	5.47	10.54	13.16	17.48	9.16	8.45	9.14	37.93
200	-52.5	222.6	-32.7	56.3	113.1	92.2	-43.5	563.7	38.69	18.65	41.05	48.21	22.21	98.71	77.00	83.37
210	-62.0	230.9	-38.9	62.9	120.5	99.9	-57.4	593.9	8.23	13.56	18.03	22.66	14.13	11.02	37.98	46.74
220	-69.5	255.5	-57.2	95.0	104.0	92.8	-121.0	557.5	3.62	13.94	13.75	12.64	7.10	4.58	8.16	24.61
230	-50.6	254.4	54.0	127.6	191.9	119.9	145.0	906.8	20.96	14.93	77.55	93.14	32.50	32.04	114.02	165.23
240	-72.5	284.4	-18.0	109.4	151.9	142.2	-5.2	828.0	12.44	14.09	21.98	27.41	26.02	20.91	37.92	89.02
250	-78.7	298.4	-20.3	119.2	165.9	145.7	23.0	874.2	3.85	16.25	8.30	18.41	12.88	10.42	29.68	40.05
260	-82.6	310.6	-20.5	121.4	197.5	139.6	97.2	984.8	6.93	20.62	29.22	40.28	22.65	23.37	58.72	80.37
270	-72.3	331.3	-29.8	146.5	217.8	107.7	184.2	883.8	51.55	17.38	52.79	84.25	96.23	58.86	145.40	93.48
280	-88.8	342.1	1.8	168.1	308.6	188.3	553.5	1387.5	7.21	17.96	18.13	40.82	34.06	15.78	138.06	108.24
290	-106.6	418.2	6.9	264.8	207.6	60.3	197.2	791.3	9.59	10.67	21.77	20.63	16.24	31.07	36.77	127.43
300	-46.6	492.8	184.6	385.8	481.1	520.4	539.1	2082.4	57.61	131.79	162.28	392.50	77.21	141.71	222.83	310.59

Table 38. Dynamic stiffness real and imaginary parts at 4000 rpm and 690 kPa (MN/m)

f	$R(H_{xx})$	$I(H_{xx})$	$R(H_{xy})$	$I(H_{xy})$	$R(H_{yx})$	$I(H_{yx})$	$R(H_{yy})$	$I(H_{yy})$	$\Delta R(H_{xx})$	$\Delta I(H_{xx})$	$\Delta R(H_{xy})$	$\Delta I(H_{xy})$	$\Delta R(H_{yx})$	$\Delta I(H_{yx})$	$\Delta R(H_{yy})$	$\Delta I(H_{yy})$
20	69.0	37.5	-59.7	19.5	161.8	35.3	110.4	110.5	5.29	2.13	4.76	4.14	8.81	4.84	5.97	8.89
30	70.4	63.1	-59.4	41.6	164.0	32.0	126.1	150.3	1.27	1.48	1.06	1.39	0.79	1.47	1.77	2.93
40	72.4	80.8	-55.4	53.4	159.4	48.9	115.8	199.5	1.37	1.39	1.15	1.18	2.14	1.52	3.03	2.77
50	70.4	93.7	-49.9	66.8	162.7	56.5	117.0	254.8	1.41	1.70	0.97	1.35	1.75	0.97	1.24	2.86
60	73.9	116.3	-53.2	72.7	169.0	60.0	136.6	279.2	47.94	43.73	48.37	35.58	115.84	87.81	113.35	66.24
70	73.1	143.4	-51.4	109.8	176.1	101.9	122.7	375.0	3.41	2.69	2.54	5.09	4.70	3.48	8.97	6.86
80	60.7	151.9	-42.1	102.4	151.3	107.4	65.6	409.9	1.36	2.02	0.71	3.46	3.51	3.63	8.63	6.06
90	65.7	178.2	-37.7	123.6	173.8	116.1	107.8	465.0	1.87	2.17	1.87	2.83	3.37	1.37	6.95	3.70
100	62.4	209.7	-40.2	143.2	189.6	139.5	106.2	529.7	2.07	2.75	2.56	3.16	3.61	6.53	9.76	12.55
110	50.9	229.4	-48.1	150.5	161.8	148.2	70.7	539.7	1.56	2.06	3.38	2.49	3.14	3.24	8.91	8.22
120	36.9	257.4	-45.3	172.9	137.2	190.9	35.5	613.9	67.35	118.25	147.29	103.33	110.68	227.32	255.58	209.75
130	60.9	254.3	-3.2	170.3	206.3	148.3	149.9	623.1	3.32	6.18	4.11	9.11	8.44	5.71	21.31	11.09
140	69.8	295.7	-3.9	222.7	207.0	219.8	65.2	755.8	4.13	6.38	8.64	7.75	7.24	5.89	12.92	10.87
150	70.4	308.5	21.6	224.3	254.9	202.4	177.2	781.0	3.04	4.64	3.80	4.36	6.35	2.76	10.70	11.26
160	46.7	330.0	-6.1	217.6	154.7	241.6	-21.6	796.8	2.73	3.56	2.90	5.20	7.26	4.18	16.90	10.21
170	44.3	340.6	5.8	244.8	179.7	244.9	28.4	883.9	4.80	5.64	8.33	8.23	6.18	3.96	12.22	10.38
180	347.2	331.1	243.8	284.1	310.7	123.5	133.2	807.9	444.84	588.51	915.24	787.64	318.51	255.22	602.17	373.14
190	52.5	366.3	39.8	251.0	247.4	240.3	132.9	931.5	3.57	5.42	5.27	8.05	8.22	6.08	12.97	13.98
200	51.3	387.1	51.9	242.4	203.7	238.2	49.9	856.4	32.50	60.63	73.90	130.84	111.45	89.54	113.86	286.61
210	50.4	433.2	69.1	324.9	285.0	319.9	169.3	1106.4	5.27	3.53	8.36	5.44	10.31	6.98	17.57	19.74
220	63.4	453.6	87.8	328.8	255.7	278.3	117.8	1058.3	2.78	3.39	3.85	4.29	6.75	9.07	13.05	24.82
230	47.5	474.7	83.1	350.1	218.6	408.3	-8.2	1261.8	3.59	3.95	7.01	6.30	16.63	11.75	33.68	24.47
240	48.2	483.3	105.4	324.9	295.7	357.0	224.9	1235.3	35.28	22.64	41.56	53.16	75.40	46.54	90.78	105.75
250	56.4	529.6	117.9	371.3	288.4	367.9	184.0	1393.6	7.82	4.47	10.59	11.72	10.69	8.72	28.40	22.73
260	52.5	544.3	145.3	363.0	314.9	436.5	307.1	1514.3	4.67	9.64	7.96	8.13	17.23	20.25	33.98	32.54
270	161.0	645.1	255.6	424.6	342.2	431.1	480.8	1499.6	262.09	303.24	239.45	240.30	465.28	536.27	420.97	432.39
280	336.3	343.2	375.1	137.9	1271.1	940.9	1246.9	2178.9	29.83	19.04	38.03	21.60	124.80	82.52	134.81	72.68
290	202.5	405.6	247.7	184.0	728.8	311.3	1036.7	1499.0	10.75	9.49	12.70	7.85	30.04	24.17	29.86	33.57
300	243.4	448.6	271.9	199.4	702.2	454.4	1182.2	1539.6	153.58	190.96	116.88	194.59	188.33	228.39	179.01	208.70

Table 39. Dynamic stiffness real and imaginary parts at 4000 rpm and 1034 kPa (MN/m)

f	$R(H_{xx})$	$I(H_{xx})$	$R(H_{xy})$	$I(H_{xy})$	$R(H_{yx})$	$I(H_{yx})$	$R(H_{yy})$	$I(H_{yy})$	$\Delta R(H_{xx})$	$\Delta I(H_{xx})$	$\Delta R(H_{xy})$	$\Delta I(H_{xy})$	$\Delta R(H_{yx})$	$\Delta I(H_{yx})$	$\Delta R(H_{yy})$	$\Delta I(H_{yy})$
20	122.6	63.6	-59.4	25.9	248.3	55.7	220.1	153.7	13.45	16.18	6.12	9.93	25.41	17.16	23.46	12.66
30	130.8	82.9	-50.6	60.4	261.5	45.4	246.4	219.4	8.03	10.28	5.69	2.25	4.49	10.97	11.87	3.79
40	125.8	98.3	-46.4	75.5	253.5	66.3	236.8	298.4	7.57	4.91	3.70	3.08	6.93	7.10	7.17	5.03
50	120.2	118.7	-42.4	96.6	257.5	76.2	247.6	379.0	5.58	3.18	2.06	3.71	5.01	1.58	3.50	4.83
60	140.2	153.2	-59.9	116.2	272.5	88.5	223.1	411.3	110.15	104.16	137.84	60.87	291.73	227.61	343.73	117.92
70	112.3	188.2	-51.1	149.7	276.2	153.0	252.3	560.9	5.69	20.28	11.18	9.80	12.02	16.67	18.69	11.72
80	130.3	196.6	-13.4	171.1	271.6	106.8	198.1	572.5	6.92	22.07	9.55	15.22	11.51	9.64	5.37	8.56
90	118.4	231.6	-18.6	189.9	280.4	141.3	268.4	672.8	5.54	12.16	10.35	6.20	7.14	6.78	6.03	15.27
100	126.2	259.0	-5.6	215.3	306.2	174.1	269.7	765.4	15.40	12.20	3.94	15.08	16.31	8.71	8.70	15.00
110	113.5	293.2	-13.6	234.5	271.4	184.5	233.6	784.2	4.28	19.24	10.88	13.84	9.73	8.60	13.85	27.95
120	137.9	328.3	20.2	287.7	317.0	232.5	267.9	931.9	185.80	121.32	264.88	174.16	388.80	220.64	549.87	327.50
130	143.0	323.0	55.6	263.6	344.2	193.9	346.8	908.0	7.15	30.39	13.38	22.59	17.71	26.85	20.07	18.15
140	174.8	367.8	83.6	320.9	390.3	263.8	314.1	1083.1	28.76	41.93	11.35	38.03	33.01	35.87	28.06	18.24
150	155.5	405.0	95.7	338.1	418.0	245.2	425.0	1102.2	10.96	48.26	7.55	41.65	34.06	33.64	37.33	23.39
160	130.4	421.6	63.4	332.8	309.2	298.4	205.7	1181.8	12.63	40.56	7.71	37.29	17.48	22.84	28.27	21.08
170	121.3	428.9	80.1	351.5	319.8	295.4	240.0	1255.2	9.30	31.65	15.90	29.98	18.15	21.23	21.59	15.62
180	65.2	570.3	-372.1	443.2	418.1	398.8	81.1	1593.1	1321.85	1267.88	1945.21	1815.63	1213.65	747.34	1784.67	1132.63
190	164.8	453.6	160.8	356.7	434.9	273.3	421.5	1291.5	24.10	34.44	19.77	30.55	22.92	28.33	12.22	20.81
200	149.9	499.9	151.5	385.9	389.5	307.4	343.1	1307.4	24.93	29.43	21.82	39.77	48.71	20.27	67.70	59.34
210	151.4	542.0	191.8	433.0	496.7	343.1	526.8	1470.3	29.62	50.45	22.98	47.39	46.91	47.10	50.31	31.81
220	171.7	540.9	216.9	429.4	449.4	298.4	453.2	1418.5	41.82	30.16	34.37	31.04	51.36	28.27	54.82	29.64
230	163.2	585.0	213.9	456.3	436.5	456.8	340.2	1719.7	29.40	47.14	20.93	35.82	25.34	37.97	13.17	37.81
240	176.1	575.2	252.5	413.4	533.4	370.6	625.5	1596.8	53.34	33.86	82.50	47.93	98.84	56.74	171.75	86.10
250	157.0	625.9	251.5	470.9	505.7	360.9	612.4	1682.3	17.29	30.23	14.88	22.75	29.70	22.67	28.27	28.44
260	155.5	662.5	269.6	497.1	455.8	422.8	581.3	1840.4	23.36	30.23	13.15	29.09	43.72	27.22	33.72	31.47
270	170.4	757.7	372.3	541.2	476.5	428.6	856.3	1814.2	86.04	115.50	349.84	249.98	178.52	183.59	571.24	524.47
280	205.5	922.9	410.5	733.7	-128.6	970.1	-57.0	2945.0	49.17	37.76	46.09	41.38	193.64	65.35	246.03	107.79
290	628.8	1060.9	851.9	728.4	703.2	1330.1	1505.5	2861.4	48.61	27.78	49.22	39.02	96.69	145.99	103.53	153.00
300	838.0	589.6	886.1	181.7	1217.5	957.8	2120.1	2011.7	240.59	270.10	240.32	274.30	485.65	341.27	481.52	344.25

Table 40. Dynamic stiffness real and imaginary parts at 6000 rpm and 0 kPa (MN/m)

f	$R(H_{xx})$	$I(H_{xx})$	$R(H_{xy})$	$I(H_{xy})$	$R(H_{yx})$	$I(H_{yx})$	$R(H_{yy})$	$I(H_{yy})$	$\Delta R(H_{xx})$	$\Delta I(H_{xx})$	$\Delta R(H_{xy})$	$\Delta I(H_{xy})$	$\Delta R(H_{yx})$	$\Delta I(H_{yx})$	$\Delta R(H_{yy})$	$\Delta I(H_{yy})$
20	26.3	17.5	-40.7	2.0	122.3	8.9	64.3	53.8	2.04	1.48	1.55	1.02	6.05	1.87	4.14	3.17
30	24.8	27.0	-40.8	1.3	121.6	12.0	65.4	76.9	1.70	1.66	1.09	0.67	5.68	1.19	3.64	4.56
40	21.3	37.7	-40.3	-1.5	120.0	16.4	62.9	99.5	1.89	2.23	1.25	0.81	5.49	0.88	3.98	5.40
50	19.7	47.8	-40.5	-0.7	119.1	20.0	58.1	121.7	1.65	2.96	1.47	0.86	5.10	1.17	3.43	6.44
60	22.2	65.2	-46.1	5.6	104.5	28.0	43.3	139.4	20.85	20.25	20.19	16.98	45.22	48.45	41.88	49.51
70	17.4	63.3	-37.0	1.6	121.5	38.6	34.1	175.5	2.23	3.34	0.95	1.51	5.61	2.22	4.01	9.24
80	14.3	71.7	-38.9	-0.4	126.0	34.4	39.2	207.2	2.75	3.86	0.91	1.56	5.91	2.50	3.48	11.85
90	8.6	80.8	-34.6	-1.5	124.5	39.8	31.5	228.1	2.43	4.01	0.86	1.22	5.77	2.51	2.29	11.68
100	6.4	90.2	-37.0	-2.7	123.4	36.7	16.9	255.1	3.25	4.90	2.27	2.52	15.84	8.50	6.64	15.04
110	-3.8	101.8	-36.6	-4.0	123.9	47.6	20.6	274.1	1.46	5.13	1.47	2.57	6.21	2.46	4.41	15.13
120	-4.7	109.0	-36.8	-4.2	129.0	48.7	-3.2	300.0	19.80	12.84	13.66	27.31	60.81	34.37	57.91	78.62
130	-6.5	118.8	-31.2	1.0	126.3	46.2	17.2	323.1	2.12	5.92	0.97	2.80	6.10	5.40	3.53	18.94
140	-15.4	129.7	-38.1	0.3	129.8	70.2	-20.3	355.3	2.28	6.36	2.23	2.54	6.54	3.49	2.18	20.22
150	-18.5	140.7	-34.8	7.6	136.0	68.8	-4.3	393.4	2.01	6.79	1.27	3.63	7.17	4.25	1.64	24.11
160	-23.3	151.8	-35.7	-2.2	117.4	72.0	-27.7	382.8	3.16	8.54	1.53	6.59	7.64	5.27	1.73	25.61
170	-33.3	158.9	-36.7	4.7	116.4	70.9	-38.8	418.1	3.10	7.92	5.07	4.59	7.73	4.55	4.51	25.35
180	244.2	509.9	-214.1	218.0	245.4	79.8	-35.6	519.5	1663.15	1216.80	549.87	451.81	98.73	561.14	176.18	90.39
190	-43.7	177.6	-33.5	10.9	133.4	73.1	-37.7	476.3	4.09	8.68	4.30	6.70	7.01	3.76	4.01	25.59
200	-59.2	188.9	-42.1	-3.9	121.0	78.7	-70.0	472.6	13.33	32.21	10.46	12.56	14.93	34.91	8.68	39.59
210	-70.0	197.6	-54.8	17.1	126.5	102.5	-95.9	558.8	1.73	9.84	5.22	4.79	9.34	2.39	12.40	24.61
220	-74.5	219.0	-51.2	32.3	125.7	112.4	-110.0	614.5	2.90	10.07	5.89	3.37	5.96	2.28	9.74	25.36
230	-78.9	234.5	-51.8	13.1	114.6	132.1	-144.0	614.4	1.61	12.05	3.48	3.88	9.61	5.84	4.06	34.29
240	-80.8	261.8	-37.7	49.0	115.9	151.2	-96.2	715.5	2.03	14.15	7.49	9.16	8.10	8.09	15.87	41.65
250	-94.8	288.8	-52.7	72.5	138.5	144.8	-71.5	801.3	3.78	11.23	4.41	2.72	8.78	6.57	11.34	35.64
260	-68.3	331.4	-27.7	72.6	119.3	195.6	-51.5	889.8	4.27	22.18	8.45	7.19	7.94	14.90	13.77	30.59
270	-46.1	336.8	-26.2	103.6	252.4	214.0	142.5	1114.2	6.59	16.74	5.54	14.31	21.85	20.58	15.58	53.65
280	-70.0	324.4	-31.6	80.5	203.1	156.0	221.1	1137.0	7.82	13.82	3.12	14.75	19.45	13.53	23.54	71.40
290	36.5	442.4	-43.4	181.8	272.7	296.0	365.6	1368.0	10.86	46.12	15.44	19.13	46.92	45.49	50.40	74.76
300	85.0	189.9	116.2	61.8	546.0	-87.2	945.5	1405.5	51.29	55.50	35.53	44.55	245.98	225.58	124.74	143.52

Table 41. Dynamic stiffness real and imaginary parts at 6000 rpm and 345 kPa (MN/m)

f	$R(H_{xx})$	$I(H_{xx})$	$R(H_{xy})$	$I(H_{xy})$	$R(H_{yx})$	$I(H_{yx})$	$R(H_{yy})$	$I(H_{yy})$	$\Delta R(H_{xx})$	$\Delta I(H_{xx})$	$\Delta R(H_{xy})$	$\Delta I(H_{xy})$	$\Delta R(H_{yx})$	$\Delta I(H_{yx})$	$\Delta R(H_{yy})$	$\Delta I(H_{yy})$
20	44.92	21.22	-44.08	2.06	135.12	7.85	74.73	49.43	1.85	2.48	1.20	0.99	4.18	2.56	3.61	3.34
30	42.94	35.93	-47.81	9.13	136.29	16.42	72.70	79.73	1.64	1.90	0.84	0.69	3.32	0.94	2.39	3.54
40	43.42	44.76	-47.01	10.62	135.89	22.31	67.88	106.53	2.05	2.59	0.94	1.31	3.59	1.35	2.67	4.50
50	42.39	53.20	-45.07	14.33	135.38	26.11	64.89	133.59	1.67	2.04	0.81	0.67	3.45	1.31	2.45	4.85
60	43.68	66.58	-50.80	13.67	133.90	30.86	65.16	145.74	22.85	20.26	14.98	24.08	37.63	57.52	55.90	31.08
70	40.84	74.99	-42.78	24.66	136.17	41.26	52.47	184.13	2.66	3.23	1.66	1.93	3.53	2.76	1.51	7.93
80	32.49	87.80	-43.84	18.86	109.49	59.56	0.02	251.59	2.09	4.27	1.78	1.97	2.52	1.83	7.34	9.22
90	31.70	96.18	-42.08	25.39	138.33	54.95	40.47	248.46	2.40	3.52	1.04	2.44	4.59	2.50	2.76	9.72
100	28.50	110.58	-45.40	26.83	143.16	53.90	31.50	278.37	3.49	4.48	2.69	3.39	9.15	5.46	6.44	10.57
110	20.13	120.81	-39.21	27.97	128.74	67.54	26.01	286.97	2.56	4.41	1.09	2.98	4.39	2.93	3.46	10.90
120	32.93	145.32	-49.96	50.40	175.66	77.58	9.62	362.06	34.53	32.74	35.41	51.41	90.47	66.40	97.59	112.70
130	12.11	142.91	-35.42	35.31	136.46	67.49	25.06	332.81	2.45	5.13	2.00	4.28	4.32	2.06	3.42	11.42
140	6.66	157.37	-44.16	43.22	132.88	96.64	-16.78	375.98	3.03	5.16	3.21	4.79	3.32	3.01	2.63	13.92
150	8.04	173.72	-35.37	59.17	144.85	86.95	14.02	397.85	2.62	7.20	3.62	3.79	3.67	2.84	2.41	13.88
160	0.48	182.05	-35.75	41.88	128.74	126.95	-36.13	448.48	3.48	6.62	3.75	5.61	6.11	2.08	10.50	17.46
170	-3.01	193.98	-44.67	63.84	133.26	114.27	-38.96	471.85	6.11	8.21	8.13	7.60	3.33	4.36	2.92	14.18
180	59.48	499.26	-82.59	309.21	224.44	165.78	12.69	542.11	1222.71	1553.69	1069.89	569.90	261.83	534.30	216.53	316.78
190	-18.26	217.37	-30.78	71.78	157.27	117.06	-10.44	508.49	4.52	9.82	8.98	11.12	5.40	2.95	4.29	15.71
200	-24.68	245.40	-26.42	94.76	128.51	109.56	-64.12	490.16	12.64	12.36	19.42	18.07	18.81	7.91	11.70	28.48
210	-27.12	255.04	-41.40	112.74	145.20	136.39	-53.22	556.68	4.39	10.69	3.14	7.90	4.20	4.03	7.91	19.69
220	-19.26	298.13	-22.04	154.06	109.56	109.82	-106.02	504.79	3.36	8.98	3.44	3.91	1.84	6.05	4.13	20.45
230	11.21	277.75	46.38	158.47	306.64	169.31	159.64	816.55	4.01	11.47	6.44	12.71	9.07	12.59	10.81	40.44
240	11.16	321.93	32.09	158.17	274.16	158.69	97.10	725.86	8.25	18.95	16.13	22.13	11.64	37.98	23.88	52.61
250	32.89	293.85	81.76	141.76	270.20	86.15	117.10	725.61	3.91	17.94	4.08	14.91	13.33	12.54	13.18	30.84
260	-14.85	265.51	45.56	71.76	186.26	86.94	37.29	758.24	5.59	9.22	6.17	8.45	6.34	4.88	14.79	24.20
270	16.46	314.34	60.03	117.46	179.72	107.86	97.73	797.26	4.35	17.43	4.53	15.79	5.60	9.56	6.46	28.90
280	-7.65	265.66	90.11	50.90	316.82	45.45	349.71	1062.36	10.84	9.90	13.52	6.91	29.13	13.45	34.99	51.99
290	-16.26	271.45	65.83	34.81	124.13	114.94	174.86	818.47	7.66	11.38	7.88	10.15	24.20	36.05	18.97	86.28
300	-21.55	267.80	114.80	-12.32	462.28	214.63	368.17	1567.11	26.68	106.67	97.63	116.40	107.01	94.04	168.82	186.75

Table 42. Dynamic stiffness real and imaginary parts at 6000 rpm and 690 kPa (MN/m)

f	$R(H_{xx})$	$I(H_{xx})$	$R(H_{xy})$	$I(H_{xy})$	$R(H_{yx})$	$I(H_{yx})$	$R(H_{yy})$	$I(H_{yy})$	$\Delta R(H_{xx})$	$\Delta I(H_{xx})$	$\Delta R(H_{xy})$	$\Delta I(H_{xy})$	$\Delta R(H_{yx})$	$\Delta I(H_{yx})$	$\Delta R(H_{yy})$	$\Delta I(H_{yy})$
20	93.4	27.5	-55.6	12.7	177.9	18.5	102.5	49.4	8.14	7.44	3.07	2.89	23.41	3.64	12.03	12.39
30	82.1	50.6	-59.2	25.3	189.0	20.5	121.8	79.7	8.37	8.73	2.34	2.40	20.48	3.06	11.89	16.22
40	83.9	64.6	-58.0	30.1	182.2	37.3	108.1	106.5	9.39	11.28	2.53	3.21	21.08	4.12	12.39	20.99
50	82.2	76.2	-54.8	39.5	184.3	45.2	108.0	133.6	10.93	13.46	2.26	4.62	18.07	5.90	10.23	23.96
60	87.0	106.5	-62.1	61.1	177.3	78.4	92.1	145.7	81.77	66.55	42.59	67.64	165.82	164.49	101.31	152.78
70	85.6	111.7	-52.2	62.2	194.6	71.1	104.4	184.1	14.64	18.32	2.23	9.03	23.49	14.70	9.90	38.52
80	74.2	121.6	-49.8	61.7	174.3	85.4	74.0	251.6	13.60	16.14	1.16	7.18	27.75	15.09	11.61	45.87
90	74.4	137.0	-48.8	69.3	192.2	92.3	89.7	248.5	14.54	15.53	2.47	7.98	28.26	14.62	11.13	48.50
100	73.7	154.7	-52.4	77.3	191.4	98.6	78.0	278.4	14.42	17.83	5.08	8.25	31.84	12.55	15.21	56.39
110	60.0	177.8	-49.8	85.3	182.8	111.1	78.0	287.0	10.79	18.93	1.58	8.69	30.14	10.52	10.35	53.26
120	69.4	185.4	-39.2	97.0	206.4	99.7	82.8	362.1	61.92	69.75	57.76	85.04	138.08	144.69	137.24	176.23
130	59.8	197.9	-28.4	99.7	197.7	107.7	89.8	332.8	8.05	23.89	1.61	11.19	27.14	12.29	5.62	61.60
140	54.6	224.3	-44.4	120.2	197.2	155.8	34.2	376.0	10.79	26.09	5.21	13.78	34.33	12.34	17.40	71.42
150	65.3	244.7	-21.1	143.0	230.0	154.3	101.4	397.9	13.73	27.90	9.20	14.82	31.00	10.98	18.30	70.36
160	47.2	256.0	-33.4	118.1	166.4	187.2	-9.1	448.5	15.39	29.17	12.04	16.04	31.45	19.58	10.37	79.48
170	41.8	266.7	-35.7	142.9	184.9	186.9	9.3	471.8	14.55	30.76	6.76	22.13	30.50	19.62	10.68	85.58
180	-390.5	323.3	-275.2	265.0	95.7	320.8	-7.3	542.1	2125.69	1682.87	1502.70	1280.01	847.12	599.74	590.27	475.37
190	35.5	293.4	-9.4	158.9	221.6	181.5	69.1	508.5	14.83	37.46	5.97	26.81	38.36	18.76	16.22	94.72
200	28.5	313.9	-10.8	167.1	180.2	198.5	-14.8	490.2	21.10	62.52	31.23	18.23	71.39	45.30	19.88	104.14
210	16.4	342.3	-21.5	207.9	227.0	243.4	40.6	556.7	8.95	33.48	13.86	15.09	36.28	14.30	19.31	90.76
220	19.2	374.0	-9.3	219.9	202.9	220.9	15.1	504.8	7.03	40.97	11.58	21.01	27.36	15.76	8.65	90.67
230	10.6	387.2	-8.6	224.4	187.2	314.6	-45.2	816.6	11.22	44.53	13.13	29.19	30.18	34.76	10.57	125.67
240	16.0	413.0	12.6	247.0	249.2	299.0	87.3	725.9	23.94	46.42	40.33	40.07	59.02	43.40	66.48	154.97
250	22.3	459.2	15.2	287.8	214.9	301.2	15.4	725.6	20.76	52.14	25.89	40.08	52.32	21.43	37.40	114.69
260	28.1	459.7	47.6	266.8	235.8	367.5	70.7	758.2	28.07	36.61	39.03	20.29	35.66	23.87	18.19	122.69
270	85.2	599.8	87.0	365.7	277.0	446.4	206.6	797.3	23.31	33.61	27.35	13.02	35.31	52.88	37.90	156.35
280	386.0	274.8	326.8	106.5	976.6	884.1	685.1	1062.4	91.62	61.24	76.74	44.31	306.59	204.30	242.11	280.73
290	155.7	332.3	145.8	146.2	590.8	307.5	613.2	818.5	41.96	47.39	42.25	24.00	130.91	38.26	142.87	146.30
300	194.4	369.3	168.5	163.2	768.7	220.0	895.2	1567.1	299.84	159.97	236.37	148.65	1170.54	1165.75	817.59	1049.17

Table 43. Dynamic stiffness real and imaginary parts at 6000 rpm and 1034 kPa (MN/m)

f	$R(H_{xx})$	$I(H_{xx})$	$R(H_{xy})$	$I(H_{xy})$	$R(H_{yx})$	$I(H_{yx})$	$R(H_{yy})$	$I(H_{yy})$	$\Delta R(H_{xx})$	$\Delta I(H_{xx})$	$\Delta R(H_{xy})$	$\Delta I(H_{xy})$	$\Delta R(H_{yx})$	$\Delta I(H_{yx})$	$\Delta R(H_{yy})$	$\Delta I(H_{yy})$
20	152.9	42.7	-67.1	28.9	263.2	16.8	181.9	98.2	6.09	5.04	6.46	4.68	10.89	4.90	7.35	6.73
30	138.0	68.4	-65.3	40.7	271.5	24.8	206.7	146.6	5.14	6.40	5.40	2.59	11.26	4.13	5.69	9.34
40	138.9	89.9	-66.0	53.1	260.5	50.9	189.0	203.1	3.27	6.06	5.69	2.54	7.66	3.78	6.18	7.93
50	136.3	107.5	-62.7	68.3	261.5	64.7	190.4	260.0	3.42	8.12	5.52	3.39	7.55	5.98	5.46	12.12
60	118.3	146.8	-78.8	68.0	186.3	110.3	164.4	250.9	73.07	94.49	82.61	60.42	184.20	235.88	224.02	134.49
70	144.2	155.4	-57.6	105.6	280.1	102.9	191.5	367.3	6.44	7.94	4.09	5.23	11.11	8.30	7.58	13.98
80	139.2	167.8	-42.0	117.8	249.9	97.5	136.5	395.3	7.40	9.17	4.42	6.35	11.52	6.38	7.04	15.80
90	138.6	190.5	-47.6	128.8	290.2	130.2	191.0	483.1	6.04	7.89	3.47	4.96	10.38	5.57	6.43	15.41
100	126.6	207.5	-56.9	125.2	265.3	167.1	135.2	546.3	23.03	17.53	15.47	23.32	19.86	42.57	42.09	34.00
110	119.1	242.5	-50.6	154.3	281.3	152.8	180.9	560.5	6.94	8.03	4.90	7.49	13.30	5.22	7.99	18.17
120	93.3	243.8	-41.8	119.0	219.6	151.1	127.7	516.9	120.00	117.90	159.95	84.86	236.59	242.06	329.12	156.43
130	129.3	269.2	-16.6	180.9	299.0	145.1	205.8	627.0	6.97	11.76	6.28	10.53	16.71	9.15	10.49	26.93
140	127.9	303.7	-23.7	213.4	303.5	209.4	148.7	746.9	7.55	13.13	6.19	10.37	13.47	7.39	7.63	28.05
150	141.3	330.0	7.7	238.8	340.7	202.5	234.0	796.0	8.47	13.88	6.40	14.42	13.70	6.19	11.37	27.54
160	122.6	349.5	-12.9	221.0	280.4	253.3	115.8	834.0	7.85	15.28	8.23	12.52	13.91	6.22	12.73	27.05
170	117.3	365.9	-8.4	253.2	292.9	250.7	133.5	889.0	9.88	15.71	12.83	13.40	15.70	7.10	10.62	30.62
180	547.0	1477.5	-135.0	1346.6	920.5	442.8	562.4	1337.6	2149.98	4977.10	4771.23	3853.47	1827.63	2361.50	1177.05	3165.82
190	123.3	390.6	35.1	271.2	351.9	239.0	236.8	951.4	10.05	15.84	16.58	16.26	13.34	9.58	9.93	32.05
200	98.5	502.4	17.9	416.6	230.9	242.6	16.0	920.7	199.77	243.73	140.10	292.02	204.03	199.66	259.94	143.20
210	102.7	450.3	43.1	329.1	363.0	300.0	229.4	1094.4	15.10	15.31	18.76	20.18	19.38	7.12	23.88	28.87
220	107.6	478.5	57.7	339.6	333.9	278.0	194.0	1047.5	6.87	15.12	12.26	10.75	14.62	6.23	16.33	33.23
230	101.8	503.4	50.8	349.2	321.5	388.0	124.0	1254.1	5.18	17.70	9.14	13.23	14.31	12.32	8.56	44.90
240	114.1	530.2	86.2	376.8	398.4	367.9	300.0	1283.9	18.51	26.84	39.25	35.11	32.84	46.13	73.23	83.73
250	113.3	568.7	85.7	411.6	394.4	352.3	291.7	1319.6	6.39	21.43	12.08	13.84	24.72	14.88	14.26	50.97
260	113.8	584.9	103.9	410.4	340.4	390.2	260.9	1405.9	13.51	19.53	18.78	15.13	33.24	10.48	28.49	45.16
270	98.2	670.0	103.0	474.7	311.2	436.9	314.2	1488.8	9.34	7.73	21.26	11.85	28.17	16.47	31.37	35.43
280	151.0	805.1	175.5	579.0	-134.5	842.9	-237.9	2134.8	16.19	22.09	19.70	27.27	29.88	42.19	28.09	81.82
290	542.2	807.2	500.6	580.0	638.0	1088.6	807.0	2224.9	32.19	59.56	36.06	37.34	63.69	62.64	52.81	72.03
300	490.8	502.8	473.5	296.2	920.1	799.7	1314.9	1818.8	275.75	173.31	248.48	146.50	863.56	320.83	761.56	248.19

Table 44. Dynamic stiffness real and imaginary parts at 6000 rpm and 1379 kPa (MN/m)

f	$R(H_{xx})$	$I(H_{xx})$	$R(H_{xy})$	$I(H_{xy})$	$R(H_{yx})$	$I(H_{yx})$	$R(H_{yy})$	$I(H_{yy})$	$\Delta R(H_{xx})$	$\Delta I(H_{xx})$	$\Delta R(H_{xy})$	$\Delta I(H_{xy})$	$\Delta R(H_{yx})$	$\Delta I(H_{yx})$	$\Delta R(H_{yy})$	$\Delta I(H_{yy})$
20	165.0	44.8	-67.3	22.9	299.0	67.7	280.3	146.7	80.95	30.52	86.71	9.97	149.79	50.72	142.37	54.78
30	176.5	56.5	-41.7	34.6	316.6	12.8	332.2	134.5	31.63	75.91	42.28	61.71	23.01	136.03	45.99	121.06
40	161.3	72.1	-45.3	49.2	283.9	42.6	296.4	213.3	29.36	33.07	9.72	45.70	54.61	39.28	32.73	69.09
50	160.1	99.9	-45.9	70.5	299.6	68.8	300.6	288.5	16.84	39.27	14.75	23.76	20.69	63.38	25.88	33.25
60	198.4	132.0	-34.5	142.0	366.2	114.9	313.6	456.1	239.60	255.54	119.56	243.51	564.69	626.70	293.89	591.27
70	178.2	130.6	-24.7	115.9	332.7	72.4	332.5	405.0	8.41	36.70	15.99	5.47	15.30	53.14	17.21	8.77
80	176.2	146.0	-16.1	132.6	317.1	77.8	281.0	462.1	20.90	34.66	23.11	10.28	10.87	61.78	32.44	18.57
90	158.2	188.8	-35.4	142.6	337.8	130.9	313.9	555.5	23.95	36.85	30.36	11.15	14.84	61.48	44.69	25.83
100	170.7	192.9	-15.5	152.4	340.5	162.0	337.2	632.0	58.16	10.66	48.07	49.67	136.79	113.54	216.60	97.08
110	148.9	225.4	-22.1	164.9	315.8	154.9	300.0	642.9	35.59	22.28	15.23	44.50	47.71	22.13	24.28	58.83
120	148.0	244.7	-24.6	184.5	303.4	188.1	252.6	714.8	90.92	139.10	161.87	103.65	138.88	346.10	346.61	270.24
130	169.4	243.6	19.5	194.4	343.5	140.3	341.6	716.6	29.52	15.60	23.66	16.02	37.50	12.12	31.28	23.24
140	161.5	276.9	11.1	226.0	363.7	193.6	313.6	843.1	29.46	15.01	14.00	20.49	42.10	8.10	35.74	15.51
150	181.4	294.7	48.5	245.0	399.2	171.0	398.8	872.7	18.97	20.43	23.42	15.37	13.48	37.19	26.74	34.13
160	162.5	329.5	7.6	245.8	352.8	262.7	246.5	1009.5	14.18	27.99	48.63	12.93	24.53	33.54	57.90	42.41
170	150.1	343.0	20.9	276.2	353.2	224.1	306.2	1008.6	14.47	19.24	20.97	44.01	21.47	17.46	14.58	57.03
180	768.1	264.5	722.5	180.8	528.2	-160.1	506.5	593.5	4031.37	2817.29	5347.76	2354.82	1566.79	2858.05	1868.60	3410.99
190	173.3	363.0	84.4	287.5	406.3	212.4	416.5	1059.6	12.83	19.82	34.10	22.97	14.60	20.44	33.04	43.63
200	146.0	298.5	241.5	98.3	437.7	250.1	443.5	1274.8	145.11	464.01	553.35	678.65	493.64	72.70	539.31	719.03
210	152.4	415.5	92.3	335.9	399.5	269.3	383.9	1179.0	12.65	8.81	8.04	15.38	14.31	15.06	14.02	35.47
220	166.8	440.5	107.3	351.4	411.5	267.1	392.7	1205.4	20.37	8.71	31.93	17.31	13.55	18.82	30.31	24.63
230	153.9	475.9	93.6	376.0	395.2	370.6	334.8	1406.2	10.43	32.19	30.02	72.28	24.46	35.26	13.71	96.28
240	163.0	485.6	128.6	360.6	465.7	312.2	516.0	1356.9	29.52	31.08	55.11	60.63	50.73	42.04	110.78	51.25
250	165.2	514.6	137.2	396.7	454.3	300.1	541.7	1418.4	20.65	18.49	47.12	19.76	10.93	26.16	39.84	45.24
260	149.3	538.6	138.8	404.2	403.6	337.9	485.5	1515.9	12.33	22.20	15.53	39.75	24.20	11.71	39.54	40.05
270	157.5	592.2	159.3	453.7	419.1	335.1	618.4	1521.3	20.42	34.36	16.16	35.57	10.97	34.76	13.41	43.57
280	197.0	630.8	218.1	467.0	143.6	554.8	66.5	1973.6	47.32	16.25	44.65	14.31	30.75	15.27	48.75	26.90
290	218.2	753.0	213.1	582.7	314.3	520.1	739.5	1786.5	59.29	47.73	74.34	34.10	47.76	58.83	41.33	107.65
300	316.2	799.8	359.7	628.4	216.8	628.6	917.8	1779.7	99.29	79.55	101.46	76.95	295.50	135.13	237.44	193.29

Table 45. Dynamic stiffness real and imaginary parts at 8000 rpm and 0 kPa (MN/m)

f	$R(H_{xx})$	$I(H_{xx})$	$R(H_{xy})$	$I(H_{xy})$	$R(H_{yx})$	$I(H_{yx})$	$R(H_{yy})$	$I(H_{yy})$	$\Delta R(H_{xx})$	$\Delta I(H_{xx})$	$\Delta R(H_{xy})$	$\Delta I(H_{xy})$	$\Delta R(H_{yx})$	$\Delta I(H_{yx})$	$\Delta R(H_{yy})$	$\Delta I(H_{yy})$
20	30.9	14.7	-52.8	1.8	155.4	12.0	84.8	46.6	3.71	4.53	3.48	3.45	12.85	5.51	8.45	7.12
30	29.7	21.8	-50.7	-1.6	157.4	14.6	86.9	64.7	3.65	4.39	2.66	1.95	6.99	4.96	5.48	3.46
40	24.7	32.6	-51.7	-5.2	156.2	17.6	84.1	84.9	3.37	4.32	3.08	1.56	7.74	2.41	6.03	5.51
50	22.9	41.3	-50.9	-5.4	155.0	20.1	79.5	104.2	3.27	4.26	2.53	1.13	8.63	4.01	6.62	7.62
60	27.6	51.4	-49.5	2.2	148.0	30.8	58.0	133.3	26.60	19.10	21.37	18.82	51.14	57.04	32.60	52.05
70	16.6	56.0	-49.8	-9.1	159.6	39.8	58.8	159.7	4.95	7.24	4.45	3.51	5.80	2.19	2.86	5.49
80	14.3	65.7	-54.8	-6.5	157.0	33.8	61.8	175.0	4.43	5.37	3.14	3.30	9.25	3.82	3.07	13.59
90	10.2	74.7	-51.7	-6.7	152.7	38.4	50.0	190.3	4.07	9.09	5.00	3.75	5.73	4.66	2.43	13.64
100	6.6	84.0	-51.3	-4.6	154.9	43.7	42.9	217.7	6.13	7.69	3.73	5.42	9.15	5.00	3.97	19.47
110	-0.5	94.8	-50.4	-5.3	151.1	50.3	34.8	240.3	7.01	8.07	3.57	7.33	10.64	7.46	7.09	24.63
120	-1.7	101.8	-41.8	-1.3	154.3	54.4	40.3	260.2	26.43	21.80	15.73	24.82	77.40	49.81	68.72	68.54
130	1.6	108.5	-33.5	-2.4	148.5	42.3	16.2	278.7	8.99	6.80	8.46	6.26	15.31	7.07	5.70	33.50
140	-9.4	121.4	-43.7	-5.0	155.6	67.6	-1.2	311.5	8.54	12.61	3.96	5.50	12.55	7.77	6.57	29.47
150	-11.5	131.2	-43.1	2.2	159.4	71.5	11.9	339.8	2.83	9.35	3.25	4.74	11.61	7.01	3.40	33.72
160	-17.4	139.2	-44.7	-4.9	149.2	78.0	-7.5	347.5	4.39	11.53	5.02	6.65	9.85	5.09	5.00	29.53
170	-27.0	146.5	-44.2	-3.9	145.2	73.3	-9.1	371.2	5.75	14.38	6.83	8.28	11.77	8.17	4.63	34.25
180	-165.9	702.6	-333.0	184.1	238.3	182.4	-24.3	482.4	1453.75	1390.08	862.47	715.52	194.20	409.10	191.92	178.66
190	-35.5	164.7	-42.1	0.6	155.0	84.4	-23.9	422.6	5.67	10.39	7.70	9.04	11.61	5.82	8.51	36.16
200	-46.2	174.1	-48.8	-9.2	144.4	93.9	-51.6	437.7	5.38	12.69	4.62	5.62	14.60	5.74	5.84	36.50
210	-55.5	186.2	-61.3	11.8	154.2	113.1	-65.5	505.2	3.78	12.85	3.05	4.58	15.14	6.61	5.86	41.40
220	-59.0	204.7	-55.8	26.9	157.5	124.5	-74.3	570.1	1.48	9.83	4.41	4.50	11.24	5.00	8.99	42.09
230	-69.9	218.7	-68.4	-3.1	151.1	148.8	-117.6	594.4	1.71	12.56	3.70	3.22	11.14	10.17	11.11	46.14
240	-63.2	239.5	-35.5	27.7	153.9	147.5	-45.1	634.1	4.66	10.73	6.67	13.06	17.05	13.18	22.42	52.72
250	-70.2	269.6	-42.2	72.9	177.4	139.1	2.0	761.9	4.59	12.60	8.39	14.08	18.11	7.97	8.28	50.14
260	-55.2	303.5	-28.2	41.2	124.6	176.2	-21.5	782.8	14.73	20.90	6.69	16.52	28.95	21.83	10.81	50.95
270	10.5	305.3	19.5	99.4	312.3	164.2	332.0	1073.7	25.18	58.44	71.30	142.06	111.25	45.69	256.56	161.02
280	-31.1	282.0	-3.5	57.0	252.8	103.8	349.2	1056.9	21.01	23.79	9.84	19.46	14.02	14.79	29.79	60.93
290	66.0	306.4	41.2	82.2	366.8	179.3	801.2	1283.9	71.08	67.00	35.08	44.56	61.81	55.18	65.57	98.01
300	-14.2	240.2	10.6	-2.2	551.1	-210.9	1525.4	1031.5	86.22	84.70	108.81	41.11	121.67	169.06	48.40	227.44

Table 46. Dynamic stiffness real and imaginary parts at 8000 rpm and 345 kPa (MN/m)

f	$R(H_{xx})$	$I(H_{xx})$	$R(H_{xy})$	$I(H_{xy})$	$R(H_{yx})$	$I(H_{yx})$	$R(H_{yy})$	$I(H_{yy})$	$\Delta R(H_{xx})$	$\Delta I(H_{xx})$	$\Delta R(H_{xy})$	$\Delta I(H_{xy})$	$\Delta R(H_{yx})$	$\Delta I(H_{yx})$	$\Delta R(H_{yy})$	$\Delta I(H_{yy})$
20	49.4	18.0	-48.4	-2.9	167.9	7.8	89.1	40.3	3.80	3.79	9.80	3.20	17.42	9.67	18.53	4.01
30	49.4	30.5	-49.9	3.6	168.2	17.1	84.4	65.6	5.38	4.92	9.82	2.06	17.62	6.01	11.68	8.41
40	48.7	38.0	-49.6	3.0	168.1	20.2	81.8	87.7	5.99	5.59	10.15	2.60	17.65	7.10	11.59	11.12
50	48.7	46.5	-48.7	7.0	167.3	25.3	77.5	111.2	6.07	7.14	9.27	3.31	17.99	8.04	8.79	15.69
60	52.6	60.1	-48.8	8.4	161.7	35.9	77.4	131.2	28.00	35.92	40.73	24.16	45.82	68.83	55.87	48.01
70	47.1	64.9	-46.7	12.4	164.6	36.5	65.8	151.5	5.15	10.27	10.00	4.23	15.42	5.97	6.79	20.18
80	39.0	75.2	-47.3	6.2	144.6	63.9	20.1	216.4	3.95	10.86	8.17	4.31	15.79	8.83	7.47	25.28
90	36.3	83.3	-49.1	11.0	165.7	50.9	53.9	203.8	4.60	12.55	9.33	6.15	17.02	6.86	1.14	31.19
100	30.6	97.5	-51.1	13.4	168.3	59.5	47.5	228.7	5.40	17.38	10.49	10.33	18.76	14.74	7.74	42.43
110	27.3	104.3	-44.5	15.9	157.9	62.2	40.5	242.8	4.90	15.19	5.59	10.35	19.40	7.11	4.32	45.06
120	33.5	116.0	-40.1	25.3	167.5	55.9	41.6	266.6	47.87	48.54	44.07	44.29	110.05	121.18	128.79	119.71
130	18.5	126.4	-35.8	12.1	165.7	57.1	20.3	284.5	4.81	22.18	3.74	6.38	28.31	11.73	10.32	60.98
140	13.0	135.2	-43.8	22.5	155.2	89.5	1.2	312.2	3.47	19.15	4.66	9.15	20.59	9.97	6.43	60.68
150	17.2	151.2	-41.7	39.1	161.1	83.4	11.7	329.3	3.23	21.26	4.55	8.62	18.79	9.82	7.17	62.28
160	7.3	155.8	-36.6	21.8	168.9	123.7	-1.4	394.1	4.10	23.87	4.98	8.68	17.74	11.72	7.30	63.94
170	3.8	170.1	-47.9	38.6	155.9	105.6	-12.6	389.9	4.99	21.80	8.99	10.20	18.00	10.84	6.55	67.36
180	-104.8	69.9	-100.1	19.4	120.0	118.1	-25.1	417.7	1162.5	639.36	649.78	664.27	179.80	326.42	218.94	148.58
190	-9.1	196.1	-37.7	48.4	169.9	113.8	-7.0	430.5	9.18	27.84	7.88	15.81	27.57	14.11	10.18	79.89
200	-10.8	208.9	-37.7	54.4	156.7	117.0	-23.8	428.3	8.33	29.33	6.09	16.26	28.18	9.66	13.90	76.65
210	-11.6	224.4	-39.3	78.1	155.6	130.9	-43.0	464.1	3.81	25.19	5.47	10.62	23.36	6.71	10.35	72.01
220	14.1	271.9	-13.1	124.9	109.4	135.2	-108.5	457.0	10.33	36.23	8.18	21.76	13.45	6.40	12.22	68.77
230	30.0	222.9	59.3	88.9	316.1	133.3	156.5	652.3	9.24	34.33	11.87	22.22	38.44	21.67	24.88	103.51
240	59.5	264.6	53.9	114.5	294.8	140.0	88.9	635.2	14.02	35.49	18.29	24.02	49.70	27.91	44.35	111.95
250	41.1	220.4	71.9	70.6	269.2	96.3	83.9	635.8	10.96	26.99	22.93	18.25	50.25	6.01	40.18	102.55
260	-15.0	218.0	17.3	33.5	236.8	80.6	61.3	676.7	6.35	29.48	11.28	11.73	29.28	18.15	16.52	88.25
270	18.0	242.6	43.3	65.9	227.3	126.1	100.2	729.2	9.86	25.70	18.33	8.73	20.78	15.62	35.66	114.13
280	-20.0	230.8	44.6	21.8	371.7	47.4	347.0	991.9	5.01	29.85	8.86	7.59	38.07	11.07	56.15	139.40
290	-17.4	249.0	34.4	32.9	200.2	46.9	266.5	724.2	3.79	33.70	9.21	15.33	16.21	33.89	71.30	65.84
300	-46.5	290.3	24.8	45.4	514.4	205.9	360.7	1429.5	61.76	60.00	90.17	75.14	45.99	39.45	64.49	127.48

Table 47. Dynamic stiffness real and imaginary parts at 8000 rpm and 690 kPa (MN/m)

f	$R(H_{xx})$	$I(H_{xx})$	$R(H_{xy})$	$I(H_{xy})$	$R(H_{yx})$	$I(H_{yx})$	$R(H_{yy})$	$I(H_{yy})$	$\Delta R(H_{xx})$	$\Delta I(H_{xx})$	$\Delta R(H_{xy})$	$\Delta I(H_{xy})$	$\Delta R(H_{yx})$	$\Delta I(H_{yx})$	$\Delta R(H_{yy})$	$\Delta I(H_{yy})$
20	103.7	18.8	-53.7	8.7	206.7	2.7	110.1	46.1	4.28	3.60	6.78	2.51	11.36	3.14	9.45	2.50
30	93.0	33.1	-52.5	13.7	201.7	5.2	114.7	71.7	3.08	1.77	1.74	0.96	12.18	2.69	6.18	2.76
40	92.4	45.0	-53.8	17.4	196.8	16.5	107.0	100.2	2.43	2.80	3.68	2.13	12.50	1.50	6.70	3.98
50	88.9	54.0	-51.9	22.7	195.2	20.5	106.5	129.7	1.89	5.05	3.41	1.40	10.88	2.88	4.72	5.80
60	100.8	52.9	-46.9	34.1	222.8	17.9	111.2	170.3	69.81	49.70	46.33	49.93	159.14	91.38	72.76	122.07
70	87.2	78.9	-52.5	33.2	196.5	42.8	96.8	179.5	3.54	3.83	4.40	2.99	6.86	4.39	5.60	7.26
80	76.6	90.2	-52.6	32.2	181.8	57.1	75.2	213.6	2.46	4.69	1.92	1.43	10.57	3.80	2.75	4.91
90	82.6	107.6	-56.7	42.5	201.2	48.3	94.7	240.4	1.80	10.22	5.69	1.83	23.19	4.01	4.16	15.30
100	78.3	123.4	-59.2	50.9	194.8	58.6	93.8	265.5	4.79	8.56	6.11	5.62	13.53	7.44	9.33	16.07
110	74.1	136.8	-57.6	57.3	186.3	61.8	98.3	285.6	2.65	8.24	6.08	2.73	20.08	3.34	10.96	23.93
120	62.4	154.8	-63.2	55.9	170.4	101.2	55.2	304.0	32.28	67.93	63.30	46.69	99.23	123.53	107.23	135.30
130	70.6	144.5	-41.3	54.0	176.2	66.9	71.9	331.4	3.14	7.54	3.95	5.57	15.65	8.66	13.53	22.99
140	67.7	162.3	-50.9	67.4	161.4	91.8	42.4	353.7	5.31	8.54	3.87	6.69	12.41	4.15	7.05	22.49
150	69.5	180.9	-44.0	90.3	183.6	106.1	68.3	398.4	3.21	9.04	4.43	4.52	10.37	6.47	5.70	20.86
160	60.8	186.9	-46.0	74.0	158.2	121.3	46.1	409.7	4.63	7.86	5.25	6.05	14.20	3.95	5.15	32.45
170	52.8	201.9	-49.6	90.9	164.3	119.6	42.2	436.9	5.12	10.15	5.98	8.37	12.74	6.56	7.66	21.37
180	-68.3	81.7	-64.6	-56.2	104.4	136.3	-5.2	428.0	1305.63	1088.28	654.88	1052.86	451.97	331.21	378.29	169.89
190	42.8	228.6	-42.2	104.3	175.9	130.2	61.7	485.3	5.21	9.24	6.51	7.13	12.63	6.13	7.01	31.30
200	39.1	241.2	-47.7	103.5	153.7	136.9	29.9	474.6	4.65	12.92	4.26	7.04	12.22	2.93	5.69	28.82
210	27.2	260.3	-56.9	125.0	156.5	167.2	24.1	543.9	4.05	10.93	3.98	5.43	12.90	4.66	9.06	24.91
220	25.8	290.3	-58.1	142.2	142.4	160.9	8.8	531.5	3.09	12.42	4.79	5.38	10.03	4.40	4.61	24.85
230	23.0	298.9	-55.5	140.7	142.3	228.2	-3.5	650.1	3.73	10.15	5.61	3.39	8.79	3.45	4.69	30.91
240	18.6	329.4	-53.8	165.6	176.2	225.1	56.8	679.7	6.35	13.73	16.27	13.39	18.58	16.22	30.09	41.10
250	35.5	382.6	-51.7	216.3	143.1	218.2	9.6	689.2	4.33	14.18	3.00	6.30	15.04	11.76	10.34	51.30
260	67.7	373.9	-1.8	207.2	151.7	268.2	48.3	791.3	9.06	14.04	9.46	5.06	25.54	13.61	24.60	45.88
270	63.7	432.4	-3.9	248.3	201.8	330.8	118.6	863.5	87.03	77.48	85.14	94.20	69.92	63.66	77.93	68.17
280	218.3	195.3	122.0	91.3	589.1	402.9	366.7	1114.3	18.44	15.77	11.82	15.22	53.98	26.38	30.53	45.09
290	132.4	256.7	59.1	121.3	387.4	235.2	390.4	913.5	9.23	20.81	6.49	8.43	19.83	13.10	22.43	37.60
300	97.0	308.9	24.6	144.7	418.2	264.6	501.9	950.7	58.52	73.01	74.08	67.01	37.76	46.29	37.17	59.50

Table 48. Dynamic stiffness real and imaginary parts at 8000 rpm and 1034 kPa (MN/m)

f	$R(H_{xx})$	$I(H_{xx})$	$R(H_{xy})$	$I(H_{xy})$	$R(H_{yx})$	$I(H_{yx})$	$R(H_{yy})$	$I(H_{yy})$	$\Delta R(H_{xx})$	$\Delta I(H_{xx})$	$\Delta R(H_{xy})$	$\Delta I(H_{xy})$	$\Delta R(H_{yx})$	$\Delta I(H_{yx})$	$\Delta R(H_{yy})$	$\Delta I(H_{yy})$
20	164.1	21.0	-72.1	19.6	288.5	-18.9	181.1	58.4	9.87	13.10	8.55	7.15	34.85	38.06	20.63	16.75
30	142.7	49.9	-69.7	24.8	272.8	-9.3	192.2	95.6	9.75	17.12	8.60	4.12	15.71	16.87	21.61	10.21
40	140.9	73.7	-73.4	33.4	255.7	26.9	170.6	136.4	14.61	19.91	8.95	8.32	12.34	9.15	13.42	6.68
50	137.8	89.2	-70.4	44.4	255.6	39.9	170.6	185.1	16.67	20.47	6.82	9.56	8.47	7.66	13.03	12.62
60	174.1	96.1	-63.2	63.2	319.5	46.6	187.2	234.7	135.82	190.21	114.74	112.43	260.88	454.78	288.12	216.35
70	144.4	123.7	-68.6	68.2	269.7	73.2	159.8	263.9	21.93	22.47	8.33	17.01	18.15	18.29	8.97	26.22
80	144.9	138.0	-57.5	83.5	245.6	79.7	110.7	297.2	21.67	27.75	4.84	22.18	23.19	24.19	8.37	31.28
90	142.6	162.1	-67.6	90.3	282.7	109.9	149.8	366.1	18.68	22.29	3.99	18.93	27.63	27.04	12.34	43.03
100	140.3	179.1	-65.0	98.9	282.6	127.0	137.7	405.4	23.34	25.69	7.24	19.29	30.41	41.67	10.38	50.99
110	141.4	196.0	-59.2	113.6	286.8	130.6	146.7	447.6	19.78	28.53	5.71	17.11	35.10	31.85	13.24	52.94
120	127.9	167.3	-41.5	92.5	236.3	65.3	139.6	425.0	87.03	88.99	121.61	62.55	159.52	224.39	268.09	136.41
130	138.5	172.5	-14.2	76.9	263.4	146.6	97.9	557.4	22.97	11.25	21.92	12.49	41.46	25.92	24.46	89.05
140	127.1	223.9	-43.4	127.8	278.6	156.6	120.0	576.9	14.13	37.53	12.58	30.60	44.59	33.89	21.62	79.25
150	133.6	251.7	-29.6	157.8	306.2	153.5	179.6	613.2	17.93	35.26	9.44	27.88	38.73	6.70	33.35	70.76
160	118.7	267.5	-44.5	138.8	265.5	187.3	125.2	637.0	14.29	44.87	7.77	25.13	25.83	13.24	23.63	72.38
170	109.9	293.5	-47.0	166.9	265.0	184.7	120.5	664.8	16.86	42.55	11.25	31.96	26.03	12.01	20.18	72.27
180	843.3	408.2	323.9	428.0	495.4	-80.8	316.2	595.5	2137.2	1379.4	2172.6	1317.3	434.43	1190.9	927.92	832.50
190	112.4	318.0	-23.9	189.5	297.3	188.9	169.4	732.6	20.03	49.73	11.74	36.53	31.86	22.29	27.47	77.98
200	109.2	344.1	-31.2	199.0	271.7	210.9	113.9	734.1	22.37	45.60	12.29	35.07	28.58	28.46	14.96	85.93
210	102.9	362.6	-23.4	229.4	293.9	237.3	142.4	828.9	25.64	51.11	15.60	47.72	44.74	21.64	37.78	95.91
220	104.1	380.4	-14.7	237.1	284.2	226.2	131.2	813.1	27.39	47.17	23.35	41.14	40.71	19.01	33.10	88.13
230	98.7	395.4	-18.9	238.3	276.2	300.7	97.9	962.3	24.88	50.18	18.76	43.48	42.15	32.78	25.38	115.07
240	93.6	416.0	-8.1	260.4	318.7	284.7	195.6	991.5	40.74	51.94	47.39	62.72	72.24	42.47	100.60	136.21
250	83.0	451.9	-18.7	288.0	317.3	280.0	192.6	1025.5	17.51	55.07	14.49	45.76	50.82	31.80	41.84	116.93
260	74.3	469.3	2.6	307.2	282.3	285.6	170.1	1087.1	20.28	53.26	35.79	56.76	64.81	15.39	44.25	125.68
270	53.8	526.2	-36.2	366.5	230.5	309.6	164.8	1099.0	63.32	53.18	192.55	50.94	84.00	68.64	100.27	306.36
280	88.9	627.4	7.9	387.0	-77.0	570.7	-158.3	1489.7	32.37	48.94	37.46	45.94	21.04	49.84	30.95	162.13
290	378.1	776.8	188.8	571.3	327.5	919.4	340.7	1726.9	27.84	55.85	38.00	52.62	72.46	100.04	75.80	212.93
300	512.6	569.8	361.1	440.3	725.3	805.3	840.4	1658.4	428.30	222.39	411.57	231.06	253.67	324.39	269.75	336.69

Table 49. Dynamic stiffness real and imaginary parts at 8000 rpm and 1379 kPa (MN/m)

f	$R(H_{xx})$	$I(H_{xx})$	$R(H_{xy})$	$I(H_{xy})$	$R(H_{yx})$	$I(H_{yx})$	$R(H_{yy})$	$I(H_{yy})$	$\Delta R(H_{xx})$	$\Delta I(H_{xx})$	$\Delta R(H_{xy})$	$\Delta I(H_{xy})$	$\Delta R(H_{yx})$	$\Delta I(H_{yx})$	$\Delta R(H_{yy})$	$\Delta I(H_{yy})$
20	204.6	44.2	-101.8	45.6	283.6	59.2	184.2	126.0	28.22	53.79	6.89	30.84	17.61	49.62	28.43	21.19
30	168.5	52.3	-78.9	26.6	312.8	10.0	253.2	115.4	10.10	9.16	6.44	13.91	9.44	6.33	5.02	8.76
40	161.7	84.5	-90.4	42.2	293.6	51.4	223.2	174.0	9.73	14.28	4.91	8.93	13.49	9.42	5.56	7.02
50	154.4	87.2	-79.4	56.3	297.3	50.7	237.6	223.4	9.27	8.25	5.77	3.45	6.31	5.84	5.20	4.37
60	164.1	92.1	-74.5	78.2	289.2	32.0	241.2	261.8	73.40	142.59	125.92	76.48	207.12	358.99	313.03	212.58
70	163.2	130.6	-79.3	88.5	312.6	72.4	237.0	304.3	10.46	9.58	5.78	3.25	9.50	8.19	5.72	7.84
80	160.6	137.1	-62.5	92.4	295.5	76.0	206.2	350.2	15.82	12.68	10.19	8.62	11.14	7.15	10.85	9.22
90	163.7	162.1	-68.9	104.9	321.9	105.1	237.8	414.2	9.30	12.24	8.78	9.66	9.62	7.04	10.48	13.95
100	162.7	186.5	-68.4	119.9	320.0	120.9	230.7	454.6	11.75	10.19	5.75	8.20	8.37	9.21	8.58	11.62
110	167.9	212.0	-60.5	138.3	312.1	128.7	233.8	479.6	14.54	15.20	7.53	14.43	12.88	7.77	5.61	16.54
120	187.7	220.0	-49.9	164.2	366.9	113.2	251.4	561.3	83.01	19.93	76.43	74.50	168.03	87.48	189.85	133.91
130	170.2	197.6	-22.8	132.4	305.0	142.2	223.1	573.1	9.29	12.05	17.38	9.28	15.68	27.23	27.82	42.68
140	164.1	249.2	-42.5	169.4	300.7	171.0	199.6	635.9	6.95	13.73	7.41	11.37	24.59	7.52	16.09	19.23
150	168.5	271.3	-22.7	194.1	352.2	164.4	263.6	668.5	3.70	7.73	4.90	8.48	5.19	6.48	8.59	14.86
160	148.4	272.9	-38.5	155.0	314.3	211.4	184.6	725.8	8.51	14.09	9.72	13.88	7.92	7.53	8.93	18.67
170	141.1	308.5	-40.3	202.3	312.6	201.3	203.4	744.6	10.70	15.38	7.60	13.15	9.96	7.07	10.03	18.65
180	-1002.7	44.0	-641.3	-614.2	-137.7	686.4	-368.9	834.7	8084.56	3186.58	4143.98	5754.87	3492.89	3443.73	3891.38	957.02
190	152.9	334.4	-3.1	221.3	361.6	205.2	267.6	814.8	6.45	14.53	11.69	10.11	7.66	9.53	7.30	24.06
200	137.2	345.1	-16.9	215.9	329.8	216.1	210.2	807.8	7.22	17.79	4.66	17.79	4.76	9.30	7.65	26.49
210	138.3	387.9	-2.9	269.7	345.9	252.7	231.8	893.1	12.77	12.18	11.13	14.98	13.20	9.14	9.23	33.28
220	147.8	399.1	4.9	269.8	361.5	254.5	232.2	922.3	5.60	20.05	6.25	17.67	4.48	7.27	8.33	18.98
230	130.9	423.9	-5.7	263.7	336.1	321.7	189.2	1040.4	10.68	10.25	6.44	14.20	8.80	7.51	10.26	32.33
240	142.5	441.7	22.2	297.8	412.3	282.1	342.7	1065.3	8.75	17.90	15.74	15.85	21.58	26.89	33.55	36.50
250	140.5	482.7	14.8	340.1	396.8	288.9	337.4	1119.6	5.81	18.14	7.77	13.35	12.73	4.85	12.21	24.14
260	123.5	495.2	13.8	330.7	349.8	308.1	286.2	1176.0	9.51	29.50	13.14	21.68	14.23	18.06	16.20	17.99
270	126.1	544.2	30.4	417.7	354.1	295.8	336.5	1198.7	77.07	38.51	140.22	157.09	47.49	81.21	171.19	164.04
280	152.1	568.9	76.4	371.5	139.8	443.5	6.8	1461.6	15.16	19.78	20.24	19.65	14.58	5.55	22.01	34.47
290	162.4	683.6	40.7	480.5	244.7	458.0	424.8	1389.1	10.32	16.28	13.91	16.67	10.06	17.08	14.40	46.87
300	275.7	764.8	144.5	582.5	249.1	607.6	557.3	1502.9	32.86	37.49	29.43	38.60	31.99	23.25	38.78	50.78

Table 50. Dynamic stiffness real and imaginary parts at 10000 rpm and 0 kPa (MN/m)

f	$R(H_{xx})$	$I(H_{xx})$	$R(H_{xy})$	$I(H_{xy})$	$R(H_{yx})$	$I(H_{yx})$	$R(H_{yy})$	$I(H_{yy})$	$\Delta R(H_{xx})$	$\Delta I(H_{xx})$	$\Delta R(H_{xy})$	$\Delta I(H_{xy})$	$\Delta R(H_{yx})$	$\Delta I(H_{yx})$	$\Delta R(H_{yy})$	$\Delta I(H_{yy})$
20	31.7	16.2	-50.1	2.9	192.1	10.6	98.2	45.6	5.94	4.06	3.43	2.35	11.75	5.02	7.49	4.27
30	29.5	17.2	-44.9	-6.7	189.6	2.9	106.0	53.5	3.50	2.36	2.51	1.29	8.55	18.95	15.40	11.42
40	25.4	28.9	-46.3	-8.6	190.6	11.5	105.2	75.3	4.39	2.45	2.12	1.79	8.02	10.97	12.55	6.25
50	23.1	37.1	-46.2	-9.4	186.0	12.4	102.3	90.1	2.69	2.56	2.63	3.62	7.58	12.38	14.86	4.14
60	25.4	49.5	-53.3	-6.0	167.0	18.6	81.4	97.2	32.78	26.30	11.32	32.95	36.86	78.41	64.79	37.87
70	20.6	51.1	-45.9	-14.2	187.3	34.0	85.3	133.8	2.40	2.78	2.62	3.24	7.72	14.15	15.94	5.01
80	20.1	62.1	-51.6	-8.9	187.8	26.7	95.1	150.4	1.56	3.98	3.39	6.16	10.75	19.82	24.69	5.59
90	17.0	67.0	-47.9	-13.7	183.6	32.9	82.7	160.9	2.72	3.00	2.04	4.32	8.29	20.86	22.58	5.23
100	13.5	73.8	-48.0	-13.7	185.4	35.4	79.6	182.0	2.45	4.86	3.17	4.38	8.95	19.91	25.17	6.29
110	8.0	80.3	-46.1	-14.6	177.5	41.0	70.3	195.7	2.75	3.96	2.85	4.70	9.88	20.71	23.11	8.33
120	4.2	93.7	-53.2	-14.1	195.2	54.4	56.8	231.7	17.83	19.00	18.46	19.30	74.28	60.99	72.97	89.80
130	7.9	95.0	-44.0	-10.8	169.6	38.5	59.2	228.4	8.47	4.54	3.34	6.72	19.18	30.86	25.86	24.63
140	-0.4	108.1	-52.7	-8.6	168.4	45.6	57.9	249.6	8.99	7.34	12.03	9.22	13.96	40.40	48.85	18.87
150	1.6	117.3	-47.1	-2.8	166.2	51.8	47.0	261.0	17.10	6.05	4.80	17.53	22.22	43.00	41.53	36.52
160	-9.1	124.0	-48.4	-14.8	166.0	66.1	20.5	285.8	8.69	6.00	13.95	6.26	13.05	29.73	32.35	15.47
170	-17.4	127.3	-29.4	-13.7	158.3	60.3	16.4	278.4	9.46	12.87	23.38	6.65	23.75	36.01	43.43	19.59
180	-159.0	596.4	-422.7	-64.7	244.2	156.6	-36.0	403.7	572.90	721.36	411.49	487.36	202.36	132.82	139.16	108.94
190	-16.7	143.7	-41.5	-0.9	157.2	73.6	14.1	339.1	14.00	6.67	10.93	9.49	35.21	35.95	37.54	39.11
200	-28.3	157.5	-54.3	-9.1	156.1	87.7	-11.5	372.4	13.02	5.55	10.11	4.77	26.04	28.42	28.20	17.28
210	-37.7	167.8	-64.2	9.5	157.9	93.9	-6.5	410.1	18.22	4.40	13.04	18.33	37.77	40.18	59.81	37.80
220	-38.4	189.0	-59.6	22.0	158.9	115.2	-19.0	471.7	19.99	4.90	8.02	19.71	40.09	35.99	55.08	41.63
230	-48.9	200.1	-74.2	-2.7	160.9	137.0	-44.8	517.3	17.05	6.59	17.42	10.45	43.00	31.63	50.55	25.78
240	-35.8	223.4	-39.3	12.1	149.0	140.2	-0.4	522.8	18.86	7.76	14.98	12.43	47.71	22.90	28.20	48.05
250	-27.2	256.4	-31.8	60.6	170.3	121.1	79.0	634.5	25.72	9.37	17.05	17.72	65.52	24.38	68.57	68.20
260	-8.7	286.2	-53.1	22.4	104.4	197.4	40.4	668.7	27.45	8.93	22.68	17.86	57.79	17.19	53.87	60.36
270	97.6	233.8	43.3	72.6	408.4	143.8	440.8	967.2	31.47	21.86	25.58	24.28	102.26	52.20	92.43	154.96
280	15.4	235.6	-26.4	40.1	276.4	82.5	470.6	945.4	26.13	22.79	17.76	13.67	126.20	30.47	90.55	133.98
290	49.2	214.5	-16.2	30.5	369.1	38.6	1076.8	939.1	19.01	26.46	20.49	19.78	157.65	121.68	179.12	253.37
300	-11.1	245.0	-32.7	58.5	309.4	-382.2	1673.6	433.7	64.85	37.97	98.54	83.84	164.90	204.68	192.52	432.78

Table 51. Dynamic stiffness real and imaginary parts at 10000 rpm and 345 kPa (MN/m)

f	$R(H_{xx})$	$I(H_{xx})$	$R(H_{xy})$	$I(H_{xy})$	$R(H_{yx})$	$I(H_{yx})$	$R(H_{yy})$	$I(H_{yy})$	$\Delta R(H_{xx})$	$\Delta I(H_{xx})$	$\Delta R(H_{xy})$	$\Delta I(H_{xy})$	$\Delta R(H_{yx})$	$\Delta I(H_{yx})$	$\Delta R(H_{yy})$	$\Delta I(H_{yy})$
20	118.0	3.2	-51.6	-0.6	239.6	3.2	118.4	44.5	11.93	4.81	17.60	0.87	20.04	4.15	13.03	4.71
30	107.8	27.4	-53.0	10.4	248.2	-1.3	131.4	65.3	5.02	3.04	12.47	5.12	21.71	6.75	14.29	7.85
40	105.4	36.1	-53.6	10.2	239.0	2.5	123.8	87.3	7.07	4.55	14.46	3.91	23.17	8.19	12.81	12.52
50	100.7	43.3	-51.4	15.1	234.4	2.3	124.3	109.1	7.66	5.25	13.28	2.87	25.59	5.17	13.17	14.64
60	113.8	49.2	-52.3	24.7	252.9	12.7	121.8	141.8	107.17	61.47	55.97	43.10	179.18	126.01	87.18	92.09
70	100.2	67.9	-53.7	23.4	232.6	12.1	120.0	151.2	5.17	7.47	13.61	3.54	23.04	8.18	8.74	20.16
80	91.2	75.1	-51.7	22.5	210.7	30.2	99.2	181.7	3.57	9.20	14.68	2.49	32.88	15.42	14.80	32.43
90	91.5	87.9	-56.7	26.4	227.7	29.1	114.7	203.1	4.50	8.79	13.88	4.98	31.53	10.43	11.35	28.46
100	83.4	97.3	-56.0	27.4	220.6	28.7	112.9	214.9	3.23	12.00	15.88	3.19	34.49	7.74	14.88	31.56
110	77.4	111.9	-60.3	31.2	209.5	32.9	108.4	229.7	5.74	9.17	15.41	4.88	36.42	7.90	8.75	35.07
120	71.9	116.4	-61.1	34.7	194.5	30.4	90.4	248.7	36.03	32.71	38.63	26.63	75.79	99.42	86.71	83.16
130	69.8	128.6	-55.1	43.9	192.6	36.5	88.7	269.1	4.37	13.20	13.69	2.33	33.96	4.92	5.41	41.59
140	59.0	144.1	-60.7	50.9	179.8	58.1	68.2	290.1	3.88	18.39	17.28	6.63	37.48	7.24	13.05	48.71
150	67.8	159.7	-55.1	65.9	183.7	76.2	62.3	325.0	3.08	13.89	8.58	8.01	30.10	10.25	9.54	40.65
160	62.0	165.8	-52.7	51.8	178.4	96.2	56.3	364.4	10.40	20.37	18.05	7.95	45.24	7.83	15.56	74.35
170	61.0	194.2	-55.3	65.6	194.0	85.5	44.4	371.3	8.94	21.61	15.60	9.19	48.11	19.84	9.81	80.81
180	97.7	315.2	-119.3	190.1	211.8	115.2	73.8	433.4	664.69	973.51	672.54	793.80	274.29	145.19	179.27	242.98
190	44.9	202.3	-50.1	79.1	187.4	114.2	63.1	436.5	8.22	14.18	6.45	6.82	30.71	10.06	11.16	58.45
200	40.4	212.0	-51.2	79.2	170.1	115.3	51.2	426.2	6.10	25.05	5.79	8.81	35.34	6.95	12.60	72.86
210	27.2	225.9	-55.3	92.2	160.9	132.1	32.1	454.8	4.22	19.81	3.25	10.91	35.24	20.54	25.10	55.40
220	20.8	254.3	-60.0	103.2	148.8	132.4	18.1	466.9	6.18	19.32	6.26	14.22	28.78	16.86	7.48	52.35
230	22.2	267.6	-51.6	108.0	146.5	193.5	17.2	570.5	4.82	19.32	4.43	7.41	48.48	20.58	37.11	98.48
240	14.2	299.4	-63.5	132.0	169.5	204.8	55.6	612.1	18.06	13.25	21.61	15.78	46.96	45.03	42.46	63.96
250	18.4	342.7	-68.4	161.8	170.1	207.6	63.9	632.3	6.11	15.97	6.77	6.66	39.99	27.22	34.65	72.84
260	65.5	352.8	-16.5	174.3	176.0	222.3	88.1	686.4	5.80	17.03	10.24	1.95	27.00	43.74	32.18	69.58
270	110.4	395.1	1.4	200.1	165.2	285.0	110.0	728.6	7.07	14.10	11.66	4.48	18.33	35.34	26.32	76.65
280	218.9	243.6	89.9	112.3	524.9	431.1	321.9	1027.3	5.39	19.43	7.72	9.63	32.89	47.33	78.31	117.01
290	126.0	246.9	41.9	103.2	376.1	197.1	390.9	789.8	9.98	20.93	11.43	9.12	28.44	18.11	52.74	113.83
300	99.2	289.7	15.9	123.8	372.2	224.0	478.5	801.3	56.15	107.94	100.35	178.73	80.92	69.58	222.87	166.79

Table 52. Dynamic stiffness real and imaginary parts at 10000 rpm and 690 kPa (MN/m)

f	$R(H_{xx})$	$I(H_{xx})$	$R(H_{xy})$	$I(H_{xy})$	$R(H_{yx})$	$I(H_{yx})$	$R(H_{yy})$	$I(H_{yy})$	$\Delta R(H_{xx})$	$\Delta I(H_{xx})$	$\Delta R(H_{xy})$	$\Delta I(H_{xy})$	$\Delta R(H_{yx})$	$\Delta I(H_{yx})$	$\Delta R(H_{yy})$	$\Delta I(H_{yy})$
20	117.99	3.16	-51.62	-0.63	239.64	3.17	118.39	44.48	12.31	6.52	8.41	4.36	14.04	6.85	10.73	2.89
30	107.80	27.44	-52.97	10.36	248.20	-1.30	131.35	65.34	3.30	2.24	3.36	2.57	9.61	7.11	6.83	5.15
40	105.43	36.08	-53.63	10.21	239.01	2.47	123.85	87.30	5.43	2.84	4.94	2.30	11.68	2.77	8.43	3.32
50	100.67	43.27	-51.43	15.05	234.42	2.32	124.29	109.12	4.73	2.73	5.06	1.56	9.03	2.77	6.02	2.80
60	113.83	49.18	-52.34	24.74	252.88	12.66	121.82	141.75	82.23	80.66	39.63	42.62	168.56	147.47	87.46	68.30
70	100.21	67.89	-53.65	23.43	232.62	12.06	119.95	151.19	6.87	4.85	6.62	3.06	9.06	4.31	7.06	4.90
80	91.17	75.14	-51.68	22.45	210.75	30.20	99.19	181.72	3.13	4.44	5.74	1.10	7.92	2.41	3.15	5.06
90	91.48	87.91	-56.73	26.41	227.66	29.09	114.68	203.13	3.22	5.87	6.24	1.60	8.23	4.04	5.23	7.26
100	83.36	97.27	-55.96	27.45	220.57	28.72	112.87	214.85	3.61	7.45	8.08	2.85	12.97	4.88	5.18	12.98
110	77.43	111.93	-60.28	31.22	209.52	32.90	108.45	229.73	6.53	6.72	8.62	4.04	11.55	5.97	7.75	10.24
120	71.87	116.43	-61.11	34.66	194.53	30.44	90.42	248.70	32.73	38.10	24.50	27.38	111.82	72.37	59.71	69.92
130	69.83	128.65	-55.10	43.91	192.58	36.54	88.68	269.13	2.13	5.99	6.87	4.46	9.70	6.18	9.84	14.92
140	59.03	144.05	-60.75	50.86	179.85	58.08	68.24	290.08	2.51	7.74	8.40	5.45	8.50	4.26	5.10	13.73
150	67.78	159.72	-55.13	65.94	183.75	76.24	62.34	325.01	5.73	8.48	4.06	8.67	8.77	6.57	7.60	17.59
160	61.96	165.83	-52.66	51.85	178.36	96.16	56.33	364.36	5.05	8.86	3.70	6.51	16.85	10.82	5.76	26.55
170	61.03	194.24	-55.26	65.59	193.97	85.52	44.39	371.31	8.87	7.98	6.14	16.27	15.18	8.26	16.35	24.34
180	97.66	315.19	-119.27	190.14	211.79	115.17	73.80	433.44	908.68	595.05	594.13	419.16	161.75	286.92	145.75	158.00
190	44.95	202.33	-50.05	79.10	187.36	114.19	63.14	436.47	6.89	8.60	4.87	10.78	14.30	2.65	2.64	29.82
200	40.37	212.02	-51.23	79.21	170.10	115.29	51.19	426.23	2.96	3.92	4.71	3.71	16.33	4.20	6.88	30.12
210	27.22	225.92	-55.33	92.15	160.94	132.11	32.06	454.77	3.33	3.70	5.26	3.99	12.24	8.16	6.95	22.14
220	20.85	254.30	-60.02	103.22	148.78	132.43	18.10	466.91	4.21	4.47	2.74	3.56	11.97	8.51	8.54	27.13
230	22.18	267.64	-51.57	108.03	146.51	193.47	17.17	570.51	4.75	5.77	3.43	7.41	7.49	7.89	5.58	27.64
240	14.18	299.42	-63.48	131.99	169.48	204.80	55.55	612.08	8.24	11.51	9.28	9.14	12.21	16.19	16.66	36.49
250	18.39	342.70	-68.43	161.80	170.10	207.59	63.88	632.32	12.57	8.74	7.53	9.54	6.74	7.60	5.21	28.43
260	65.51	352.80	-16.55	174.33	175.96	222.30	88.11	686.39	13.14	13.24	11.34	10.50	13.45	12.02	9.81	36.10
270	110.35	395.12	1.36	200.07	165.17	284.98	109.98	728.58	11.38	19.32	6.87	15.03	20.14	21.99	14.60	28.99
280	218.93	243.58	89.86	112.33	524.93	431.11	321.92	1027.26	42.64	50.12	20.48	34.02	43.68	113.28	40.45	92.23
290	125.96	246.88	41.91	103.23	376.08	197.12	390.94	789.80	16.57	12.32	14.00	4.92	23.81	21.35	31.75	51.54
300	99.15	289.68	15.93	123.81	372.19	224.02	478.55	801.28	71.97	65.90	51.42	51.58	31.26	33.53	32.38	41.77

Table 53. Dynamic stiffness real and imaginary parts at 10000 rpm and 1034 kPa (MN/m)

f	$R(H_{xx})$	$I(H_{xx})$	$R(H_{xy})$	$I(H_{xy})$	$R(H_{yx})$	$I(H_{yx})$	$R(H_{yy})$	$I(H_{yy})$	$\Delta R(H_{xx})$	$\Delta I(H_{xx})$	$\Delta R(H_{xy})$	$\Delta I(H_{xy})$	$\Delta R(H_{yx})$	$\Delta I(H_{yx})$	$\Delta R(H_{yy})$	$\Delta I(H_{yy})$
20	207.9	12.0	81.6	10.9	317.1	6.2	110.4	56.1	259.64	3.46	86.61	9.51	383.58	28.30	130.97	5.84
30	142.8	30.3	68.0	14.8	269.0	2.4	162.1	73.5	22.51	24.05	6.37	11.56	35.17	46.94	5.77	21.28
40	141.9	40.2	68.2	19.4	265.8	16.6	142.4	112.0	39.50	8.96	11.27	11.30	63.48	26.55	16.44	21.25
50	131.7	55.1	66.1	24.0	260.3	24.3	148.0	143.9	24.14	6.99	6.83	6.47	41.07	22.32	11.34	15.70
60	133.3	61.5	66.5	33.5	255.9	28.0	152.4	171.1	107.77	72.93	48.81	69.43	257.24	135.17	84.43	165.75
70	129.2	84.8	64.0	35.3	269.3	43.7	150.9	196.5	15.44	21.82	4.72	10.05	22.68	48.28	18.49	16.13
80	125.2	81.4	53.3	41.4	238.9	49.0	105.8	233.0	11.07	17.00	8.34	2.43	28.68	15.31	9.04	7.36
90	119.6	106.7	67.0	42.6	260.5	60.4	149.2	263.0	18.62	6.96	6.83	6.98	30.04	14.51	6.46	14.14
100	111.5	118.7	65.6	46.6	255.9	61.1	148.1	282.4	17.53	11.05	8.30	7.12	30.20	6.47	4.84	14.40
110	110.1	131.9	63.7	52.0	241.2	62.0	145.1	290.0	15.72	11.67	8.01	7.54	24.93	19.21	13.22	17.22
120	100.6	145.8	66.4	55.7	227.9	90.4	120.9	321.2	34.09	52.84	46.75	19.39	77.03	126.40	107.83	62.89
130	108.5	146.3	56.6	65.2	242.7	65.0	137.5	340.3	7.76	13.15	8.79	5.28	14.63	10.29	8.20	16.89
140	98.4	166.5	61.4	76.2	234.2	93.4	114.6	387.8	9.64	12.63	7.55	7.64	20.00	6.07	3.71	20.32
150	104.6	185.0	55.4	88.4	252.1	100.6	136.6	420.4	9.51	10.67	6.88	5.87	14.92	7.19	3.31	18.88
160	105.1	191.0	57.1	74.2	223.6	118.5	91.5	442.6	14.04	11.19	11.21	8.39	17.68	23.24	10.62	23.77
170	112.0	214.9	56.5	95.7	223.3	102.6	92.5	459.3	26.64	7.52	8.78	10.77	9.55	28.98	11.32	19.59
180	304.7	463.6	78.5	325.4	336.2	110.1	158.4	529.9	963.31	804.36	588.03	834.70	373.79	302.95	323.25	233.80
190	83.0	231.8	50.1	109.6	244.8	143.5	116.7	526.0	13.10	11.92	7.94	10.44	19.43	8.02	5.49	29.16
200	75.9	248.5	53.5	112.8	222.9	153.6	83.0	518.7	9.86	10.51	4.89	9.53	17.76	5.84	7.23	33.04
210	60.2	265.2	56.0	128.0	226.4	177.7	85.3	576.2	13.85	11.82	6.51	12.17	23.09	6.93	10.93	29.78
220	64.7	285.1	50.7	139.3	231.8	179.0	79.0	594.0	13.72	10.65	7.14	6.78	16.79	13.00	11.10	28.65
230	57.7	297.5	52.6	135.1	218.6	223.5	73.7	675.1	12.00	14.43	4.20	9.85	21.09	5.74	10.38	33.94
240	54.3	321.2	52.5	154.8	257.6	220.8	137.4	714.7	13.16	16.76	11.62	8.59	10.42	22.51	24.47	32.42
250	49.8	349.7	61.3	173.8	258.8	217.3	142.9	745.1	11.95	19.78	10.16	9.61	13.41	17.42	12.26	40.50
260	46.7	374.1	57.2	182.9	225.8	238.8	120.5	793.8	11.85	17.80	5.51	10.46	19.14	6.89	15.05	37.22
270	32.6	412.3	69.1	211.8	211.0	252.0	159.6	819.0	9.95	18.10	5.05	10.09	14.22	19.57	15.21	26.09
280	56.1	466.8	41.7	221.2	56.0	404.1	1.5	1053.4	19.23	16.23	5.88	9.42	18.83	21.45	10.83	31.88
290	137.4	639.5	45.4	375.7	97.0	513.5	144.1	1028.9	40.08	36.31	25.26	27.99	30.75	34.24	14.42	33.15
300	391.7	551.1	173.9	367.9	359.3	759.9	379.8	1261.0	95.79	211.36	81.67	151.97	139.82	148.33	96.61	138.58

Table 54. Dynamic stiffness real and imaginary parts at 10000 rpm and 1379 kPa (MN/m)

f	$R(H_{xx})$	$I(H_{xx})$	$R(H_{xy})$	$I(H_{xy})$	$R(H_{yx})$	$I(H_{yx})$	$R(H_{yy})$	$I(H_{yy})$	$\Delta R(H_{xx})$	$\Delta I(H_{xx})$	$\Delta R(H_{xy})$	$\Delta I(H_{xy})$	$\Delta R(H_{yx})$	$\Delta I(H_{yx})$	$\Delta R(H_{yy})$	$\Delta I(H_{yy})$
20	190.7	-2.2	-70.9	15.6	284.6	19.1	194.1	78.7	4.26	6.96	6.20	2.76	14.93	8.74	6.03	6.38
30	186.8	19.2	-67.0	22.1	329.1	-11.6	244.4	95.7	5.89	2.88	5.13	2.29	11.14	3.47	5.21	3.56
40	167.0	46.5	-65.0	23.9	297.9	28.6	224.5	137.6	4.55	3.16	4.52	1.99	8.46	4.56	3.30	3.74
50	155.3	59.2	-61.5	28.9	293.6	30.7	232.2	174.0	4.06	3.54	5.16	1.25	5.94	3.81	4.06	2.35
60	207.4	92.7	-71.4	73.0	367.2	127.2	189.2	275.5	157.87	103.73	54.33	103.01	358.57	294.90	162.70	235.43
70	163.1	83.8	-62.0	46.9	309.6	36.7	231.2	235.5	4.66	4.38	4.06	1.76	12.62	4.49	3.23	8.09
80	165.5	87.1	-51.1	56.5	305.9	48.1	202.1	288.1	5.63	5.11	4.37	3.57	8.70	5.39	2.82	7.49
90	153.8	114.4	-62.1	57.5	311.5	73.1	231.3	327.3	6.28	4.75	3.59	3.57	12.14	3.94	5.12	8.76
100	145.6	123.3	-59.4	63.0	306.5	68.3	231.3	354.0	5.12	4.80	4.32	4.55	11.85	5.67	4.79	7.48
110	147.2	150.3	-62.1	72.2	290.9	88.1	219.7	368.2	6.91	5.26	2.21	7.07	15.65	7.65	6.42	17.66
120	150.2	143.6	-40.5	93.1	306.9	62.4	265.7	439.6	75.88	46.76	52.57	63.48	215.28	131.50	151.41	179.12
130	152.5	161.5	-49.9	89.6	301.0	91.3	212.7	433.3	6.31	5.81	2.77	7.85	14.59	10.27	10.34	18.58
140	133.3	183.6	-54.7	92.2	288.5	114.0	204.4	476.9	5.10	7.90	3.44	5.20	12.26	6.46	5.92	14.27
150	144.5	200.5	-47.1	110.2	310.5	126.0	216.1	514.3	4.51	8.93	4.45	5.35	10.88	6.81	8.70	16.45
160	140.5	207.6	-56.8	88.7	280.4	178.9	163.3	564.7	11.17	12.44	8.11	13.83	11.04	15.29	19.08	11.32
170	154.2	221.2	-43.9	107.4	245.1	136.3	155.1	561.9	18.91	16.96	12.79	18.46	25.23	14.31	17.46	16.06
180	394.0	216.5	69.5	309.5	336.8	52.2	269.9	594.6	457.11	742.53	481.39	813.12	380.54	194.50	387.64	286.89
190	132.3	260.6	-40.0	142.5	331.8	184.1	201.2	658.6	3.39	8.95	6.38	3.28	6.20	6.53	3.15	11.55
200	121.6	270.1	-42.8	141.7	305.8	190.5	160.7	652.1	3.02	8.94	4.85	4.86	8.43	6.25	6.89	14.61
210	110.9	292.5	-43.0	162.9	315.3	211.4	164.6	716.5	4.16	9.76	4.19	4.83	7.33	5.66	8.87	14.05
220	127.8	315.9	-34.3	182.9	345.2	217.8	175.9	754.1	3.51	8.61	7.13	4.28	6.90	6.22	11.10	12.42
230	107.6	326.3	-42.1	170.2	313.2	265.1	138.5	836.4	2.70	10.04	6.43	5.25	5.82	5.53	12.09	16.72
240	115.4	354.2	-36.1	203.9	378.2	253.0	239.5	889.2	15.07	22.26	19.94	30.70	48.85	39.17	49.37	67.42
250	120.5	374.4	-20.7	225.4	383.7	224.6	279.9	908.2	5.63	18.17	14.98	10.44	8.39	12.24	12.47	27.50
260	114.9	388.1	-13.5	229.9	345.8	247.9	233.6	964.0	3.16	18.71	7.86	12.56	8.09	8.33	12.82	24.61
270	114.3	404.6	-5.2	244.9	362.9	231.8	328.0	973.4	6.34	16.67	5.66	14.24	5.56	7.89	9.45	31.16
280	125.7	420.8	29.6	224.5	223.3	354.8	56.5	1187.6	5.94	13.45	4.49	11.84	6.83	7.88	13.88	27.70
290	123.0	495.8	-9.2	301.2	314.0	301.5	410.7	1088.8	5.16	21.72	5.85	17.69	9.40	21.50	13.26	35.01
300	149.8	554.6	10.5	340.0	292.9	341.4	517.1	1113.1	70.53	92.18	68.77	127.11	50.62	57.00	67.84	76.53

Table 55. Dynamic stiffness real and imaginary parts at 10000 rpm and 1655 kPa (MN/m)

f	$R(H_{xx})$	$I(H_{xx})$	$R(H_{xy})$	$I(H_{xy})$	$R(H_{yx})$	$I(H_{yx})$	$R(H_{yy})$	$I(H_{yy})$	$\Delta R(H_{xx})$	$\Delta I(H_{xx})$	$\Delta R(H_{xy})$	$\Delta I(H_{xy})$	$\Delta R(H_{yx})$	$\Delta I(H_{yx})$	$\Delta R(H_{yy})$	$\Delta I(H_{yy})$
20	223.2	7.9	-63.9	12.6	348.5	25.3	278.2	94.5	14.61	11.75	6.88	6.94	13.97	19.28	12.85	12.88
30	220.0	36.7	-68.1	28.4	395.5	-13.3	328.5	119.6	5.68	7.09	4.38	4.60	10.08	8.30	4.29	6.14
40	205.1	48.9	-63.2	30.5	366.7	29.0	308.7	171.5	2.95	3.61	2.28	2.95	10.56	5.05	4.51	4.76
50	196.5	58.6	-59.5	40.2	365.7	31.5	314.2	217.9	5.37	4.32	1.53	2.76	9.34	8.37	7.56	8.15
60	190.6	111.4	-97.4	58.4	300.2	88.2	228.5	249.9	123.65	169.61	60.82	98.47	280.28	498.63	212.34	218.54
70	206.1	98.1	-60.1	60.9	382.9	38.1	318.0	297.3	3.90	6.71	2.70	3.97	10.21	9.38	7.51	10.32
80	210.2	113.0	-54.0	74.6	365.0	60.8	281.9	346.0	1.71	5.19	1.98	3.46	5.58	7.50	5.30	6.14
90	186.4	129.5	-60.0	71.9	382.5	67.0	321.4	404.6	2.83	6.16	3.15	2.39	7.75	9.88	5.69	6.79
100	192.5	145.3	-56.6	82.7	382.2	79.9	317.6	442.1	3.82	6.69	3.76	3.53	7.44	7.68	5.18	12.66
110	169.4	169.9	-56.7	81.0	351.1	73.6	321.9	453.9	4.51	8.37	6.05	2.28	8.01	8.38	7.01	8.74
120	203.3	198.3	-69.3	129.9	481.0	156.6	289.0	636.5	65.62	131.04	104.60	97.02	224.18	377.84	284.35	323.71
130	202.7	193.8	-47.9	105.4	373.1	109.3	308.0	522.5	6.77	9.20	8.00	7.97	6.58	17.77	13.96	8.68
140	172.8	211.0	-49.1	115.7	356.9	120.5	287.0	582.8	7.61	8.61	4.52	6.97	9.39	9.04	7.39	14.56
150	192.9	216.6	-32.8	128.8	402.9	119.4	330.9	624.0	7.49	9.24	8.33	7.31	15.18	11.65	10.26	20.04
160	174.9	224.0	-55.8	108.1	362.4	193.9	235.9	737.0	13.95	10.81	5.88	12.60	11.52	12.57	27.73	28.58
170	186.6	222.7	-35.0	114.6	295.2	138.5	214.5	710.8	12.71	14.16	6.26	13.76	42.41	9.99	27.43	18.29
180	639.4	695.3	-100.1	728.9	735.4	14.1	565.7	924.9	525.17	1981.90	1374.45	1610.51	1158.39	463.29	737.73	1077.05
190	176.0	289.5	-24.3	174.4	418.4	173.4	307.4	792.2	5.70	10.02	10.05	10.10	12.30	7.62	9.69	20.77
200	175.0	300.0	-19.5	180.6	403.6	175.5	273.4	803.9	5.23	5.10	10.47	6.61	9.05	8.61	13.31	15.45
210	160.3	320.5	-15.7	199.5	408.5	190.9	291.6	865.5	4.29	6.57	7.51	7.30	8.94	4.71	8.96	18.62
220	170.1	341.2	-4.5	209.3	420.6	207.4	283.2	909.7	4.76	8.94	4.69	7.75	5.83	7.60	8.70	14.77
230	150.8	355.0	-12.4	199.3	387.0	265.0	227.5	1013.5	3.64	8.13	5.20	5.16	7.12	7.57	13.16	20.22
240	166.4	383.2	2.3	230.4	456.2	229.7	371.3	1031.8	18.55	17.44	26.74	22.36	39.94	42.57	61.96	49.42
250	159.7	415.7	4.8	263.6	464.0	230.4	404.9	1082.0	8.10	11.74	10.28	10.28	9.08	11.75	5.20	24.49
260	170.4	424.7	26.5	268.8	443.9	226.7	382.2	1088.5	4.45	9.90	6.74	9.59	8.59	7.51	12.52	23.32
270	181.4	434.7	39.2	278.8	464.0	202.5	480.7	1119.8	5.89	10.31	4.63	8.98	5.18	7.13	12.20	21.20
280	177.5	434.4	85.0	253.5	309.1	302.1	116.1	1234.5	4.90	7.04	6.17	8.11	3.24	3.08	8.32	18.69
290	164.0	493.0	29.0	310.6	423.9	265.6	587.3	1265.0	6.93	6.62	7.75	6.98	8.61	6.28	15.79	23.19
300	158.3	542.5	47.1	339.8	434.2	248.6	740.8	1253.7	29.97	49.68	70.05	66.44	33.50	24.30	50.39	64.57

Table 56. Dynamic stiffness real and imaginary parts at 12000 rpm and 0 kPa (MN/m)

f	$R(H_{xx})$	$I(H_{xx})$	$R(H_{xy})$	$I(H_{xy})$	$R(H_{yx})$	$I(H_{yx})$	$R(H_{yy})$	$I(H_{yy})$	$\Delta R(H_{xx})$	$\Delta I(H_{xx})$	$\Delta R(H_{xy})$	$\Delta I(H_{xy})$	$\Delta R(H_{yx})$	$\Delta I(H_{yx})$	$\Delta R(H_{yy})$	$\Delta I(H_{yy})$
20	93.9	11.7	-51.0	1.7	256.0	-3.0	127.2	41.7	39.28	3.75	6.62	5.74	38.58	10.53	11.91	4.94
30	91.1	24.3	-53.9	5.8	250.5	-2.9	126.8	59.4	32.84	3.73	9.90	7.63	33.87	15.99	11.38	5.80
40	88.8	26.2	-53.1	4.1	244.1	-3.0	124.1	78.2	32.31	2.71	9.00	10.21	29.48	21.45	10.17	7.64
50	84.2	31.9	-51.5	7.2	238.6	-8.5	125.1	95.3	35.22	4.31	4.98	12.76	29.17	19.28	12.62	7.06
60	87.2	62.4	-60.3	8.8	212.6	42.2	110.3	107.2	70.38	84.39	33.21	49.17	147.88	165.73	72.01	87.91
70	79.9	47.5	-50.4	10.3	232.9	7.0	118.3	143.9	35.27	2.37	6.16	17.72	18.00	27.91	18.32	9.69
80	70.6	61.6	-59.1	8.5	223.1	10.6	118.6	154.9	37.96	4.24	5.35	18.63	13.15	11.60	12.22	12.71
90	73.4	65.1	-53.0	10.2	214.8	12.6	112.6	166.3	36.62	4.42	3.77	17.40	13.78	16.04	16.70	13.50
100	76.1	70.3	-48.1	15.0	220.9	12.9	116.1	186.7	43.96	2.99	4.26	23.72	16.94	14.59	22.75	16.64
110	63.0	81.5	-54.9	13.2	205.6	16.8	107.9	195.4	33.20	7.54	4.42	13.63	12.11	22.89	30.07	20.55
120	57.0	89.3	-55.9	13.6	190.6	32.2	94.4	204.2	51.41	18.82	24.05	36.82	98.55	94.35	103.71	57.03
130	54.7	99.1	-53.9	20.7	190.8	21.9	95.2	227.9	40.88	10.45	6.19	20.41	7.20	13.06	25.47	19.37
140	40.4	109.7	-58.0	19.3	173.0	36.0	76.3	239.8	31.39	16.88	5.06	12.03	12.59	20.94	27.56	33.24
150	39.6	120.0	-59.8	28.9	183.4	57.6	68.7	277.0	49.46	18.51	14.99	22.69	41.64	31.36	25.86	31.98
160	40.6	120.9	-44.6	23.7	165.6	65.3	62.2	288.8	32.86	56.03	70.33	68.36	40.82	55.33	33.61	81.34
170	45.4	122.6	-20.9	33.0	160.2	77.2	39.9	312.5	64.42	114.03	260.24	7.44	21.53	97.95	125.41	110.69
180	263.0	85.5	50.3	99.8	167.5	15.2	78.1	306.4	980.00	1453.10	646.27	676.78	331.96	302.66	174.64	163.31
190	31.5	169.5	-52.9	54.3	165.8	99.9	42.3	369.8	5.96	6.82	59.17	8.63	40.71	12.07	19.54	61.59
200	-25.5	94.4	-38.2	-41.0	175.2	138.6	49.0	402.2	149.31	79.56	110.35	262.18	48.77	55.30	77.25	87.11
210	35.3	201.9	-50.8	86.7	188.7	151.5	35.0	462.9	22.71	18.65	46.11	41.94	55.48	44.30	27.71	63.98
220	47.8	234.4	-35.0	108.4	229.2	177.7	88.6	519.9	32.19	32.59	36.60	58.49	51.30	80.31	42.72	43.64
230	88.0	245.9	15.3	152.2	282.8	118.0	210.5	528.0	62.40	41.36	14.87	90.75	13.98	64.28	21.40	65.37
240	158.9	193.5	115.2	113.4	381.9	24.4	351.1	487.1	101.28	11.44	61.19	47.18	62.04	51.66	78.96	114.26
250	78.7	155.3	66.8	33.2	231.1	-13.0	243.6	396.1	51.49	20.94	15.16	18.49	30.97	62.41	136.61	131.94
260	35.5	165.6	14.8	2.7	181.6	15.7	186.8	447.8	29.68	20.33	14.70	15.90	62.36	119.88	307.18	135.88
270	39.2	164.4	31.5	6.7	183.4	-5.9	298.4	444.2	25.03	33.26	28.02	14.78	132.14	236.70	371.79	281.19
280	11.2	186.7	-0.3	16.0	144.9	18.8	302.3	478.5	13.49	6.24	7.93	3.80	91.13	207.37	531.94	310.94
290	-2.4	200.2	-12.4	5.8	154.8	32.7	375.5	455.0	3.66	34.33	8.50	10.20	208.22	23.53	172.07	596.31
300	-35.0	268.9	-33.1	52.5	193.3	59.0	507.8	564.8	44.26	52.69	55.24	33.77	199.57	223.44	255.16	690.62

Table 57. Dynamic stiffness real and imaginary arts at 12000 rpm and 345 kPa (MN/m)

f	$R(H_{xx})$	$I(H_{xx})$	$R(H_{xy})$	$I(H_{xy})$	$R(H_{yx})$	$I(H_{yx})$	$R(H_{yy})$	$I(H_{yy})$	$\Delta R(H_{xx})$	$\Delta I(H_{xx})$	$\Delta R(H_{xy})$	$\Delta I(H_{xy})$	$\Delta R(H_{yx})$	$\Delta I(H_{yx})$	$\Delta R(H_{yy})$	$\Delta I(H_{yy})$
20	119.1	10.9	-66.1	4.8	247.6	-1.4	133.8	41.5	3.38	3.10	1.79	1.51	10.56	3.59	5.89	2.73
30	109.7	19.7	-64.6	4.9	242.1	-4.9	139.5	58.6	6.06	4.23	1.50	2.58	13.04	2.49	4.03	2.40
40	106.9	28.7	-65.5	5.7	238.4	7.8	134.3	85.7	3.25	2.78	1.46	1.33	10.57	2.69	4.53	1.27
50	100.7	33.7	-63.8	6.9	232.1	6.9	135.1	107.3	3.27	1.04	1.24	1.93	10.51	3.65	3.38	2.37
60	108.1	47.6	-70.4	10.1	234.4	27.8	130.6	117.5	81.76	85.26	50.97	38.01	217.37	199.42	100.05	121.87
70	99.5	54.9	-66.9	13.5	228.5	16.5	127.8	144.2	3.56	2.15	1.55	2.55	9.79	4.89	4.71	3.81
80	96.3	56.7	-58.1	11.2	196.2	38.2	78.8	187.8	2.97	3.41	2.49	1.43	7.54	4.02	4.19	4.44
90	94.5	70.8	-67.7	16.6	225.7	32.8	124.7	193.5	2.74	2.58	2.53	1.96	12.16	4.25	6.61	6.05
100	87.2	80.4	-68.5	16.1	220.4	33.9	121.9	207.2	3.65	3.82	2.91	2.23	11.75	5.36	7.12	5.10
110	86.9	85.3	-63.9	20.3	204.0	38.8	110.8	211.3	4.42	3.77	3.26	2.82	14.14	8.56	9.20	12.35
120	93.0	93.7	-66.2	27.6	247.1	18.4	117.6	250.6	44.81	35.42	29.66	39.79	139.38	127.97	129.52	106.14
130	74.6	101.3	-68.9	28.8	203.1	38.4	105.1	256.5	3.38	3.78	2.87	4.14	9.09	8.04	10.91	8.54
140	65.0	111.0	-69.4	28.7	194.6	59.0	80.5	285.2	5.23	5.35	4.15	4.53	10.09	7.24	9.59	8.76
150	62.4	128.1	-72.9	39.0	199.4	68.6	84.4	316.2	4.17	8.22	4.88	5.38	6.75	1.47	6.31	9.11
160	56.8	132.1	-66.7	33.4	185.2	86.5	79.5	339.7	7.97	4.75	6.64	5.18	10.17	7.14	12.43	8.29
170	51.1	146.5	-71.9	42.0	182.9	91.2	68.4	360.4	9.38	13.46	11.01	13.49	5.32	6.33	6.84	7.96
180	471.4	543.7	-148.4	467.2	337.6	34.4	172.9	449.6	976.78	3059.01	1473.70	1605.23	857.15	439.43	323.56	570.17
190	40.7	170.7	-69.7	54.2	194.8	112.4	70.2	407.7	8.16	15.79	8.42	9.64	6.76	16.83	24.32	10.59
200	-25.6	138.3	-29.2	-25.2	154.7	437.3	-333.5	419.8	40.64	50.01	39.14	67.83	109.78	188.32	254.34	200.25
210	24.8	195.8	-77.9	64.7	182.3	141.3	36.5	444.4	3.50	11.62	5.50	6.43	6.94	9.18	10.11	11.97
220	25.4	216.6	-76.2	83.7	163.0	129.4	27.7	425.2	2.99	11.05	2.52	6.61	6.59	4.43	5.50	11.57
230	19.0	221.9	-77.0	72.0	193.7	200.4	47.6	560.4	1.80	8.38	3.41	5.63	3.48	5.19	4.37	13.16
240	8.3	249.9	-86.6	95.3	208.2	201.5	74.4	574.3	5.88	11.46	14.11	10.19	15.80	21.85	24.72	33.41
250	2.2	285.6	-99.0	117.3	224.1	235.8	77.6	642.2	4.33	11.79	6.30	10.68	10.15	12.03	12.66	27.46
260	31.7	342.7	-81.2	182.8	243.1	208.9	126.1	643.2	9.73	14.22	14.41	9.93	8.94	8.53	11.98	15.34
270	120.4	439.1	-25.7	279.5	249.7	230.2	150.1	664.8	16.33	17.29	14.64	16.67	9.74	12.42	11.59	17.86
280	300.0	300.2	146.0	208.5	510.0	268.0	376.0	870.7	27.51	40.65	22.82	26.72	44.67	54.31	38.98	43.64
290	227.8	145.3	165.2	58.5	230.6	170.8	200.5	636.2	21.15	17.31	23.52	12.33	14.45	14.24	18.91	18.84
300	78.6	252.9	15.7	35.1	382.1	349.7	211.3	962.6	91.33	63.77	84.38	79.70	45.27	44.56	37.39	32.29

Table 58. Dynamic stiffness real and imaginary parts at 12000 rpm and 690 kPa (MN/m)

f	$R(H_{xx})$	$I(H_{xx})$	$R(H_{xy})$	$I(H_{xy})$	$R(H_{yx})$	$I(H_{yx})$	$R(H_{yy})$	$I(H_{yy})$	$\Delta R(H_{xx})$	$\Delta I(H_{xx})$	$\Delta R(H_{xy})$	$\Delta I(H_{xy})$	$\Delta R(H_{yx})$	$\Delta I(H_{yx})$	$\Delta R(H_{yy})$	$\Delta I(H_{yy})$
20	169.5	-9.1	-79.0	13.1	297.7	0.7	179.4	56.1	10.53	12.06	3.36	3.43	12.80	6.97	6.31	4.00
30	150.2	17.6	-73.1	11.7	293.5	-11.0	197.8	71.7	2.32	5.34	3.14	1.61	12.09	5.28	3.22	2.83
40	137.5	30.6	-71.2	8.1	280.8	19.4	186.3	108.1	3.12	4.43	1.95	1.75	14.12	3.19	3.60	2.33
50	126.0	39.6	-69.1	9.2	271.2	14.9	191.2	137.1	5.62	2.08	2.27	2.64	13.65	3.57	2.18	2.22
60	139.3	42.6	-68.8	21.6	293.9	15.9	196.4	175.6	77.59	96.29	63.90	56.37	276.31	207.61	112.45	210.90
70	128.8	58.0	-71.3	17.2	276.3	22.2	184.7	179.7	3.88	3.52	2.41	2.89	13.93	2.76	4.49	5.92
80	124.0	56.9	-66.7	23.3	272.2	37.0	169.1	235.0	1.87	5.39	3.70	1.30	13.23	4.71	5.37	2.90
90	120.1	80.6	-76.2	22.4	275.4	51.4	176.6	248.8	1.80	4.25	3.03	3.00	15.44	5.19	6.99	5.20
100	113.2	87.8	-73.6	22.4	268.2	45.4	174.5	263.8	1.99	3.79	3.15	2.27	17.77	3.81	9.59	5.97
110	115.8	101.1	-75.1	30.1	262.8	45.7	175.4	268.4	3.23	5.20	4.53	3.96	17.99	4.98	4.79	10.12
120	101.4	108.0	-75.0	25.7	259.2	81.1	134.5	298.8	35.33	20.70	24.84	32.37	139.91	73.82	81.83	123.90
130	103.0	107.2	-71.2	37.6	260.7	37.9	165.0	325.4	3.21	6.16	4.45	2.96	12.02	7.68	5.82	8.51
140	96.0	125.5	-72.7	45.6	254.4	77.6	126.9	377.2	7.02	7.64	5.76	4.52	8.41	15.90	14.75	10.35
150	94.3	138.9	-70.1	53.2	272.4	60.5	176.5	402.6	4.67	9.28	6.56	8.10	10.70	6.83	9.65	10.48
160	84.8	147.9	-72.3	47.8	237.6	102.3	129.2	433.1	7.25	11.71	3.34	5.60	7.34	8.43	6.65	12.37
170	76.9	163.9	-76.1	57.6	235.9	107.4	123.7	466.4	3.80	13.65	7.98	9.30	6.57	10.04	8.49	5.08
180	236.3	153.8	19.8	228.6	248.3	48.3	196.2	462.4	1337.53	676.15	706.53	571.25	234.50	530.55	258.35	243.73
190	76.9	187.2	-68.6	76.0	261.3	105.6	164.0	505.8	3.47	19.88	7.96	10.34	5.32	10.69	11.56	16.04
200	49.9	214.6	-84.0	42.5	304.7	180.7	-12.5	573.1	81.02	66.60	33.45	49.87	259.91	283.19	182.30	139.76
210	57.4	214.7	-70.8	86.2	253.1	147.0	125.5	564.8	4.60	16.70	4.69	9.14	11.62	9.62	8.87	13.06
220	58.9	230.0	-68.1	99.2	241.6	144.0	111.8	545.2	2.24	14.34	2.76	6.63	8.44	3.49	8.33	10.20
230	53.9	240.2	-65.5	92.2	236.5	212.7	84.8	669.9	1.99	14.57	6.98	7.01	5.57	6.93	9.69	12.49
240	48.6	262.0	-71.3	112.3	278.5	189.4	165.4	677.3	9.29	12.52	9.84	11.46	27.72	18.35	36.61	28.74
250	41.6	287.5	-76.0	127.5	283.8	203.5	151.4	721.1	4.42	16.02	7.73	9.58	4.87	16.31	10.04	15.86
260	34.1	307.9	-80.6	136.8	283.2	213.2	179.1	756.7	3.12	22.11	7.48	11.95	13.92	12.48	8.81	20.56
270	24.7	337.0	-88.4	155.1	300.3	203.2	247.6	778.7	8.68	17.92	3.93	14.31	7.83	4.09	4.26	12.32
280	13.1	374.2	-100.3	160.0	250.9	343.8	171.9	1005.8	8.57	10.55	10.21	6.38	9.59	7.19	13.49	9.21
290	65.7	512.5	-104.1	299.2	311.5	300.0	319.5	918.3	18.90	23.07	14.23	12.55	10.61	14.94	10.58	18.34
300	193.1	585.3	12.9	399.4	364.1	322.9	451.4	956.9	130.24	128.04	80.71	97.43	66.57	64.75	47.96	44.31

Table 59. Dynamic stiffness real and imaginary parts at 12000 rpm and 1034 kPa (MN/m)

f	$R(H_{xx})$	$I(H_{xx})$	$R(H_{xy})$	$I(H_{xy})$	$R(H_{yx})$	$I(H_{yx})$	$R(H_{yy})$	$I(H_{yy})$	$\Delta R(H_{xx})$	$\Delta I(H_{xx})$	$\Delta R(H_{xy})$	$\Delta I(H_{xy})$	$\Delta R(H_{yx})$	$\Delta I(H_{yx})$	$\Delta R(H_{yy})$	$\Delta I(H_{yy})$
20	191.6	7.7	-79.9	12.0	353.0	3.9	263.6	67.8	3.46	5.02	3.14	2.70	7.27	3.80	4.16	2.79
30	184.8	22.4	-76.7	13.3	348.9	-11.8	282.9	87.6	3.89	4.65	3.21	2.25	3.47	3.16	2.57	3.00
40	169.1	37.1	-72.9	13.8	333.0	24.6	273.1	135.8	2.54	2.26	2.60	1.43	2.81	2.37	3.29	1.84
50	154.2	43.5	-67.9	17.1	321.9	22.0	278.7	170.7	2.81	3.96	3.81	1.88	4.10	5.44	5.21	3.88
60	152.9	36.9	-58.8	15.4	286.2	-38.7	331.1	189.6	78.69	156.67	63.83	67.87	171.88	535.93	203.22	214.83
70	165.4	61.6	-70.4	27.0	342.2	29.3	271.8	229.8	5.64	3.62	2.31	3.75	5.22	3.73	5.32	5.40
80	168.2	63.1	-57.8	33.2	321.9	51.8	216.5	283.2	4.71	3.44	3.08	3.98	4.17	4.56	4.70	8.88
90	152.4	88.5	-74.1	30.2	343.0	56.6	269.4	312.8	2.23	3.76	3.87	2.53	6.42	3.41	6.54	5.38
100	148.8	93.4	-70.7	33.1	344.8	50.4	266.6	336.4	3.38	4.98	4.35	3.76	7.35	5.66	6.07	8.60
110	146.3	116.9	-76.4	38.3	331.6	53.3	267.0	340.6	2.11	3.47	2.30	4.26	7.45	7.43	6.86	9.18
120	133.4	121.8	-79.3	39.0	347.2	74.5	226.3	385.7	37.92	45.60	50.49	23.81	118.90	200.34	186.18	127.57
130	136.0	122.3	-73.9	49.3	326.8	39.7	252.3	396.5	3.38	7.40	4.48	6.62	7.48	7.63	10.05	11.95
140	122.6	148.0	-79.5	59.9	322.4	77.9	218.2	467.6	3.11	6.35	4.51	4.97	12.83	6.96	9.22	11.68
150	126.7	156.3	-68.7	70.8	346.4	58.1	274.4	496.8	5.83	4.60	8.70	5.45	16.33	6.03	16.49	18.72
160	113.4	169.0	-77.3	64.2	306.0	111.1	204.9	543.9	6.61	4.45	5.60	6.47	15.04	5.97	12.23	12.25
170	108.6	185.8	-75.6	80.0	306.4	104.4	219.5	577.1	7.53	8.91	11.67	10.22	11.28	9.57	15.79	10.27
180	461.9	219.9	70.2	431.1	361.3	-42.0	387.3	569.0	556.84	790.39	445.29	708.10	418.85	214.57	300.30	284.56
190	111.8	215.6	-62.6	99.2	330.9	118.8	255.8	624.3	8.21	7.92	8.53	10.70	6.14	6.30	13.76	11.05
200	108.7	244.8	-97.0	49.7	371.9	109.4	-9.6	792.8	68.17	116.68	190.74	147.37	465.79	290.67	623.90	767.93
210	100.3	241.0	-54.5	117.2	336.8	162.0	230.4	712.2	2.69	3.57	3.25	5.03	7.76	9.90	14.61	13.27
220	103.4	256.8	-51.0	125.2	328.0	157.2	217.2	685.6	2.55	3.81	2.41	4.95	6.54	6.68	7.32	13.14
230	91.8	270.4	-59.3	120.7	322.8	224.1	180.1	822.7	2.35	3.16	3.64	2.93	6.85	6.05	9.68	11.88
240	94.7	291.3	-53.6	141.8	375.8	197.6	282.7	834.9	5.34	8.60	13.34	10.39	18.24	20.35	32.47	40.11
250	84.5	318.5	-59.9	163.2	379.6	211.7	278.7	889.4	3.38	4.96	4.63	6.45	8.09	6.42	11.87	17.85
260	85.2	333.4	-49.1	166.8	377.1	210.1	305.5	909.7	5.36	4.17	5.74	5.32	9.74	5.99	11.30	14.51
270	91.2	351.1	-45.7	186.4	405.0	175.4	410.4	918.8	3.92	8.78	7.92	8.87	9.65	7.79	12.31	22.69
280	79.2	355.3	-35.5	158.6	329.6	331.5	209.3	1226.0	3.44	5.90	3.65	5.44	8.69	9.41	13.74	19.64
290	88.7	426.6	-48.4	238.9	402.8	232.3	502.3	1044.1	3.49	8.37	4.93	6.93	11.29	7.96	14.42	17.73
300	116.6	473.0	-7.3	291.0	385.4	228.4	502.7	987.3	19.38	43.89	35.89	54.92	22.92	30.24	70.39	41.89

Table 60. Dynamic stiffness real and imaginary parts at 12000 rpm and 1379 kPa (MN/m)

f	$R(H_{xx})$	$I(H_{xx})$	$R(H_{xy})$	$I(H_{xy})$	$R(H_{yx})$	$I(H_{yx})$	$R(H_{yy})$	$I(H_{yy})$	$\Delta R(H_{xx})$	$\Delta I(H_{xx})$	$\Delta R(H_{xy})$	$\Delta I(H_{xy})$	$\Delta R(H_{yx})$	$\Delta I(H_{yx})$	$\Delta R(H_{yy})$	$\Delta I(H_{yy})$
20	224.4	13.2	-76.3	11.9	393.3	6.5	356.1	78.8	7.84	7.67	7.43	2.58	12.49	5.35	13.37	2.40
30	222.3	22.5	-73.4	19.8	396.9	-21.3	383.1	91.5	5.91	3.96	6.53	2.89	9.45	11.22	6.78	7.23
40	199.9	36.0	-68.3	20.5	374.9	22.8	371.0	155.0	2.71	4.83	4.83	1.76	5.81	2.76	6.49	3.24
50	181.6	38.1	-61.5	24.5	359.3	17.4	373.8	199.0	5.65	4.80	4.88	2.14	5.92	3.13	5.53	2.38
60	221.2	82.2	-73.1	46.2	399.4	115.3	340.7	265.7	241.15	140.40	66.96	126.95	611.36	629.20	181.60	412.47
70	199.8	63.6	-65.4	36.2	390.8	27.9	362.5	266.1	4.40	6.40	6.81	2.35	6.49	4.47	8.65	5.69
80	202.7	73.5	-56.5	44.8	382.1	55.6	317.4	340.7	4.34	7.38	4.50	3.85	11.63	5.11	8.07	5.02
90	177.6	95.4	-67.9	42.2	383.0	60.5	361.6	370.3	1.98	7.48	5.06	2.21	10.76	6.07	8.26	7.42
100	183.6	103.1	-66.7	48.5	390.1	60.5	352.3	400.3	2.41	9.98	7.01	6.61	15.70	6.10	8.59	14.22
110	172.1	128.2	-66.6	49.0	369.2	63.8	357.8	403.7	4.16	11.58	4.97	5.06	12.55	8.43	8.13	11.14
120	167.7	117.6	-53.9	66.8	385.2	68.0	370.6	491.3	35.84	48.99	36.37	55.53	164.74	175.38	138.92	230.24
130	177.8	131.6	-58.5	63.0	381.5	46.7	347.6	465.3	6.28	10.40	3.54	7.27	10.30	8.62	7.05	11.17
140	154.1	154.7	-61.2	74.8	377.7	83.4	320.9	575.4	4.34	11.61	4.15	8.36	9.90	7.49	12.51	12.70
150	169.6	153.7	-38.7	81.0	430.0	39.9	426.9	583.8	5.46	11.69	6.03	7.91	19.60	7.93	12.59	14.81
160	148.9	171.8	-63.4	73.2	367.9	110.6	310.3	635.9	4.85	14.05	7.86	8.87	11.31	9.42	18.53	11.51
170	145.9	192.1	-56.1	97.6	380.8	107.1	334.7	692.5	3.98	9.27	6.56	10.04	10.87	7.63	9.74	10.23
180	451.6	203.3	90.1	310.5	412.1	-61.0	449.8	627.1	205.62	278.77	465.52	291.53	170.82	135.63	200.50	289.10
190	149.6	220.9	-41.3	110.0	399.0	98.8	381.1	703.8	5.61	14.41	5.71	7.30	18.82	8.15	10.72	11.98
200	150.8	231.8	-52.7	102.9	360.0	114.3	226.7	781.2	17.11	31.15	34.48	45.94	134.38	66.44	227.09	130.71
210	141.4	243.9	-26.2	131.3	409.6	137.2	357.1	811.9	7.09	10.20	5.75	6.84	22.07	11.60	26.56	9.91
220	145.2	265.1	-27.9	138.4	398.4	143.0	332.4	787.2	4.89	13.77	3.44	4.71	16.71	5.43	11.02	10.61
230	131.5	275.6	-31.7	133.3	388.3	205.4	273.7	928.3	3.81	12.48	4.81	4.72	8.72	4.93	13.73	7.96
240	139.5	300.8	-25.6	155.8	450.3	167.6	412.0	927.1	7.46	13.27	11.56	10.46	18.09	12.90	30.82	26.04
250	135.9	321.5	-22.3	180.2	456.4	170.1	421.8	998.2	4.21	13.32	7.36	6.63	14.76	5.80	11.84	12.42
260	133.2	332.2	-12.2	180.7	433.2	164.4	423.1	992.2	8.65	14.50	9.77	6.48	12.69	3.38	7.75	11.98
270	143.9	342.5	0.5	195.5	475.0	131.7	553.9	1024.8	7.60	15.76	10.34	8.00	19.19	8.33	14.74	12.87
280	132.8	343.7	25.7	163.8	361.3	268.8	220.8	1265.4	9.70	17.47	11.18	7.72	6.13	8.23	8.39	11.04
290	133.4	393.1	-1.3	227.4	464.6	170.4	675.4	1126.2	3.97	21.95	7.05	13.16	13.85	11.96	10.91	18.77
300	148.2	438.3	17.0	268.0	476.0	131.3	808.6	1062.5	18.24	20.17	21.66	27.77	16.07	9.57	21.36	18.23

Table 61. Dynamic stiffness real and imaginary parts at 12000 rpm and 1655 kPa (MN/m)

f	$R(H_{xx})$	$I(H_{xx})$	$R(H_{xy})$	$I(H_{xy})$	$R(H_{yx})$	$I(H_{yx})$	$R(H_{yy})$	$I(H_{yy})$	$\Delta R(H_{xx})$	$\Delta I(H_{xx})$	$\Delta R(H_{xy})$	$\Delta I(H_{xy})$	$\Delta R(H_{yx})$	$\Delta I(H_{yx})$	$\Delta R(H_{yy})$	$\Delta I(H_{yy})$
20	249.5	30.5	-80.3	31.4	434.7	36.7	435.3	121.3	32.10	204.55	24.00	226.01	62.08	349.98	36.76	383.63
30	278.0	23.4	-41.2	28.9	488.6	-41.4	532.5	95.7	245.71	41.02	291.73	38.35	398.75	130.03	498.65	27.43
40	235.7	30.2	-61.8	20.9	428.2	5.6	473.0	161.5	69.64	32.47	82.12	44.65	121.94	51.20	148.43	69.80
50	206.0	37.4	-72.6	29.4	386.5	12.5	441.7	217.4	33.64	16.19	39.40	28.42	61.12	26.65	71.89	43.87
60	290.3	48.7	-61.4	51.1	622.8	19.2	485.7	297.9	295.53	166.50	135.08	110.79	1011.90	519.26	416.75	382.09
70	236.7	64.0	-59.3	46.6	439.6	20.5	454.1	294.3	18.45	22.58	32.55	12.15	25.11	36.92	55.19	27.49
80	228.5	80.8	-62.3	60.7	413.5	55.9	398.9	375.8	10.25	14.97	22.34	17.88	18.10	30.05	31.17	33.85
90	203.4	96.9	-65.3	59.6	430.8	61.1	454.9	430.5	13.85	17.42	5.82	34.53	27.92	29.03	29.16	64.26
100	215.9	102.3	-54.9	60.3	437.0	56.1	455.4	450.7	23.72	18.59	42.31	9.59	35.27	29.98	80.96	11.03
110	197.8	126.8	-50.0	61.0	413.4	59.5	460.6	456.9	13.82	18.95	29.35	11.37	16.35	32.06	48.54	43.26
120	199.4	115.8	-52.3	83.6	462.3	48.9	467.4	582.4	57.19	56.47	37.91	72.98	258.94	216.67	145.88	306.30
130	211.8	137.7	-49.0	78.5	435.6	47.9	447.9	532.8	10.81	18.31	28.94	11.47	15.12	30.58	38.68	39.43
140	175.2	151.8	-53.3	79.2	409.0	77.7	401.9	618.2	14.71	18.58	9.01	33.07	36.01	17.26	30.86	52.80
150	211.4	155.4	-14.7	107.9	491.7	25.4	557.1	645.5	16.70	24.25	44.16	20.02	12.33	51.37	76.80	49.84
160	175.2	175.5	-61.2	83.0	429.6	119.9	407.4	739.9	20.54	15.93	32.23	39.33	41.71	28.20	64.66	72.53
170	168.4	194.1	-46.8	104.9	428.6	100.9	437.1	760.1	22.37	14.90	39.75	32.81	34.08	28.01	73.78	36.78
180	317.8	330.1	-75.4	249.4	520.4	31.4	488.4	797.4	648.54	386.63	652.14	645.65	272.27	471.32	496.16	447.70
190	181.1	223.6	-23.5	131.5	451.1	81.0	494.9	770.5	9.89	15.09	24.45	13.13	14.29	18.41	39.85	27.82
200	181.7	224.2	-40.9	119.2	378.6	101.0	351.4	862.0	25.31	21.13	65.68	89.55	129.28	123.12	451.23	307.18
210	169.9	251.8	-18.3	155.5	456.8	118.9	463.0	889.4	8.02	12.39	10.80	8.61	17.94	16.21	23.52	32.13
220	173.3	265.8	-8.4	153.0	444.9	128.6	434.5	867.9	9.78	19.97	24.65	20.18	16.82	17.62	31.14	39.07
230	155.6	281.6	-22.2	149.7	436.0	197.7	371.5	1015.0	16.80	11.77	30.70	18.92	19.21	20.32	47.37	21.45
240	171.0	303.8	-4.1	174.5	504.0	145.8	520.4	1009.1	14.32	19.33	37.22	16.66	27.37	31.20	54.87	55.27
250	169.9	327.9	2.2	206.7	509.5	146.4	537.6	1075.0	13.32	21.97	39.32	21.95	24.21	29.10	41.70	58.51
260	169.2	336.9	15.5	205.8	489.2	138.1	555.5	1071.5	12.28	17.48	11.83	26.10	25.28	13.37	40.02	37.38
270	178.6	339.8	40.3	212.0	516.1	99.3	664.4	1076.6	9.27	17.89	21.90	10.88	20.18	17.05	22.74	44.73
280	170.8	344.7	64.1	188.6	396.9	221.0	292.1	1227.8	6.97	15.47	19.84	13.21	14.34	17.08	26.83	32.22
290	163.7	385.2	28.7	235.0	513.5	136.1	818.4	1196.3	8.02	14.72	14.24	13.45	14.15	13.69	29.72	27.26
300	171.2	426.7	45.7	259.5	526.3	100.8	959.4	1141.0	29.77	27.07	54.34	37.17	31.07	21.49	42.51	39.74

VITA

Bader K. Al Jughaiman received his B.S degree in mechanical engineering from King Fahd University of Petroleum and Minerals in Dhahran, Saudi Arabia in June 2001. Since then, Bader has been working for Saudi ARAMCO as a rotating equipment engineer. Bader obtained his M.S degree in mechanical engineering from Texas A&M in August 2006. Bader is married and has two children.

Bader can be reached at South Ghawar Producing Department, Saudi ARAMCO, Udhailiyah 31311, Saudi Arabia. Bader also can be emailed at:
bader.jughaiman@aramco.com